Design of an energy management system utilizing optimum energy consumption of a distribution level microgrid

WA Bisschoff

13273523

Dissertation submitted in fulfilment of the requirements for the degree *Magister* in Electrical and Electronic Engineering at the Potchefstroom Campus of the North-West University

Supervisor: Prof R Gouws

May 2016

Executive Summary

Currently within South Africa, net-metering policies are not yet widely implemented which hinders the adoption of residential microgrids. Without proper net-metering policies in place, the benefits of residential microgrids are limited to self-consumption as all energy fed into the utility grid is lost without remuneration. This leads to an inefficient and non-profitable microgrid system. To improve the efficiency and feasibility of a microgrid system in areas with no net-metering policy, it is of utmost importance that an energy management system (EMS) that optimises self-consumption, of the generated energy, be employed. This dissertation discusses the design, simulation, implementation, results obtained and feasibility of such an EMS.

The EMS was designed according to a typical living standard measure (LSM) group 8 residence. A simulation model was designed to represent the load profile of the residence with and without the intervention of the EMS. The EMS employed various energy saving strategies along with a strategy focussing on self-consumption. Simulation results showed that in certain scenarios, the EMS would improve the self-consumption percentage from 83% to 98%. The EMS would also reduce the energy consumption off the utility grid from 35.6 kWh per day to 12.7 kWh per day. This would be possible by actively controlling the loads to operate at specific times during the day and by reducing the amount of running hours of certain loads. To verify the accuracy of the simulation model, the EMS was installed into an experimental test station with real-world loads.

The microgrid was installed at a typical LSM group 8 residence in Potchefstroom and employed a 2 kW solar photovoltaic (PV) system with a grid-tie inverter. The control system which housed the EMS software was installed along with the solar PV and grid-tie inverter system. The control system consisted of a programmable logic controller (PLC) which controlled relays connected in series with the loads. Experimental results from the test station showed that in certain scenarios, the EMS improved the self-consumption percentage from 84% to 95%. The EMS also reduced the energy required from the utility grid from 34.2 kWh per day to 9.8 kWh per day. This was possible by efficiently controlling the loads according to the incoming solar PV profile and minimising energy consumption when little or no solar PV energy was generated.

The feasibility of the integrated system depended greatly on the initial investment capital available. In the case that the integrated system could be funded without the need for a loan, the saving on electricity costs and the investment cost would reach a break-even point within four years. In the case that a loan would be used to fund the investment, the monthly repayment cost would be covered by the monthly electricity bill savings and the total monthly cost would still be less than the monthly electricity bill without the integrated system. The adoption of the integrated microgrid system would therefore be a feasible solution to counteract rising electricity costs.

Keywords: Energy Management System, Microgrid, Distributed Generation

Opsomming

Tans in Suid-Afrika is nettometingbeleide nog nie op grootskaal geïmplementeer nie, met die gevolg dat die integrasie van residensiële mikrokragnetwerke verhinder word. Sonder behoorlike nettometingbeleidsraamwerke, word die voordele van residensiëlemikrokragnetwerke beperk tot selfverbruik. Alle energie wat in die sentralekragnetwerk ingevoer word, gaan verlore sonder enige vergoeding aan die eienaar van die mikrokragnetwerkstelsel. Dit lei tot 'n ondoeltreffende en nie-winsgewende mikrokragnetwerkstelsel. Om die rendement en winsgewendheid van die mikrokragnetwerkstelsel in gebiede met geen nettometingbeleide te verbeter, is dit van uiterste belang om 'n energiebestuurstelsel (EBS) wat selfverbruik optimaliseer ten einde in te stel. Hierdie verhandeling ondersoek die ontwerp, simulasie, implementering, resultate en winsgewendheid van so 'n EBS.

Die EBS is ontwerp volgens 'n tipiese lewenstandaardmaatreël (LSM) groep 8 inwoning. 'n Simulasiemodel is ontwerp om die vragprofiel van die woning voor te stel gesamentelik met en sonder die beheer van die EBS. Die EBS het verskeie energiebesparendestrategieë saam met 'n selfverbruikstrategie geïmplementeer. Simulasieresultate het getoon dat in sekere omstandighede sou die EBS die selfverbruikpersentasie van 83% tot 98% verbeter het. Die EBS het die energie wat benodig was vanaf die sentralekragnetwerk van 35.6 kWh per dag na 12.7 kWh per dag verminder. Dit is moontlik gemaak deur aktiewe beheer oor die vragte uit te oefen op spesifieke tye gedurende die dag en deur die vermindering van die hoeveelheid werksure van sekere vragte. Om die akkuraatheid van die simulasiemodelle te verifieer, is die EBS geïnstalleer in 'n eksperimenteletoetsstasie met werklike vragte soos geïnstalleer in 'n LSM-groep 8 woning.

Die mikrokragnetwerkstelsel was geïnstalleer in Potchefstroom en het gebruik gemaak van 'n 2 kW sonkragfotovoltaïsestelsel met 'n kragnetwerkintegreerbareomsetter. Die beheerstelsel wat die EBS-sagteware gehuisves het, was geïnstalleer saam met die sonkragfotovoltaïsestelsel en kragnetwerkintegreerbareomsetterstelsel. Die beheerstelsel het bestaan uit 'n programmeerbarelogiesebeheerder wat kontakte in serie met die vragte gehad het. Eksperimentele resultate van die toetsstasie het getoon dat in sekere omstandighede die EBS die selfverbruikpersentasie van 84% na 95% verbeter het. Die EBS het verder ook die energie wat nodig was vanaf die sentralekragnetwerk van 34.2 kWh per dag na 9.8 kWh per dag verminder. Dit is moontlik gemaak deur die vragte doeltreffend te beheer volgens die inkomendesonkragprofiel en deur die vermindering van energieverbruik wanneer min of geen solarenergie gegenereer is nie.

Die winsgewendeheid van die geïntegreerdestelsel hang grootliks af oor die beskikbare aanvanklike beleggingskapitaal. In die geval dat die geïntegreerde stelsel gefinansier kan word sonder die noodsaaklikheid van 'n lening, sal die besparing op die koste van elektrisiteit en die beleggingskoste 'n gelykbreekpunt bereik binne vier jaar. Indien 'n lening gebruik word om die belegging te finansier, sou die maandelikse terugbetalingbedrag gedek word deur die besparing en sou dit steeds minder as die maandelikse elektrisiteitkoste wees as wanneer die geïntegreerde stelsel nie geïmplementeer word nie. Die inwerkstelling van die geïntegreerde stelsel met EBS is dus 'n winsgewende oplossing om die stygende koste van elektrisiteit teen te werk.

Sleutelwoorde: Energiebestuurstelsel, Mikrokragnetwerk, Distribusiegenerasie

Acknowledgements

The completion of this dissertation could not have been possible without the inputs and participation of the names listed below.

Michelle, my wife and best friend, I would like to thank you for your endless love, patience and understanding during the six years of my under and postgraduate studies. Your words of encouragement always kept me focussed on the task at hand.

Prof. Rupert Gouws, I would like to express my sincerest gratitude for your support in my under and postgraduate studies. Since the beginning of 2012, your guidance and knowledge not only broadened my horizons but taught me the skill to confidently face any engineering challenge.

To my family, you all gave your tireless support in assisting me during this time. Thank you for the editing assistance, mechanical engineering and moral support. A special thanks goes out to my brother for all those early morning commitments.

I would like to sincerely thank the National Research Foundation for granting me the necessary financial support to complete this study.

I would also like to thank the South African National Weather Service for supplying me with historic weather data which helped improve the quality of this study.

The research project was funded by the National Research Foundation (NRF) and would not have been possible without their financial aid. The material of this study is based on research/work supported by the NRF. The research findings are that of the authors and not that of the NRF.

Table of Contents

List of Figures

List of Tables

Nomenclature

List of Abbreviations

3G	Third Generation
AC	Alternating Current
AI	Analog Input
CAD	Computer Aided Design
CFL	Compact Fluorescent Lamp
CPU	Central Processing Unit
CSP	Concentrated Solar Plant
CT	Current Transformer
DC	Direct Current
DER	Distributed Energy Resource
DFIG	Doubly Fed Induction Generator
DOD	Depth of Discharge
DPDT	Double Pole Double Throw
DSP	Digital Signal Processing
EBS	Energiebestuurstelsel
ECU	Electronic Control Unit
EMS	Energy Management System
ESS	Energy Storage System
Eskom	Electricity Supply Commission of South Africa
FLA	Full Load Amperage
FRC	Fully Rated Converter
GPRS	General Packet Radio Service
GPS	Global Positioning Satellite
GTI	Grid-Tie Inverter
HFO	Heavy Fuel Oil
HVAC	Heating, Ventilation and Air Conditioning
I/O	Input/Output
IC	Integrated Circuit
IEC	International Electrotechnical Commission
IDM	Integrated Demand Management
IP	Internet Protocol
LED	Light Emitting Diode
LSM	Living Standards Measure
LV	Low Voltage
MCU	Microcontroller
MPPT	Maximum Power Point Tracking
MV	Medium Voltage
NEMA	National Electrical Manufacturers Association
PCC	Point of Common Coupling
PFC	Power Factor Correction

PLC	Programmable Logic Controller
PV	Photovoltaic
PWM	Pulse Width Modulation
QoS	Quality of Supply
RAM	Random Access Memory
RF	Radio Frequency
RISC	Reduced Instruction Set Computer
SA	South Africa
SANWS	South African National Weather Service
SBC	Single Board Computers
SOC	State of Charge
SEF	Solar Energy Facility
SIM	Subscriber Identity Module
TCP	Transmission Control Protocol
TOU	Time of Use
UDP	User Datagram Protocol
UPS	Uninterrupted Power Supply
VSC	Voltage Source Converter
WEF	Wind Energy Facility
WTG	Wind Turbine Generator

List of Units

A	Ampere
Ah	Ampere-hours
bps	bits per second
GB	Gigabyte
GHz	Gigahertz
Hz	Hertz
KB	Kilobyte
Kg	Kilogram
kVA	Kilo Volt-Ampere
kW	Kilowatt
kWh	Kilowatt-hour
kWh/m^2	Kilowatt-hour per Square Meter
lm/W	Lumens per Watt
MHz	Megahertz
MVA	Mega Volt-Ampere
MW	Megawatt
MB	Megabyte
V	Volts
VAC	AC Volts
VDC	DC Volts
W	Watt
W/kg	Watt per Kilogram
Wh/kg	Watt-hour per Kilogram

List of Symbols

C	Carbon
h	Hours
H	Hydrogen
I	Current
N_p	Number of Primary Turns
O	Oxygen
P	Real Power
R	South African Rand
R^2	Coefficient of Determination
R_b	Burden Resistor
s	Seconds
V	Voltage
°C	Degree Celsius
η	Reduction Factor
γ	Depth of Discharge
κ	Inrush Current Factor
θ	Power Factor
ς	Safety Design Factor

Chapter 1: Introduction

This chapter is the starting point of the dissertation which establishes the foundation upon which the study is built. This chapter expands on the relevant background knowledge of microgrid systems and the role of these within the centralised power grid. A section that explains the background information on the research problem is added along with the research methodology that is followed. The dissertation structure, research questions and publications are also listed within this chapter. A conclusion is drawn at the end of the chapter to summarise key thoughts that need to be remembered.

1.1 Background

A microgrid is defined as a small independent power system consisting of locally generated alternative energy sources that can function independently or in accordance with the centralised power grid [1], [2]. Microgrids can be integrated with the centralised grid on transmission or distribution level depending on the purpose of the system. For a residential microgrid, the system is integrated on the low voltage (LV) distribution network where the power generation mediums are referred to as distributed energy resources (DERs) [2]. Typical examples of DERs include small scale wind turbines, solar photovoltaic (PV) systems, microturbines, diesel-generators, fuel cells etc.

Conventional microgrids are connected in a topology that enables the system to be grid-tied or disconnected from the grid (island-mode); a typical illustration of a microgrid system is shown in figure 1-1 [3]. The grid-tied topology is the most-common and simplest to implement since a constant balance between the generated and consumed energy is ensured by the centralised grid. In the case where the DERs connected to the microgrid generates excess energy, it is fed into the centralised grid [2], [4]. In island-mode it is not that simple since there is no additional grid to which excess energy can be fed to maintain the energy balance. Once the microgrid disconnects from the upstream distribution grid, the aim of the system is to ensure a reliable supply, whilst maintaining the energy balance in the system [4]. Islanded microgrid systems are more complex systems and requires an energy storage system (ESS) as a buffer between the DER and the loads connected to the microgrid. During the islanding period of the microgrid, the loads are supplied from the ESS while the DER recharges the ESS [2].

The popularity of microgrids have rapidly increased over the last decade as a result of certain benefits microgrids possess over a conventional centralised power grid. The uprising of society to reduce environmental pollution and promote self-generation have seen various renewable energy sources being adopted as DERs in microgrid topologies [2], [4]. According to Moussavou, Adonis and Raji (2015) and Guo, Pan and Fang (2012), some of the main advantages of the renewable sources of energy are the reduced impact on the environment and the abundance of renewable energy [5], [6].

Another key benefit associated with a microgrid system is the higher conversion efficiency compared to that of a centralised power grid [7]. Due to localised power generation within

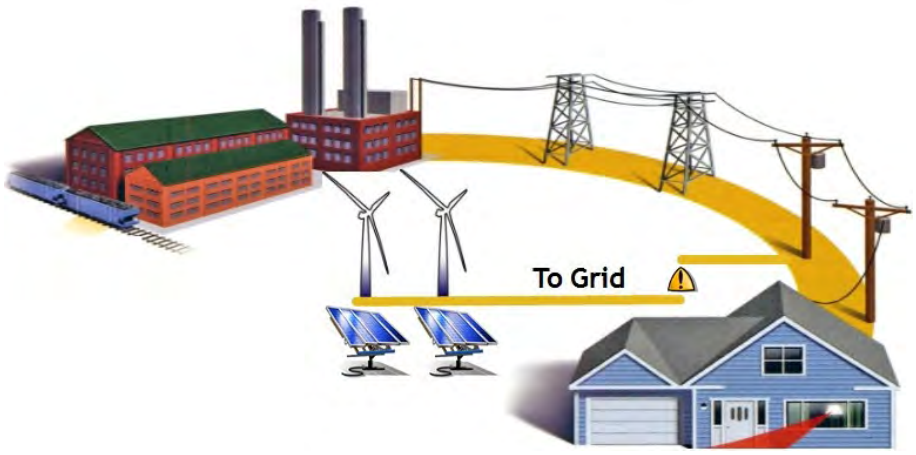

Figure 1-1: Typical microgrid system [3]

a microgrid, the need to transmit energy over long distances is eliminated which in turn eliminates transmission and distribution losses. According to Nandy and Bhattacharya (2009), it is equated that transmission and distribution losses are rarely less than 20% [8]. South African (SA) data suggests that transmission line losses are equated to between 6 and 8% whilst distribution losses, depending on rural or urban areas, are between 11 and 40% [9].

Over the past five years the world has seen numerous installations of microgrids on distribution level which utilises the benefits of both grid-tied and island-mode microgrids. Island-mode microgrids are especially popular with farmers and electricity users in rural areas that require a reliable supply of electricity. Broad-based implementation of microgrids in the urban residential sector are growing slower compared to the rural sector due to higher reliability of electricity in urban areas. The implementation of a microgrid is considered an investment with the benefit of electricity bill reduction.

1.2 Purpose of Research

1.2.1 Problem Statement

The purpose of the research study presents an economic as well as a technical problem. The economic problem addresses the financial and economical constraints that prohibits or limits the implementation of microgrids within the South African economy. The technical problem addresses engineering related constraints and limitations associated with microgrids.

1.2.1.1 Economic Evaluation

Recent press releases and media announcements made by the South African state-owned utility company, Eskom, indicates that the South African national power grid is under severe pressure [10]. A media statement made by the chief executive officer at the time, Tshediso Matona, stated that, *"We are on the brink of a total blackout"* [10].

Eskom has an installed grid capacity of 44 084 MW when all units are fully opera-

tional [11]. However, all the generation units are not fully operational and are subject to scheduled maintenance. Eskom aims to perform scheduled maintenance on at least 10% of the installed capacity per annum whilst trying to limit the unplanned outages to below 4 500 MW [10]. This translates to a net usable capacity of 35 000 MW. Eskom has made provision to increase the total capacity of the grid by implementing the "New Build Programme" which sees the construction of two new coal-fired power stations, namely Medupi and Kusile, a pumped storage facility and a wind farm [11]. To further increase the capacity of the grid, Eskom started recommissioning two old coal-fired power stations in 2005 [11], [12]. Although this relieved pressure off the grid, Eskom still had to settle buy-back contracts with heavy industrial electricity users and urge residential users to cut back on energy consumption [13], [14].

According to Eskom Integrated Demand Management (IDM) (2013), the residential sector occupies at 35% of the annual energy demand and consumes 17% of the total energy generated [15]; a summary of the capacity consumption and demand levels for each sector of SA is shown in figure 1-2. This has led to the implementation of a residential mass roll-out programme to reduce the residential demand and consumption levels. The Switch and Save residential mass roll-out programme saw the installation of energy saving and load management devices at the expense of Eskom [16]. According to Eskom IDM (2014), by winter 2014, a reduction of 1 045 MW in the residential demand division had been mandated [16]. This reduction proved to relieve pressure off the grid but further reductions in the residential sector are possible [17], [18], [19].

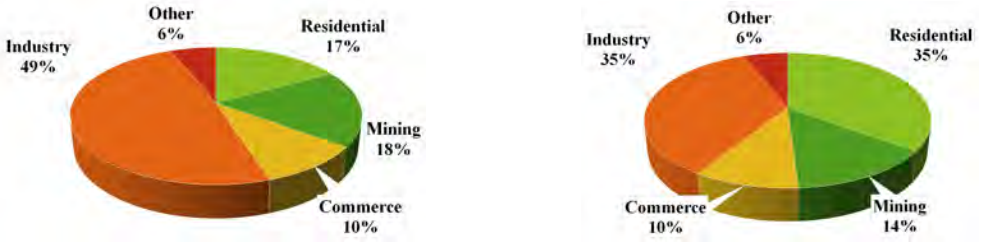

(a) Energy consumption per sector

(b) Energy demand per sector

Figure 1-2: Energy occupancy per sector in SA [15]

Rising electricity prices and unreliable supply are driving more residential electricity consumers to installing residential microgrid systems that consists of small scale renewable energy sources such as wind turbines and solar PV systems. According to Mikati et al. (2013) and Ramakrishnan et al. (2013), implementing residential microgrids have the ability to drastically improve the owner of the microgrid's reliability whilst decreasing the annual electricity bill [17], [20]. Achieving the abovementioned requires widespread net-metering policies that permits residential electricity consumers to "sell" excess generated electricity back to the utility [17], [20]. According to Lipschitz (2010), NERSA (2009) and Eskom Transmission (2015), connecting small scale (<1 MW) DERs that feeds electricity back into the grid is not permitted throughout SA unless it forms part of a municipal agreement or pre-approved pilot project [21], [22], [23]. There are certain private residential estates, such as De Zalze in Stellenbosch, which forms part of City of Cape Town Municipality that has been selected to participate as part of a pilot project. Municipalities such as Nelson Mandela Bay and City of Cape Town permits feed-in policies and according to Nelson Mandela Bay Municipality (2014), a feed-in tariff of R 1.20 per

kilowatt-hour (kWh) is offered to residential clients partaking in Port Elizabeth whereas City of Cape Town Municipality (2014) reports a feed-in tariff of R 0.56 per kWh [24], [25], [26]. These policies are becoming more popular but lacks financially feasible feed-in tariffs and users are also subject to a fixed daily charge. Feed-in tariffs are below the average cost of electricity supplied by municipalities and Eskom. The benefit of feeding electricity into the centralised grid cannot fully be utilised as in other countries such as the Americas, Belgium and Switzerland which offers competitive feed-in tariffs [27].

1.2.1.2 Technical Evaluation

The adoption of residential grid-tied microgrids are limited to the benefit of complementing the existing electricity feed. As previously is mentioned, the most common topology of residential microgrids is to connect the system in a grid-tied topology to the utility's grid and allow the excess generated energy to feed into the centralised grid. The lack of load management or feed-in tariff policies introduces the problem of wasted energy. Every kWh of energy that is fed into the utility's network is essentially wasted for the home-owner as very little or no remuneration is received for energy fed back into the grid. Figure 1-3 visually supports the abovementioned statement.

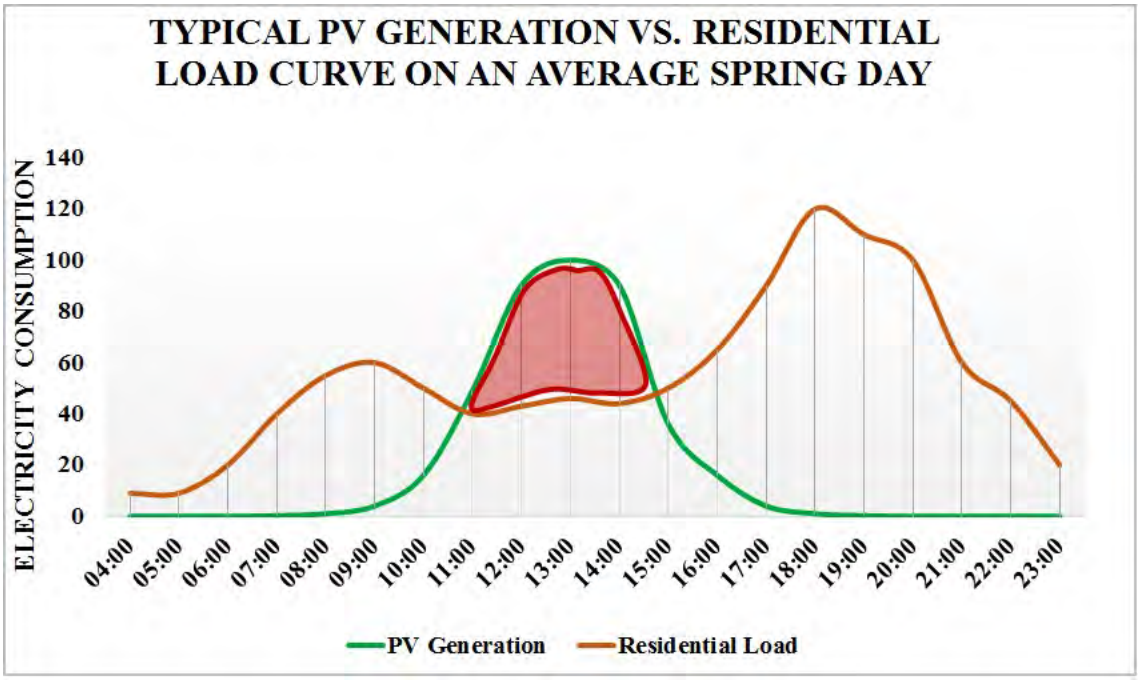

Figure 1-3: Typical solar PV generation and residential load curve

Figure 1-3 illustrates an example of a home-owner employing a grid-tied solar PV system. A typical household load curve along with an input solar PV curve is shown. The home-owner loses the excess energy where the incoming power exceeds the consumed power (red area). A reduction in the efficiency of the home-owner's microgrid is inevitable as not all of the energy generated by the microgrid is consumed locally.

1.3 Research Methodology

The study was divided into nine phases: 1) Candidate technology and literature study, 2) Conceptual and detail design, 3) Design simulations, 4) Microgrid test station construction and assembly, 5) Control system implementation, 6) Integrated system evaluation, 7) Experimental data collection, 8) Results analysis, conclusion and recommendations, 9) Verification and validation.

1.3.1 Candidate Technology and Literature Study

A comprehensive literature study needed to be done to ensure that all possible solutions to the mentioned problem statement were considered. Furthermore, a candidate technology survey was completed to ensure that the latest technology trends were kept in mind during the design phase.

1.3.2 Conceptual and Detail Design

After the completion of the literature and candidate technology study, the formed conceptual design was developed into a theoretical detailed design. During the theoretical design phase, all specifications, standards and integrations between components was determined to ensure sound theoretical design. The technology survey was actively used as a basis for the theoretical design which simplified the conversion process from a theoretical design into a fully practical detail design.

1.3.3 Design Simulation

Individual and integrated system simulations were performed to ensure that a basis was formed to which the experimental test data could be compared. Powerful mathematical modelling software such as MATLAB® and Simulink® was used to simulate the energy and control system. The input energy profiles for the photovoltaic cells was simulated using PVsyst, which is software that uses historic geographical and system installation details to produce expected energy yields. In a similar manner the control system was comprehensively simulated using the mathematical packages described above.

1.3.4 Microgrid Test Station Construction and Assembly

This phase saw the finalised detail design taken from mere drawings to a fully assembled and constructed test station. The microgrid's hardware was constructed and installed such that it was suitable for collecting accurate test data. It was critical that thorough electrical installation was done to adhere to the regulations of the Occupational Health and Safety Act (No. 85 of 1993) [28]. This was critical as the microgrid system was tested in an environment where people were unaware of the hazards present.

1.3.5 Control System Implementation

The control system was responsible for the active management of the microgrid and was critically important to ensuring the success of the study. The energy management software system was written in a cross-platform C++ application called Qt Creator. The system

controller ran in a server-client topology where the data was sent and received data to/from the Qt application to ensure optimal system performance. The Qt application also acted as the integration point between all the communication protocols.

1.3.6 Integrated System Evaluation

After the microgrid's hardware and software sub-systems were finalised, the integration between the sub-systems commenced to produce an integrated system. The integration tests consisted of testing input-to-output relations to ensure that the software and hardware systems were operating as expected.

1.3.7 Experimental Data Collection

After satisfactory results were obtained from the simulations, the same process had to be followed by the experimental test station. The experimental test station system was tested in real-time testing conditions that allowed the collection of the experimental test data. The test data was automatically captured and stored within a MySQL database on the server; this enabled easy retrieval of the data for analysis purposes.

1.3.8 Results Analysis, Conclusion and Recommendations

During this phase, all the captured data was processed into information by means of statistical correlations, mathematical approximations and graphical illustrations. This information was then critically analysed and compared against the simulation data to draw scientific conclusions and recommendations.

1.3.9 Verification and Validation

The verification and validation of the study was critical to ensure that the study meets the requirements which it is intended for. Verification and validation complements each other and is intended to raise the following two questions: 1. Verification - "Are we building the system right?" 2. Validation - "Are we building the right system?". Verification and validation of the system were done on the design, simulation and results chapters.

1.3.10 Key Research Questions

This section states the three primary research questions that should be answered at the end of the study. The questions listed below dictates the objectives and provides a performance measure of the study.

1. Is it financially feasible to implement a residential microgrid with an EMS?
2. If net-metering is to be implemented in the South African utility network, how does this influence the feasibility of a residential microgrid with an EMS? How does the benefits of net-metering weigh up against localised consumption (self consumption)?
3. Technically, how much energy reduction is possible without excessively disrupting the daily routine of residential energy consumers?

1.4 Dissertation Overview

A brief overview of the dissertation is discussed in this section. Chapter 2, the literature study chapter, provides an in-depth discussion of the available sources of energy, energy storage mediums, system controllers and integration technologies. Also, various case studies are presented to research the practical application of each component. The information gathered in the literature study forms the basis of the research and is used extensively during the design phase.

Chapter 3 is a dedicated design chapter and consists of design specifications, requirements and assumptions. These are used to form a conceptual design which ultimately leads to a detailed design of the integrated system. The detail design includes component selection and compatibility checks for both the hardware and software design. Extensive use of mathematical software such as MATLAB® and CAD software such as Solidworks® is made. The design chapter describes the theoretical system that is simulated in Chapter 4.

Chapter 4 is the simulation chapter which consists of three simulation models that describes three scenarios. The simulation models are built using Simulink® modelling software. Each of the simulation models are simulated to represent a 24-hour cycle. The simulated scenarios are analysed and the results are summarised at the end of each simulation discussion. The results obtained from the simulation models are compared to the experimental results obtained in Chapter 5. This validates and verifies the accuracy of the simulation model to that of a real-world system.

Chapter 5 discusses the detailed implementation of the experimental test station, how the experimental system is tested and how the results are obtained. The experimental results are then analysed and combined to produce meaningful results which can be interpreted. The interpreted experimental results are then used to determine the technical and financial feasibility of the controlled microgrid system. The experimental results are also verified and validated to ensure that measurements were made correctly.

Chapter 6 is the closing chapter which summarises the literature, design, simulations and experimental results of the dissertation. This chapter also discusses recommendations and future work proposals that can be implemented to improve the performance of the residential microgrid. The validation and verification of the study is also summarised in this chapter and highlights the methods that were used validate and verify the study.

The appendices attached at the back of the dissertation includes written articles, a Turnit-In report to prove originality and a DVD which contains additional content relating to the study. These appendices are all supplementary to the main document and are frequently referenced to.

1.5 Publications and Peer Reviews

Throughout the study, a conscious effort was made to gather inputs from industry professionals on the research topic. This was done by participating at two conferences namely

the Afrikaans Youth Symposium as well as the International Conference on the Domestic Use of Energy. Both of these conferences yielded publications and presentations; the citations for each publication are shown below. Two additional articles were written to summarise the study and were submitted to the Journal of Energy in South Africa and the Journal of Energy Conversion and Management. Feedback on these articles has not yet been received. All of the articles are added in Appendix A for further reading.

- W.A. Bisschoff and R. Gouws, "Energy management system for a residential grid-tied micro-grid", in Proceedings of the Twenty Third Conference on the Domestic Use of Energy, Cape Town, South Africa: Cape Peninsula University of Technology, Apr. 2015, pp. 85–91, ISBN: 978-0-9922041-8-1.

  Article abstract:
  With the national power grid under tremendous pressure, there are enormous pressure exerted on residential electricity consumers to cut-back on electricity consumption to ensure a reliable supply. This has led to residential electricity users wanting to generate their own electricity through solar and wind systems, more formally known as distribution energy resources (DERs). The possibility of DERs currently exists within the centralised power grid, but is currently not well supported by Eskom and local municipalities. There are currently very little widely implemented policies regarding net-metering and feed-in tariff structures amongst Eskom and municipalities. Thus, excess generated energy fed into the grid is used elsewhere without any benefit going to the owner of the DER. By implementing an active energy management system (EMS) alongside the grid integrated system, electricity generated by the DER can be consumed locally by the residential loads. The EMS achieves an electricity consumption reduction of 23.4 % compared to a system with no EMS. Further results show that the EMS compensated system shows a cost saving of R19.17 per day which translates to a reduction of 51.4 % compared to a system with no EMS.

- W.A. Bisschoff and R. Gouws, "Ontwerp van ‘n energiebestuurstelsel vir optimale energie verbruik en effektiwiteit van ‘n distribusievlakmikrokragnetwerk", Studentesimposium in die Natuurwetenskappe, Pretoria, South Africa, Nov. 2014, pp. 21.

  Article abstract (Afrikaans):
  Onlangse persvrystellings en media aankondigings deur die Suid-Afrikaanse staatsbeheerde nutsmaatskappy, Eskom, dui daarop dat die nasionale kragnetwerk onder geweldige druk is. Daar word enorme druk deur residensiële- en industriële elektrisiteitsverbruikers uitgeoefen om betroubaarheid van ‘n stabiele kragnetwerk te verseker. Die moontlikheid van ‘n mikrokragnetwerk bestaan binne die huidige gesentraliseerdekragnetwerk, maar word tans nie baie goed ondersteun deur Eskom en streeksmunisipaliteite nie. Mikrokragnetwerke verwys na kragopwekking deur onafhanklike kragprodusente op distribusie- en transmissievlak. Mikrokragnetwerke kan as ‘n selfstandige-, kragnetwerkgeïntegreerde- of hibriedekragnetwerke opgestel word. Sodoende met hierdie topologieë kan die mikrokragnetwerk aanvullend wees tot die gesentraliseerdekragnetwerk. In eerstewêreldselande soos België en Switserland word mikrokragnetwerke baie goed ondersteun waarby die nutsmaatskappye oortollige gegenereerde elektrisiteit by die mikrokragnetwerk terugkoop. Dit is egter nie die geval in Suid-Arika nie en oortollige gegenereerde

elektrisiteit gaan verlore. 'n Residensiële energiebestuurstelsel kan die bogenoemde probleem oorkom deur aktiewe monitering en bestuur van die mikrokragnetwerk se inkomende- en uitgaande energie.

- W.A. Bisschoff and R. Gouws, "Experimental Energy Management System for Residential PV Systems in Non-feed-in Tariff Countries", Submitted to the Journal of Southern Africa (JESA) on 6 November 2015. ISSN: 1021-447X.

  Article abstract:
  Currently within South Africa and other developing countries, net-metering policies are not yet widely implemented which hinders the adoption of residential PV systems. Without proper net-metering policies in place, the benefits of residential PV systems are limited to self-consumption as all energy fed into the utility grid is lost without remuneration. This leads to an inefficient and non-profitable PV system. To improve the efficiency and feasibility of the PV system in countries with no feed-in policy, it is of utmost importance that an energy management system (EMS) that optimises self-consumption, of the generated energy, be employed. The EMS presented in this paper focusses on self-consumption and reducing the energy consumption off the utility grid. Experimental results obtained from a real-world system showed that the local energy consumption percentage increased by 15-20% when compared to a PV system with no EMS.

- W.A. Bisschoff and R. Gouws, "Practical considerations for controller selection in residential energy management systems: A review", Submitted to the Journal of Energy Conversion and Mangement on 13 November 2015. ISSN: 0196-8904.

  Article abstract:
  A review of the wide variety of system controllers available on the market along with the practical applicability of each is discussed in this paper. The system controllers that are discussed include programmable logic controllers, microcontrollers and single board computers. These controllers are generally not competing for the same market share however, some of the capabilities of these controllers overlap with one another which makes the selection of an appropriate system controller a complex decision. The practical considerations of controller selection are discussed in this article along with a practical example thereof. The practical example that was used to illustrate controller selection was a residential energy management system which would be installed alongside a grid-tied 2 kWp photovoltaic system. The aim of the energy management system is to ensure that all the photovoltaic generated energy is consumed locally within the residence and not fed into the distribution network. Such a system is applicable in areas where no net-metering policies are in place.

1.6 Conclusion

The introductory chapter was used to cover relevant background theory on microgrids and how it fits into the modern power system. The identified problem was described in terms of an economic and technical aspect which clearly defined the purpose of the research. The research methodology section exhibited the requirements to complete the study on a scientific level. By following the research methodology described above, it was possible

to introduce a conceptual design of the microgrid and EMS (shown in later chapters). Section 1.5 illustrated that the content of the dissertation was submitted to international conferences and journals to obtain as much feedback from field experts as possible.

The purpose of research gave insight into the content that needs to be covered in the literature study. The literature study covered in Chapter 2 covers theoretical background knowledge, candidate technology and case studies of similar projects. An overview of the key topics that is discussed in the literature study is shown in figure 2-1. The structure of the dissertation that is followed is shown below.

Chapter 1: Introduction

Chapter 2: Literature Study

Chapter 3: Design

Chapter 4: Simulations

Chapter 5: Construction, Assembly and Testing

Chapter 6: Conclusion and Recommendations

Appendix A: Publications and Peer Reviews

Appendix B: Turnit-In Report

Appendix C: DVD Content

Chapter 2: Literature Study

2.1 Introduction

This chapter contains the necessary research on the components and technologies that were required for the study. The literature study presents information regarding the required components and applicable case studies that hosted similar characteristics of residential EMSs. A simplified block diagram illustrating the content that is covered in the literature study is shown in figure 2-1. A complex functional block diagram that illustrates the interrelationship between the contents of the literature study is shown in figure 2-2.

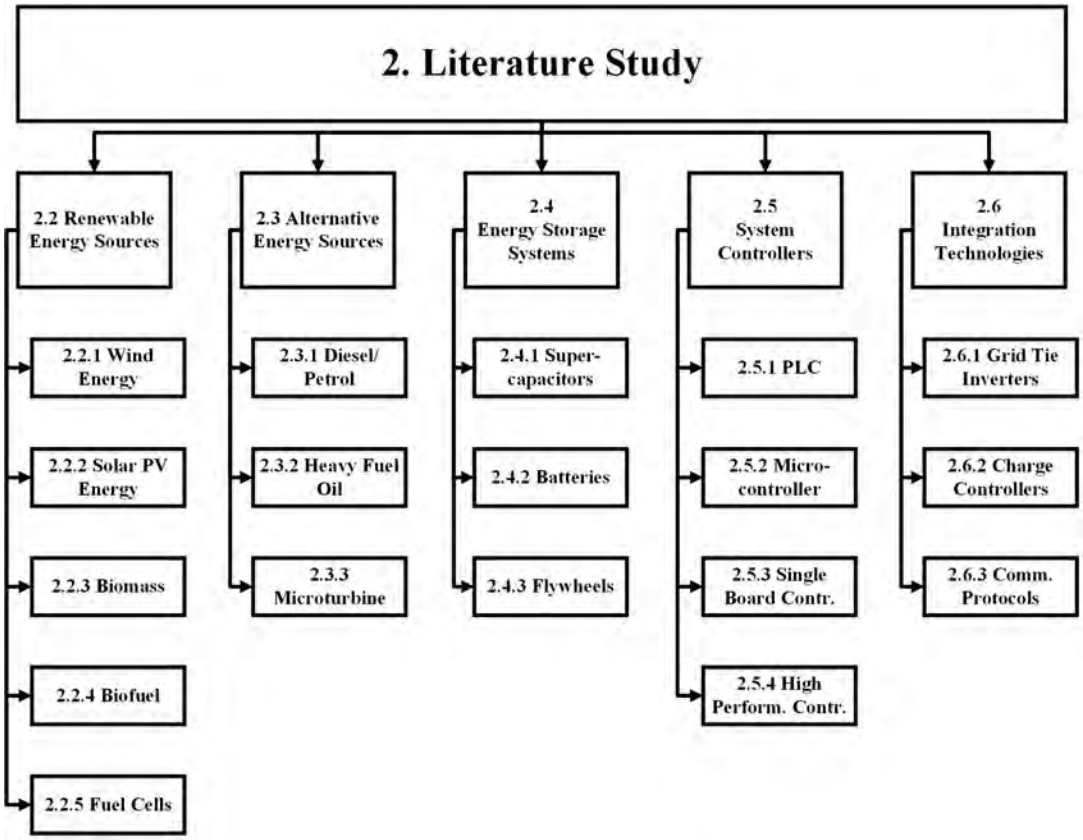

Figure 2-1: Literature study overview

2.2 Renewable Energy Sources

As mentioned in the introductory chapter, distributed energy generation refers to local electricity generation on the LV distribution network (230/400 V). From figure 2-3, an overhead summary of a power system is shown to indicate the generation, transmission and distribution networks associated with a centralised power system [29]. Therefore, the focus of DERs lie within the distribution network and is discussed accordingly.

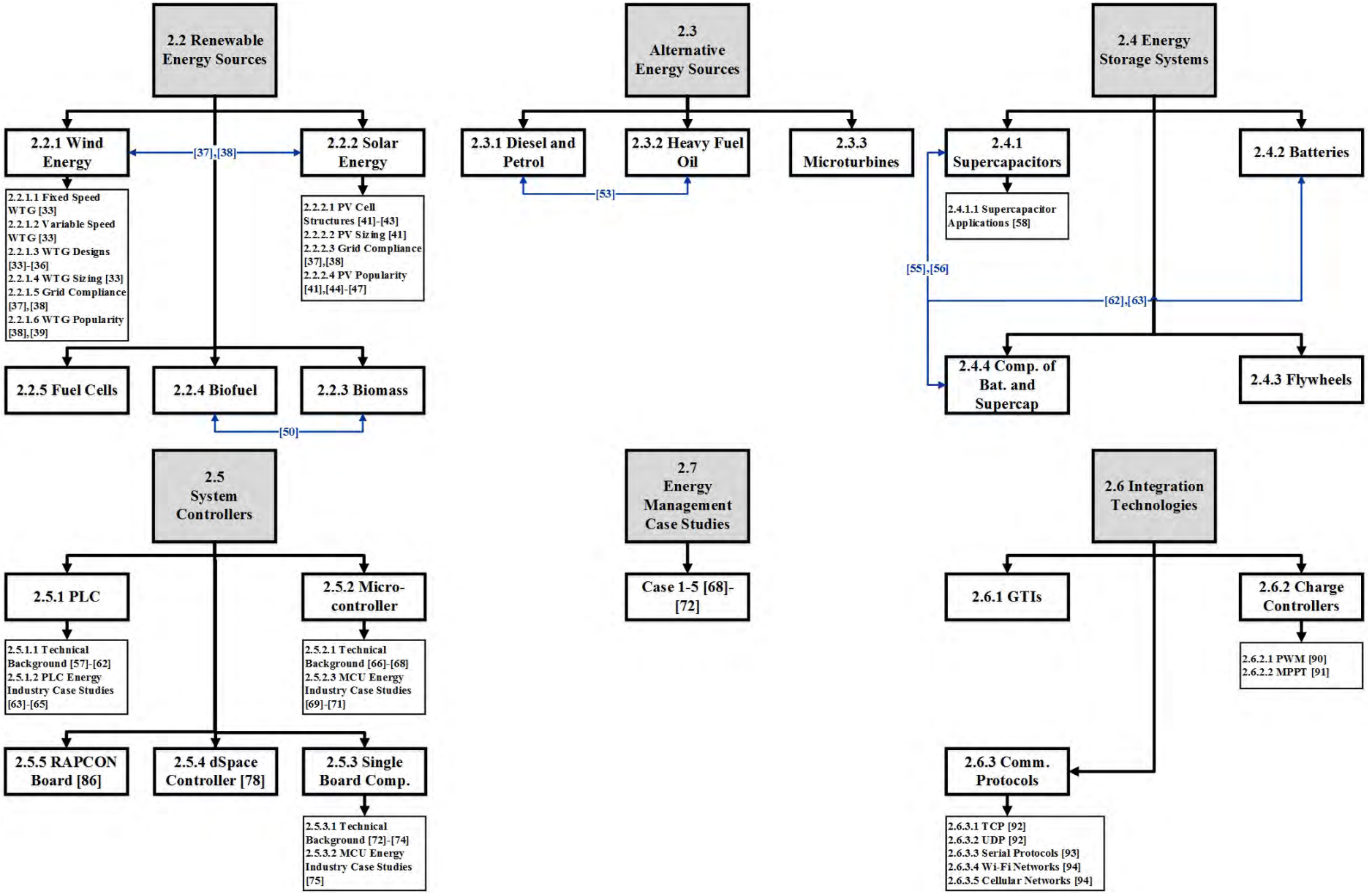

Figure 2-2: Literature study overview

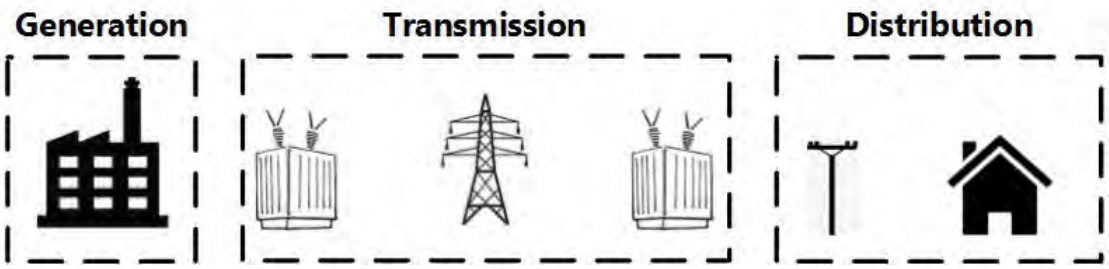

Figure 2-3: Power system network [29]

A general agreement amongst governments across the globe have been reached that confirms that fossil fuels are limited and also one of the main contributors toward global climate change. According to Brown (2012), Delucchi and Jacobson (2013), the world's energy need can be met entirely with just wind, water and solar power [18], [30]. However, according to Smil (2014) and Trainer (2013), the world cannot be powered solely by renewable energy sources [31], [32]. However, a broad-based implementation of renewable energy sources can greatly reduce the dependency on fossil fuels according to sources Smil (2014) and Trainer (2013) [31], [32].

Figure 2-4 illustrates the applicable sources of energy that is discussed in the following section. It should be noted that the shaded blocks shown in figure 2-4 represent content beyond the scope of the study; reasons relating to this is also discussed in the sections that follow.

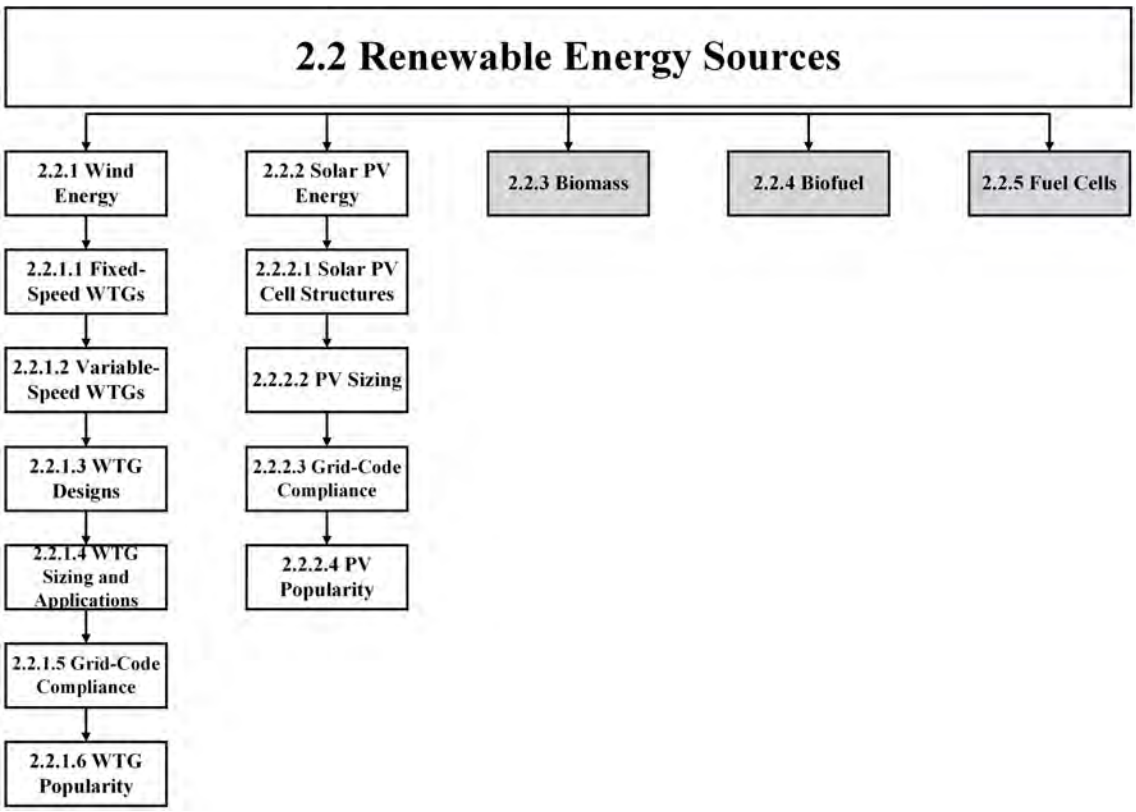

Figure 2-4: Literature study content on renewable energy sources

2.2.1 Wind Energy

A wind turbine generator (WTG) is a piece of equipment that harnesses the power of wind to capture its energy and convert it into electricity. The basic components include the blades, low-speed shaft, gearbox and high-speed shaft which is connected to the generator. These are components housed inside the WTG nacelle and enables electricity generation; a descriptive figure illustrating the main components of a WTG is shown below [33].

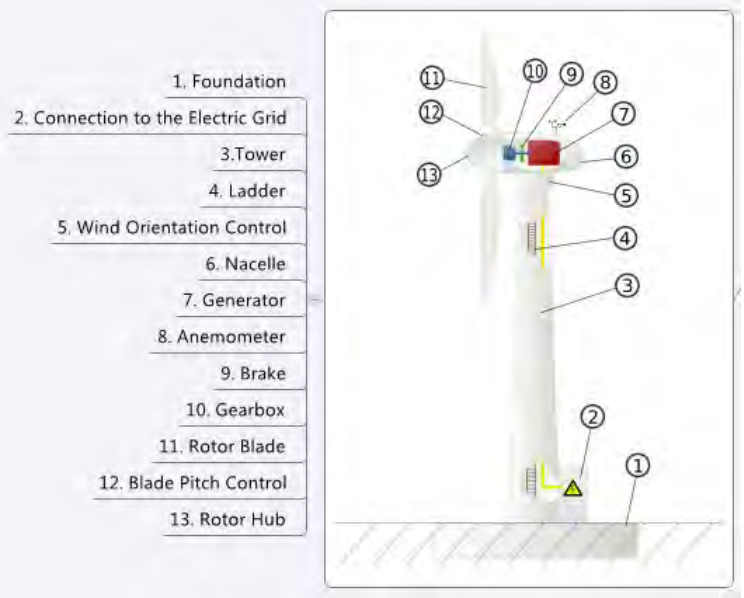

Figure 2-5: Wind turbine generator [33]

A WTG generates electricity as wind passes through the blades and generates lift which exerts a rotational force. The blades of the WTG are connected to the low-speed shaft inside the nacelle which is fed into a step-up gearbox. The high-speed shaft is connected to the output side of the step-up gearbox which is fed to the generator. The step-up gearbox increases the speed of the low-speed shaft such that the high-speed shaft rotates at a speed suitable for efficient electricity generation. The power output from the generator is fed to a transformer which steps up the voltage to an appropriate voltage for power transmission [33]. Figure 2-6 illustrates this description above and shows the internal components of the nacelle.

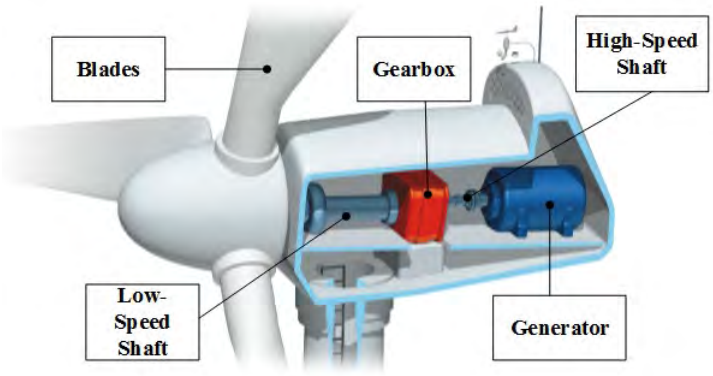

Figure 2-6: Overview of nacelle contents [33]

As the demand for more wind energy increased, various WTG architectures were introduced into the market. These architectures are divided into two groups namely fixed and variable-speed WTGs.

2.2.1.1 Fixed-Speed WTGs

Fixed-speed WTGs are some of the first turbines used in the generation of electricity through wind. A squirrel-cage induction machine is operated as a generator with varying slip to have a fixed rotor speed and constant power output. The squirrel-cage induction generator absorbs reactive power and it is therefore necessary to connect power factor correction (PFC) capacitors to the output. These capacitors are switched in/out accordingly to allow power generation at unity power factor [33]. Figure 2-7 shows a schematic diagram of a fixed-speed WTG [33]. A soft-starter is included in the diagram which is used to slowly build up magnetic flux to limit excessive transient currents during the energising of the generator.

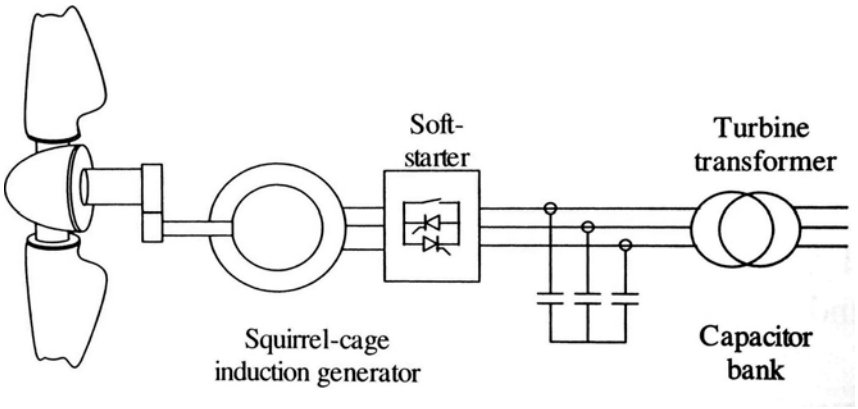

Figure 2-7: Fixed-speed WTG [33]

2.2.1.2 Variable-Speed WTGs

Variable-speed WTGs have emerged into the market to accompany the addition of large-sized WTGs to the grid. There are various grid code requirements that must be adhered to for a grid-tied WTG and the introduction of variable-speed WTGs simplified the conformance to grid codes. Variable-speed configurations are commonly in the form of a doubly fed induction generators (DFIG) or a fully rated converter (FRC) with a synchronous/induction generator [33].

DFIG Turbines

A DFIG turbine contains a wound-rotor induction generator and a bi-directional power converter to receive or send current from/to the rotor winding. The bi-directional converter acts as a voltage source converter (VSC) to control the voltage fed into the rotor winding and permits variable-speed operation. An advantage of a DFIG system is that power can be delivered through the stator and the rotor. As an example, when the generator is operating above the synchronous speed, power is delivered to the grid through the stator and the rotor via the bi-directional converter. Whenever the rotational speed drops below the synchronous speed, power is absorbed by the rotor through the converter [33]. Figure 2-8 illustrates a schematic diagram of a DFIG turbine [33].

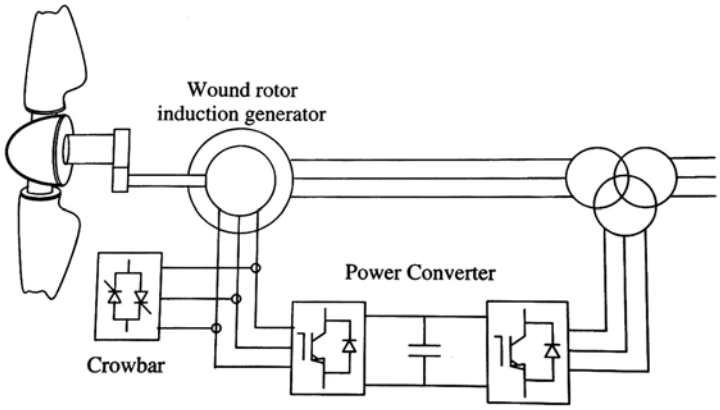

Figure 2-8: DFIG turbine [33]

FRC Turbines

Due to the output of the generator being isolated from the power grid, FRC turbines are very flexible in a sense that various types of generators such as induction, synchronous and permanent magnet may be used. The output terminals of the generator are fed to a power converter which rectifies the output and inverts the rectified signal which conforms to the grid codes. This way variable speed operation is achieved by the turbine [33]. A schematic diagram of a typical FRC turbine is shown in figure 2-9 [33].

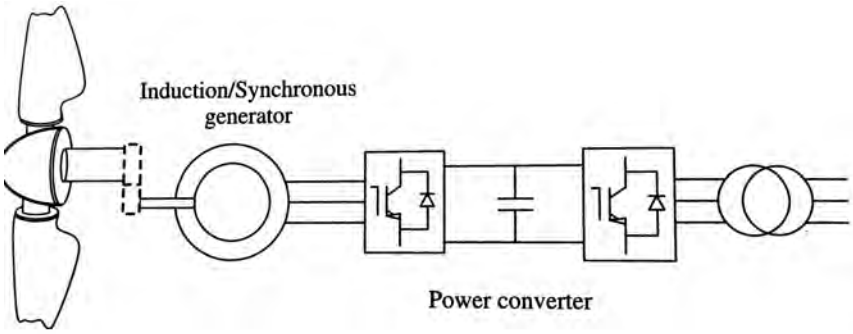

Figure 2-9: FRC turbine [33]

2.2.1.3 WTG Designs

WTGs come in various shapes and sizes with each having a unique application. There are two types of structural designs associated with WTGs namely horizontal and vertical axis. Horizontal axis WTGs hosts all of the equipment in the nacelle on top of the tower which must be directed face-on into the wind. These designs are preferred for large-sized WTGs as higher towers can be constructed to achieve higher power generation capacity. Horizontal axis turbines employ a Darrieus design which is a high-tech airfoil design that operates on the same principle as lifting force of an aeroplane wing. Horizontal axis designs achieve the highest efficiencies with an overall efficiency ranging from 40-45% [34].

The opposite is true for vertical axis turbines as the rotor shaft is vertically aligned and most of the equipment is installed at ground level. The advantage of this design over horizontal axis WTGs are that the equipment is more accessible which simplifies maintenance. Vertical axis designs are preferred where the turbine is constructed on top of a building. Buildings tend to redirect wind over the top of the building which is better

swept up by vertical axis blades.

Generally there are two types of vertical axis turbine designs, the Savonius and Darrieus rotor designs. The Savonius design operates in a similar manner than an anemometer with an efficiency ranging from 5-10%. The Darrieus design for vertical axis turbines are less efficient than the horizontal axis design [34]. This is due to the swept area of a horizontal axis turbine always faces into the wind creating more lift with all of the blades. The opposite is true for vertical axis turbines' where the blades are faced perpendicular to the wind which allows only a part of the swept area to generate lift. This leads to an overall efficiency ranging from 25-35% [34]. A visual illustration of the various WTG designs is shown in figure 2-10 [35], [36].

(a) Darrieus H. turbine

(b) Darrieus V. turbine

(c) Savonius turbine

Figure 2-10: Different WTG designs [35], [36]

2.2.1.4 WTG Sizing and Applications

WTGs are classified as small, intermediate and large relating to the rated power output. Small WTGs are classified as turbines having a power output rating of less than 10 kW, intermediate WTGs are rated between 10 and 500 kW and large WTGs have a power rating greater than 500 kW [33]. Table 2-1 summarises the capacities associated with various applications [33].

Table 2-1: Wind turbine applications according to size

Small (<10kW)	**Intermediate (10-500 kW)**	**Large (>500 kW)**
-Urban and rural residence -Agricultural -Remote location powering	-Powering small villages -Hybrid power systems -Distributed generation	-Commercial wind farms -Off-shore wind farms

2.2.1.5 Complying with Grid Codes

According to National Energy Regulator of South Africa (NERSA) (2014) connecting any source of renewable energy generation equipment in a power plant configuration which feeds into the national electricity grid, several technical requirements and standards must be met [37]. According to NERSA (2014), all renewable energy power plants are classi-

fied into three categories according to size [37]. A summary of the categories are shown below [37].

1. **Category A: 0 - 1 MVA**

   This category permits a connection to the low voltage (LV) network with a power rating of less than 1 MVA. This category is sub-categorised into three power levels:

   [A1] 0 - 13.8 kVA

   [A2] 13.8 - 100 kVA

   [A3] 100 kVA - 1 MVA

2. **Category B: 1 - 20 MVA**

   This category permits a connection to the medium voltage (MV) network with a power rating between 1 and 20 MVA.

3. **Category C: 20 MVA or higher**

   This category permits a connection to the medium/high voltage (MV or HV) network with a power rating greater than 20 MVA.

However, to connect a wind energy facility (WEF) to the national electricity grid, the WTG shall adhere to all the requirements as set out in the International Electrotechnical Commission' (IEC) Technical Specification Series, TS-61400 and adhere to the "*South African national grid for Wind Turbines connected to Distribution or Transmission Systems*" [38]. The technical requirements and standards for integrating a WEF at a point of common coupling (PCC) is compiled by NERSA and discussed below [37], [38].

Frequency Requirements
Whenever the WEF is in operation, it must adhere to the frequency profiles as shown in figures 2-11 and 2-12 [38]. The rules associated with the frequency profiles are discussed below.

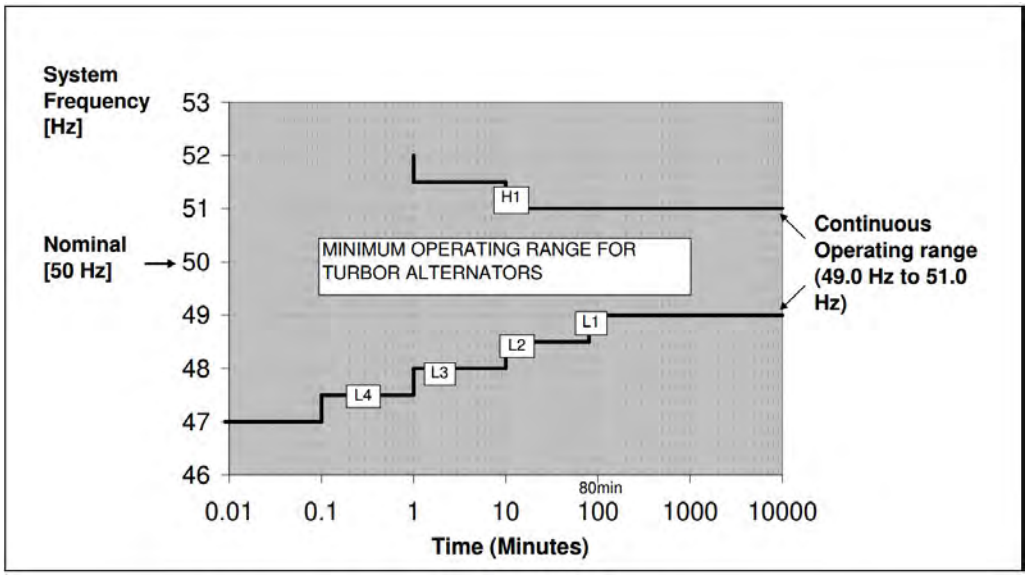

Figure 2-11: Minimum frequency operating range of WEF (Cumulative over lifespan of WEF) [37]

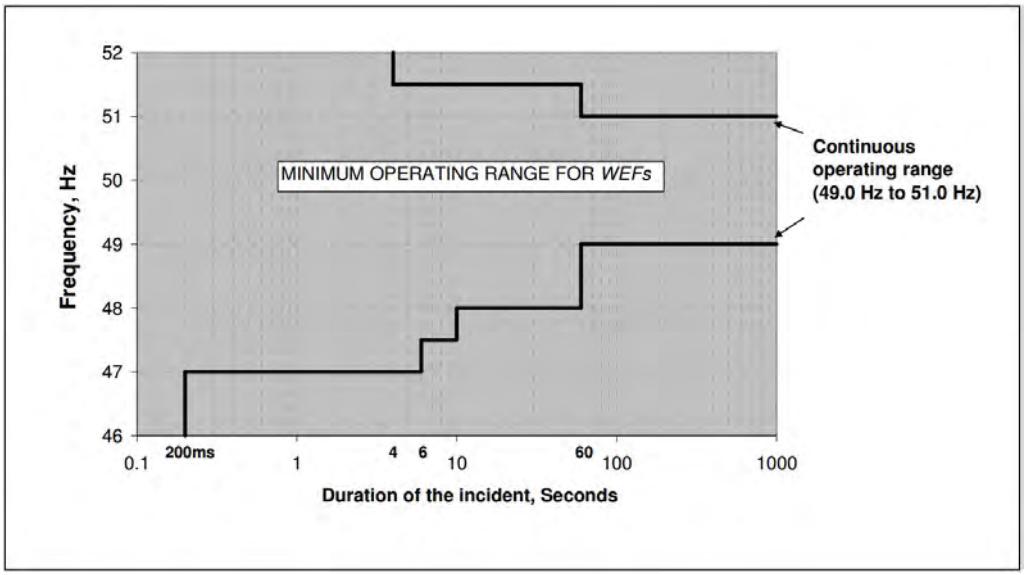

Figure 2-12: Minimum frequency operating range of WEF (During a system frequency disturbance) [37]

The following rules apply for the operation of the WEF [38]:

1. Individual tripping of WTGs should commence as soon as the turbine operates outside the defined ranges and according to the tripping philosophy set up by the system operator.

2. The WEF should remain connected to the distribution or transmission network for a falling (not rising) rate of frequency change of 0.5 Hz per second, provided that the system frequency is still within the continuous frequency characteristic.

3. A frequency response system should be included in the WEF that should match the profile of the power-frequency response curve shown in figure 2-13 [38].

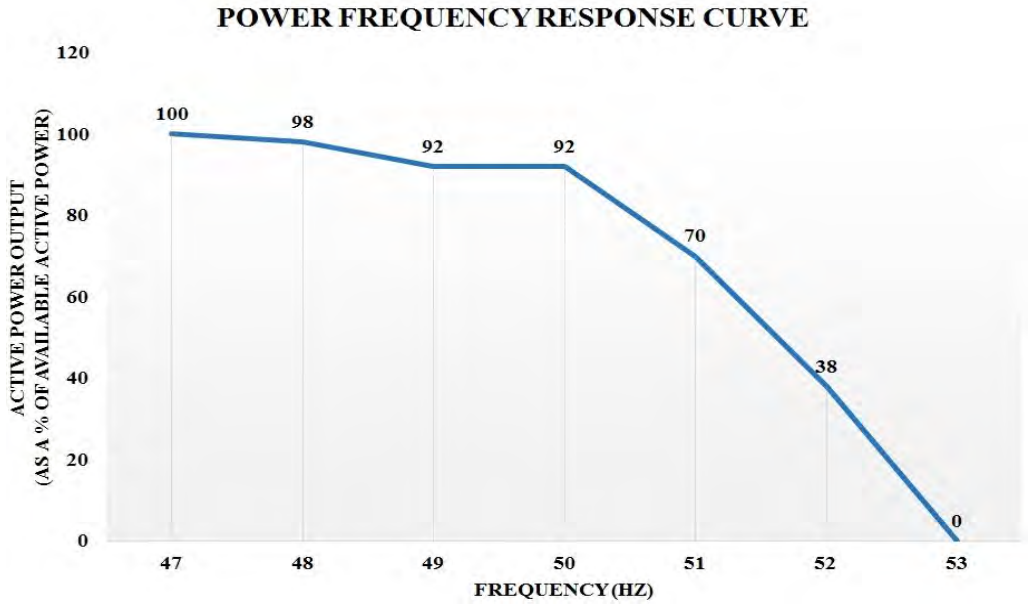

Figure 2-13: Power-frequency response curve [38]

For the frequency response system further requirements should be implemented as discussed below [38]:

1. A frequency dead-band setting capable of being manually set to between 0 and 0.5 Hz on each WEF. The setting shall be set according to the Grid Code.

2. Under continuous operating frequency (49.5 to 50.5 Hz), the WEF should be able to deliver power of at least 95% of the available active power.

3. If the frequency rises above the 50.5 Hz mark, the WEF should reduce power output to the output shown in figure 2-13. The reduction should be in the order of 1% of rated capacity per second [38].

Voltage Requirements
In a similar manner as the frequency requirements, there are voltage requirements that must be adhered to at the PCC. These requirements are listed and discussed below [38].

1. Voltage quality distortion levels outputted by the WEF should not exceed the levels supplied by the local distributor and NERSA.

2. The WEF should contain a closed-loop control system which constantly monitors and adjusts the voltage at the PCC. A manual adjustable telemetered set-point should also be included which can be adjusted within 90% to 110% of the nominal voltage at the PCC.

3. The maximum permissable voltage change at the PCC once a switching operation have been performed should not exceed 2%.

Power Factor Requirements
For WEFs rated less than 20 MW, a constant supply of reactive power output should incur a power factor less than 0.975 lagging or leading at the PCC. For WEFs greater than 20 MW, the power factor should not be less than 0.95 lagging or leading at the PCC. Also, no WEF should consume reactive power from the PCC to allow the WEF to start up [38].

2.2.1.6 WTG Popularity

Wind energy are becoming one of the most popular forms of electricity generation globally with an annual increase of 25-30% over the last decade [18]. The most attractive advantages of wind generation is that there are no fuel costs associated with the electricity generation process and wind is an undepletable source of energy. The popularity growth of wind energy are not only limited to large scale wind farms but also to smaller scale plants. These smaller scale plants are typically implemented by commercial and residential customers that are exploring self-generation possibilities. Figure 2-14 shows the growth of wind energy generation since the year 2000 [39]. Since the beginning of 2000, the installed wind energy capacity has grown from 17 400 MW to nearly 290 000 MW (2012). This translates to a growth percentage in excess of 1600% since 2000.

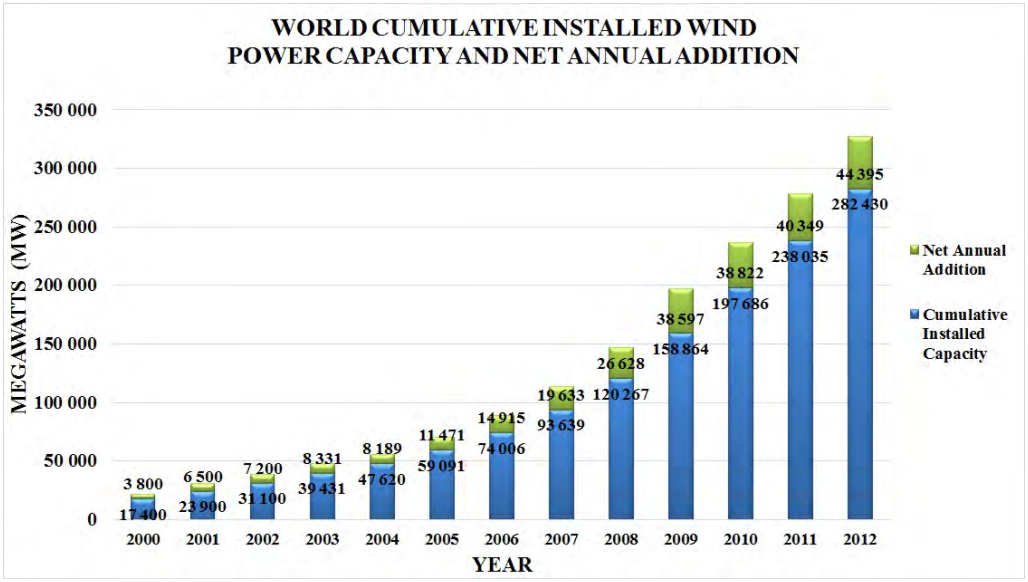

Figure 2-14: Total wind generation installed capacity [39]

From the statistics shown above, electricity generation from wind has increased significantly over the past 15 years. A map illustrating the mean wind speed across the world is shown in figure 2-15 [40]. The measurements are made at 80m above ground level.

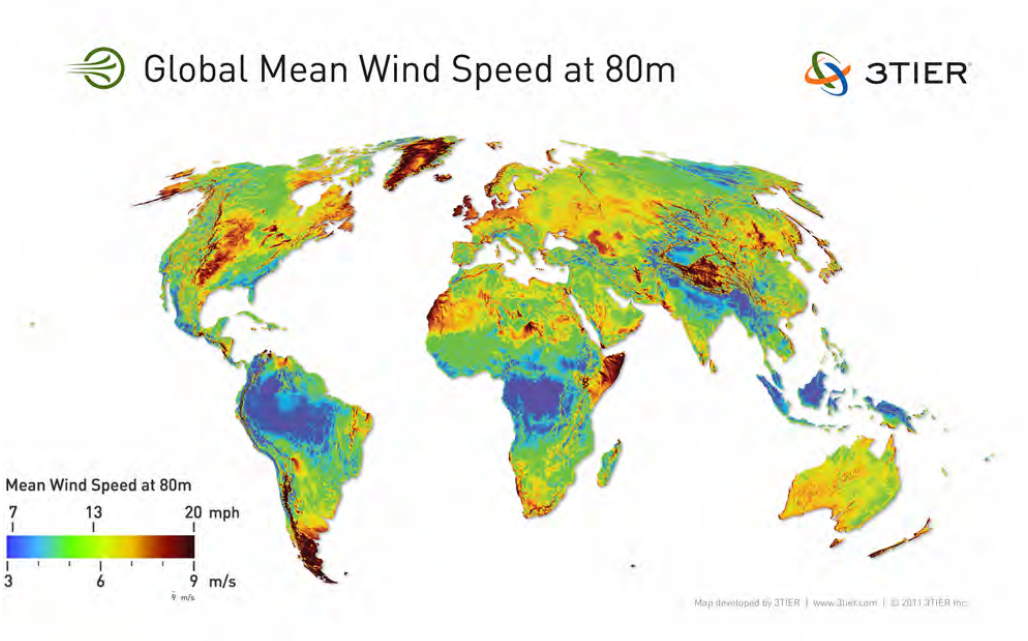

Figure 2-15: Global mean wind speed [40]

In a similar fashion as the global map shown above, specific wind speed data can be obtained for Southern Africa. A map illustrating South African specific data is shown in figure 2-16 [40]. From figure 2-16 it is evident that the wind speeds in South Africa are average to above average in comparison with the rest of the world. The coastal regions are especially wind rich which permits a feasible solution for WTG installations.

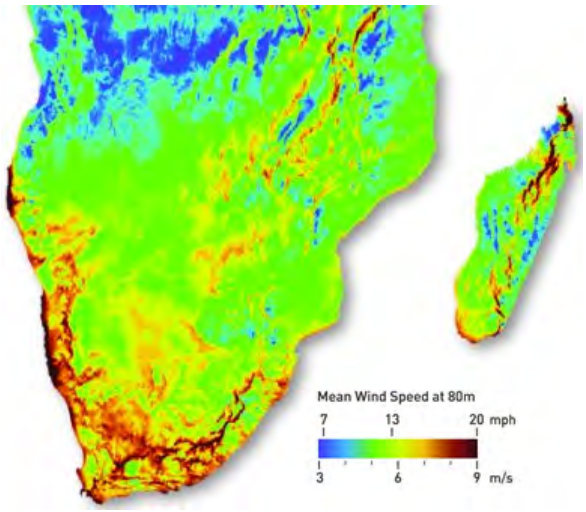

Figure 2-16: Southern Africa mean wind speed [40]

2.2.2 Solar Photovoltaic Energy

A solar photovoltaic (PV) cell is a semiconductor device, such as silicon, which relies on the photoelectric effect (the ability to emit electrons when light shines on it) to free up electrons in the semiconductor material. Once these electrons are freed, an electrical imbalance must be created within the cell to enable electric current to flow. This is done by stacking an n- and p-type structure onto each other which permits the flow of electric current [41]. A module of multiple cells are electrically connected and built onto a frame to create a single solar PV panel.

2.2.2.1 Solar PV Cell Structures

The are many different solar PV cell structures available on the market but generally boils down to two types, monocrystalline and polycrystalline. As the name implies, monocrystalline cells are manufactured from only one silicon ingots which are cylindrical in shape. The manufacturing process of monocrystalline cells are more advanced than that of polycrystalline cells and therefore increases the cost considerably. The polycrystalline manufacturing process is simpler as raw silicon is melted and poured into a square mould, cooled down and cut into square wafers [41].

Monocrystalline solar PV cells have a higher conversion efficiency than polycrystalline cells as the highest quality silicone is used to manufacture these cells. The efficiency of monocrystalline solar PV cells vary between 15% to 20% as opposed to the polycrystalline cells' range of 13% to 16%. This characteristic causes the monocrystalline cells to be more expensive than the polycrystalline cells. Monocrystalline cells can be identified by a single dark coloured cell with rounded edges and polycrystalline cells by its bright blue colour and rectangular shape [41]; figure 2-17 shows mono and polycrystalline cells next to each other [42], [43].

2.2.2.2 Solar PV Sizing

The capacity sizing of any solar PV system is a critically important factor to consider when installing such a system. Installing an oversized/undersized solar PV system may

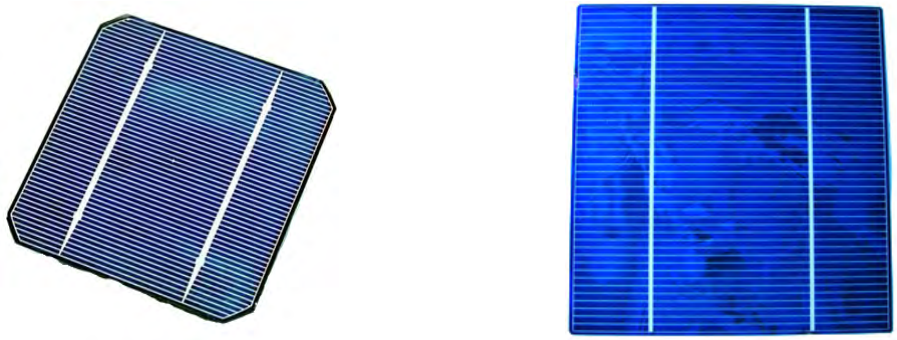

(a) Monocrystalline solar PV cell (b) Polycrystalline solar PV cell

Figure 2-17: Solar PV cell structures [42], [43]

lead to unreliable supply or excessive initial costs. To successfully size a solar PV system the following factors should be taken into account [41]:

- Solar radiation data for the site

  Radiation data for specific sites are based on global irradiation data on a horizontal surface. Global irradiation data can be converted to information relating to the radiation level usable by a solar PV panel; this rating is expressed in kWh/m^2.

- Electrical load profile

  The load data provides insight into the amount of energy that is required to power all the loads during certain periods throughout the day.

- Importance of continuous supply (standalone only)

  In cases where the site is very remote without a possible grid connection, continuous supply of energy is of utmost importance and the necessary capacity adjustments, such as larger capacity, should be made.

2.2.2.3 Complying with Grid Codes

In a similar fashion as with the WEF, connecting a LV solar energy facility (SEF) to the national electricity grid requires adherence to the specification set out in the national grid code [37]. The technical requirements and standards for integrating a SEF at a point of common coupling (PCC) is compiled by NERSA and discussed below.

Frequency Requirements
The frequency requirements of SEFs are very similar to those discussed with WEFs and similar graphs applies to SEFs; figures 2-18 and 2-19 illustrates the frequency profiles that should be adhered to [37].

1. If the frequency of the SEF is greater than 52 Hz for longer than 4 seconds, the SEF should disconnect from the grid.

2. If the frequency of the SEF is less than 47 Hz for long than 200 milliseconds, the SEF should disconnect from the grid.

3. The SEF should remain connected to the distribution or transmission network for a falling (not rising) rate of frequency change of 1.5 Hz per second, provided that the system frequency is still within the continuous frequency characteristic.

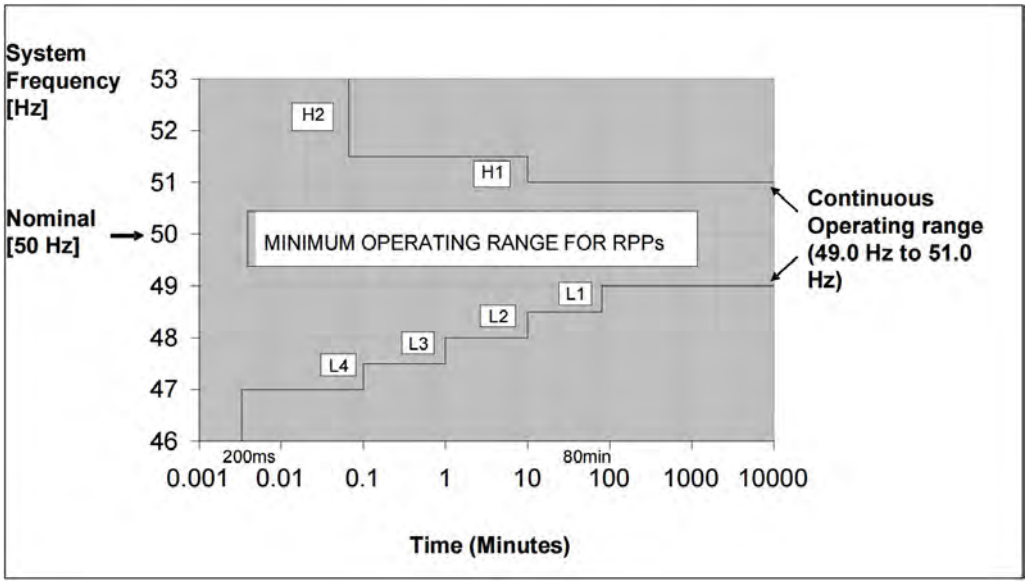

Figure 2-18: Minimum frequency operating range of RPP (Cumulative over lifespan) [37]

4. For continuous operation, the frequency should vary between 49 and 51 Hz.
5. A frequency response system should be included in the SEF that should match the profile of the power-frequency response curve shown in figure 2-20 [37].
6. During higher than normal frequency operating conditions, a reduction in active power should be implemented to stabilise the frequency according to the profile shown in figure 2-20.
7. If the frequency rises above the 50.5 Hz mark, the WEF should reduce power output to the output shown in figure 2-20.
8. If the frequency of the SEF exceeds 52 Hz for more than 4 seconds, the SEF should be disconnected from the grid.

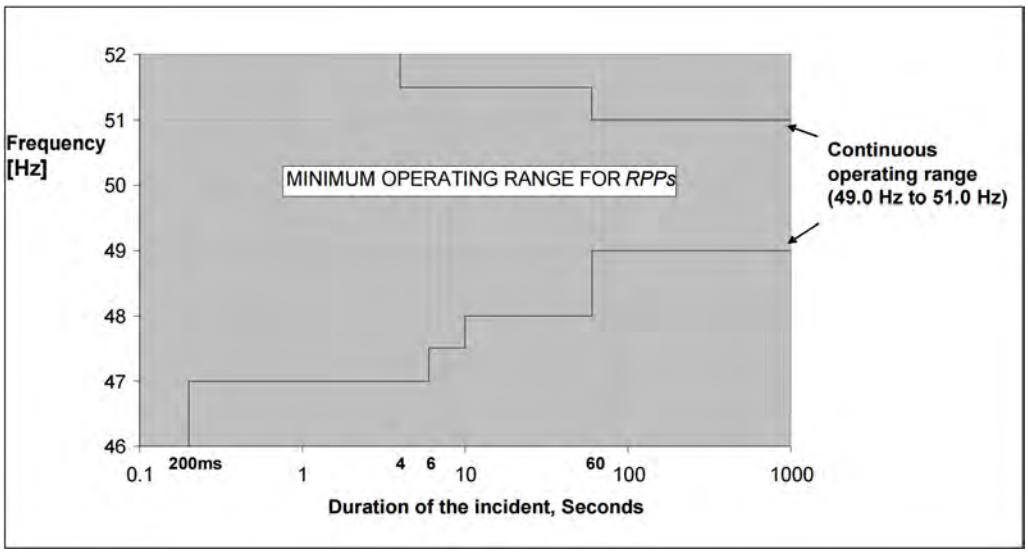

Figure 2-19: Minimum frequency operating range of RPP (During a system frequency disturbance) [37]

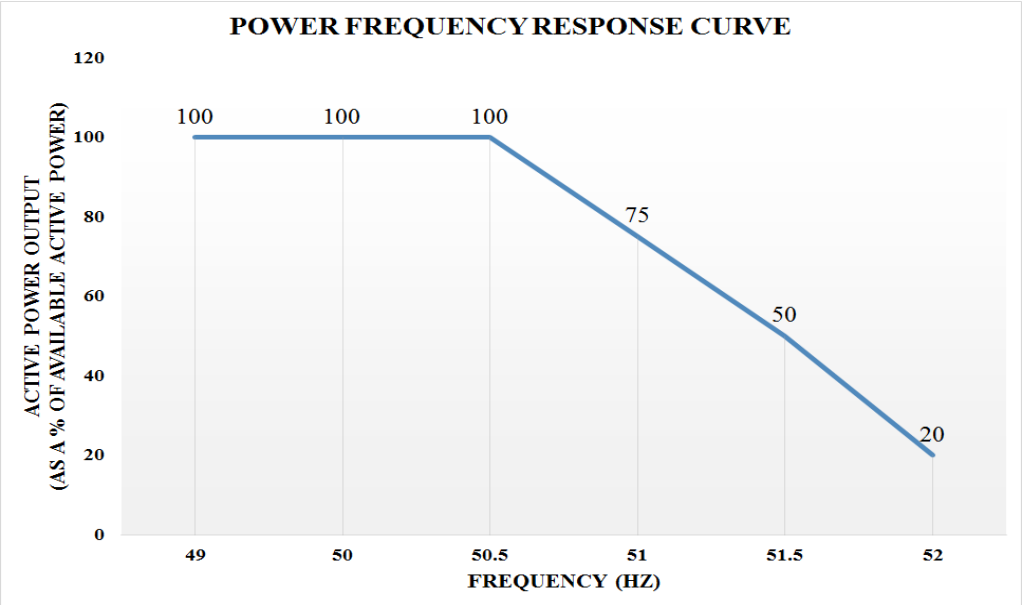

Figure 2-20: Power-frequency response curve [37]

Voltage Requirements

There are standards and requirements set-out for both normal and abnormal operating conditions of the SEFs. In case of abnormal operation, different requirements must be met than with normal operating conditions. The voltage requirements as set-out in "*Grid Connection Code for Renewable Power Plants (RPPs) Connected to the Electricity Transmission System (TS) or the Distribution System (DS) in South Africa*" describes the difference between normal and abnormal operation and each of the requirements associated with each state [37]; these requirements are listed below.

1. The SEF should be able to operate at a voltage -15% to +10% of the nominal voltage at the PCC.

2. In case of a sudden voltage drop/increase which extends beyond the abovementioned range, figure 2-21 applies and the maximum disconnection time must be adhered to as listed in table 2-2 [37].

Table 2-2: Maximum disconnection times for RPPs [37]

Voltage Range at POC	**Maximum Trip Time (s)**
V < 50%	0.2
50% < V < 85%	2
85% < V < 110%	Continuous Operation
110% < V < 120%	2
V > 120%	0.16

Power Factor Requirements

For SEFs rated less than 1 MVA, a constant supply of active power output should incur a power factor of no less than 0.95 lagging or leading at the PCC. This should be available from 20% of rated power [37]. The default power factor should be set at unity.

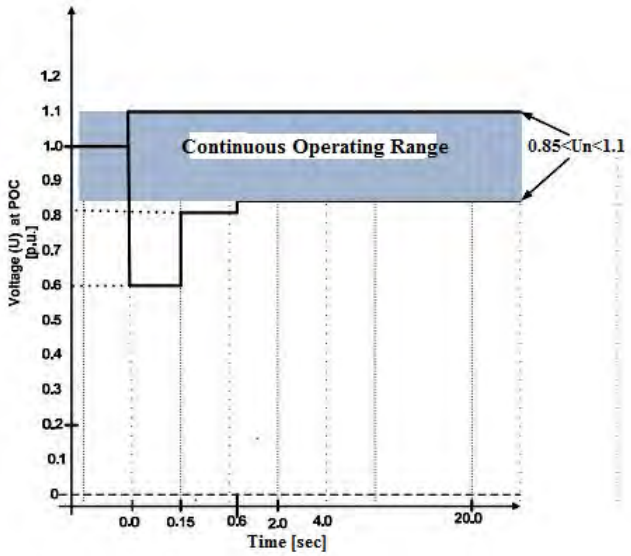

Figure 2-21: Voltage ride through capability for the RPPs of category A-1 [37]

2.2.2.4 Solar PV Popularity

In a similar fashion than with WTGs, a rapid growth rate in the installation of solar PV systems and plants has been seen over the past 15 years. Annual global growth rates of 25-40% have been seen over the past 15 years which signifies the worldwide expansion of solar PV generation [44]. The annual growth of solar PV installations are shown in figure 2-22 [44].

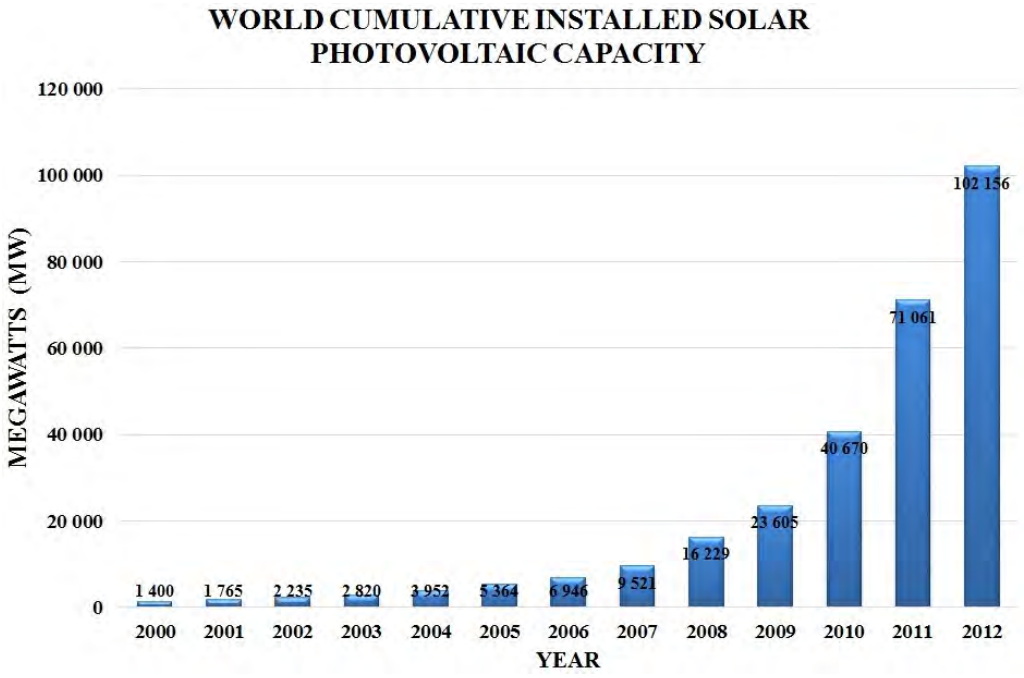

Figure 2-22: Total PV generation installed capacity [44]

Solar PV plants and small solar PV generation systems are fast becoming the preferred method of power generation over conventional coal-fired power stations as this source of energy can be erected in a short time and in any area with a fair bit of solar irradiation.

According to Markvart (2004), the solar irradiation level is the most important factor that determines the capable power output of a solar PV cell [41]. Solar irradiation levels vary greatly around the world but from the solar irradiation map shown in figure 2-23, it is evident that the desert like regions are the best locations to install solar PV cells as an energy source [45].

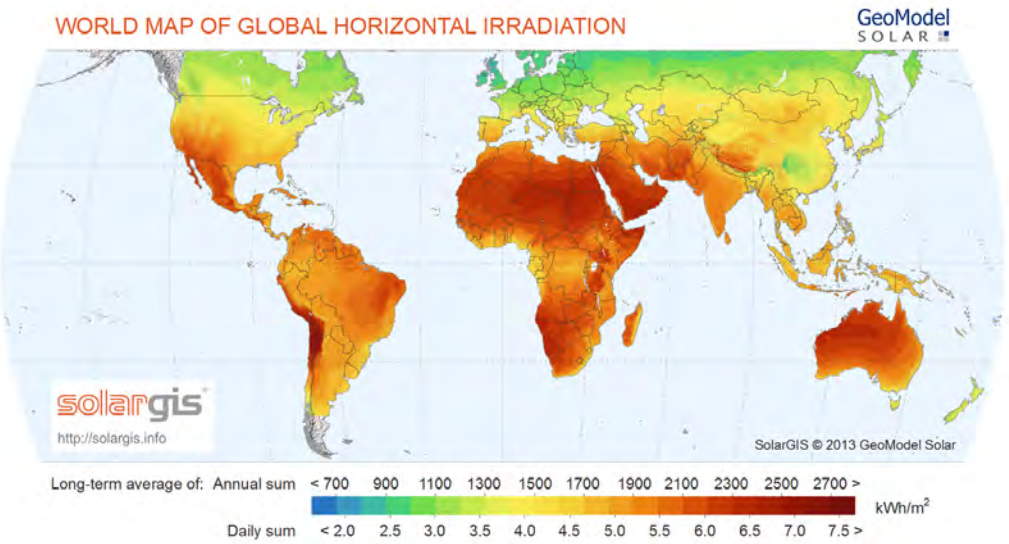

Figure 2-23: Map showing solar radiation levels across the world [45]

From the world map shown above, it can clearly be seen that Southern Africa has some of the highest solar irradiation levels in the world; this feature makes Southern Africa a prime location to benefit from solar PV energy generation. A map showing the solar irradiation levels in Southern Africa is shown in figure 2-24 [46].

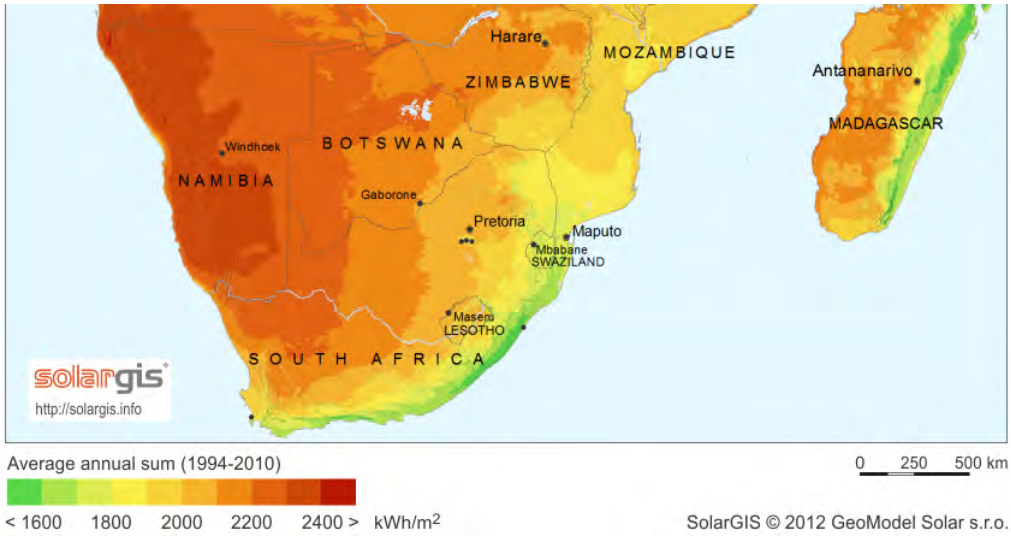

Figure 2-24: Map showing solar radiation levels in Southern Africa [46]

Up until 2010 the South African solar PV industry consisted of nothing more than a few small scale off-grid installations situated in the rural areas of the country. An initiative led by the South African Department of Energy to financially support the construction of large scale solar PV plants led to several companies stepping forward to erect these plants.

The construction of 18 large scale PV plants commenced in 2013 and upon completion a capacity of 630 MW is expected to be added to the national grid [47].

2.2.3 Biomass

Biomass is one of the oldest forms of renewable energy which captures the energy of the sun through the process of photosynthesis. Chlorophyll, a molecule contained in plants, captures the sun's energy by decomposing carbon dioxide into carbohydrates. Carbohydrates are complex chemical compound consisting of carbon (C), hydrogen (H) and oxygen (O) [48]. Once carbohydrates are heated to a certain extent, the captured carbon, hydrogen and oxygen are released in the form of carbon dioxide and water. This releases the energy captured from the sun during the photosynthesis phase. Examples of biomass sources are energy crops, crop residues, forest residues and municipal/industrial waste.

There are two ways of converting biomass into biopower namely direct combustion or gasification [48]. Direct combustion refers to the age-old principle of burning biomass and producing heat. This heat is used to heat water to produce steam. In turn, the steam is fed to a turbine which is connected to a generator. The process of gasification is a modern way of processing biomass to produce synthetic gas (syngas) [48]. Syngas is created by controlling the amount of oxygen during the burning process and consists of a mixture of hydrogen and carbon monoxide. The electricity generation process using syngas is very similar to the direct combustion process, with the only difference being the burning process [48]. The use of biomass to generate electricity is a complex process which requires a great deal of maintenance and supervision. This in turn steeply increases the initial investment and running costs for such a system. Another drawback of such a system is that it is a bulky system which requires a large area [49]. Hence, this causes the use of biomass to fall beyond the scope of the study.

2.2.4 Biofuel

Biomass and biofuel are closely related with the difference being that biofuel is a processed form of biomass. As mentioned above, syngas is produced by the gasification of biomass [49]. Syngas is one form of processed biofuel. Two other forms of biofuel are biodiesel and bioethanol. Biodiesel is produced through the extraction of oils from plants and mixing it with a small portion of regular diesel (usually 15%) [49]. Bioethenal is produced through the process of fermentation and is also mixed with regular gasoline to produce a cleaner form of fuel [49], [50]. As previously mentioned, the process to produce electricity from biofuel or biomass is a very complex process which increases costs considerably. Therefore, the use of biofuel falls beyond the scope of this study.

2.2.5 Fuel Cells

Fuel cells are electrochemical devices that combine fuel and oxygen to produce electric energy, heat and water as a by-product. The electrochemical process is non-combustive and highly efficient compared to the traditional heat engine [51]. Similar to a battery, a fuel cell employs both an anode and cathode with an electrolyte. The performance of a fuel cell is driven by the electrolytic composition which ultimately determines the design of the fuel cell. An overview of the electricity generation process for a fuel cell is shown in figure 2-25 [51].

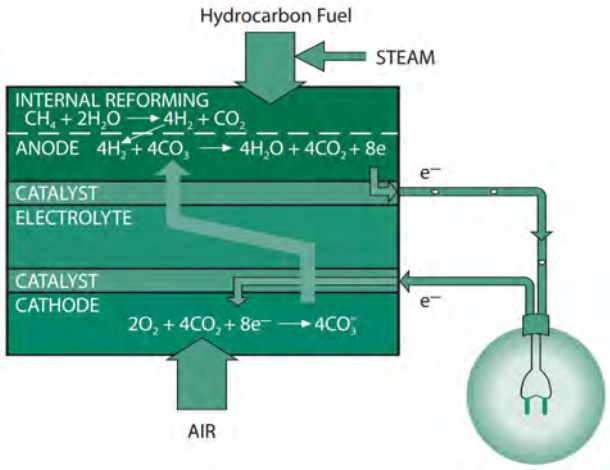

Figure 2-25: Fuel cell process [51]

Fuel cells are a still in early development phases and therefore the initial investment costs of fuel cells are extremely high. As technological advances in fuel cells come forward, the price of fuel cells may decrease. The current price of fuel cells makes this an unfeasible option for a residential energy system and hence falls beyond the scope of this study.

2.3 Alternative Energy Sources

Non-renewable and portable energy sources are considered in this section to present thorough research on all possible sources of energy. Non-renewable energy sources are very reliable forms of energy and has this distinct advantage over all renewable energy sources. The alternative energy sources that are discussed in this section is shown in figure 2-26.

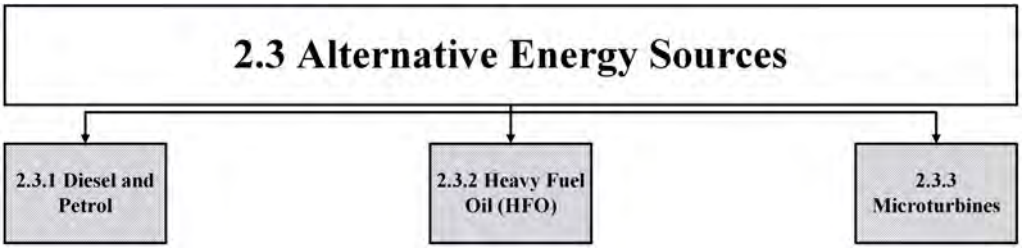

Figure 2-26: Literature study on alternative energy sources

2.3.1 Diesel and Petrol

Diesel and petrol generators are fossil fuel driven engines whose output shaft is connected to the rotor of an electric generator. This form of electricity generation is very popular in industry due to the output-power-to-size ratio and the reliability of the fossil fuel based engine. However, the running and fuel costs of fossil fuel electricity generation are much higher than the utility generated electricity and hence places this alternative source of energy beyond the scope of this study [52].

2.3.2 Heavy Fuel Oil (HFO)

Heavy fuel oil is another form of fossil fuel that is used in regions where diesel and petrol theft is a problem. Fuel oils are classified in different numbers according to the carbon chain length and the boiling point. HFO generators are specially designed machinery which can deal with the high viscosity of the oil. The viscosity of HFO is very high and requires preheating to at least 100°C to enable the flow thereof. An example of an HFO sample along with a genset is shown in figures 2-27a and 2-27b [52], [53].

(a) Heavy fuel oil sample

(b) HFO genset

Figure 2-27: HFO sample and genset [53]

Currently within the borders of South Africa, HFO is not commonly used for small sized applications and requires specialised machinery to generate electricity. Hence, the use of an HFO generator falls beyond the scope of the study.

2.3.3 Microturbines

As the name implies, microturbines are small-scale versions of the large steam driven turbines typically found in coal-fired power stations and concentrated solar plants (CSPs). Both coal-fired power stations and CSPs use steam that feeds into a turbine that is connected to the rotor of an electric generator. Once the steam passes through the blades of the turbine, a rotational motion is initiated which rotates the rotor of the generator. Steam turbines along with the steam generation process are very complex and expensive. Therefore, a significant initial investment has to be made to implement a microturbine and hence falls beyond the scope of the study.

2.4 Energy Storage Systems

The use of an energy storage medium is becoming increasingly popular with the use of renewable energy sources. An energy storage medium allows the use of energy at a later time when it is required. The efficiency of the storage system directly impacts the system's performance and hence requires an in-depth study on energy storage systems (ESS). The systems that are discussed in the following section are shown in figure 2-28.

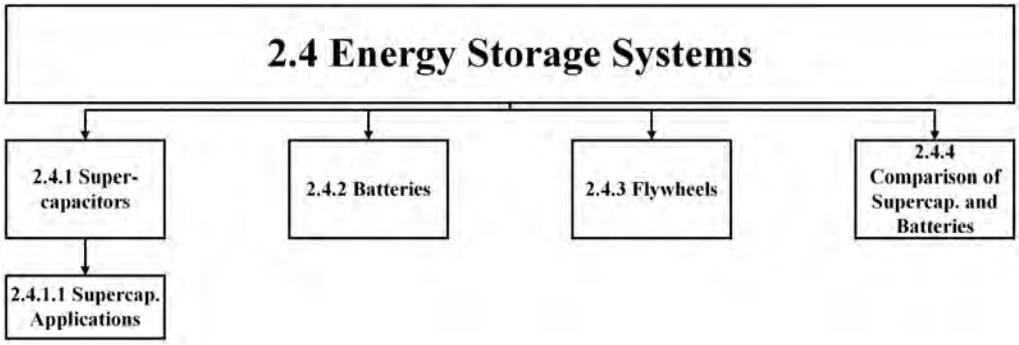

Figure 2-28: Literature study on energy storage systems

2.4.1 Supercapacitors

Supercapacitors are commonly referred to as double-layer capacitors with the ability to store thousands of capacitive charge [54]. This enables the supercapacitors to deliver a large jolt of energy within a very short period; this is referred to as a power dense energy source. The opposite is true for batteries which are energy dense devices; these types of devices better suited for long energy delivery at low to medium output current. Supercapacitors are renowned for their exceptional power density rather than energy density. These power dense devices not only have the capability to discharge quickly but also have the capability to fully recharge at the same rate. This is a superior characteristic that supercapacitors possess over other energy storage devices. The charge time of supercapacitors are only limited by the current delivering capability of the charging unit [55].

One drawback associated with an supercapacitor is that it has a very low output voltage which typically ranges from 2.5-2.7 V. This drawback can be overcome by connecting the supercapacitors in a series topology which would increase the output voltage. However, connecting capacitors in series causes a decrease in capacitive charge of the capacitor bank and in essence, decreases the energy delivery time. Also, the charging of a capacitor bank becomes more complex as external voltage balancing circuits are required to prevent damage to the supercapacitors. There are two balancing schemes that can be implemented namely passive and active balancing [56].

Passive balancing is used in applications where the supercapacitors do not charge/discharge regularly. The balancing is established by placing a resistor in parallel with each capacitor in the bank. Active balancing is used in application where the supercapacitors are constantly charged and discharged. The active balancing circuit keeps the voltage of the capacitor bank below a fixed value. According to Xu, Shaojun and Liu (2009) energy is constantly transferred from the highest charged supercapacitor to the least charged supercapacitor [56].

Once the balancing scheme of the supercapacitors is implemented, the applications of these devices are stretched over a very wide variety as discussed in the following section; figure 2-29 illustrates a leading manufacturer's supercapacitors [57].

(a) Maxwell supercapacitors

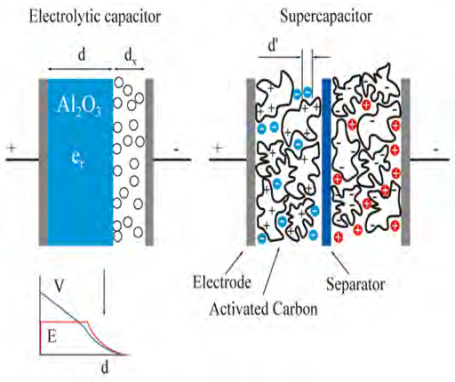

(b) Supercapacitor internal architecture

Figure 2-29: Supercapacitors [57]

2.4.1.1 Supercapacitor Applications

As stated in the preceding section, the supercapacitor has the ability to charge/discharge at a very fast rate and therefore most of the applications listed below make extensive use of this property.

1. Regenerative braking schemes
    - The Bombardier lightweight railroad system in Germany uses supercapacitors to capture the kinetic energy caused by braking. This energy is re-used to increase the acceleration of the railcar and to power intersection switches. The number of load cycles per year these capacitors perform are estimated to be between 100 000 and 300 000. This is an energy saving of up to 30% per year [58].
    - In some parts of the United States, the buses have been fitted with supercapacitors to accelerate and to improve top speed. These buses incorporate a hybrid electrical drive system and can accelerate to a speed of 50 km/h within 17 seconds. The supercapacitors recuperates about 38% of the energy used by the bus which is equivalent to 1.7 litre/km [58].
2. Energy storage
    - Another application of supercapacitors is in backup storage devices such as UPSs. These devices provide power for a short period of time after the power has gone out.
    - Solar PV panels are typically connected to supercapacitors in order to store the captured energy. Once again this is a favoured application of the fast charging capability.

2.4.2 Batteries

As stated above, batteries are energy dense devices and not power dense devices. However, new-age batteries such as lithium-ion and lithium-polymer batteries are a huge improvement on the acid based batteries in terms of power density. The different types of batteries are listed and compared in table 2-3 [59], [60].

Table 2-3: Rechargeable batteries' comparison [59], [60]

Characteristic	Ni-Cad	Ni-MH	Lead Acid	Lithium-Ion	Lithium-Polymer
Energy Density (Wh/kg)	35-55	43-70	30-40	90-200	130-200
Power Density (W/kg)	50-150	250-1100	180-200	750-1250	Up to 2900
Life Cycles	1500	600-800	500-800	500-1000	Up to 1000
Operating Temp. (°C)	-20 to 60	-20 to 60	5 to 40	-40 to 60	0 to 60
Maintenance	1-2 Months	2-3 Months	3-6 Months	None	None
Recharge Time	3-6 Hours	3-6 Hours	3-6 Hours	1-2 Hours	1-2 Hours

From table 2-3, it can be seen that newer technology batteries such as lithium and Ni-MH batteries surpasses the older technology based lead acid and nickel cadmium batteries in all aspects. However, there is one aspect of new technology batteries that cannot be met with lead-acid batteries and that is the ability to deep cycle. Lead-acid batteries have the ability to discharge up to 85% of its capacity without drastically affecting the lifespan of the battery. The opposite is true for lithium based batteries which have a drastic decrease in lifespan once a deep cycle has been performed. It is therefore critically important that the aspects addressed in table 2-3 are taken into consideration when selecting a battery for a certain application.

2.4.3 Flywheels

A flywheel energy storage system is a high inertia rotating wheel, usually placed within a vacuum chamber to reduce friction, that harnesses the energy generated by the rotation of the wheel [61]. The flywheel energy storage system operates on the principle of conservation of energy which states that energy cannot be created or destroyed but rather converted to another form of energy. In the case of a flywheel, electrical energy to a fed motor is used to rotate a flywheel that is connected to the rotor of the motor; this way electrical energy is stored as rotational energy. Once the electrical energy feed to the motor is removed, the flywheel connected to the rotor now drives the motor as a generator and converts the rotational energy back into electrical energy; figure 2-30a illustrates the abovementioned configuration along with an example in figure 2-30b [62].

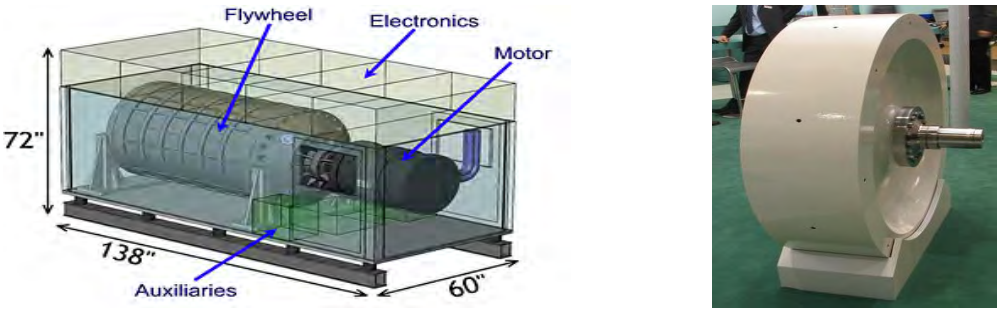

(a) Principle of flywheel energy storage

(b) Example of a flywheel design

Figure 2-30: Flywheel [62]

2.4.4 Comparison of Supercapacitors and Batteries

As previously stated, batteries and supercapacitors are opposites of one another. Batteries discharge energy at a fairly constant voltage over a longer period of time and requires hours to recharge to full capacity. Supercapacitors are superior devices in terms of very fast charging and discharging of energy. However, a drawback of a supercapacitor is that as it discharges, the output voltage decays exponentially until completely depleted [55]. Supercapacitors then become without use when the voltage drops below the load's required voltage level. The main differences between batteries and supercapacitors are summarised in table 2-4 [54], [55], [59], [60].

Table 2-4: Comparison of supercapacitors and batteries [54], [55], [59], [60]

Batteries	Supercapacitors
High energy storage	Low energy storage
Long charge/discharge time	Short charge/discharge time
3-8 years of reliable service	Unlimited life cycles
85% discharge depth	Full discharge depth
Constant output voltage	Decaying output voltage
Efficiency: 45-85%	Efficiency: 85-98%

2.5 System Controllers

The system controller is of utmost importance and ultimately determines the performance of the entire control system. Selecting an unsuitable system controller for a required application leads to performance related and integration issues and therefore in-depth research is performed on suitable controllers. Figure 2-31 illustrates the topics that are covered in this section.

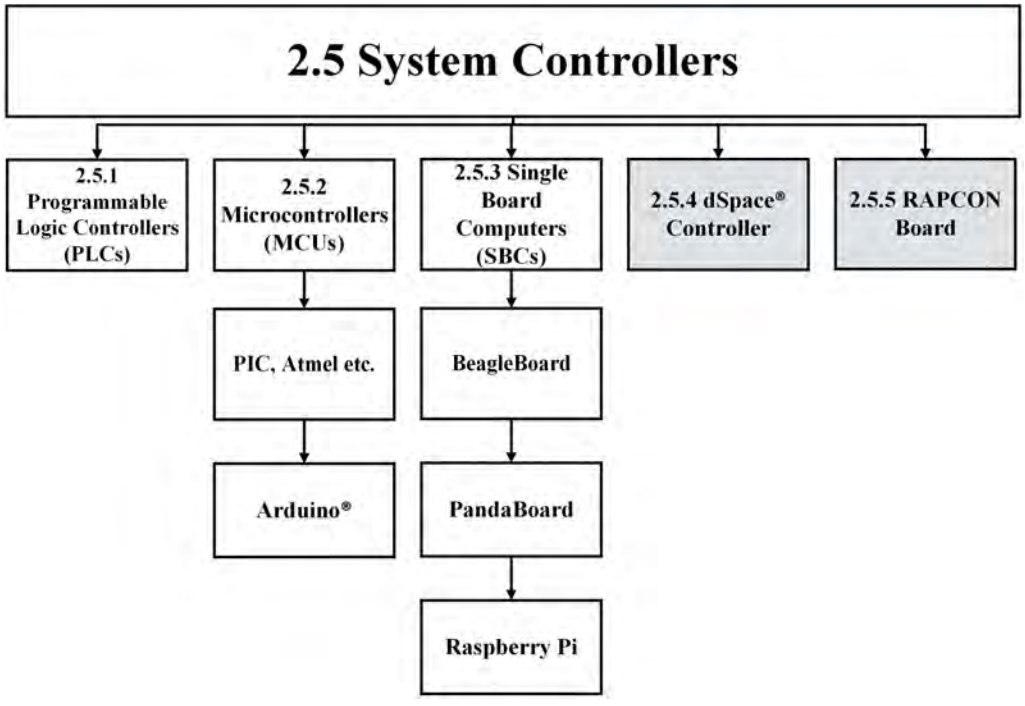

Figure 2-31: Literature study on system controllers

2.5.1 Programmable Logic Controller (PLC)

2.5.1.1 Technical Background

A PLC is a solid-state digital computer used to control and automate electromechanical processes such as production lines in factories, building energy management systems and heating, ventilation and air conditioning (HVAC) systems [63]. PLCs are renowned for their robustness and capability to withstand harsh environments such as excessive temperatures, dusty/smoke conditions and vibration. These devices have a built-in non-volatile memory bank hosting an independent operating system which makes standalone and real-time automation possible. Automation through these devices is made possible by the fact that inputs can be obtained from sensors, calculations can be performed in real-time and the appropriate actuators can be activated based on the inputs [63]. A Siemens PLC is shown in figure 2-32a along with a diagram illustrating the cycling process in figure 2-32b [64].

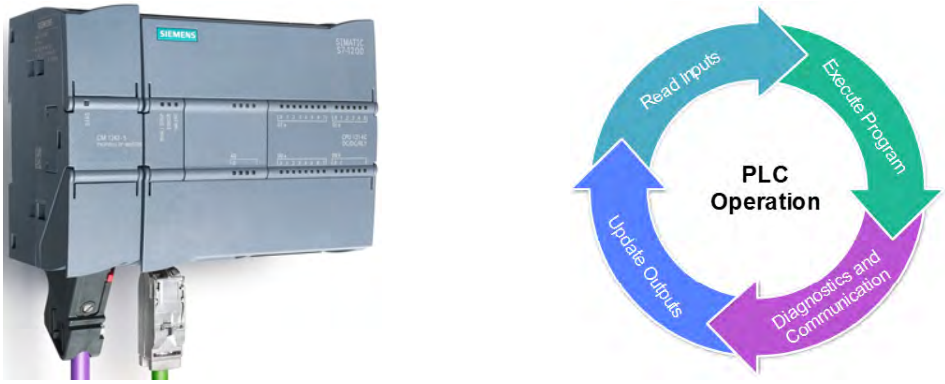

(a) Siemens S7-1200 series PLC

(b) PLC cycling process

Figure 2-32: Basic PLC system [64]

As mentioned above, some of the main advantages of a PLC is the robustness and reliability under extreme conditions and the simple programming techniques that can be employed to control the PLC [65], [66]. All the programming techniques associated with a PLC are based on logical structure such as AND, OR, NOT, XOR etc. [63]. This structure of programming permits the use of logical gates and basic truth tables to control the PLC in a desirable manner. These logical structures are also presented in graphical forms to ensure an user friendly programming environment; the most widely used graphical environments include ladder and functional block diagrams. Another notable advantage of PLCs are the simplified redesign of established circuits. Alterations to the circuit are easily done without rewiring the entire circuit, only logical program code alterations needs to be made. This ensures a time-efficient solution to rectify a fault or alteration to an established circuit [63]. In support of time-efficiency, PLCs can be programmed in such a way that the PLC autonomously detects faults within an electromechanical system and sends/displays error messages accordingly. This permits easy diagnostics and troubleshooting which again reduces the off-line time during a fault condition [63], [67]. The most popular graphical forms, ladder and functional block diagrams, are shown in figure 2-33 [63], [67].

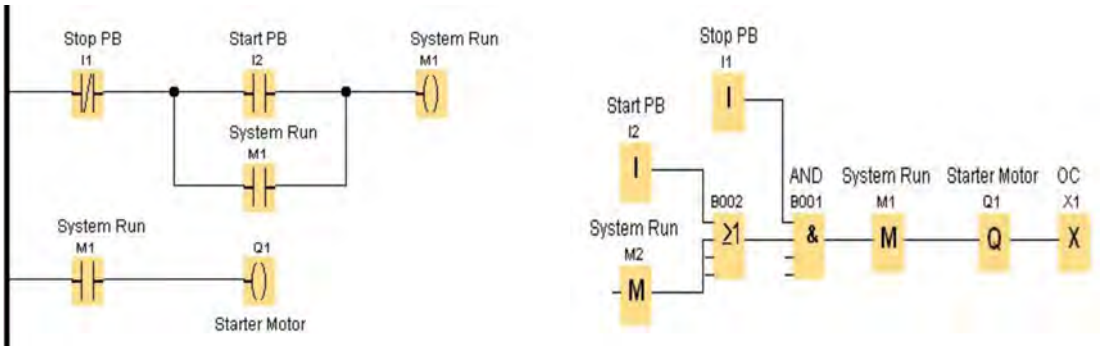

(a) Ladder diagram (b) Functional block diagram

Figure 2-33: Graphic forms of PLC programming [63], [67]

There are few disadvantages associated with a PLC with the most significant being the cost implication in simple control systems. The initial cost of a PLC can be significant and therefore in the case of simple control systems, it may be too expensive to implement as the controller. As the complexity of a control system increases, the more cost effective solution a PLC becomes. A PLC contains numerous internal contacts, timers, counters etc., if all of these internal components are occupied by sensors and actuators, the PLC is performing the maximum number of operations possible and operating cost effectively [66].

To summarise the description of a PLC, a formal definition is supplied according to the National Electrical Manufacturers Association (NEMA) (2010) [68]:

"A programmable controller is a digitally operated electronic system, designed for use in an industrial environment, which uses a programmable memory for the internal storage of user-orientated instructions for implementing specific functions such as logic, sequencing, timing, counting and arithmetic to control, through digital or analog inputs and outputs, various types of machines or processes. Both the PLC and its associated peripherals are designed so that they can be easily integrated into an industrial control system and easily used in all their intended functions." [68]

2.5.1.2 PLC Energy Industry Case Studies

PLCs are considered the leading systems controller for industrial applications due to the wide range of advantages listed above [63]. Typical industry applications are listed and discussed below.

1. Home automation system

   In a study by Yilmaz (2010), a home automation system implementing a PLC was designed and constructed [69]. The main purpose of this system was to automatically control the lighting, wall outlets, gas and water system of a home to optimise energy consumption. The control of the wall outlets came from connecting several of the outlets onto the relays controlled by the PLC. In a similar manner, the distribution panel lighting switches were also connected to the PLC's relays; however, the control of these lighting switches was performed using a single keypad as input device. The keypad was strategically placed within the home which allowed

centralised lighting control. With a low pressure gas system present in the home, Yilmaz (2010) decided to implement a gas safety system into the home which shuts down the gas inflow in case of a leakage [69].

2. Small building renewable energy source management system

   In the study presented by Balasevicius, Dervinis and Sarkauskas (2011), a small building energy management system consisting of renewable energy sources and a diesel generator were developed [70]. Solar PV and wind power plants of up to 5 kW was considered alongside a 10 kW diesel generator. The aim of the project was to minimise energy consumption from the national grid and expend all the locally generated energy. According to Balasevicius et al. (2011), the small building was divided into ten sections of electric loads, each connected to a triac-bank which is connected to the sources of energy [70]. The control system consisted of a power meter connected at each load section. The control strategy that was followed was to first connect the building to the utility company's grid and determine the power required by each section. Once this was established, the available energy from the wind, solar and diesel generator was determined. Based on these measurements, the PLC determined and controlled which load sections could be connected to the sources of energy.

3. Fuzzy logic building energy management system

   This study presents a building energy management system that offers distributed control of the indoor comfort level whilst reducing the energy consumption. According to Kolokotsa et al. (2002), the system used a smart card unit, controlled by a user, to adjust the indoor illuminance and HVAC settings according to the user's smart card [71]. In cases where a smart card was not presented, the system assumed no-one was present and switched off all the lights and HVAC. A PLC performed fuzzy logic algorithms to determine the sensor inputs, actuator outputs and to send data across a communication network. There were several illuminance and temperature sensors connected to the control system which determined the comfort level according to the user's inputs. In addition, the PLC collected data from various users' smart cards and stored the data to adapt the control strategy.

2.5.2 Microcontrollers (MCUs)

2.5.2.1 Technical Background

A microcontroller (MCU) is comparable to a small computer because of various similarities in architectural design. Similar to a computer, an MCU has a reduced instruction set computer (RISC) processor, variable random access memory (RAM) and input/output (I/O) peripherals [72]. A MCU also contains an instructions set which hosts the program code embedded by the programmer. These devices contain numerous features which make these embedded devices very attractive when considering control systems; some of the features are listed below [72].

- Programmable digital I/O
- Programmable analog I/O
- Serial I/O
- Timers

- Interrupts on timers and inputs

Some of the main advantages of MCUs are the reduction in size, weight and cost compared to other controllers consisting of a separate processor, memory module and I/O devices. The reduction to a single integrated circuit (IC) permits the implementation of cost effective embedded systems. The downside to MCUs is that in cases where high processing power is required, the MCU may fall short of the expected demand. An image of a single IC and generic internal architecture of an MCU is shown in figures 2-34a and 2-34b respectively.

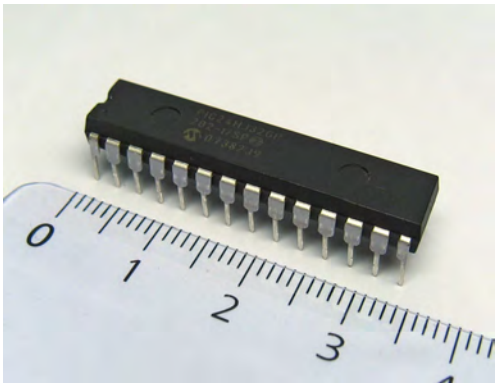

(a) Single IC microcontroller

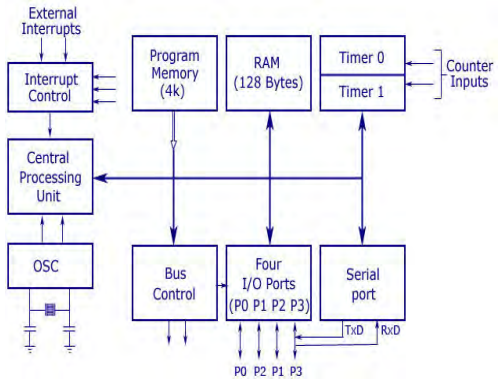

(b) Microcontroller architecture

Figure 2-34: Microcontroller illustration and architecture [72], [73]

MCUs are devices which receives a low direct current (DC) voltage as input and outputs a similar DC voltage as a control signal. Therefore, MCUs requires a stepped down and rectified signal which generates a trend that MCUs are suitable in only low system voltage applications [72], [73]. Some low system voltage projects include global positioning satellite (GPS) based systems, radio frequency identification (RFID) systems, mobile communication systems and environmental monitoring systems [72], [73]. However, with the emerging of more robust and versatile MCUs, industrial applications are becoming more apparent as discussed in the following section [73], [74]. A brief summary containing performance features of low-to-high end microcontrollers are shown in table 2-5. The MCUs listed below are from the leading MCU manufacturer Microchip®.

Table 2-5: MCU features [72], [73]

Characteristic	**PIC16F84**	**PIC24EP32**	**PIC32MX170**
Operating Speed	16 MHz	32 MHz	64 MHz
Peripheral Features	13xI/O pins, 4xInterrupts, 1xTimer, 1xPWM	21xI/O pins, 8xInterrupts, 5xTimers, 3xPWM	34xI/O pins, 10xInterrupts, 5xTimers, 8xPWM
Program Memory	8 KB	32 KB	256 KB
Data RAM	68 bytes	4 KB	64 KB

2.5.2.2 Arduino® Microcontrollers

Arduino®, another microcontroller manufacturer, follows an open-source platform as development environment [75]. Arduino® focuses on developing students' MCU control skills and therefore has created a simpler programming language that is understood more easily. Some of the Arduino® development boards have the capability to interface with MATLAB® and Simulink® and can be programmed by designing a Simulink® control system model.

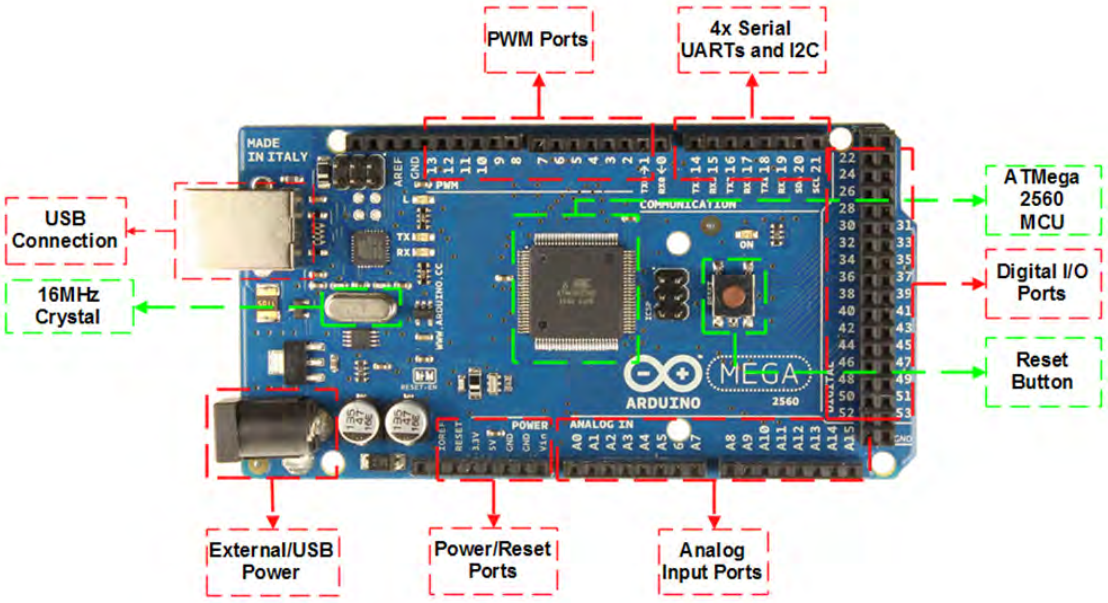

Figure 2-35: Arduino® development controller [76]

The development board shown in figure 2-35 is a standalone board with analog/digital input/output pins, communication ports etc. [76]. These pins and ports are used to connect the development board to external peripherals such that the processor is able to interface with the real world. A summary of the forms of microcontrollers' characteristics are shown in table 2-6 [75], [76].

Table 2-6: Arduino® microcontroller comparison [75]

Arduino Microcontroller	Raw Microcontrollers (PIC, Atmel, etc.)
Simpler programming logic	Complex programming logic
Not durable in harsh conditions	Not durable in harsh conditions
MATLAB®/Simulink® integration	No unnecessary components pre-built
Cost effective	Very low cost
Pre-assembled PCB	Requires custom built PCB
Fast processing	Fast processing

2.5.2.3 MCU Energy Industry Case Studies

MCUs are conventionally not used in heavy current applications as the control unit; however, there are exceptions which are discussed below.

1. MCU based energy management system for a stand-alone microgrid

   In this case study, Belvedere et al. (2012) presented an energy management system that consisted of a battery storage system, fuel cells and solar PV emulator [77]. The system was interconnected in such a way that a small distributed network of 4.5 kW was formed which was not connected to the utility grid but rather formed its own 230 V AC bus. The two networks were isolated from one another and is never connected simultaneously. A 5 kW load emulator was connected to the bus to emulate various loads connected to the network. The main objective of the control strategy for the MCU system was to connect and disconnect the fuel cells and solar PV emulator to optimise the charging of the battery bank. Based on the battery bank state-of-charge, the MCU decided which source of energy, battery or utility grid, should supply the loads [77].

2. MCU and solar PV based energy management system

   In this case study, Ghodki (2013) presented a study which contained a distribution system consisting of solar PV power and the utility grid [78]. A monitoring system employing smart metering was used to measure the amount of electrical energy consumed by the load and based on these measurements, the MCU controlled the power flow. The control of the power flow was established by using relays to connect the solar PV system and the utility grid in a parallel connection to the load [78]. The MCU measured the power consumed by the load and based on the capacity of the solar PV system, a decision was made regarding which source of energy, solar PV or utility, was used to power the load [78].

3. MCU home energy management system

   In the case study presented by Pisica et al. (2013) a prototype home energy management system was designed and implemented [79]. The main objective of this study was to make use of dynamic tariff monitoring and scheduling home appliances operation according to those tariffs. This way loads was shifted to a time frame where more generation capacity and a lower tariff was available. In this manner, electricity savings was increased by a scheduling pattern. The system also consisted of a web page that hosted all the scheduling, time frames and connected appliances. According to Pisica et al. (2013), the additional distributed generation was advised to further increase electricity savings [79].

2.5.3 Single Board Computers (SBCs)

2.5.3.1 Technical Background

Single Board Computers (SBCs) are becoming more popular as these small sized devices have the properties of a completely functional computer [80]. Similar to a conventional computer, SBCs also hosts an embedded processor, memory module and I/O ports. Although these are low-end 8/16 bit processors, basic dynamic RAM and limited I/O peripherals, these devices still offer competitive computational power at a fraction of the cost and size of industrial controllers. A feature and functionality overview of some of these SBCs are shown in table 2-7; only a few of the most popular SBCs available on the market are listed [80].

Table 2-7: Single board computers overview [80], [81], [82]

Characteristic	BeagleBoard Black	PandaBoard ES	Raspberry Pi
Memory	1 GB	1 GB	1 GB
Processor Speed	Cortex A8: 1 GHz	Cortex A9: 2 GHz	ARM A7: 900 MHz
Display	Micro HDMI: 1080p	HDMI: 1080p	HDMI: 1080p
Interfaces and Ports	2xUSB, SATA	2xUSB, 3.5mm Audio Jack, RS-232	4xUSB, 3.5mm Audio Jack
Connectivity	1 Gbit/s Ethernet	2 Gbit/s Ethernet, WLAN, Bluetooth	1 Gbit/s Ethernet
Storage	Internal Flash: 2 GB	Expandable. SD Card: 32 GB	Expandable SD Card: 32 GB
Peripheral Features	UART, PWM, A/D, Timers	UART, PWM, A/D, Timers	UART, PWM, A/D, Timers
Operating System	Ubuntu, Windows Embedded, Android	Ubuntu, Android	Linux, Raspbian OS

From table 2-5 and 2-7 it is evident that SBCs have superior processing power when compared to microcontrollers. This is the main reason SBCs are the preferred choice in cases where digital signal processing (DSP) and other processor intensive calculations must be performed [81], [82]. An image of a Raspberry Pi is illustrated in figure 2-36a along with a visual summary of its features in figure 2-36b [80].

(a) Credit card size Raspberry Pi SBC

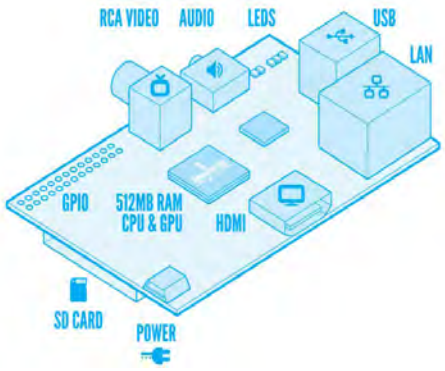

(b) Raspberry Pi visual illustration of features

Figure 2-36: Raspberry Pi [80]

These powerful boards are driven by Linux based operating systems; some of these systems include Android, Angstrom and Ubuntu. These are all open-source products and therefore support is dependent on the community. A competitor of the Raspberry Pi, the Panda Board, is shown in figure 2-37 with the main specifications [83].

2.5.3.2 SBC Automation Case Studies

There is a shortfall of energy management studies using SBCs which is due to the fact that SBCs are fairly new on the market and studies have not yet been conducted in this manner. However, there is a home automation system powered by SBCs which is discussed below.

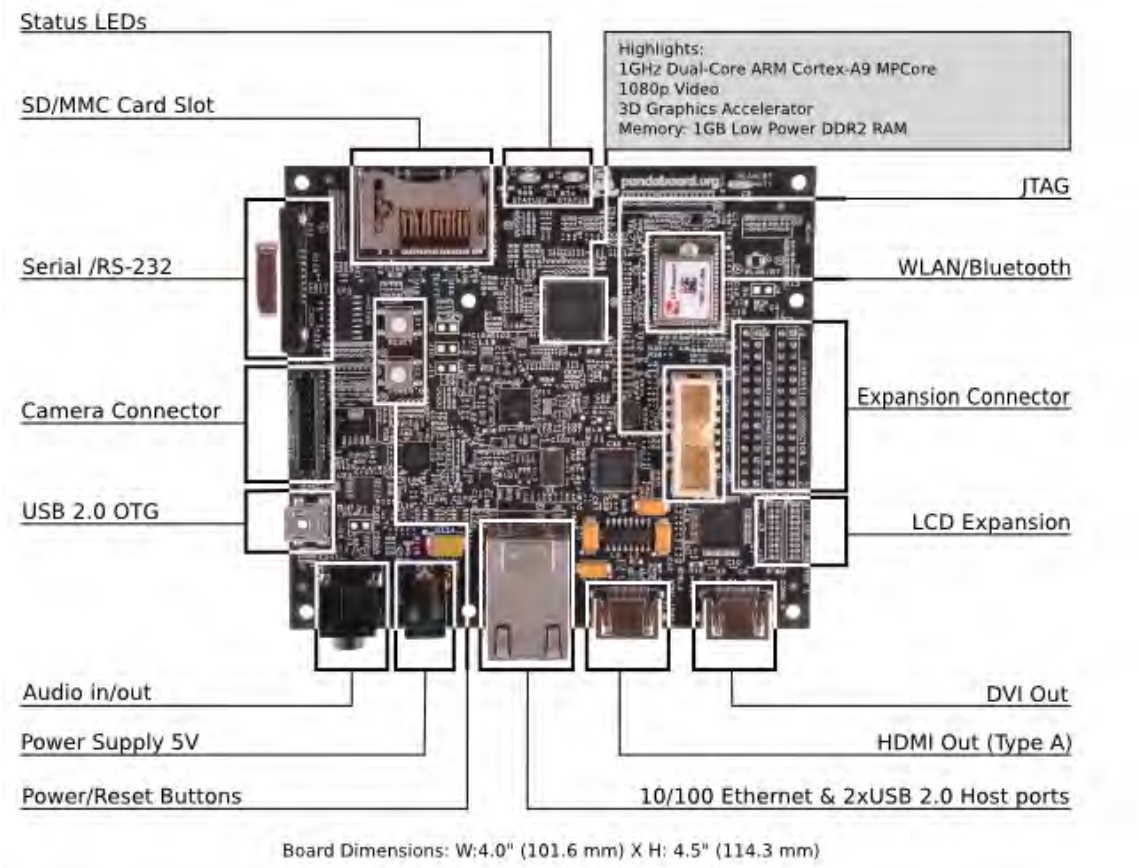

Figure 2-37: Panda board [83]

1. SBC home automation system

   In the study presented by Ramses et al. (2013), a home automation system was implemented to control various loads by using a mobile device [84]. A Raspberry Pi SBC was used as a server to connect the home onto the internet. The user was then able to access the server through the mobile device's internet connection and control several of the loads from a centralised point. The main actuator was controlled through wireless network communication received from the SBC and relays were used to connect and disconnect the loads [84].

2.5.4 dSPACE® Controller

dSPACE® controllers are high performance boards that are used in systems that require fast performing real-time control applications [85]. Some of these applications include the electronic control units (ECUs) in the automotive industry, cabin control in aeroplanes and medical equipment such as respiratory machines. These controllers host extremely powerful processors and are very reliable. It has the capability to fully integrate with MATLAB® and Simulink® [85]. This includes all toolboxes ranging from fuzzy logic to neural networks. dSPACE® controllers have been extensively used in the automotive industry especially in electric drive technology for the past decade. Typical applications of electric drive technology include electric power steering, electric brake systems, electric vehicles and so on; figure 2-38 shows a dSPACE® controller.

Figure 2-38: dSPACE® controller [85]

2.5.5 RAPCON Board

The RAPCON board has been designed and manufactured to extend the real-time operation of MATLAB® and Simulink®. This makes the RAPCON board an extremely powerful board which enables the board to operate between MATLAB® and Simulink®. This board has been designed to operate on a Microsoft® Windows platform and support MATLAB® versions R2007b through to R2015a. The main features of the RAPCON board is summarised in table 2-8 [86].

Table 2-8: RAPCON features [86]

Feature	Specification
MATLAB® Version Support	R2007b-R2015a
Baud Rate	460800 baud
Analog Inputs	8, 0-5 V, 12 bit res.
Digital Inputs	8, 0-5 V, 8 lines
Analog Outputs	2, 0-5 V, 12 bit res.
Digital Outputs	8, 0-5 V, 8 lines
H-Bridge Outputs	Supply Voltage, 5 A
Sampling Rate	15.2 kHz

RAPCON boards are especially popular in mechatronic applications due to the real-time integration, on-board H-bridge and easily expandable boards. The RAPCON board is supplied with dedicated software which makes this a favourable controller amongst educational and industrial users alike. Figure 2-39 shows an image of the RAPCON controller [86].

Figure 2-39: RAPCON board [86]

2.6 Integration Technologies

As discussed in Chapter 1, there are two types of microgrid topologies, grid-tied and standalone. The former is discussed in this section as this is the topology that is applicable to this study. A typical rooftop grid-tied system is shown in figure 2-41 for illustration purposes [87], [88]. Within this section, the grid-tie inverter (GTI), battery charge controllers and communication protocols are briefly discussed as illustrated in figure 2-40.

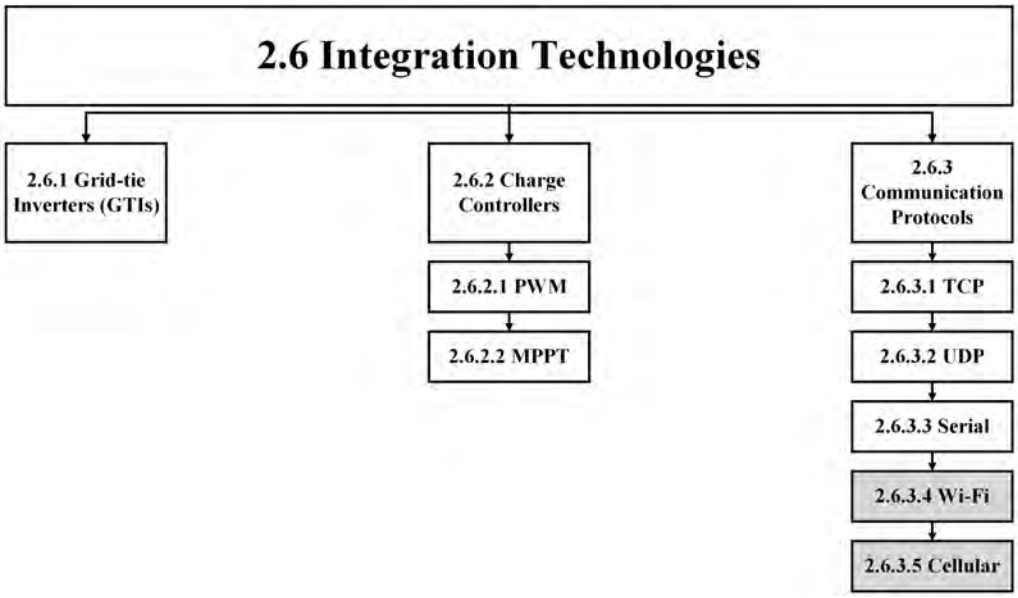

Figure 2-40: Integration technology topics

2.6.1 GTIs

GTIs consist of exactly the same components as stand-alone inverters with the exception that GTIs can synchronise with the grid voltage and frequency. Once the GTI is in sync with the grid, the output relay of the GTI is closed and energy starts feeding into the grid. A critical performance aspect which usually separates a low-quality GTI from a high quality GTI, is the ability to conform to the quality of supply (QoS) standards of the grid the GTI is connected to. The QoS requirements that GTIs should adhere to in South Africa were discussed previously. Due to these requirements, GTIs are fairly expensive pieces of equipment in the installation of grid-tied microgrids. More information on these follows in the design chapter.

2.6.2 Charge Controllers

To ensure that the battery is charged optimally, it is of utmost importance to use a battery charge controller. Charge controllers are primarily used as a link between the batteries and solar PV panels. Connecting the solar PV panels directly to the battery causes permanent damage to the battery.

There are two types of charge controllers available on the market, Pulse Width Modulation (PWM) and Maximum Power Point Tracking (MPPT). Both models operate on the

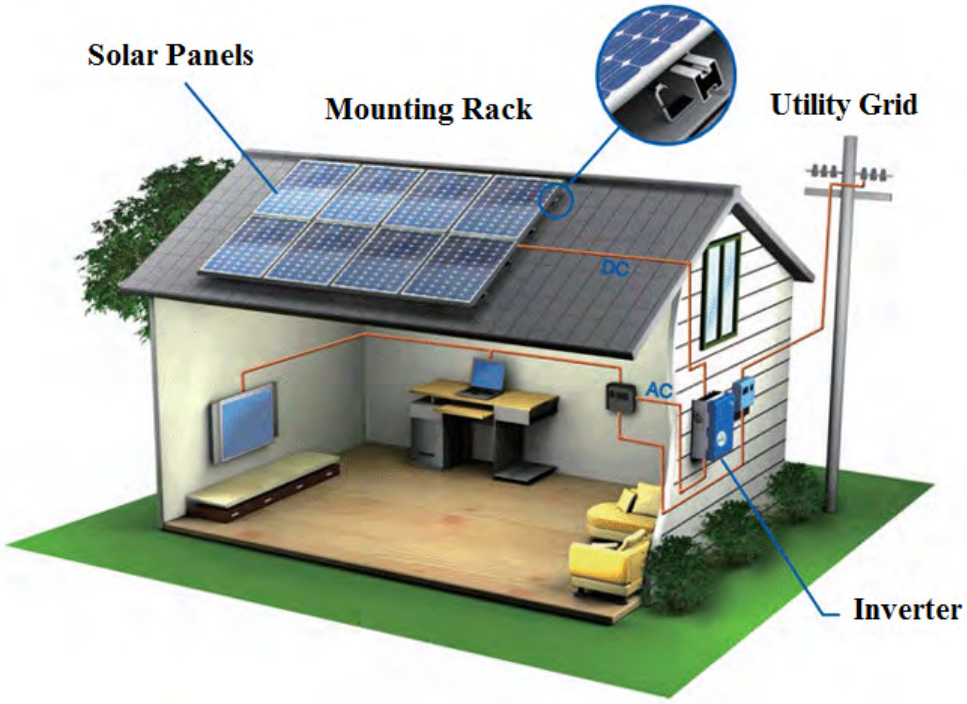

Figure 2-41: Rooftop grid-tie system [88]

principle of charging the battery at the optimal voltage which is a bit higher than the measured battery voltage. The two mentioned technologies both achieve this characteristic but in different manners [89].

2.6.2.1 PWM

PWM charge controllers work as a closed-loop control system which first measures the battery voltage and then determines the optimal charging voltage. The controller takes into account the input voltage from the solar PV panels and adjusts the output voltage to that of the optimal charging voltage through the principle of PWM. The basic principle of PWM is shown in figure 2-42 [90].

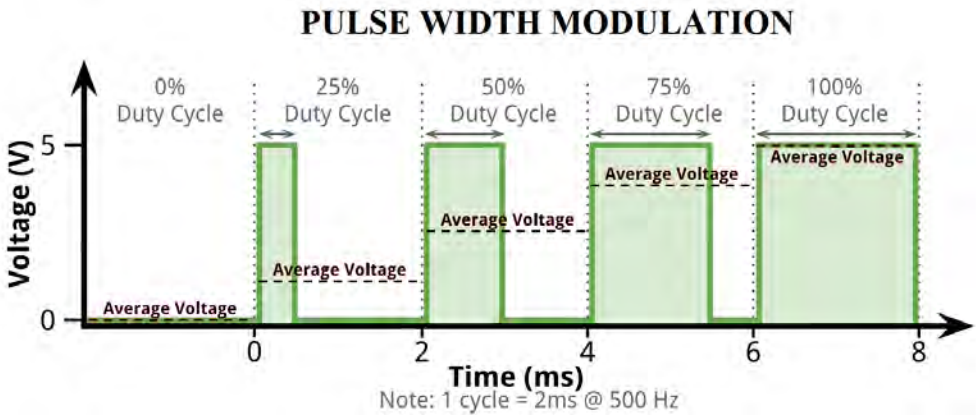

Figure 2-42: Principle of PWM [90]

2.6.2.2 MPPT

MPPT charge controllers also operate in a closed-loop control system that constantly adjusts the output of the charger to match the maximum power point of the solar PV panel. The I-V curves shown in figure 2-43 illustrate the operating principle of the MPPT controller [91].

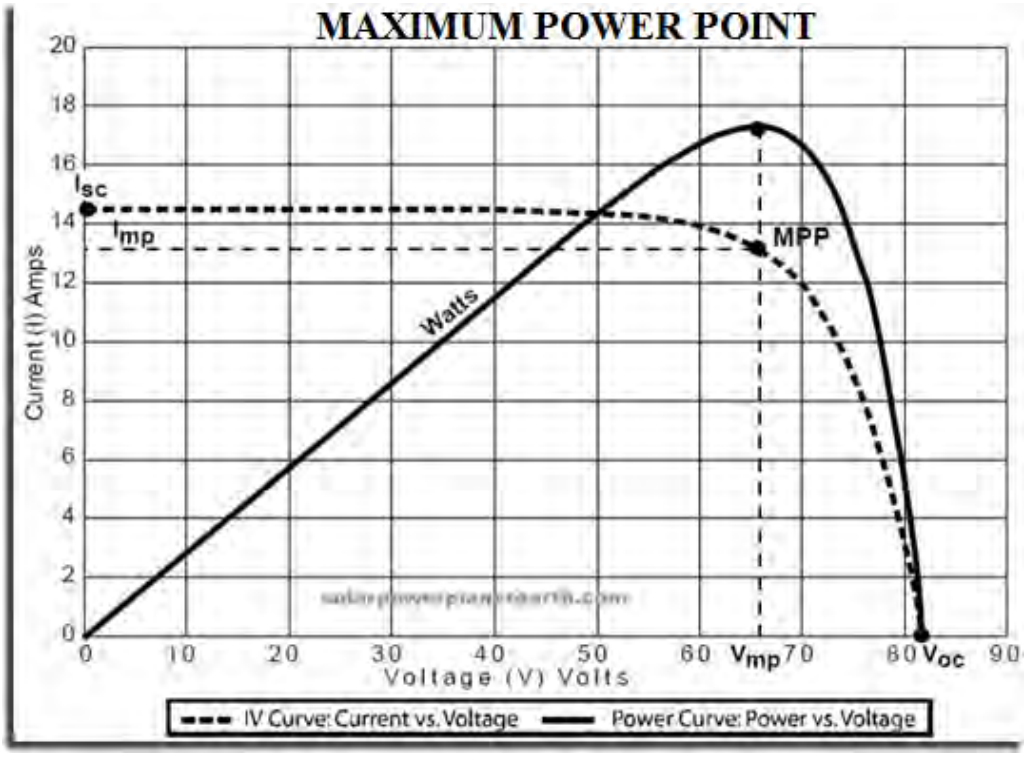

Figure 2-43: Principle of MPPT [91]

Comparing these two controller technologies against one another yields the following conclusions as summarised in table 2-9.

Table 2-9: Comparison of PWM and MPPT charge controllers [90], [91]

PWM	MPPT
Lower conversion efficiency	Highest conversion efficiency
Low investment costs	High investment costs
Cannot have parallel strings	Permits parallel strings
Lower voltage implies normal fuse protection is possible	Operates at higher voltage and requires special protection

2.6.3 Communication Protocols

Communication protocols are considered a critical component as these are the mediums that information regarding measurements and component statuses are synchronised within a network. A loss within the communication system may cause the system to a halt which in turn may cause malfunctions and permanent damage to components. Therefore, as in the previous section a comprehensive study of the standardised communication protocols

are discussed. Figure 2-44 provides an overview of covered protocols in the following section.

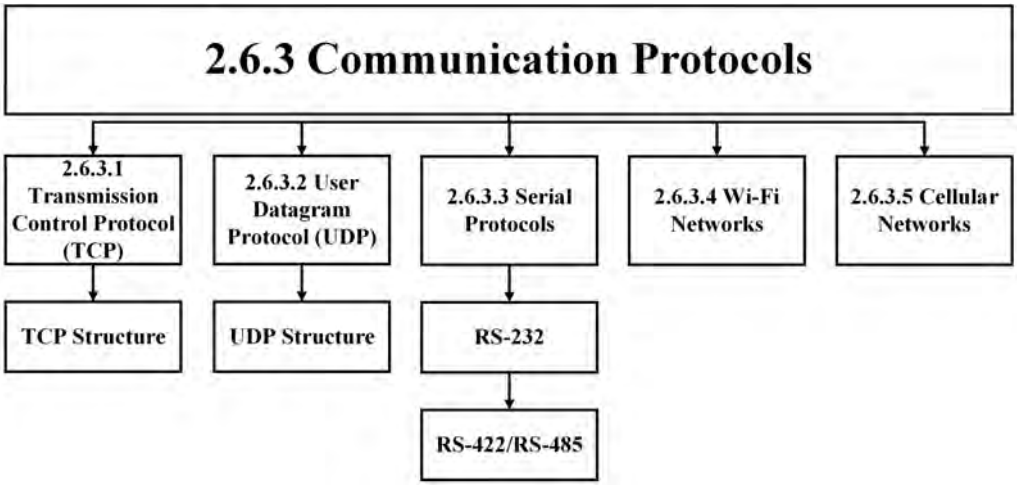

Figure 2-44: Literature study on communication protocols

2.6.3.1 Transmission Control Protocol (TCP)

Transmission Control Protocol (TCP) is a transport protocol which ensures reliable data stream delivery between applications. Data transfer is ensured by making use of sequenced acknowledgements within the transmission packets. TCP was developed due to a wide variety of programs and software packages running on the same computer. This introduced problems of dataset streams getting lost between programs and software packages. The TCP protocol was developed to ensure that each program or software package sent and received the correct data stream. This was accomplished by introducing TCP port numbers, referred to as sockets, along with unique IP addresses of the start and end points. Some of the main services that TCP offer are listed and discussed below [92].

- Exceptional reliability — Reliability in TCP connections are ensured by sequencing bytes with a forward acknowledgement number that tells the destination which byte should be sent to the source. Another feature to enhance the reliability is to retransmit bytes after a specified time of unacknowledged bytes. This allows the TCP protocol to handle misread, duplicate, lost and delayed packets [92].
- Efficient flow control — Flow control is regulated by the receiving end which embeds a sequence number in the acknowledgement packets. This sequence number indicates the number of bytes that can be received without overflowing the internal buffers.
- Full-duplex operation — TCP permits full duplex communication which enables the sending and receiving end to send and receive packets simultaneously [92].
- Multiplexing — Multiple upper-layer datasets can be multiplexed and sent over a single connection. No additional processing or connections are required [92].
- Stream data transfer — Stream data transfer offers the advantage of reducing the additional processing required by the sending and receiving end during the preparation of the data that needs to be sent. Without data stream transfer, the sending and receiving ends would require applications to chop and unite data blocks before/after sending [92].

TCP Protocol Structure
The TCP header file shown in table 2-10 represents the structure that is used to transmit and receive TCP packets across a network [92].

- Source Port — Identifies point at which source process receives TCP service
- Destination Port — Identifies point at which destination process receives TCP service
- Sequence Number — Indicates the number assigned to first byte of data in the current message
- Acknowledgement — Contains the sequence number of the next byte that the sender expects
- Data Offset — Number of 32-bit words in the TCP header show where the data begins
- Reserved — Usually 0, intended for future expansion of protocol
- Control Bits — Carries all the control information in the form of bits
- Window — Indicates the size of the internal buffer of the sender end
- Checksum — Indicates if header was damaged during transmission
- Urgent Pointer — Points to first urgent data byte in pointer
- Option and Padding — Specifies TCP options
- Data — Carries actual data that must be transmitted

Table 2-10: TCP protocol header structure [92]

<table>
<tr><td colspan="5">16 bit</td><td colspan="4">32 bit</td></tr>
<tr><td colspan="5">Source Port</td><td colspan="4">Destination Port</td></tr>
<tr><td colspan="9">Sequence Number</td></tr>
<tr><td colspan="9">Acknowledgement Number</td></tr>
<tr><td>Offset</td><td colspan="2">Reserved</td><td>U</td><td>A</td><td>P</td><td>R</td><td>S</td><td>F</td><td>Window</td></tr>
<tr><td colspan="8">Checksum</td><td>Urgent Pointer</td></tr>
<tr><td colspan="9">Option and Padding</td></tr>
<tr><td colspan="9">Data</td></tr>
</table>

2.6.3.2 User Datagram Protocol (UDP)

UDP provides a very simple transport protocol but at the expense of reliability. UDP has the same objective as with TCP, to ensure that the sent data reaches its correct destination. This is done by using UDP port numbers. However, UDP ensures no reliability, flow control or error handling functions. This significantly simplifies the UDP headers and reduces traffic on the network due to less bytes that needs to be transferred. UDP is however useful where the flow control and error handling is controlled by the application [92].

UDP Protocol Structure
In a similar fashion as the TCP protocol, the UDP protocol also contains a header file which is used to transmit and receive packets across a UDP network. The structure of the header file can be seen in table 2-11 [92].

- Source Port — 16 bits. An optional port which may be used to include a port number to which a reply can be directed
- Destination Port — 16 bits. Port related to the destination address
- Length — 16 bits. Length of the user datagram that will be transmitted

- Checksum — 16 bits. Contains information regarding IP header, UDP header and the data
- Data — Carries actual data that must be transmitted

Table 2-11: UDP protocol header structure [92]

16 bit	32 bit
Source Port	Destination Port
Length	Checksum
Data	

2.6.3.3 Serial Protocols

Serial communication is divided into three groups, each based on the principle of operation. The RS-232 protocol was the first to be developed and is also the simplest.

RS-232
RS-232 is by far the simplest protocol of the serial communication family and has therefore been adopted in a large portion of applications such as commercial and industrial data communication. Although RS-232 is a simple protocol, full-duplex communication is possible which permits simultaneous communication between two devices. This protocol is of the 3-wire type hosting a sending, receiving and ground wire. The data is transferred by a sequence of binary bits. The bits, logical 1 and 0, are represented by either a +12 V or a -12 V signal. The speed at which the bits are transferred is determined by the preset baud rate and is measured in bit per second (bps). Transmission distance is a drawback of the RS-232 protocol as longer lines introduce noise and voltage drops. Since the logical binary values are based on fixed voltage levels, a voltage drop close to the threshold value may cause data being transferred incorrectly. This is even more so for added noise on the line, a steep pulse can cause a 0 to be interpreted as a 1. These problems led to the development of the RS-422 protocol [93].

RS-422/RS-485
As mentioned above, the RS-232 protocol uses absolute voltage levels to define the logical binary values. The RS-422 protocol works in a different manner and makes use of differential signals to overcome long distance voltage drops and noise on the line. Differential signal transmission implies that a bit value is obtained from relative voltage is flowing from the positive signal terminal to the negative signal terminal. This doubles the number of wires required by the RS-422 protocol but reduces noise and voltage drop effects significantly. This permits the RS-422 protocol to be used across longer distances at a much higher baud rate [93].

RS-485 is an expansion of the RS-422 protocol which allows the connection of multiple senders and receivers in a network topology. The RS-232 and RS-422 protocols are handy in peer-to-peer connections between senders and receivers but do not perform as well as the RS-485 protocol in a network topology. RS-485 allows multiple senders and receivers to be connected to the same node in a network with each device having its own unique address [93].

2.6.3.4 Wi-Fi Networks

This is a form of communication in robotics where a device is controllable through the internet via a Wi-Fi connection [94]. For this type of communication, a wireless network adapter must be installed into the control computer with another adapter installed into the device that requires control. The adapter installed into the computer converts digital signals into radio frequency (RF) signals, in turn the receiver adapter converts the RF signals back to digital signals. For safe control over the Wi-Fi network, authentication and security measures must be taken. This form of communication is not used in microgrid topologies and falls beyond the scope of the study.

2.6.3.5 Cellular Networks

Cellular communication operates in a similar fashion to Wi-Fi networks but with the exception that general packet radio service/third generation (GPRS/3G) networks are used. These are the networks that are used to establish communication between cellphone users. These connections require a subscriber identity module (SIM) card that is registered at a service provider which enables the use of the cellular networks. These network providers charge a certain rate for the use of their network and also depends on amount of data usage by the network [94]. These networks broadly cover large deserted areas of land which permits communication from very remote areas. This form of communication is not used in microgrid topologies and falls beyond the scope of the study.

2.7 Energy Management Case Studies

This section serves to list and provide a short description of applicable EMS case studies that apply to this study. The main focus of this section is to dissect the control strategy followed by each study.

1. Predictive power control for PV plants

   This study presents a predictive model control approach to manage energy generated by a grid-tied PV power plant in real-time [95]. The aim of the control system is to optimise economic revenue by utilising an energy storage medium to store energy when solar PV generation is greater than the load requirement. Perez et al. performed the study by designing a simulation model and a real-world testing station where predictive control could be exercised [95]. The results indicated that the predictive model was executed during three specific times of the day, namely, before sunrise, mid-day and late afternoon. The study highlights the fact that real-time prediction ensures that the solar PV system is economically feasible.

2. Hierarchical control scheme for a PV and battery system

   Lampropoulus et al. presents a study where a hierarchical control scheme is defined for the energy management of a battery and a solar PV system integrated with the grid [96]. The aim of the study is economic optimisation of the integrated system by employing predictive control techniques. The control strategy utilises a three-level scheduling system, namely, day-ahead, intra-hour and real-time. The

first two levels ensure accurate scheduling, whereas the real-time level adapts according to residential demand, PV generation, network capacity and other technical constraints [96]. The study found that the accuracy of the forecasting techniques was the ultimate driven in economic feasibility and emphasis was placed on ensuring that forecasting should be done as accurately as possible.

3. Rule-based home EMS considering demand response application

   This study presents an intelligent rule-based technique to manage the power consumption of various appliances [97]. Ahmed et al. further incorporated a demand response feature into the control strategy [97]. The control system accepts the following inputs to determine the scheduling of the appliances: customer comfort level, preference setting and priority of appliance. The appliances that were considered for the study included an air conditioner, water heater (geyser), tumble dryer and electric vehicle. The proposed rules that were set-up are as follows:

   (a) Determine power rating
   (b) Identify user inputs (comfort, preference and priority)
   (c) Read demand response signal indicating the amount of load to shed
   (d) Calculate expected demand according to user settings. Readjust according to demand response signal within the user's requirements

   The study consisted of a simulation and found that it was an effective solution to manage the household power demand within an imposed demand limit.

4. Local energy management unit for residential applications

   The local energy management unit described by Romero et al., consisted of three primary goals [98]. The first one was to limit the demand exerted on the grid during peak times. This allowed the user to consume less energy off the grid [98]. The second goal was to ensure a constant power consumption rather than a large power swing. The third goal was to maintain the continuous power consumption under a reference limit. Based on the results from the experimental system, it was found that it is possible to maintain a constant power consumption and demand using a residential EMS [98].

5. Energy management strategy of a renewable-based residential microgrid

   This study proposed an energy management strategy for a residential microgrid which comprised of a PV system and small wind turbine. The microgrid was connected through a battery system to the utility grid to ensure power balance in the system [99]. The control strategy accepted inputs such as the battery SOC, the power at each microgrid node and load/renewable energy forecasts. The inputs allowed the control system to optimise battery usage and reduce power fluctuations due to switching loads. The control system was simulated and experimentally tested. The study showed that the power swing variability was reduced by up to 54.5% [99]. Energy consumption calculations were not calculated but is expected to also have a slight reduction.

2.8 Conclusion

The literature study provided background knowledge on distributed energy sources such as solar PV, wind etc. Further insight into control systems, integration technology and energy storage system associated with microgrids was gained. Finally, research studies conducted by peers in the field of energy management were discussed in the last section of Chapter 2. A great deal of insight was gained on how other studies addressed issues related to residential microgrids. All of these studies have enabled this study to progress to a design phase.

The design phase is structured into four main topics which move from project requirements into detail design. The first phase of the design contains the necessary project requirements, specifications and assumptions. After the scope of the project has been properly defined, a conceptual design follows which includes component specification and integration. Finally, a detailed design is done which specifies all the individual components' functionalities and applicability. The detail design then further specifies the detailed integration of each of the individual components. The fully integrated design is done comprehensively such that a simulation model can be built on the design. The conceptual and detail designs are discussed in the following chapter, namely Chapter 3.

Chapter 3: Design

3.1 Introduction

To ensure that the integrated system was designed properly, an assessment of the specifications and requirements was necessary. The integrated system design was divided into smaller subsystem designs which was assessed independently to ensure that the specifications and requirements were met. The project requirements is discussed in the first part of Chapter 3 and is followed by a conceptual and detail design of the energy and control system. During the design chapter various engineering decision-making processes and principles was followed to produce an integrated system design. Figure 3-1 provides an overview of the chapter's layout.

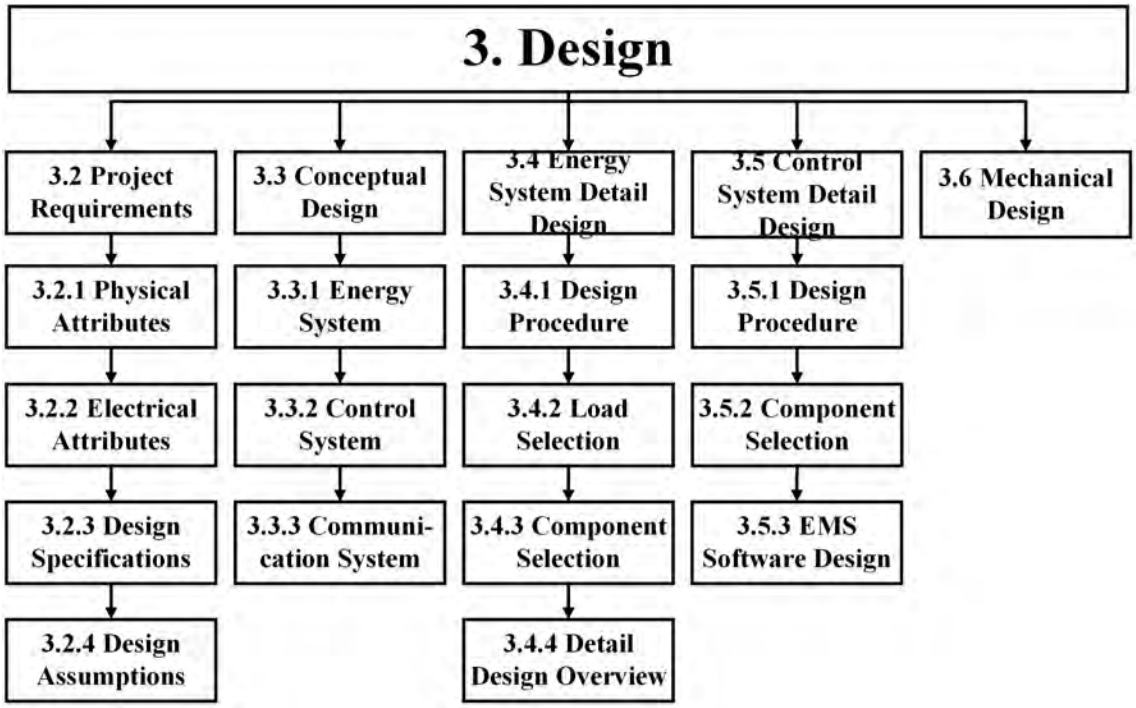

Figure 3-1: Structure of design chapter

3.2 Project Requirements

The project requirements section was divided into four categories namely physical and electrical attributes, design specifications and design assumptions. The project requirements were based on the NRS034-1:2007 standard which describes electricity consumption patterns of different income groups in South Africa, namely living standards measure (LSM). Within the NRS034-1:2007, the electricity demand and consumption profiles of the various income groups were described. This provided a guideline of which income groups were the most likely to implement a residential microgrid system. The classes ranged from the lowest income group (LSM 1) to the highest income group (LSM 10);

the groups were updated according to the latest published data and consumer price index (inflation). Table 3-1 illustrates the updated data of the NRS034-1:2007 standard.

Table 3-1: Classification of domestic consumers

Consumer Class	LSM Class	Income Range (Gross R/Month)
Rural settlement	LSM 1 (Low-end)	0 to 1 735
Rural village	LSM 1 and 2	1 735 to 2 456
Informal settlement	LSM 3 and 4	2 456 to 3 996
Township area	LSM 5 and 6	3 996 to 8 063
Urban residential I	LSM 7	8 063 to 13 059
Urban residential II	LSM 8	13 059 to 17 845
Urban complex	LSM 9	17 845 to 25 028
Urban multistory/estate	LSM 10	25 028 and higher

Analysis of the updated ranges and according to the South African Department of Energy, it was evident that the middle to high income classes (LSM 8 to LSM 10) were the most likely to implement a residential microgrid system [100]. Hence, for the study, the physical and electrical attributes were set-up according to the LSM 8 income group.

3.2.1 Physical Attributes

As mentioned above, the specifications of the study were set-up according to a modern middle to high income class (LSM 8) home. According to the South African Audience Research Foundation, a LSM group 8 residence had the following physical attributes [101]:

- Three Bedrooms, with the main bedroom having an en-suite bathroom
- Two Bathrooms, one independent and one en-suite
- One air conditioning unit and a swimming pool
- A kitchen with a built-in gas stove and oven with a laundry room fit for a washing machine and tumble dryer
- Two lock-up garages with a wall/fence enclosing the house

3.2.2 Electrical Attributes

The equivalent electrical attributes and appliances corresponding to the abovementioned physical attributes were as follows:

- One 3 kW (150 litre) geyser, with the geyser wired to supply the kitchen, laundry room and the bathrooms
- One 9 kg washing machine (0.55 kW) along with a 9 kg tumble dryer (2.2 kW)
- A swimming pool pump (0.55 kW)
- A standard two door refrigerator (0.25 kW)
- A standard dishwashing machine (1.8 kW)

A detailed residential floor plan that visually illustrates the characteristics described above is shown in figure 3-2 and is used as a reference to support the explanation of the specifications.

Figure 3-2: LSM class 8 home floor plan

3.2.3 Design Specifications

According to a study presented by Bokanga, Raji and Kahn (2014), a standalone DC microgrid for South African rural areas was designed and illustrated that a significant energy consumption reduction was possible by implementing low power LED DC lights [102]. The implementation of DC security lights were therefore included in the design specifications. The design specifications was drafted to establish what was needed in terms of technical design. The system specifications that were set are listed below:

- The residence should host a DC security light system that activates during night time and remains switched on for the duration of the night without interruptions. The DC light system should be used to provide light to the pool area and the rest of the yard. The maximum allowed instantaneous power consumption of the entire DC light system should not exceed 75 W
- Load control should only be exercised over continuous running loads which excludes indoor lighting
- The energy storage capacity should not exceed a capacity of 2 kWh
- The microgrid system should be used as a supplement to the available utility grid and not as a standalone system

3.2.4 Design Assumptions

The following design assumptions were made to narrow down the scope of the study:

- Residential customers were billed on a flat rate of R 1.85 per kWh. This corresponded to the Eskom HomePower Standard (>600 kWh per month) tariff structure

- The equipment that were connected to the grid, such as the GTI, complied to the grid-code at the PCC
- Inrush currents of the loads were disregarded and not factored into the EMS
- Lighting and other loads not mentioned above were disregarded.

3.3 Conceptual Design

The residential microgrid system was divided into the three sub-systems as illustrated in figure 3-3. The first sub-system, namely the energy system, solely consisted of hardware and was responsible for the physical connection between the DER, GTI, ESS, charge controller and loads. The communication and control sub-systems operated alongside each other to manage the hardware as efficiently as possible. The control and communication sub-systems consisted of both hardware and software. More detailed descriptions of the conceptual design is discussed in following sections.

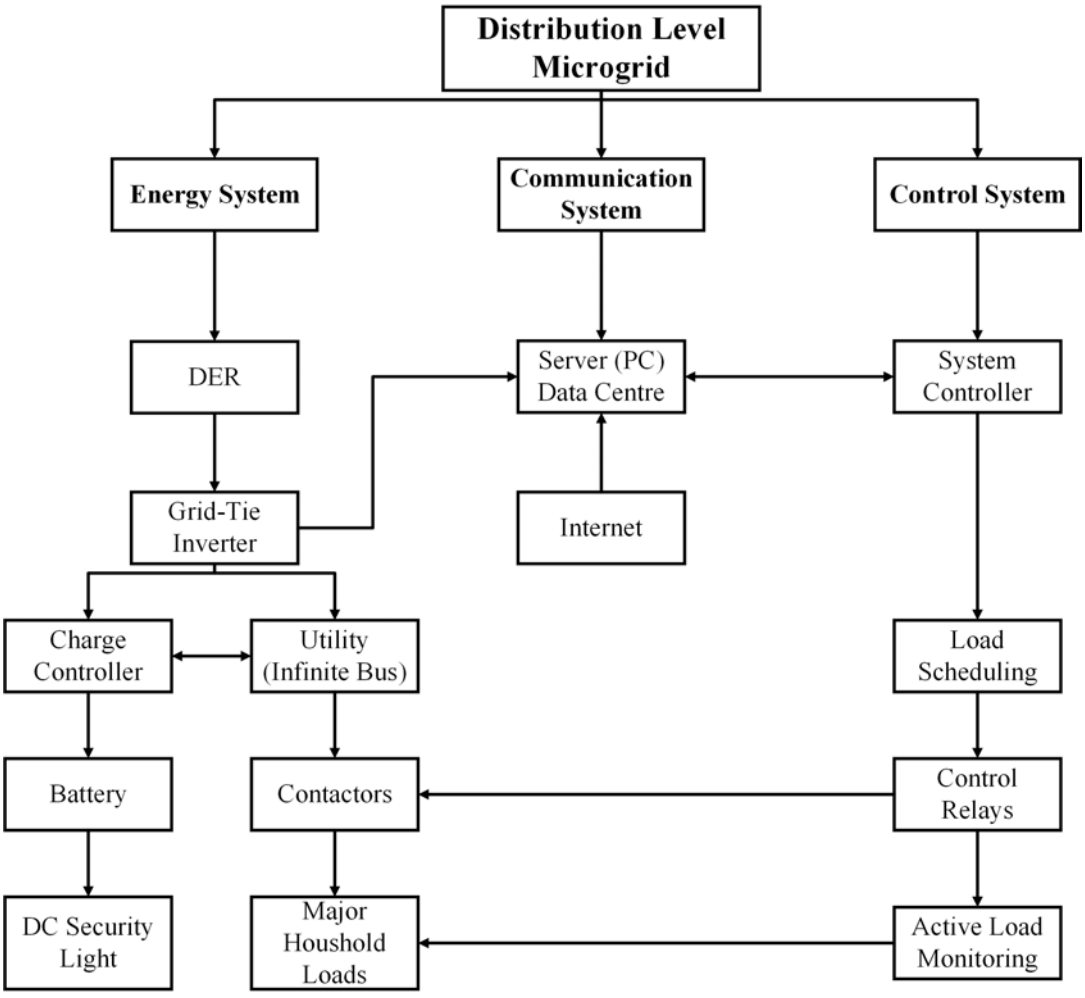

Figure 3-3: Conceptual design

3.3.1 Energy System

The energy system associated with the residential microgrid system was a combination of a DC security light system, DER, GTI and controllable household loads. The selection

of the abovementioned components are evident from the detail design section introduced later in this chapter. As can be seen in figure 3-3, the objective of the energy system was to integrate the DER, GTI, battery and other hardware into a topology that could be connected with each other and the utility. A basic diagram that describes the microgrid's interconnection to the utility is shown in figure 3-4.

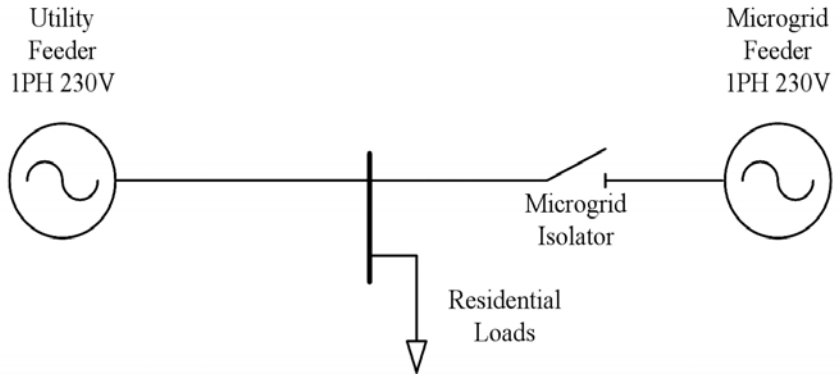

Figure 3-4: Basic single line diagram of microgrid and utility integration

The DER was connected via the GTI to the utility grid such that energy generated by the DER could supply the loads connected in the residence. To actively control the loads in the residence, it was essential that electronically controllable switches, such as contactors or relays were installed in series with the loads that needed to be controlled. By doing so, full control could be exercised over which loads are connected/disconnected to/from the utility and microgrid. Figure 3-5 illustrates the integrated energy system concept along with how the DC security light system fitted into the energy system.

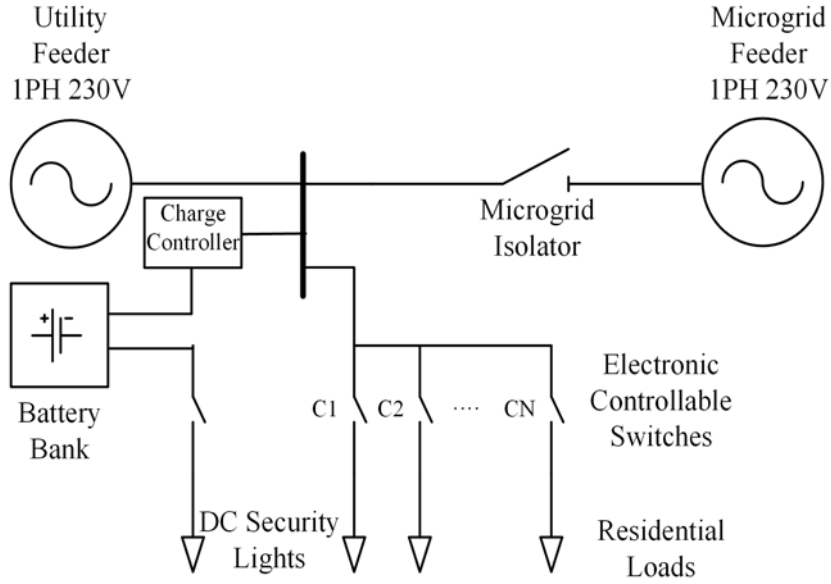

Figure 3-5: Microgrid grid integration and load control

3.3.2 Control System

The control system made use of multiple control strategies which was based on short and long-term inputs. Primarily, for the short-term inputs, the control system ensured that as

much as possible of the energy generated by the DER was consumed locally and power consumption off the grid was minimised. In the case where power generation exceeded power consumption, more loads were switched on to reduce the excess energy. The state-of-charge (SOC) of the battery was also fed to the system controller that aided in the decision-making processes regarding the DC security light system.

Long-term inputs included daily expected energy, weather patterns and user priority settings. The main purpose of the long-term inputs was to further ensure the optimising of the energy usage within the system. The control system made use of these inputs to schedule the loads at times which would ensure maximum local consumption. A summary of the short and long-term inputs that were used are shown in figure 3-6.

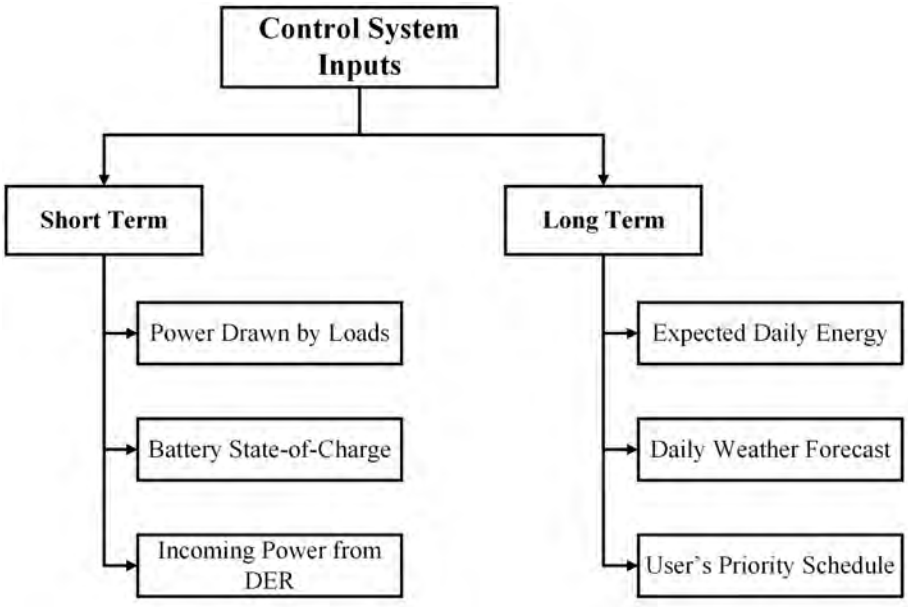

Figure 3-6: Summary of short and long-term inputs to the control system

3.3.3 Communication System

The communication system was used to ensure that short and long-term data are communicated and synchronised across the microgrid system. The short-term control strategy communicated the current drawn by the loads, battery SOC and incoming power from the DER through the network to a centralised server. This allowed the server to analyse the received measurements, create an energy consumption profile and alter the short-term control strategy to balance incoming power with the power drawn by the loads.

Further objectives of the communication system was to obtain weather predictions from an internet RSS feed, accepting user inputs and storing all relevant information in a MySQL database for further analysis. The communication system's topology is illustrated in figure 3-7.

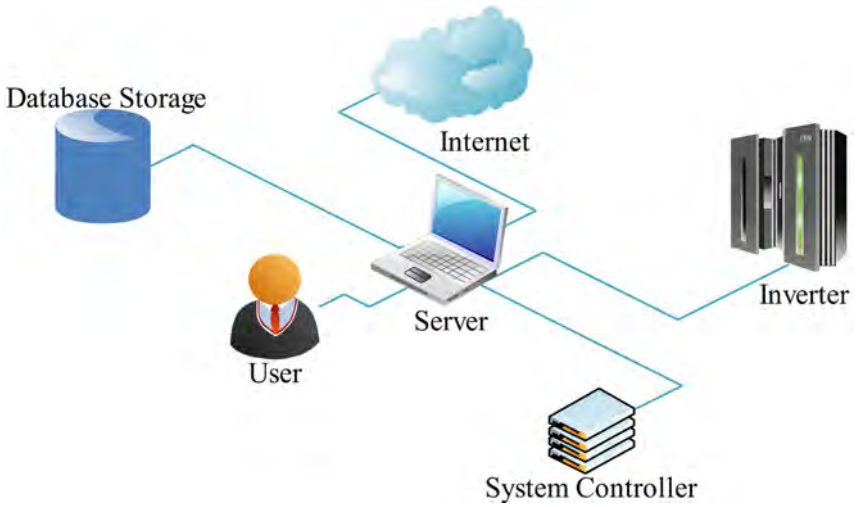

Figure 3-7: Communication system topology

3.4 Energy System Detail Design

3.4.1 Energy System Design Procedure

The energy system design procedure was the logical procedure followed to ensure proper engineering detail design of the energy system. The procedure is described below to provide insight into the energy system detail design.

- The first approach that was taken towards the energy system design was to determine which loads had to be controlled by the control system. Research on previous residential energy saving studies along with evaluation of the project requirements, a decision was made to which loads should be managed to minimise power consumption off the grid and maximise energy savings.
- Once the loads were selected, the power levels of the loads had to be established. The first step to determining the power levels was to consider the power ratings of the selected loads. This was obtained from the manufacturers' datasheets and nameplates for the selected loads. Hereafter, the current levels that would be present in the circuit was calculated to determine the protection grading that was required.
- With knowledge of the power and current levels of the loads, detailed component selection commenced. The major components in the energy system design included the DER, GTI and DC security light system. The detailed component selection of the abovementioned components are discussed in the sections below. The DC light system was an independent design due to the separate low voltage source and loads.

3.4.2 Selected Loads

As mentioned in the design procedure above, it was essential to have adequate knowledge on the loads that could be effectively managed to maximise savings. Therefore, the following section contains research on energy saving and power consumption of loads in a residence.

3.4.2.1 Geyser Energy Saving

Geysers are cylindrical insulated water tanks that are used to heat the incoming cold water to a temperature that is suitable for use within a household. A geyser consists of a heating element and thermostat with a controllable switch. The thermostat is set to a desired temperature. When the water temperature is below the set point, the switch is closed and the geyser element is switched on. The heating element's power ratings are in the range of 3 kW for a 150 litre tank and 4 kW for a 200 litre unit [103]. Once the water is heated to the desired temperature, the switch opens and the geyser element is switched off. Power consumption within an electric geyser is consumed in one of two ways [104]:

- When hot water is used, water is drawn from the geyser into the pipes which then needs to be replaced with cold water. The mixture of hot and cold water causes the geyser's temperature to stabilise well below the desired temperature. This causes the heating element to be switched on.
- When the geyser temperature drops as a result of the temperature difference between the ambient air and the geyser's tank temperature. This is known as standing losses. The greater the difference, the greater the heat loss. This causes the geyser to switch on and off periodically to maintain the geyser temperature. Figure 3-8 illustrates the concept of standing losses. This figure is based on the assumption that no hot water is drawn from the geyser.

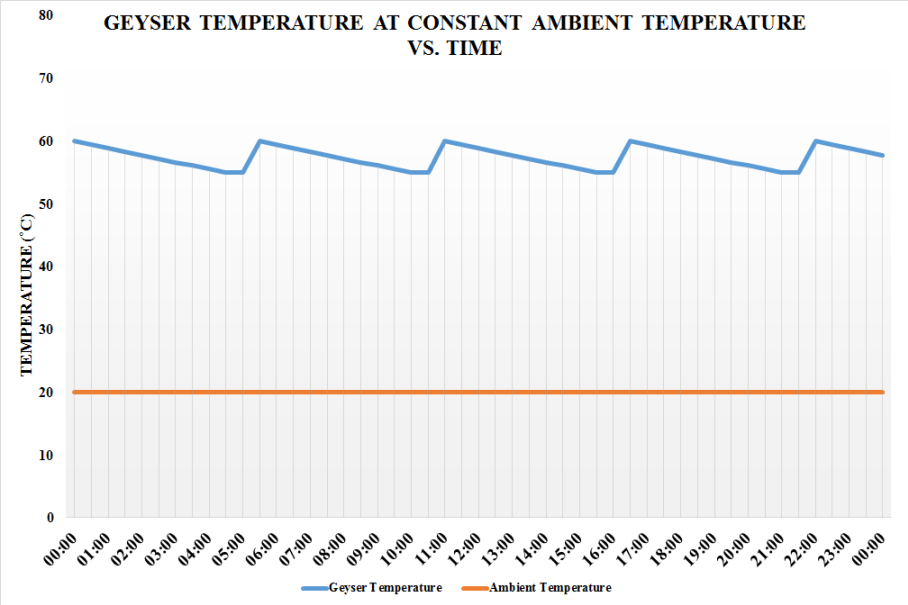

Figure 3-8: Geyser temperature at constant ambient temperature

According to experimental data collected by Catherine et al. (2012), standing losses can vary from 1.012 to 2.531 kWh/day which equates to a cost of at least R 56.16 per month (R 1.85 per kWh) [105]. Therefore, by eliminating standing geyser losses, significant monthly savings can be achieved. Table 3-2 illustrates typical saving that can be achieved if standing losses were to be eliminated.

Table 3-2: Summary of geyser standby losses

Description	kWh/month	Cost (R)/month
Standing losses	30.3-75.9 kWh	R 56.16-R 140.42

3.4.2.2 Swimming Pool Energy Saving

There are numerous energy-efficient swimming pool pumps available on the market designed to reduce energy consumption. However, these high efficiency pumps often require a significant initial investment. An alternative energy saving incentive that can be implemented, is to reduce the running time of the swimming pool pump. On average, swimming pool pumps run the filtration system for a period of roughly 10 hours per day (8 AM to 6 PM). Eskom studies suggests that if the swimming pool pump is correctly sized to the volume of the swimming pool, a runtime of 4-5 hours is sufficient for filtration and cleaning [16]. Assuming a 0.55 kW single speed swimming pool pump running for 10 hours per day will result in a monthly energy consumption of 165 kWh. Running the same motor for a total of 6 hours per day results in an energy consumption of 99 kWh per month, which is a 40% reduction. This translates to a saving of R 122.10 (R 1.85 per kWh) per month. Table 3-3 summarises the energy usage and savings potential.

Table 3-3: Summary of swimming pool energy consumption

Daily Runtime	kWh/month	Cost (R)/month
10 hours	165 kWh	R 305.25
6 Hours	99 kWh	R 183.15

3.4.2.3 Residential Energy Usage

In a study presented by Harris, Kilfoil and Uken (2008), it was found that the electricity consumption within a typical South African household can be disseminated down as shown in figure 3-9 [106].

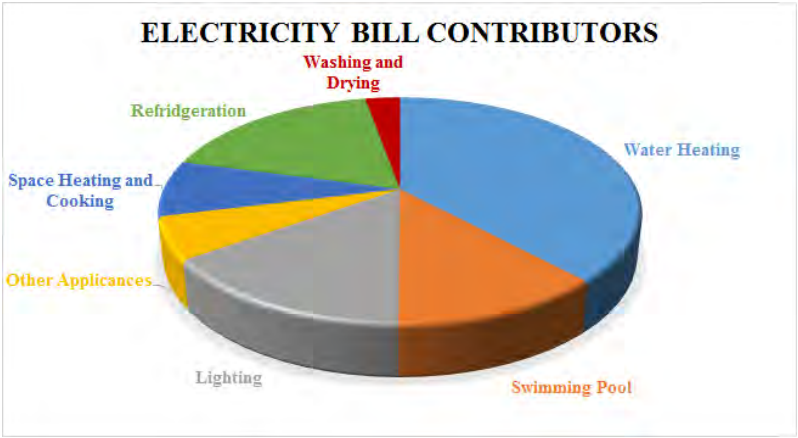

Figure 3-9: Major electricity bill contributors in a home

As expected the majority of electricity consumption within a residence are due to loads running on a continuous basis such as the geyser, refrigerators, swimming pool pumps etc. Based on this known fact, by actively controlling the continuously running loads and other residential loads such as the washing machine, tumble dryer and night-time security lighting, significant energy savings can be achieved. Therefore, the loads selected that were selected to be actively controlled are shown in table 3-4.

3.4.2.4 Load Current Levels

The current draw of the loads was calculated by using the rated power, voltage and power factor. These calculations were sufficient for residential circuit protection purposes. The continuous current level calculations was used for protection purposes are also included in the table and is calculated using eq. (3.1).

$$I = \frac{P}{V \cdot \theta} \tag{3.1}$$

Where P represents the power rating of the load and θ is the load's power factor. The calculated load current draw is calculated in table 3-4.

Table 3-4: Load power levels

Appliance	Power Rating (W)	Voltage Rating (V)	Power Factor (Approx.)	Current Draw (A)
Geyser	3 kW	220-240 V	1.0	12.5-13.6 A
Swimming Pool Pump	0.55 kW	220-240 V	0.8	2.9-3.1 A
Washing Machine and Tumble Dryer	0.55/2.2 kW	220-240 V	0.8	3.1-12.5 A
Battery Charger	0.25 kW	220-240 V	0.95	1.1-1.2 A
Dishwashing Machine	1.8 kW	220-240 V	0.8	9.4-10.2 A
Refrigerator	0.25 kW	220-240 V	0.8	1.5-1.7 A

3.4.2.5 Circuit Breaker Sizing

Successfully grading a circuit breaker for protection purposes requires knowledge of the load connected to it. The information presented in table 3-4 could therefore be used to calculate the circuit breaker requirements. The minimum current breaking capacity of the circuit breaker was calculated by using eq. (3.2). The formula took into account the safety design factor and inrush current.

$$I = \frac{P}{V \cdot \theta} \cdot \kappa \cdot \varsigma \tag{3.2}$$

Where P represents the power rating of the load, θ is the load's power factor, ς is the safety design factor and κ is the inrush current factor. According to eq. (3.2), the following circuit breakers were required as shown in table 3-5. It is important to note that the current draw for the refrigerator and battery charger were very low compared to the rating of the circuit breaker. This introduces various problems that are not discussed here. To counter these, the refrigerator was connected to the geyser's circuit breaker and the battery charger and system controller were connected on the same circuit breaker.

3.4.3 Energy System Component Selection

3.4.3.1 Distributed Energy Resource

The test location, shown in figure 3-10b, was in the town of Potchefstroom in the North-West Province of South Africa. The annual solar irradiation and average wind speed

Table 3-5: Circuit breaker specification

Appliance	Load Current (A)	Design Factor (%)	Inrush Current Factor	Required CB (A)	Standard Sized CB (A)
Geyser	13.6 A	20	1 x FLA	16.32 A	25 A
Swimming Pool Pump	3.1 A	20	4 x FLA	14.88 A	16 A
Washing Machine and Tumble Dryer	12.5 A	20	2 x FLA	30.00 A	30 A
Battery Charger	1.2 A	20	1.5 x FLA	2.16 A	*16 A
Dishwasher	10.2 A	20	2 x FLA	24.48 A	25A
Refrigerator	1.7 A	20	2 x FLA	4.08 A	*25 A

across Southern Africa is presented in the figures 3-10a and 3-10c [40], [45]. Taking the information presented in these graphs into account, an informed decision regarding the most appropriate source of energy could be made.

(a) Solar resource [45] (b) Location of test site (c) Wind resource [40]

Figure 3-10: Maps of Southern Africa's solar and wind resources

By evaluating figures 3-10a and 3-10b, it could be seen that the annual solar irradiation for the test site location was between 2000 and 2200 kWh/m^2. This was an above-average solar irradiation compared to most parts of South Africa. As opposed to the solar irradiation level, the mean wind speed at the test location (6 m/s) was below-average and would yield very little energy in the case of a WTG. Hence, the testing site could be fully utilised by implementing a solar PV system as DER.

Table 3-6 shows technical characteristics of three solar PV panel models that would be adequate for the intended application [107]. There were many other solar PV panels available on the market, however those listed in table 3-6 were available from local suppliers that could be supplied within the designated timespan and budget. The nature of this study was primarily research based and therefore the main driver of component selection was the cost of the components. Hence the use of local manufacturers and the low-cost solar PV panels came into play. All the solar PV panels listed in table 3-6 were technically adequate for the purpose of testing and within the predetermined budget. Two of the models were of the polycrystalline type and one was of the thin-film type.

Table 3-6: Solar panel comparison [107]

Manufacturer	Model	Maximum Efficiency (%)	Power Rating (W)	Open Circuit Voltage (V)	Short Circuit Current (A)	Module Type
Sunmodule	SW-180	15.3%	180 W	44.4 V	5.4 A	Poly-crystalline
Solar Frontier	SF-165-S	13.4%	165 W	110.0 V	2.2 A	Thin-film
Omnipower	60-245/3B	16.2%	245 W	37.5 V	8.8 A	Poly-crystalline

Thin-film solar PV panels are manufactured in a low-cost manner which reduces performance characteristics such as efficiency and operating lifetime. This is seen as the Solar Frontier solar PV panels offer an efficiency of 13.4% compared to the 15.3% and 16.2% offered by the polycrystalline panels. However, for the purpose of this study, these performance characteristics was disregarded as the slightly higher efficiency significantly increased the cost. The cost of the Solar Frontier thin-film panel totalled to R12.90/W as opposed to R14.12/W for the polycrystalline cells.

Another advantage of the Solar Frontier thin-film panel was the high open-circuit voltage (110.0 V) and low short-circuit current (2.2 A). This reduced the voltage drop across the wiring from the solar PV panels to the GTI. Hence, the combination of low cost along with low line losses provided enough reason to choose the Solar Frontier SF-165-S thin-film solar PV panels for the study. Figure 3-11a provides an image of the chosen solar PV panels along with its I-V performance curve which shown in figure 3-11b. The complete technical datasheet of the Solar Frontier SF-165-S is added on the DVD (Appendix C).

(a) SF-165 solar panel

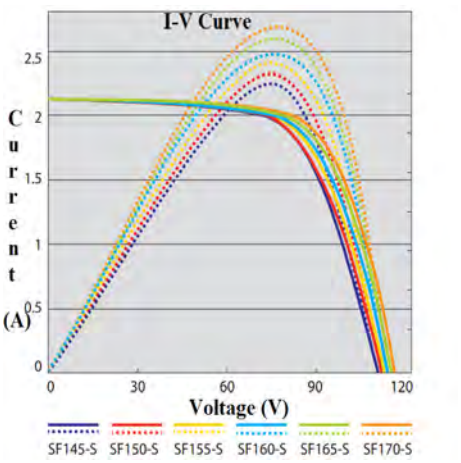

(b) SF-165 I-V curve

Figure 3-11: Solar Frontier SF-165-S [107]

3.4.3.2 Grid-Tie Inverter

As mentioned above, only local suppliers whom could deliver components at the lowest possible cost and within the specific timespan were considered. There were three GTIs

that cleared this criteria and are shown in figure 3-12 below [108], [109], [110].

(a) Kaco Powador 2002 [108] (b) SMA Sunnyboy [109] (c) Steca Coolcept [110]

Figure 3-12: Grid-tie inverters

The GTIs shown in the figures above were all manufactured by market leading companies whom guaranteed that the GTIs passed the criteria for integration with the South African grid code as explained in Chapter 2. Further technical aspects such as efficiency, input voltage range, inverter power rating and possible communication protocols are shown in table 3-7 [108], [109], [110].

Table 3-7: Grid-tie inverter comparison [108], [109], [110]

Manu-facturer	**Model**	**Maximum Efficiency (%)**	**Power Rating (kW)**	**Input Voltage Range (V)**	**IP Rating**	**Comm. Protocols**
Kaco	Powador 2002	95.9%	1.65 kW	125-510 V	IP54	RS-232 RS-485
SMA	Sunnyboy 3000TL	97.0%	3.2 kW	175-500 V	IP65	RS-232 RS-485 Bluetooth
Steca	Coolcept	98.6%	1.85 kW	160-500 V	IP21	RS-232 RS-485 Ethernet

The most critical specifications which ultimately determines the most suitable GTI are shown in table 3-7. By evaluating the inverters' efficiency it could be seen that the GTIs fell within a very narrow band ranging from 95.9% to 98.6%. Based on these efficiencies any of the three GTIs were adequate since there were very little difference. The power rating of the GTIs was one of the components that primarily increased the cost of the inverter. For the study to be thoroughly tested, the use of a 2 kW inverter was adequate. Hence, to keep costs to a minimum the SMA Sunnyboy 3000TL was disregarded.

The input voltage range stated in table 3-7 refers to the voltage range of the GTI's MPPT controller. Since fluctuating weather conditions influence the voltage of the solar PV panels, a wide MPPT voltage range would permit energy conversion from the solar PV panels to the loads. The MPPT voltage range of the Kaco Powador 2002 slightly exceeded that

of the Steca Coolcept. The Kaco Powador permitted a voltage swing of 385 V as opposed to the Steca Coolcept's voltage swing of 340 V.

The IP rating of both units were sufficient as the installation was indoors in a low-dust and low-humidity environment. As for the communication protocols, both GTIs had serial (RS-232 and RS-485) communication interfaces which were sufficient. It can be seen that both inverters were adequate for the task at hand, however, the main driver of component selection still remained cost. The Kaco Powador 2002 was readily available at the university's laboratory and would not incur in any costs. The Kaco Powador 2002 was therefore selected as the GTI for the study. The datasheet of the Kaco Powador GTI 2002 is added on the DVD (Appendix C).

3.4.3.3 DC Light System

Security Lighting
In order to choose a lighting system that would be sufficient as night time security lights, factors such as the size of the yard, required luminosity and power consumption were all factors that had to be taken into account. According to the specifications set out in section 3.2, the security light system was not allowed to exceed an instantaneous power consumption of more than 75 W.

Recent developments in lighting technology has lead to a wide range of possibilities in the security lighting industry. There are primarily four types of bulbs used for residential security lighting: LED, compact fluorescent lights (CFL), halogen and incandescent bulbs. Incandescent bulbs are phasing out of the market due to its inefficiencies. Governments around the world have started to ban the manufacturing of incandescent lamps to favour the adoption of low power LED and CFL lights [111]. LED lights are becoming more popular due to benefits such as longer lifespan, lower power consumption and high luminosity. However, LED lighting remain an expensive technology to adopt. CFL lighting is an acceptable alternative to LED lighting as it offers sufficient lifespan, similar power consumption and luminosity compared to LEDs. Halogen bulbs offer the benefit of very high luminosities at low cost but lack the low power consumption benefit of LED and CFL lights. Figures 3-13b to 3-13c shows the different bulbs used in floodlights.

(a) CFL floodlight (b) LED floodlight (c) Halogen floodlight

Figure 3-13: Floodlight designs

A comparison between the bulbs are shown in table 3-8. The table describes the relationship between the cost, luminous efficacy of radiation and lifespan of the three technolo-

gies. The selected lights shown in table 3-8 were selected to deliver a similar luminosity of a 60 W incandescent bulb.

Table 3-8: Comparison of LED, CFL and halogen lights

Bulb Type	**Cost (Est.)**	**Lifespan (Hrs. at 3 hrs/day)**	**Power Consumption (W)**	**Luminous efficacy of radiation (lm/W)**
LED	\$11.00 to \$22.00	15 000 to 25 000	9-12 W	62-69
CFL	\$1.50 to \$7.00	8 000 to 12 000	13-15 W	56-58
Halogen	\$1.00 to \$2.75	985 to 1 250	43 W	13-17

Comparing the information presented above, a decision regarding the most appropriate security bulb could be made. Bearing in mind the maximum power consumption design specification (75 W) and the number of zones that required lighting (four), the LED floodlights were the most appropriate technology. The LED floodlights offered the lowest power consumption at the highest luminous efficacy. The low power consumption permitted the use of a lower capacity battery to power the security lights. Therefore, for the four zones of lighting that were required, three LED floodlights of 10 W each and one 20 W LED floodlight were required. This yielded a total power consumption of 50 W that was to be supplied by the battery.

Battery Sizing

When performing the design and sizing of a battery system, it is important to know the continuous load requirement, hours of operation and the battery system voltage. Furthermore, factors such as depth-of-discharge (DOD), battery capacity reduction and the probability of a no-charging day should also be taken into account. The design specifications required that the battery system should be able to supply the 50 W DC security light system for a minimum of 10 hours and a maximum of 12 hours, depending on the season.

The selected system voltage as mentioned above was 12 V. Taking into account the above-mentioned design considerations, the depth of discharge of a battery can greatly influence the number of service years as shown in figure 3-14. The ideal design would be to choose a depth-of-discharge close to the knee of the curve shown in figure 3-14. According to figure 3-14, this represented a 30% DOD (only 30% of the battery's capacity is used) and would significantly increase initial investment costs. Therefore, the cycle depth design specification was set at a maximum DOD of 50% and translated to roughly 979 cycles.

The specifications set in section 3.2 required the DC security light system to operate every night and therefore the battery was charged everyday. This eliminated the probability that the battery might not be charged during the day and therefore this design consideration was neglected. The final design consideration that was taken into account was the percentage of available storage capacity which was primarily influenced by the ambient air temperature at which the battery operates. The graph illustrated in figure 3-15 shows the influence of ambient temperature on the available storage capacity of a battery [112].

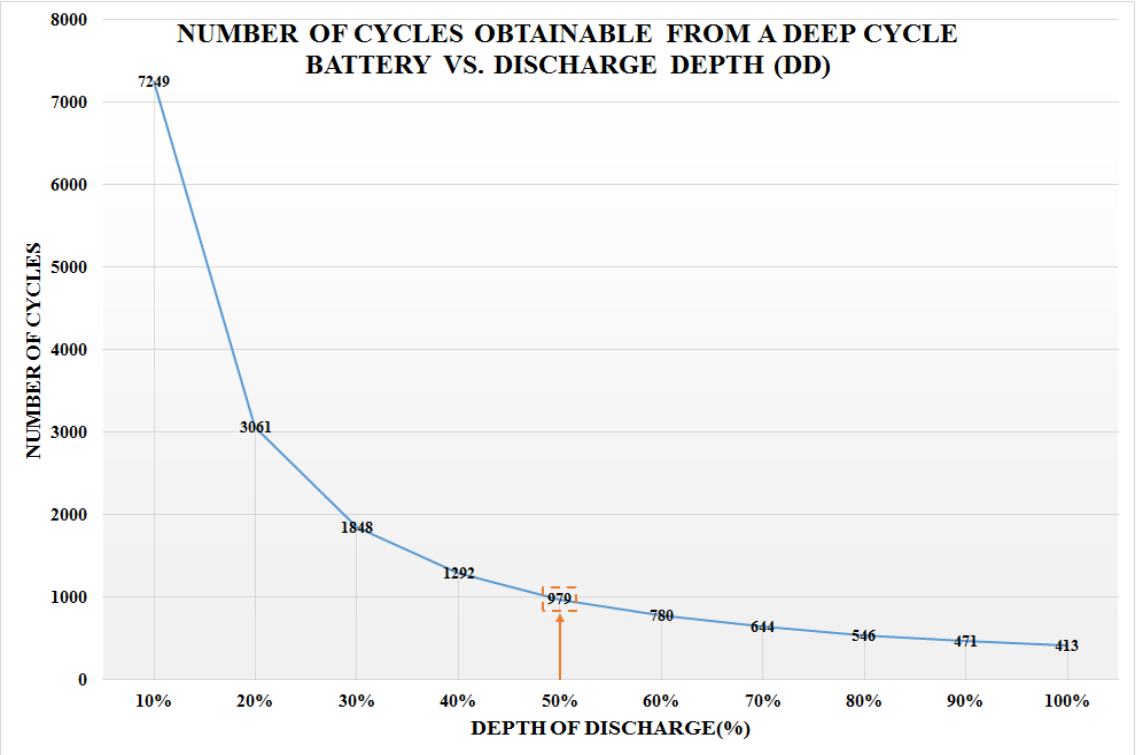

Figure 3-14: Number of cycles vs. DOD

The storage capacity of a battery declines as the ambient temperature decreases. The storage capacity of a battery is therefore at its lowest during the winter season and these conditions were considered when selecting a storage capacity reduction factor for the design.

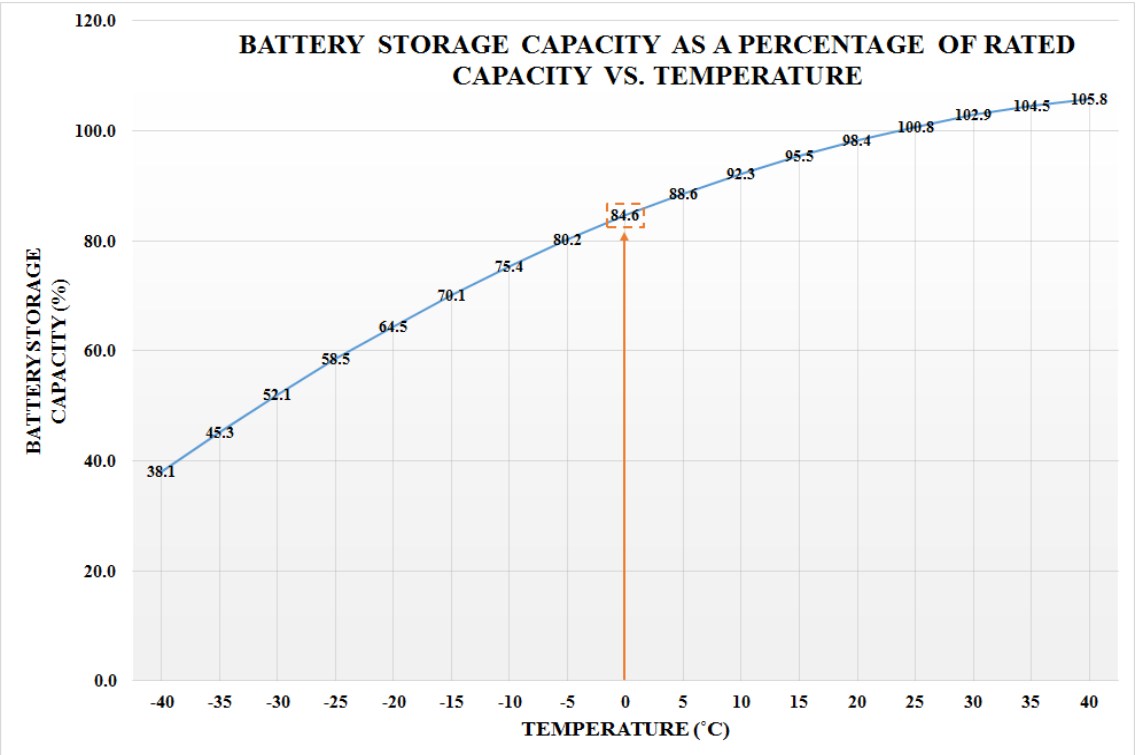

Figure 3-15: Battery storage capacity vs. ambient air temperature curve

Average winter temperatures vary greatly throughout the regions of South Africa; however the average winter temperatures for the town of Potchefstroom, where testing was conducted, are shown in figure 3-16 (data provided by the South African National Weather Service (SANWS)) [113].

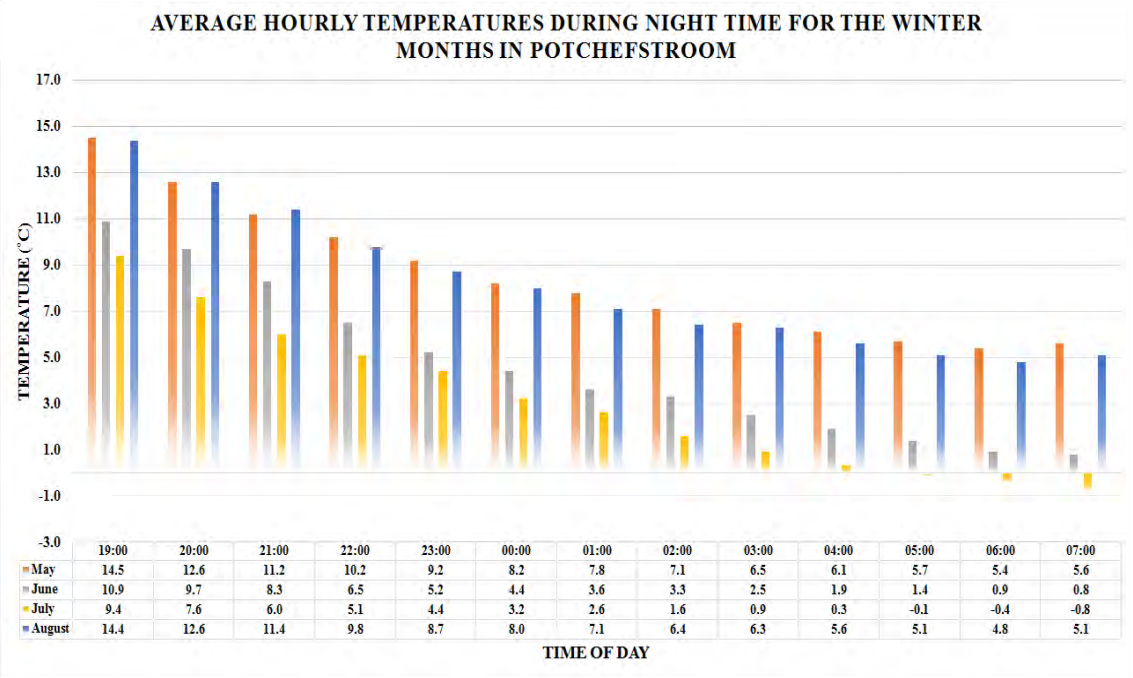

	19:00	20:00	21:00	22:00	23:00	00:00	01:00	02:00	03:00	04:00	05:00	06:00	07:00
May	14.5	12.6	11.2	10.2	9.2	8.2	7.8	7.1	6.5	6.1	5.7	5.4	5.6
June	10.9	9.7	8.3	6.5	5.2	4.4	3.6	3.3	2.5	1.9	1.4	0.9	0.8
July	9.4	7.6	6.0	5.1	4.4	3.2	2.6	1.6	0.9	0.3	-0.1	-0.4	-0.8
August	14.4	12.6	11.4	9.8	8.7	8.0	7.1	6.4	6.3	5.6	5.1	4.8	5.1

Figure 3-16: Average temperatures during the winter months in Potchefstroom [113]

By examination of the weather data, an assumption regarding the minimum average temperature during winter months was made. The majority of the temperatures during the night seldom dropped below 0°C, however a worst-case design approach was followed and therefore the design specification was set at 0°C. By analysing the curve shown in figure 3-15, it can be seen that at 0°C, a battery storage capacity reduction of 15.4% is applicable. A summary of the design specifications are shown in table 3-9.

Table 3-9: Summary of battery sizing specifications

Description	Design Specification
Load power consumption (W)	50 W
System voltage (V)	12 V
Hours of operation	12 hrs
Days without charging	0
DOD (%)	50%
Battery storage reduction factor (%)	15%

A battery's capacity rating is given in ampere-hours (Ah) and therefore the design requirements was calculated to match this unit. To calculate the required ampere-hour rating to meet the specifications set out in table 3-9, the formula shown in eq. (3.3) was applied.

$$Ah_{rating} = \frac{(P_{load})(T_{operation})}{(\gamma)(1-\eta)(V_{sys})(n+1)} \tag{3.3}$$

Where γ represents DOD, η represents the reduction factor and n implies days without charging. When applying eq. (3.3) for a wide range of capacity reduction factor and discharge depths, the following curves were obtained as shown in figure 3-17.

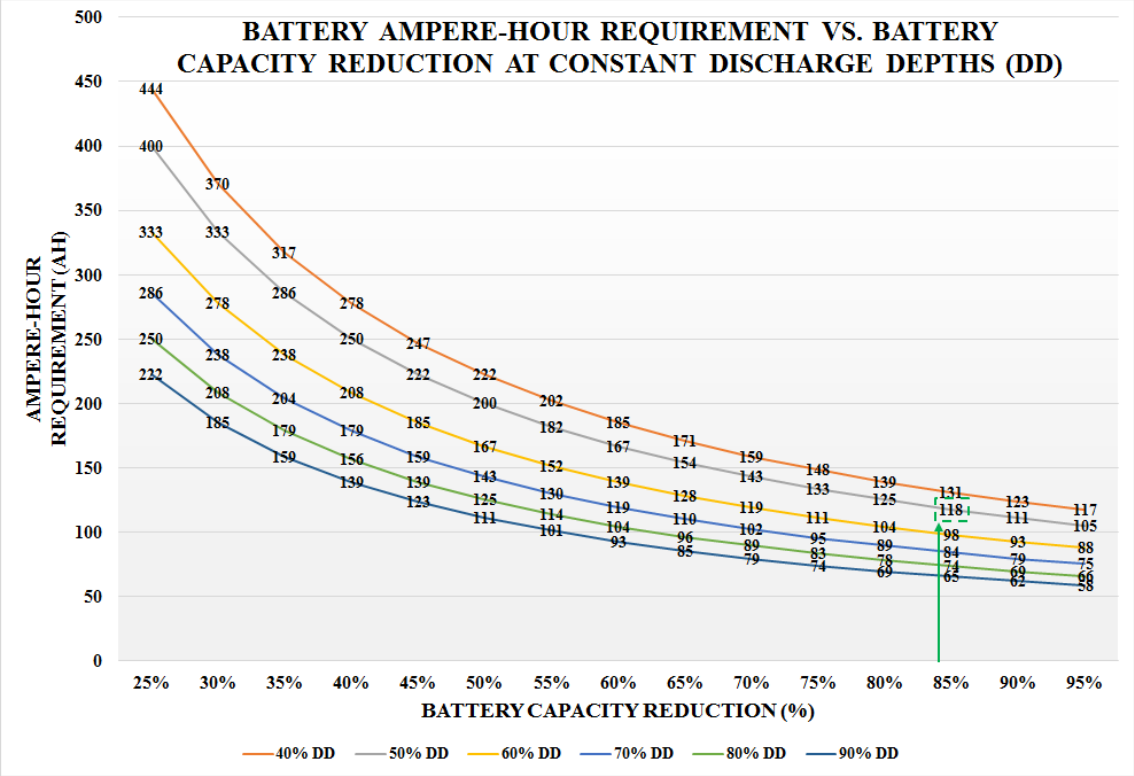

Figure 3-17: Battery ampere-hour requirement at various capacity reduction factors and discharge depths

By calculation and from figure 3-17, it can be seen that for a 50% capacity discharge and a 85% capacity reduction, a battery with a capacity rating of 118 Ah was adequate.

Battery Selection

The battery capacity rating determined in the preceding section was not a standard size and alterations on the design according to the suppliers' stock was needed. A list of available batteries according to the suppliers' stock lists are shown in table 3-10.

Table 3-10: Batteries available by suppliers

Manu-facturer	Battery Type	Capacity (Ah)	Nominal Voltage (V)	Operating Temp. (°C)	Weight (kg)
Royal	VRLC	102 Ah	12 V	-18 to +40°C	24.8 kg
Maximus	VRLA	105 Ah	12 V	-40 to +50°C	24.5 kg
Exide	VRLA	100 Ah	12 V	-40 to +50°C	24.1 kg

All of the listed batteries were very similar to one another and the only notable difference between these were the cost. All of these batteries were deep-cycle batteries available

from local suppliers. The Maximus 105 Ah battery was selected, based solely on cost, as the battery that supplied the DC light security system during night time. Since the Ah-rating was less than that of the recommended design calculations, it was necessary to check if the Ah-rating was sufficient. To ensure that the battery was sufficient, back substitution into eq. (3.3) was required. Reordering eq. (3.3) yielded a new equation namely eq. (3.4).

$$\gamma = \frac{(P_{load})(T_{operation})}{(Ah_{rating})(1-\eta)(V_{sys})(n+1)} \tag{3.4}$$

Applying eq. (3.4), the DOD of the battery equated to 56% which was still a sufficient number of life cycles according to figure 3-14. Figure 3-18 presents an image of the selected battery.

Figure 3-18: Maximus 105 Ah deep cycle battery

Battery Charge Controller

The battery charge controller was used to charge the battery throughout the day such that the battery could power the DC security lights during night-time. It was of critical importance that the charge controller fully recharged the battery before the end of the day. Failing to do so would have resulted in the DC security light system running out of power before it was supposed to. Charge controllers are rated on the input current rather than the output current and therefore special care was taken when selecting the charge controller.

After careful consideration of the controllers available from local suppliers, an appropriate controller was selected to ensure that the battery received adequate charge during the day. The ACDC Dynamics SLX20 charge controller was a 20 A, PWM-controlled charge controller. It accepted an input voltage range between 15 and 24 VDC and converted it to the optimal charging voltage. The charge controller is shown in figure 3-19 below.

Figure 3-19: ACDC Dynamic SLX20 charge controller

3.4.4 Energy System Detail Design Overview

The single line diagram of the energy system is shown in figure 3-20 and illustrates all the load circuit breakers (CB1 to CB5), current transformers (CT101 to CT105), meters (M1, M2), contactors (CR1 to CR6), loads and power sources. The interconnection of all the components are shown in figure 3-20. It should be noted that the auxiliary circuit breaker that powered the system controller are not shown on the diagram.

3.5 Control System Detail Design

3.5.1 Control System Design Procedure

The control system design procedure was the logical sequence followed to ensure proper engineering detail design of the control system. The procedure described below provided insight into the control system detail design.

- The first approach taken towards the control system design was to determine the components that were required to implement the control system. The two components that required selection was the system controller and current measurement device.
- The second and most important step was to determine the operation and logical sequence of the control system. The control system detail design required communication systems to be in place that allowed synchronised communication across the network along with the decision-making rules that the system controller needed to adopt.

3.5.2 Control System Component Selection

3.5.2.1 System Controller

The system controller was the most critical component of the study and special care was taken to ensure that the best possible system controller was selected. The requirements expected of the controller were in line with the components of figure 3-20 and the control system inputs shown in figure 3-6. As can be seen in figure 3-20, there were six contact relays (CR1-CR6) that operated at a voltage of 12 VDC, five current transformers (CT101-CT105) that measured the load current and one battery SOC meter (not shown on diagram). The load current drawn by the loads along with the incoming power from the GTI was communicated to/from the system controller at 10 second intervals. Therefore, the minimum specifications of the system controller were:

- 6 outputs to switch the load relays
- 6 analog inputs to read load currents from CTs and battery SOC
- High speed communication protocols to transfer load current and incoming power information

Controllers of different types (PLC, microcontroller and SBC) were under consideration as shown in table 3-11. All of the listed controllers were sufficient based on the expansion boards that were available for the specific controller.

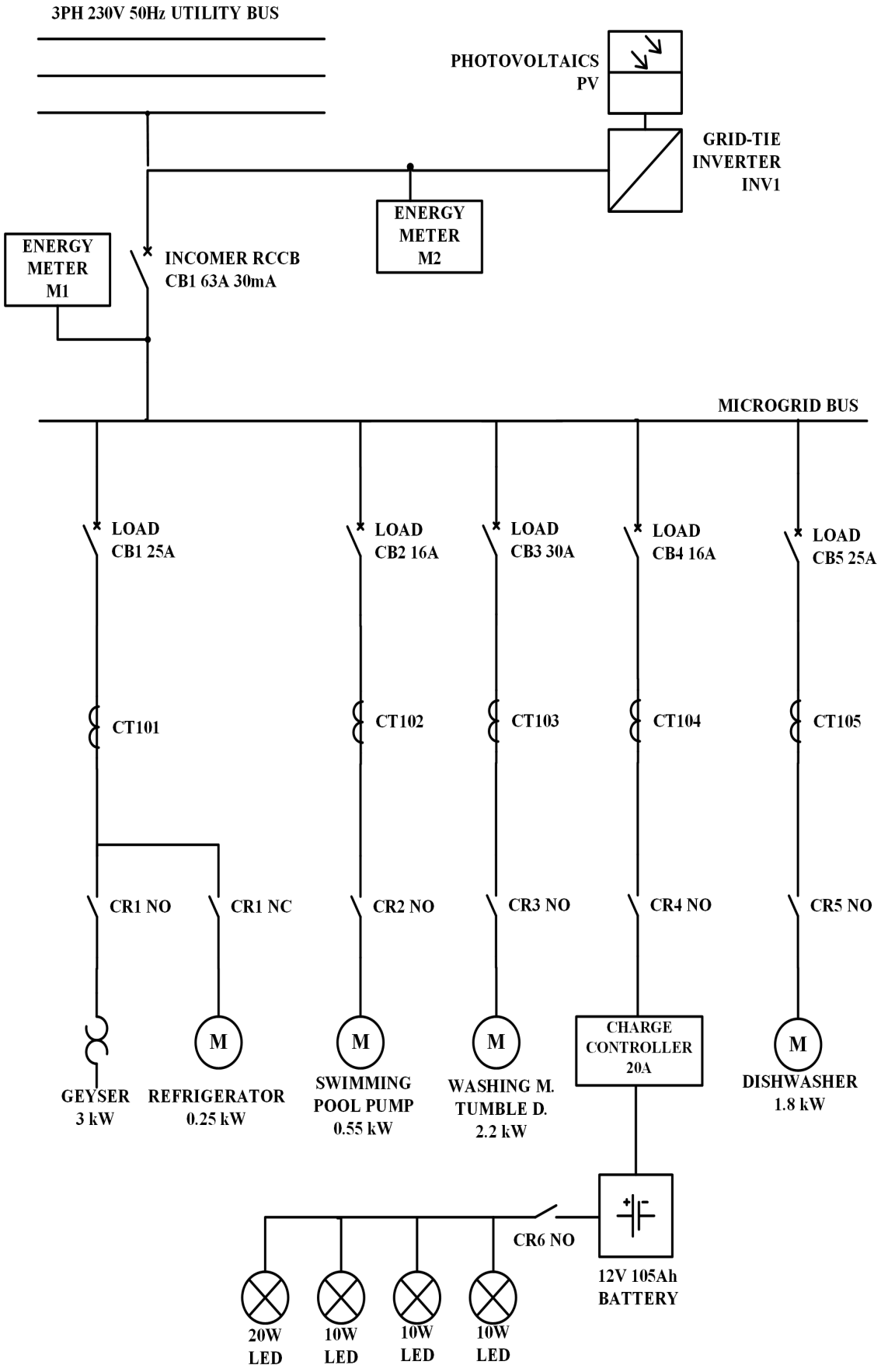

Figure 3-20: Energy system single line diagram

Table 3-11: Comparison of controllers

Manu-facturer	Model	Input Voltage (V)	Input Ports	Output Ports	Comm. Protocols	Data Memory
Siemens	S7-1200	85-264 VAC	2AI (0-10 V) 8DI (24 V) Expand.	6 Relays (3 A) Expand.	TCP UDP Expand.	50 KB
Allen Bradley	Micrologix 1100	240 VAC	10DI (24 V) Expand.	6 DO Expand.	TCP UDP Expand.	64 KB
Arduino	Mega2560	7-12 VDC	16AI /O (0-5 V) 54DI/O (5V) (Configured as input/output)		RS-232 Expand.	256 KB
Raspberry	Pi 2B	5 VDC	40GPIO (Configured as input/output)		TCP UDP RS-232 RS-485	1 GB

Only the market leading controller(s) of each type (PLC, microcontroller and SBC) were considered. This was due to the fact that adequate after sales support was required since implementation of the controller required performing non-standard tasks. The listed manufacturers all offered extensive after sales support and would be able to assist with technical problems. The input voltage of the Siemens and Allen Bradley PLCs were equal to voltage levels typically found in South African homes and therefore did not require any AC-DC converters to power the controller. The opposite was true for the Arduino® and Raspberry controllers which operated on low voltage DC power supplies and therefore required AC/DC converters to step down the voltage.

In terms of the input and output ports, the number of analog input (AI) ports had to be greater or equal than the number of ports listed in the requirements above. Both the PLCs could easily be expanded in terms of AI and output ports. The number of input ports on the Arduino® and Raspberry were sufficient but an additional expansion board was required to switch the 24 VDC relays. In terms of communication protocols, the PLCs had on-board ethernet ports with the option to expand to serial ports using additional expansion boards. Expansion boards for the Arduino® were also available which could easily be added to have ethernet capabilities. The Raspberry had both on-board ethernet and serial communication capabilities which eliminated the requirement to add expansion boards. It was possible to use any of the controllers as expansion boards enabled the controllers to meet all the requirements. Hence, a trade-off analysis was performed to determine the controller that would be used. Table 3-12 presents a practical evaluation rather than a technical evaluation of the controllers.
From table 3-12 it was evident that the Siemens S7-1200 PLC was the best suited system controller. The decision was mainly driven by the fact that the Siemens software, hardware and after sales support were superior compared to its competitors. The selection of the Siemens S7-1200 required an additional AI module to be added to meet the number of required AI ports. The Siemens AI module that was compatible with the Siemens

Table 3-12: Controllers trade-off analysis

		Evaluation Criteria							
		Cost	**Life Expectancy**	**Ease of Implementation**	**After Sales Support**	**Software Ease of Use**	**Robustness**	**Size**	**Score**
	Weight	0.15	0.2	0.2	0.1	0.2	0.1	0.05	**1**
Controllers	Siemens S7-1200	2	5	5	5	5	5	2	**4.4**
	Allen Bradley 1100	2	5	5	4	4	5	2	**4.1**
	Arduino Mega2560	5	3	4	5	5	2	5	**4.1**
	Raspberry PI 2B	4	3	3	4	2	2	5	**3.05**

S7-1200 series was the SM1231 AI module. This module had 8 AI ports with 13 bit resolution and could accurately read voltage levels ranging from -10 to 10 V and current levels 4-20 mA. Figure 3-21 shows the Siemens S7-1200 along with the SM1231 AI module. The technical datasheets of these devices are added on the DVD (Appendix C).

(a) Siemens S7-1200 CPU

(b) Siemens SM1231 AI module

Figure 3-21: Siemens S7-1200 CPU and SM1231 AI module [64]

3.5.2.2 Current Transformers

The current transformers (CTs) that were used in the study was for load current measurement purposes and was made available by the School of Electric, Electronic and Computer Engineering at the North-West University. Therefore, only an application design was required to ensure that the CTs were compatible with the Siemens SM1231 AI module. The performance curves obtained from the technical datasheet on the DVD (Appendix C) are shown in figure 3-22.
Only the linear part of the performance curve is shown since a CT should never be operated near the saturation region. The provided CT only started to saturate at a primary current above 30 A and was therefore adequate as a measurement device. According to

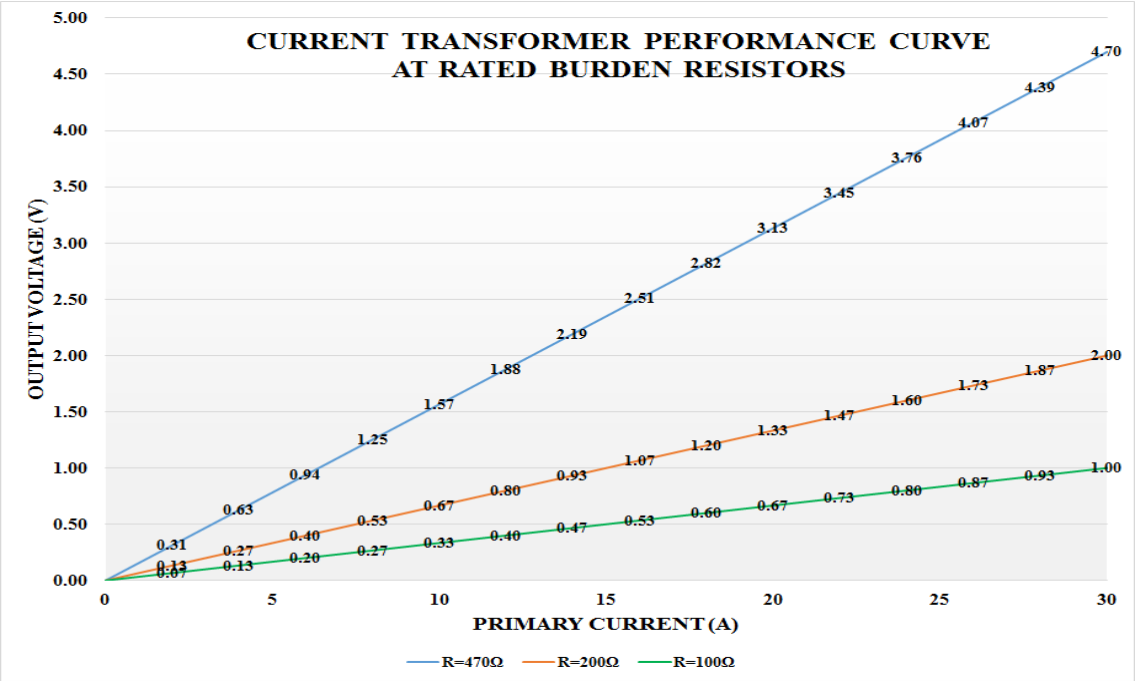

Figure 3-22: CT performance curve

the datasheet of the Siemens SM1231 AI signal module, a voltage swing of -10 to 10 V was allowed and therefore any of the burden resistors would deem adequate for measuring purposes. For practical purposes, a preference was placed on a higher swing voltage and therefore the highest possible burden resistor was selected, i.e. the 470Ω resistor. This provided a voltage swing of 0-5 V. To calculate the primary current from the output voltage, eq. (3.5) was applied.

$$I_p = \frac{V_o \cdot N_p}{R_b} \tag{3.5}$$

Where V_o represents the output voltage, N_p represents the number of primary turns (in this case 3000) and R_b represents the burden resistor value (in this case 470Ω).

3.5.3 EMS Software Design

The EMS software design is discussed according to the three phases in which it operated. The first phase was the initialising phase where all communication interfaces were set up to allow secure and reliable communication between the integrated system. After the initialising phase was completed and secure connections were made between components, the second phase started which required the user's daily requirements. Once the requirements were added, the server made a connection to the internet and downloaded the weather forecast for the day ahead. Based on these forecasts, the EMS made calculations to determine the best time to schedule the loads. These calculated times were then communicated to the PLC controller which set the timers to start the loads. The third phase was the continuous cycle where the PLC actively monitored which loads had to be switched on/off to maintain balance between solar PV generation and load consumption. During this phase, all the parameters were monitored and communicated back to the server for data storage. Figure 3-23 shows the flow diagram of the three phases along with the discussion thereof.

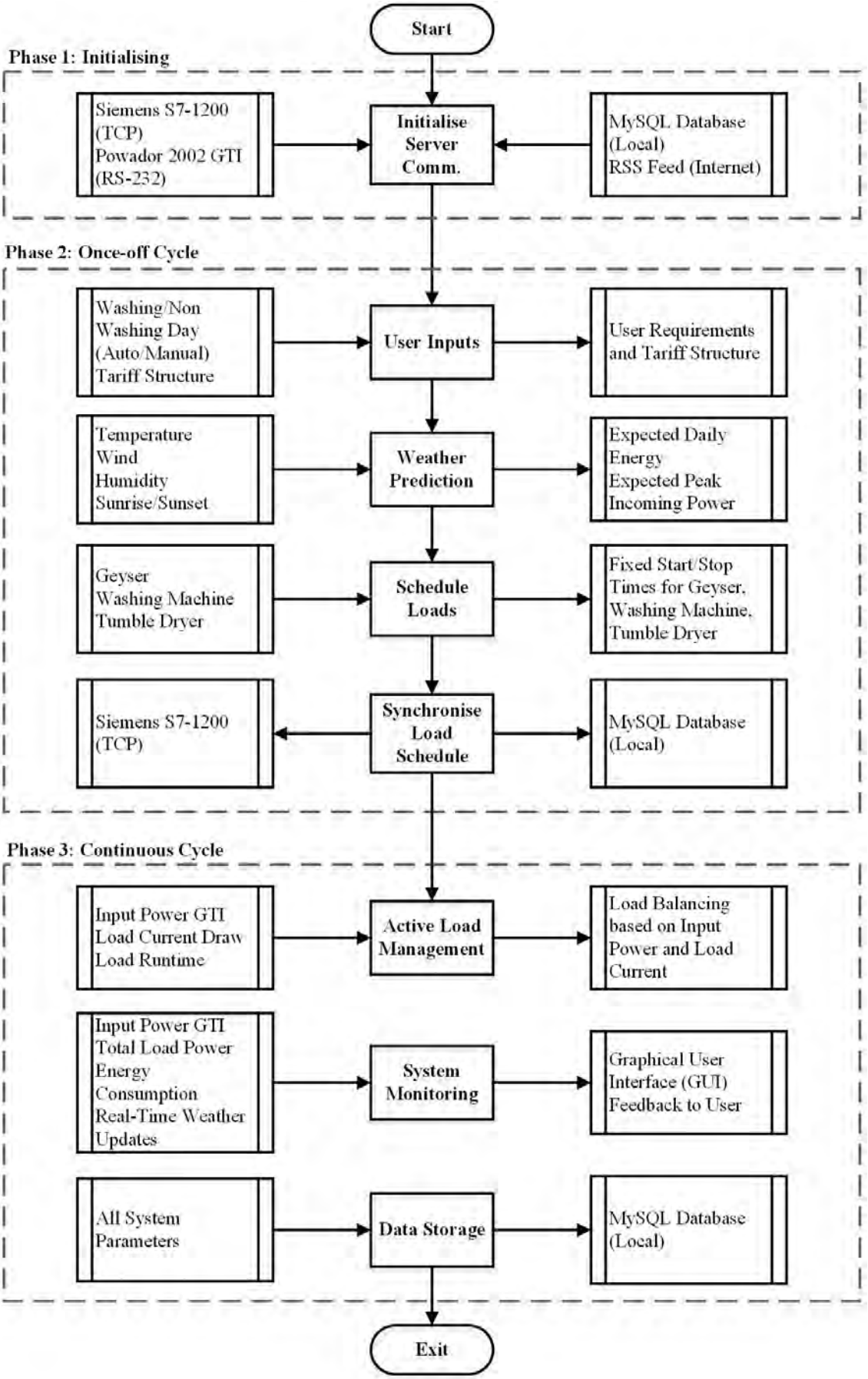

Figure 3-23: EMS flow diagram

3.5.3.1 Phase 1: Initialising

Each of the four communication systems used by the PLC, GTI and server is briefly discussed according the information presented in figure 3-24. The communication protocols that were used included RS-232, TCP/IP and a local database connection. Figure 3-24 visually illustrates the procedures that were followed to enable communication between the hardware and software systems.

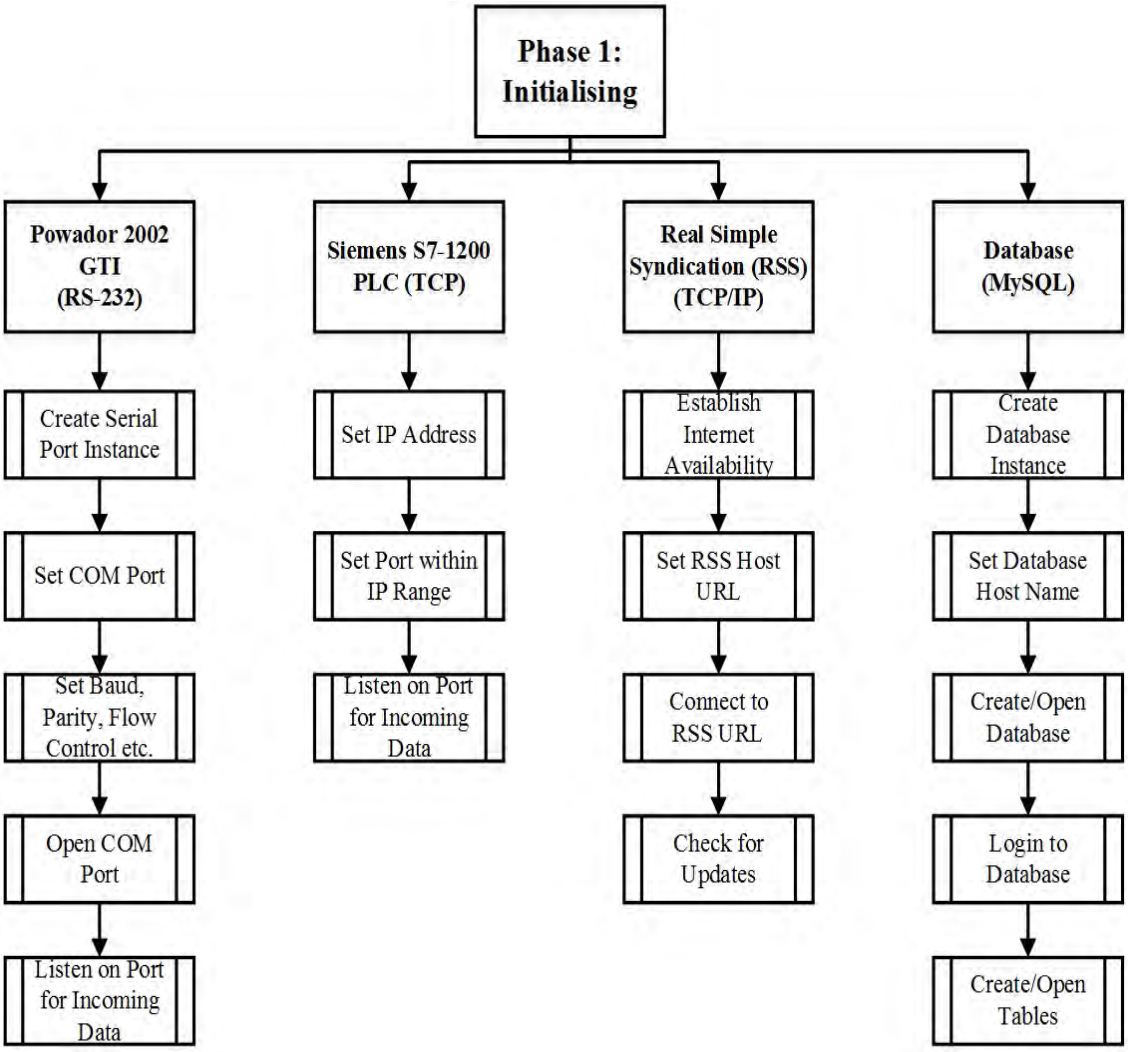

Figure 3-24: EMS phase 1

MySQL Database

The MySQL database was a critical part of the EMS software as it was used to store all the parameters of the integrated system such as the incoming power, load data, weather data etc. The EMS software had full access to the database whenever it was required and was therefore able to insert or extract data as required. The database had numerous tables which held all the data in a structured manner. The tables' columns were data type protected along with primary key ID allocated to prevent incorrect data being inserted into the fields. Incorrect data input into the tables would have caused critical errors and system faults. Figure 3-25 shows the database tables along with the field of each table.

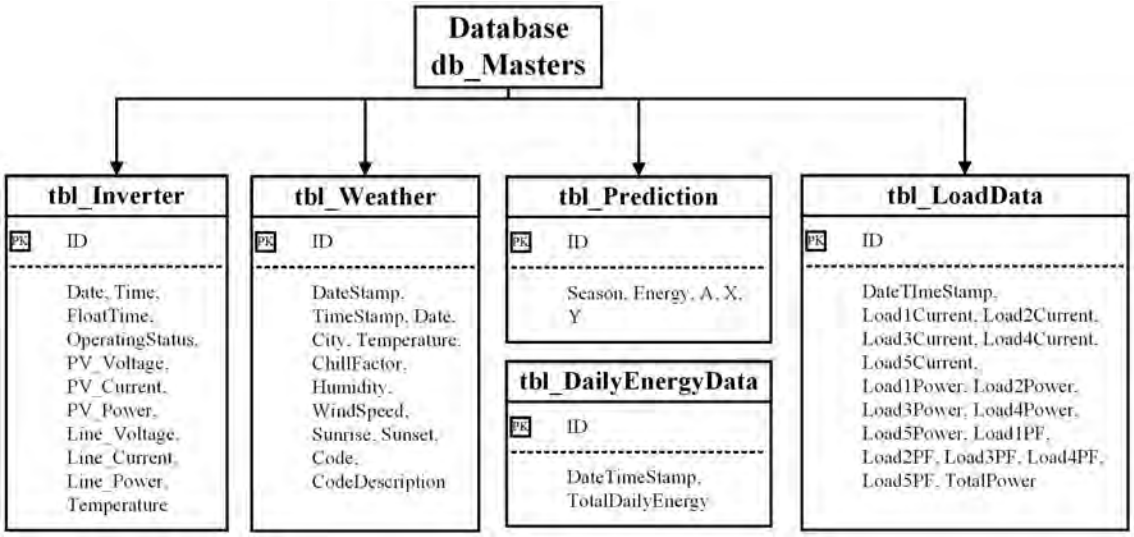

Figure 3-25: Structure of database and tables

Powador 2002 GTI

The manner in which the Powador 2002 GTI transmitted the measured parameters is shown in figure 3-26. The parameters were captured continuously with a routine update sent to the server every 10 seconds. The server was therefore set up to continuously listen and accept incoming connections from the GTI.

Column 1	2	3	4	5	6	7	8	9	10
00.00.0000	00:05:30	5	363.8	0.37	134	226.1	0.53	103	23
00.00.0000	00:05:40	5	366.0	0.39	142	226.1	0.53	112	23
00.00.0000	00:05:50	5	359.5	0.41	147	226.1	0.53	116	23
00.00.0000	00:06:00	5	369.8	0.42	155	226.1	0.58	118	23
00.00.0000	00:06:10	5	377.0	0.43	162	226.1	0.63	131	23
00.00.0000	00:06:20	5	373.6	0.45	168	226.1	0.63	133	23
00.00.0000	00:06:30	5	364.0	0.48	174	226.1	0.68	146	23
00.00.0000	00:06:40	5	364.3	0.49	178	226.1	0.68	146	23

Figure 3-26: Powador 2002 GTI serial data transmission log

The transmitted parameters were disseminated into columns as shown in figure 3-26. Each parameter was extracted separately from the incoming string and stored into the *tbl_Inverter* table for historic data analysis. The explanation of each parameter is shown in table 3-13.

Table 3-13: Explanation of transmission log

Column	Meaning	Column	Meaning
1	Place holder	6	Generator power in W
2	Daily running time	7	Line voltage in V
3	Operating state	8	Grid feed current in A
4	Generator voltage in V	9	Power fed into the grid in W
5	Generator current in A	10	Temperature of the unit in °C

Siemens S7-1200

The Siemens S7-1200 PLC was responsible to transmit real-time load data across the TCP

network at regular intervals (every 10 seconds). The PLC therefore accepted the role as the client and whenever data needed to be transmitted, a request was sent to the server which then acknowledged whether data could be transmitted. The server and the PLC were both set up to allow the transmission of data and minimise the risk of data loss.

RSS Feed

The RSS feeder was used to download the latest weather data for the test site location. This allowed the EMS software to make an approximation of the expected input energy and peak input power. This further enabled the EMS software to determine the time at which peak input power was available and to schedule the loads accordingly. It was therefore critical that the weather updates were as accurate as possible to prevent incorrectly scheduled loads. There were very few companies that provided accurate, up-to-date, and downloadable weather updates for the test site location. The best-known and trusted company offering this service was Yahoo® Weather. Full control over the information was permitted for nearly any location in the world. Therefore, the EMS software made use of Yahoo® Weather to obtain accurate weather data. An example of the Yahoo® Weather page for the test site location is shown in figure 3-27.

Figure 3-27: Yahoo® weather page for test site location

3.5.3.2 Phase 2: Once-off Cycle

The second phase that the EMS software went through was performed once in a 24-hour cycle and made use of the user's requirements and weather data to schedule some of the loads according to the estimated solar PV input profile. Figure 3-28 shows the four parts of the second phase.

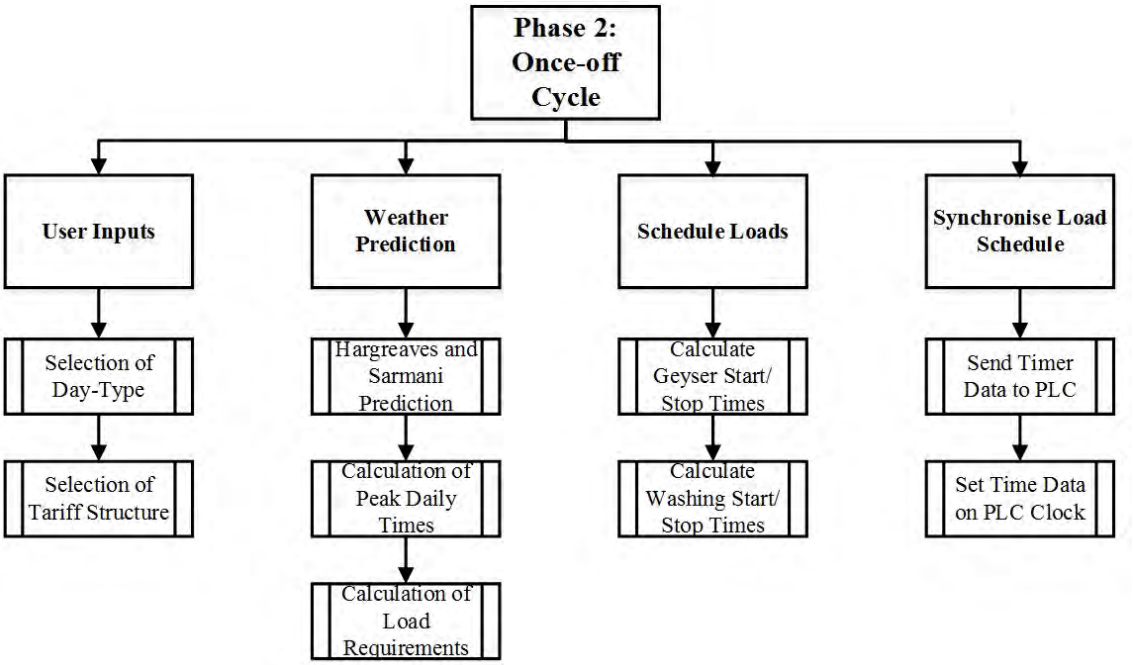

Figure 3-28: EMS phase 2

User Inputs

The user input cycle required the user to select between two types of days any LSM 8 household goes through namely a laundry day and a normal non-laundry day. During a laundry day, the washing machine and tumble dryer were switched on whereas on normal non-laundry days these loads were disregarded. A further option was available on a laundry day which allowed the user to manually select the time at which the washing should start. If no manual time was selected, the system automatically calculated the optimal time to switch on these appliances according to the estimated solar PV input profile. A screenshot of the user input section of the EMS software is shown in figure 3-29.

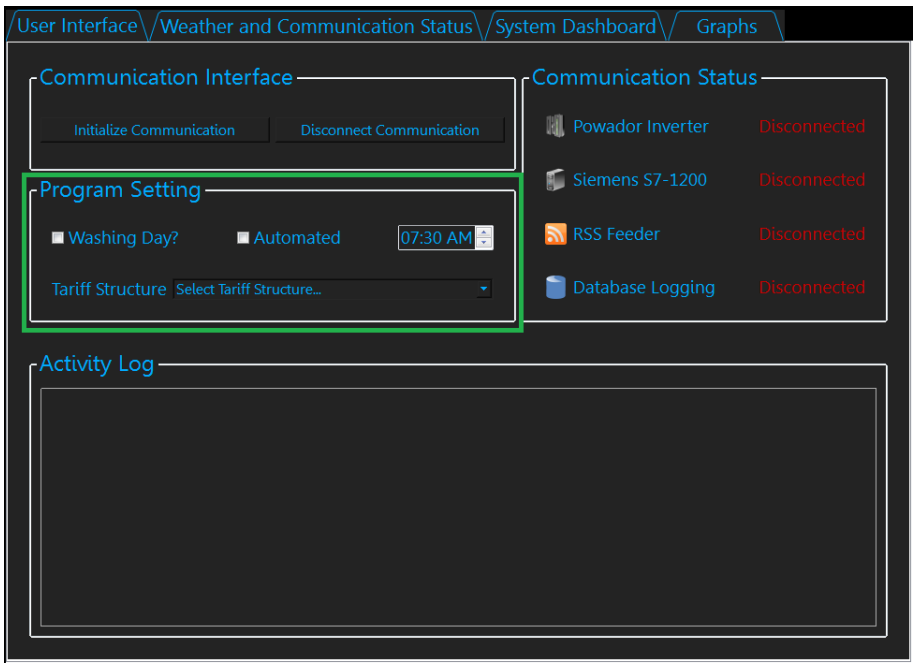

Figure 3-29: EMS software interface

Weather Prediction

The amount of energy obtained from solar PV panels are directly correlated to the amount of solar radiation obtained from the sun. According to Hargreaves and Samani (2000), a simple equation using minimal weather data can be applied to estimate the solar irradiation which in turn is directly correlated to solar PV performance [114]. This estimation method had a performance accuracy which yielded a coefficient of determination (R^2) of 0.7904 and was sufficient for the purpose of this study [115]. The equation to estimate the solar irradiation is shown below and labelled as eq. (3.6) [114].

$$R_s = KT \cdot R_a \cdot (T_{max} - T_{min})^{0.5} \tag{3.6}$$

Where T_{max} and T_{min} refers to the maximum/minimum daily temperatures, R_a refers to the extraterrestrial radiation (mm/day) and KT the empirical coefficient. According to Hargreaves and Samani (2000) a KT value of 0.162 is recommended for inland areas [114]. The Hargreaves and Samani method was tested for the test site location in Potchefstroom based on historic weather data obtained from the SANWS. The graph illustrating the correlation between actual daily energy yield from the solar PV panels and the Hargreaves-Samani index is shown in figure 3-30.

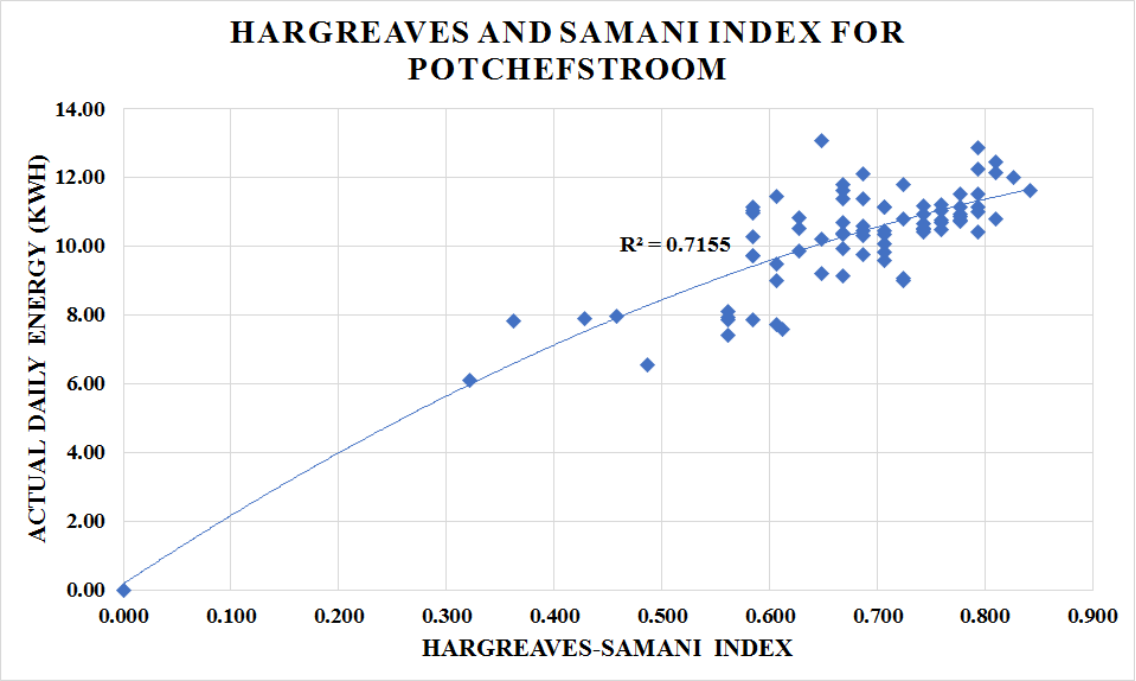

Figure 3-30: Hargreaves-Samani index in Potchefstroom

From figure 3-30 it is seen that $R^2 = 0.7155$ which is an acceptable data fit. To accurately predict the weather is a very complex process which cannot be done without expensive and high accuracy weather stations; however making use of this estimation model provided enough insight such that the EMS could improve its performance and efficiency.

Schedule Loads

The EMS software system scheduled loads such as the geyser, washing machine and tumble dryer based on the weather prediction as described above. The EMS software further used the sunrise and sunset time, season and user requirements (laundry or non-laundry day) to calculate the most appropriate time of day to switch on the abovementioned loads.

Synchronise Load Schedule
The EMS software synchronised the load schedule once the daily weather prediction was done and the user selected the type of day. The timer data were sent to the PLC during the early morning before sunrise. Based on the timer data that were sent, the PLC set the internal timers to switch accordingly when the time came.

3.5.3.3 Phase 3: Continuous Cycle

The third and final phase of the EMS software was the continuous cycle which repeated throughout the day. Within this phase the EMS actively monitored the battery charger, swimming pool, DC light system and refrigerator according to the available power coming in from the GTI. During this cycle, the EMS also stored all new weather data, load data and GTI data in real-time with accurate time-stamps.

Active Load Management
During the continuous cycle, the PLC was in complete control of managing the demand and consumption according to the incoming power from the GTI. The PLC abided by the pre-programmed EMS rules that reduced demand and minimised consumption. The loads were divided into a priority scale that allocated the importance of each load during the day. These priorities changed as the day went on with the focus to minimise disruption to the comfort level of the residents.

System Monitoring and Data Storage
As mentioned above, the system was actively monitored in real-time throughout the day. Every decision made by the PLC was recorded and monitored with the EMS software interface. These decisions along with all of the load, GTI and weather data were captured and stored in a secure database every 10 seconds. This ensured that there was enough samples for the PLC to make accurate decisions but also maintain simplicity.

3.6 Mechanical Design

To ensure that the microgrid testing station was compact and as safe as possible, an enclosure that housed all the components was designed and constructed. This was not a critical part of the study but rather an addition to ensure that the user remained safe from dangerous voltage levels. Some of the major components were drawn to scale in Solidworks® and is shown in figure 3-31. The complete system model was drawn to the exact dimensions as stated in the individual product's datasheets.

3.7 Validation and Verification

The validation of the design was done by ensuring that the design was performed according to the specifications and requirements as stated in the first part of the this chapter. The specifications described in the beginning of the chapter were closely followed to ensure that the detail design strictly complied with the specified requirements. During the validation, a concious effort was made to design according to the manufacturers application guide and relevant standards.

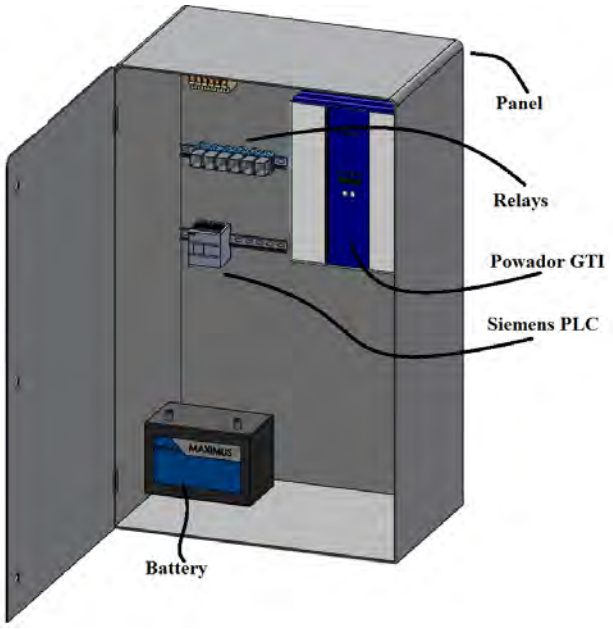

Figure 3-31: Test station design

The verification of the design chapter was done by means of simulation to ensure that the designed system responded to the inputs as per design. This is done in the simulation chapter and is omitted from this chapter. The verification of the design chapter is discussed in the following chapter.

3.8 Conclusion

The design chapter started with the project requirements that included the physical and electrical attributes, design specifications and assumptions that were taken into account. A conceptual design of the integrated system was introduced to provide some insight on how the detail design would be handled. The detail design consisted of three major sections namely the energy, control and mechanical system design.

During the energy system detail design phase, the loads, DER, GTI, battery and DC security lights component selection was done along with the application design. In a similar manner the control system detail design saw the system controller, communication system and measurement equipment be selected. The integrated design of all the components was discussed including the mechanical design.

The foundation of the design has now been laid and requires the integrated design to be simulated within the software environment. The simulation packages that were used to simulate the integrated design include MATLAB®, Simulink® and PVsyst. The results obtained from the simulations gave insight into what alterations to the design had to be made. The simulations was also a form of verification of the project which were critical to ensuring proper design. All the simulation results were captured and shown in Chapter 4.

Chapter 4: Simulation

4.1 Introduction

In this chapter all the simulation models for the energy and control systems are illustrated along with the simulation results. The software packages that were used included MATLAB®, Simulink® and PVsyst. The MATLAB® and Simulink® packages are mathematical modelling software packages that allow the building and simulation of complex control systems. PVsyst is an integrated software package hosting a comprehensive database of all the GTIs and solar PV panels available on the market. Some of the simulation model parameters such as the solar PV panel orientation, location, tilt, manufacturer and model were incorporated into the simulation model which yielded accurate simulation results. PVsyst compiled a report on the simulation results which included the solar PV module loss factor, cost of investment, annual cost, energy cost, expected monthly energy and economic viability.

The first of the five sections in this chapter discusses the optimal power rating of the solar PV panels that yielded the highest overall system efficiency. Thereafter, an integrated system design was done with PVsyst to verify the engineering detail design. The remaining three sections are illustrated and discussed the three scenarios on how the control system was simulated. The first scenario referred to the simulation model of an uncontrolled system. This was followed by two scenarios where active control over the system was performed. The first controlled system referred to a typical normal household day with no laundry that needed to be done. The second scenario where laundry needed to be done was simulated as a second controlled system. After the five sections are discussed, a conclusion is drawn to summarise the simulation chapter.

4.2 Optimal Solar PV Panel Power Rating

To establish the optimal power rating of the solar PV system required extensive use of the Simulink® simulation model added on the DVD (Appendix C). To determine the amount of energy absorbed by the loads, the daily energy yield from the solar PV system was first determined. This was done using approximation functions based on data obtained from PVsyst's meteorological data and the PVsyst simulations. These approximation functions for various daily energy yields is shown in figure 4-1.

From these approximation functions, the simulation model parameters such as the instantaneous and peak power output from the solar PV system were calculated. Other parameters that the simulation model required was the weather information such as sunrise and sunset time, minimum and maximum temperature and humidity. Inserting these parameters into the simulation model yielded the simulation results shown in table 4-1.
Table 4-1 summarises the results obtained from the simulation model. The third column of table 4-1 shows the percentage of the solar PV energy that was absorbed by the loads. This specifies the overall efficiency of the microgrid system. It was critical to specify the solar

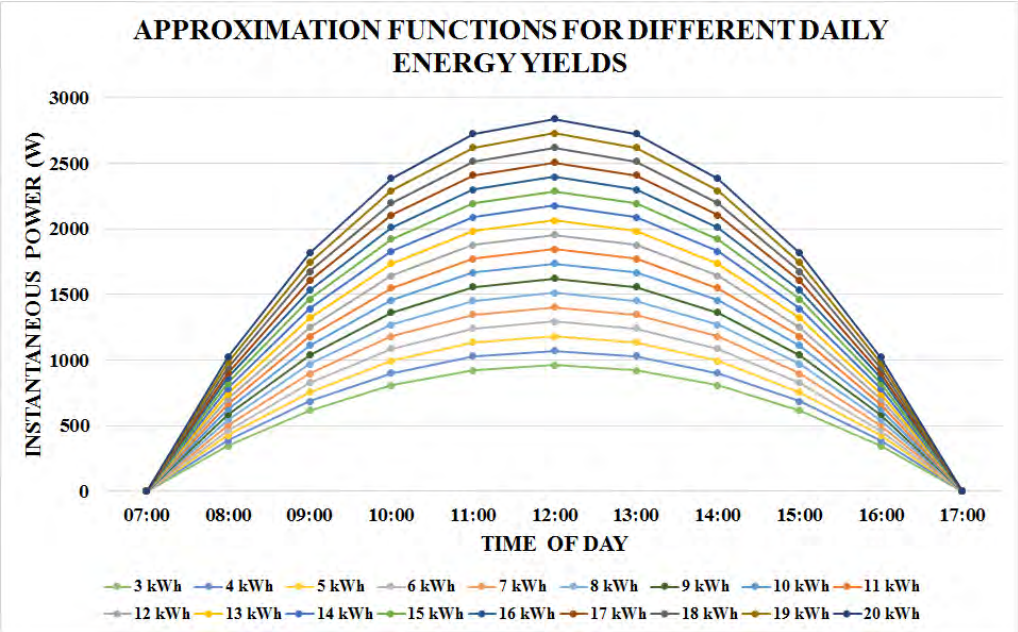

Figure 4-1: Approximation functions

PV system power rating such that the control system could operate at maximum efficiency. Figure 4-2 shows the efficiency utilised by the control system versus the daily energy yield from the solar PV system. The efficiency versus daily energy yield in figure 4-2 shows a gradual decline in the efficiency at daily energy yields greater than 15 kWh. This was due to the daily energy yield approaching the total daily load requirement. As these two values approach one another, the efficiency started to decline.

Table 4-1: Simulation efficiency results

PV Energy Input (kWh)	PV Energy Lost (kWh)	PV Energy Absorbed (%)	Total Load (kWh)	Percentage Eskom Supplied (%)	Percentage PV Supplied (%)
4.660	0.125	97.3	25.28	82.1	17.9
6.524	0.129	98.0	25.62	75.0	25.0
8.387	0.160	98.1	25.99	68.3	31.7
9.786	0.131	98.7	26.38	63.4	36.6
10.252	0.121	98.8	26.48	61.7	38.3
12.581	0.137	98.9	26.90	53.7	46.3
14.911	0.300	98.0	27.72	45.5	52.7
16.775	0.496	97.0	27.40	40.6	59.4
18.173	0.658	96.4	27.51	36.3	63.7
20.969	1.087	94.8	27.68	28.2	71.8
22.367	1.442	93.6	27.74	24.6	75.4

From figure 4-2 it was deduced that the highest efficiencies were obtained when the daily energy yield fluctuated between 8 and 12.5 kWh. It was therefore essential to specify the solar PV system power rating such that the daily energy yield was obtained within these ranges.

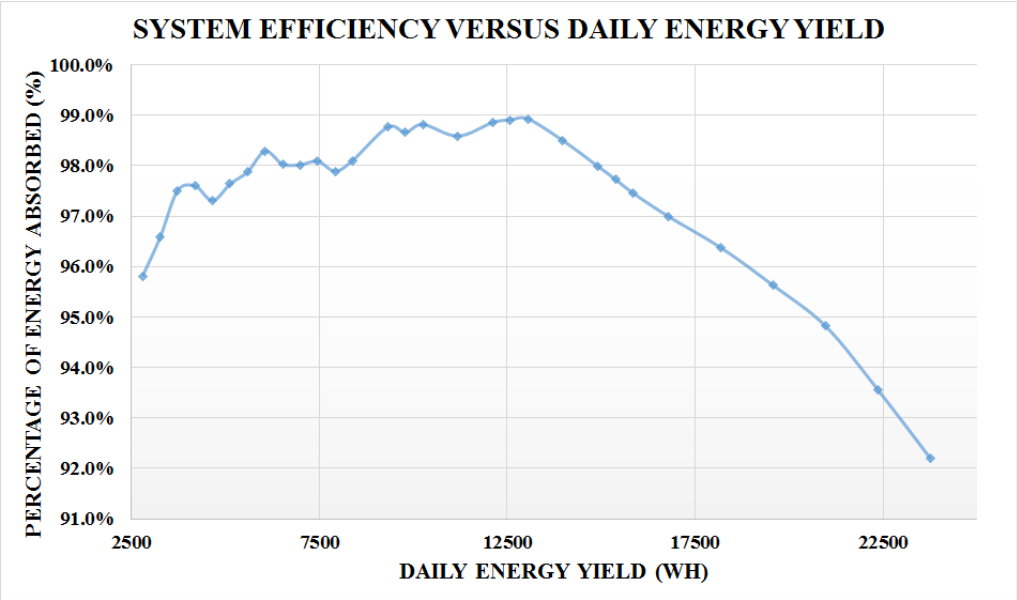

Figure 4-2: Efficiency versus daily energy yield

The probability density function of the daily energy yields for a 3 kW solar PV system, according to historic data from PVsyst are added on the DVD (Appendix C). Following a statistical approach of applying the mean plus/minus one standard deviation of a dataset, 68% of the daily energy yield was within the 12.5 to 18.1 kWh range. The efficiency of the system would have resulted in a less than optimum efficiency. Considering the probability density function of a 2 kW solar PV system as shown in figure 4-3, it was seen that for 68% of the time the daily yield would be between 8.2 to 12.1 kWh. This was very close to the desired PV energy input and therefore, a 2 kW solar PV system would yield optimum efficiency.

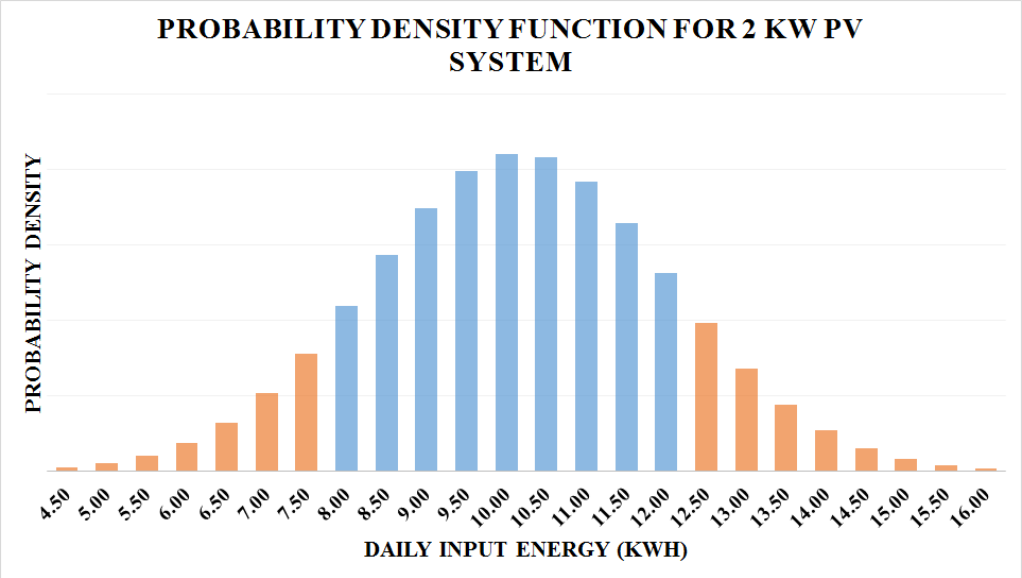

Figure 4-3: Probability density function for daily energy yield of a 2 kW solar PV system

4.3 Solar PV Design Simulation (PVsyst)

A PVsyst simulation was performed to validate and verify the compatibility between the Solar Frontier CIS solar PV panels and Powador GTI. The simulation model also provided valuable information regarding the expected daily energy yields, system losses and economic feasibility. The simulation model was set up to ensure that very accurate results were obtained. The comprehensive PVsyst report is added on the DVD (Appendix C); take note that the meteorological data from Bloemfontein, South Africa was used as the software did not have specific data for Potchefstroom. However, according to weather data provided by the SANWS, the meteorological data between Potchefstroom and Bloemfontein are very similar and for all practical purposes was accepted to be equal [113]. A summary of the key parameters and results are shown in table 4-2.

Table 4-2: Summary of PVsyst simulation parameters results

Simulation Parameter	Simulation Result
Array Manufacturer and Model	Solar Frontier SF165
Number of PV Modules	12 (3 Series, 4 Parallel)
Array Global Power	1980 Wp
Array Total Area	14.7m^2
Inverter Manufacturer and Model	Kaco Powador 2002
Inverter Operating Voltage	125-510 V
Array Orientation (Tilt)	30°
Produced Energy	4178 kWh/year
Performance Ratio	84.6%
Energy Cost	1.84 ZAR/kWh
Running Cost	2000 ZAR/year

4.4 Uncontrolled System Simulation

After the sizing calculations and PVsyst integrated design simulation, the focus was shifted to the control of the microgrid system. The aim of the simulation model was to represent a real-world system as accurately as possible which could be used to gather meaningful simulation results. The uncontrolled system model represented a residence with all the loads as mentioned in the design chapter along with a 2 kW solar PV system. The simulation model was built from measured data along with theoretical assumptions. In the following section, the uncontrolled simulation model is discussed along with the parameters of the building blocks.

4.4.1 MATLAB® and Simulink® Model Parameters

As can be seen from figure 4-4 there were 8 fundamental building blocks in the simulation model. Each of these fundamental blocks contributed towards the integrated model and is therefore discussed accordingly.

- **Block 1:** This group of blocks contained the information necessary to generate the approximated solar PV input profiles as defined in figure 4-1. The approximation

formulas were defined in these function blocks. A system gain parameter was included to vary the solar PV panel's power rating along with an adjustable constant to vary the total daily energy yield. A summary of the parameters are shown below.

Model Parameter	Value	Interpretation
Solar PV Panel Rating (Gain)	0.667	2 kW
Daily Energy Yield (Constant)	1.1	8.87 kWh

- **Block 2:** This block hosted the switching times of the geyser that were measured based on normal usage without any load control. The switching times were approximated from the measured data taken from a typical LSM 8 household. The power consumption of the geyser was simulated as the heating element had a power rating of 3 kW which was either switched on or off. The parameters of the geyser simulation block is shown below.

Model Parameter	Value	Interpretation
Switching Times	Varies	Throughout day
Geyser Power Cons.	3000	3 kW

- **Block 3:** This block hosted the swimming pool switching times throughout the day. Typically swimming pools are switched on early in the morning and switched off in the late afternoon by making use of a timer. Therefore, the simulation block contained the switching times along with the power consumption of the swimming pool pump. The swimming pool pump used a standard 0.55 kW energy-efficient induction motor and was included in the simulation block.

Model Parameter	Value	Interpretation
Switching Times	800-1700	08h00 to 17h00
Pool Pump Power Cons.	500	0.55 kW

- **Block 4:** This block contained the switching times and power consumption of the modern refrigerator. This data was based on research that suggested that modern refrigerator compressors are switched on roughly 80-90 % of the time depending on environmental conditions. Modern refrigerators are very energy efficient with low power consumption. The regular switching was simulated using a pulse generator which had a 85 % on-time. The simulation block parameters are shown below.

Model Parameter	Value	Interpretation
Switching Times	0.85	85% on-time
Refrigerator Power Cons.	300	0.3 kW

- **Block 5:** The battery charger's parameters were captured in this simulation block and was based on the manufacturers' specifications and whenever sufficient incoming solar PV power was available. The duration of the on-time of the charge controller depended on the SOC of the battery. In this scenario, a calculated assumption was made that the battery would roughly be at 40% capacity after one night's DC security light operation. The simulation block parameters are shown below.

Model Parameter	Value	Interpretation
Charging Start Time	700	Sufficient PV
Battery Charger Power Cons.	250	0.25 kW
Estimated Charge Time	450	4:30 hours

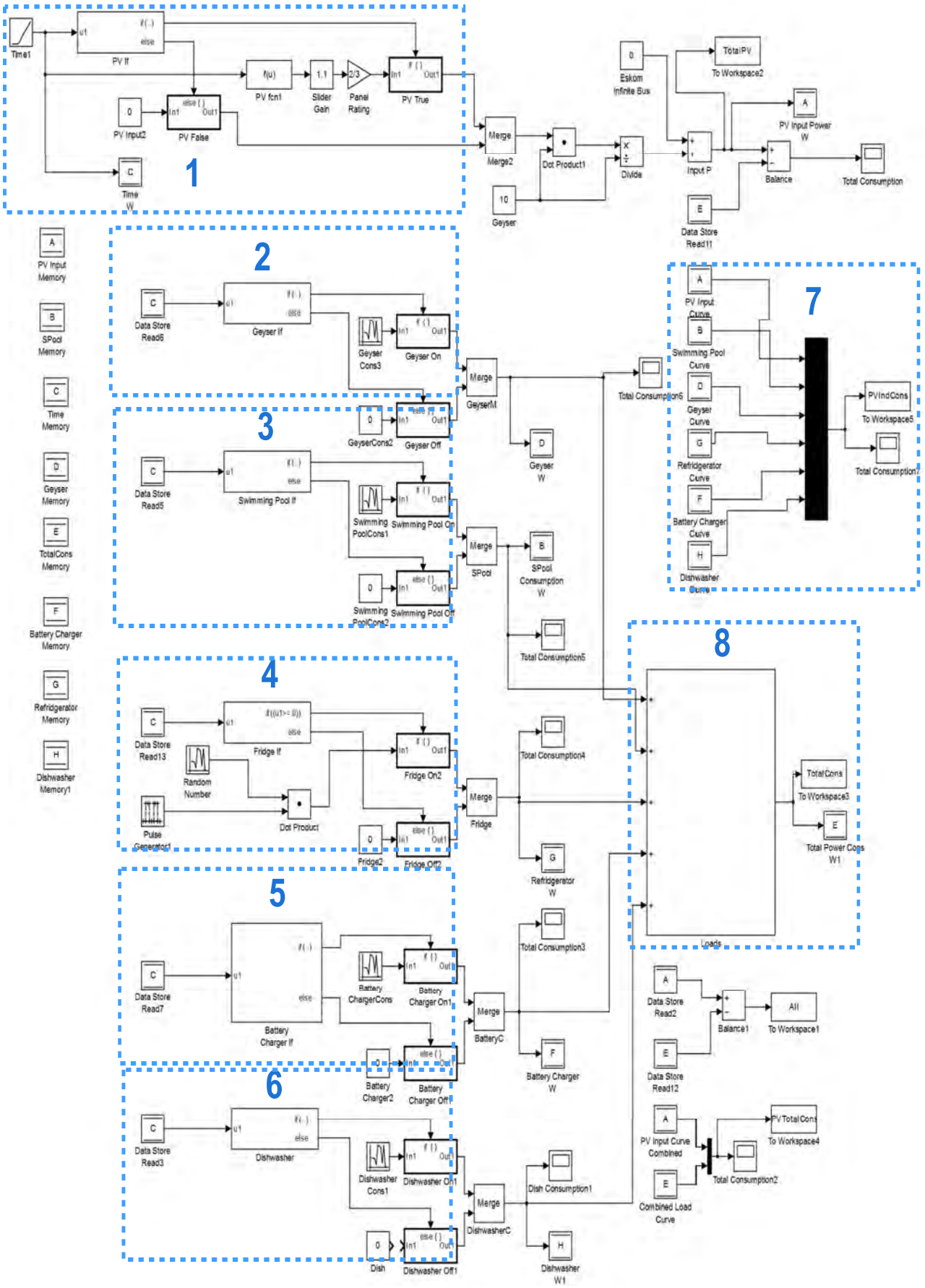

Figure 4-4: Uncontrolled Simulink® model

- **Block 6:** This block contained the parameters to simulate the dishwasher operating conditions and were based on a modern dishwashing machine's specifications. The total power consumption of the dishwasher was fairly high due to the heating element in the dishwasher. The dishwasher was also a fairly simple load as it consists of a motor and a heating element operating in conjunction with one another. These machines operate continuously for at least 45 to 90 minutes and therefore 60 minute cycles were selected as the runtime parameter. Also, according to the manufacturer's datasheet, the power consumption of the selected dishwasher was in the order of 1.8 kW. According to measured data, these machines were switched on during mid-morning which then completed the washing cycle within 90 minutes. The parameters for the dishwasher simulation block is shown below.

Model Parameter	Value	Interpretation
Washing Start Time	900	09h00
Estimated Runtime	100	1 hour
Dishwasher Power Cons.	1800	1.8 kW

- **Block 7:** This block was used to sum the approximated solar PV input profile and individual load data gathered from the simulation onto a single axis. This graph is shown in the simulation results section below.
- **Block 8:** This block captured all the individual loads and added them together to create a total load power consumption curve. This graph in turn was compared to the solar PV input curve and plotted on the same axis. This graph is also shown in the simulation results sections below.

4.4.2 Simulation Results

The simulations were performed at an accelerated pace to represent a complete 24-hour cycle spanning from midnight to midnight (adjusted scale in figures). Throughout the simulation each simulation block responded to the solar PV input profile and time variable as explained above. After the simulation model completed its 24-hour cycle, the individual and combined load curves, as shown in figure 4-5 and 4-6, were generated to illustrate the results in a graphical manner.

Figure 4-5 illustrates each individual loads' switching times along with the power consumption. The solar PV input profile was also added to the graph to illustrate at which time the loads were switched with respect to the solar PV input profile. Figure 4-5 was then combined to form a single graph that illustrated the combined load consumption with respect to the solar PV input profile; this graph is shown in figure 4-6. The annotations made on the graphs represents issues of importance and are discussed accordingly and in chronological order below.

- **Note 1:** It can be seen from the geyser's load profile, that the standby losses were contributing to the energy consumption off the utility grid which could be eliminated to increase energy savings.
- **Note 2:** The second annotation illustrates that the geyser was switched on at times when there was little or no incoming power coming from the solar PV system. This raised the issue of excessive energy consumption off the utility grid.
- **Note 3:** The overlapping area where the geyser, swimming pool pump, battery charger and dishwasher were all switched on simultaneously, resulted in an exces-

sively high energy demand (see note 5). Although South African residential energy consumers are not billed for excessive energy demands at the moment (as with industrial consumers), it may be an incentive that might be adopted in the near future.

- **Note 4:** The fourth annotation illustrated the starting time at which the swimming pool and battery charger were scheduled to start during day time. There was still room for improvement when to start these loads such that load consumption from the incoming solar PV power could be optimised. It should also be noted that the swimming pool was operated throughout the entire day (7-10 hours of run-time).
- **Note 5:** The combined load curve illustrated the maximum power demand that neared the 6 kW range. This has caused by numerous loads being switched on simultaneously.

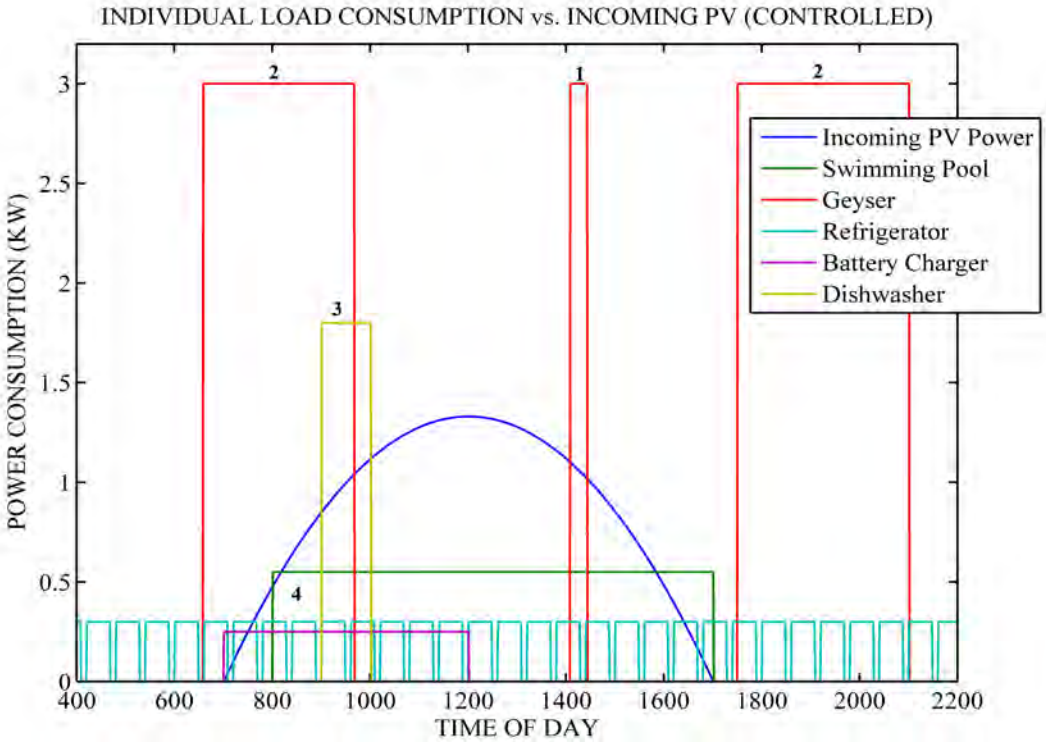

Figure 4-5: Individual load vs. incoming PV plot (Uncontrolled)

- **Note 6:** This annotation is an extension of the first annotation to illustrate that standby losses of the geyser could be eliminated.
- **Note 7:** The significance of this annotation is that the geyser was running solely off the utility grid. This significantly increased the energy consumption off the grid. There was no need for the geyser to be switched on at this stage as no hot water was required after 22h00.
- **Note 8:** This annotation highlights the incoming solar PV power that was not consumed by local loads and that was lost to the grid.

A summary of the simulation results is shown in table 4-3. From the table it can be seen that the total daily energy consumption by all the loads were 35.63 kWh with the solar PV supplying only 20.66% (7.36 kWh) of this total. The percentage of solar PV energy that was absorbed by the loads (overall system efficiency) were 83.01%. The

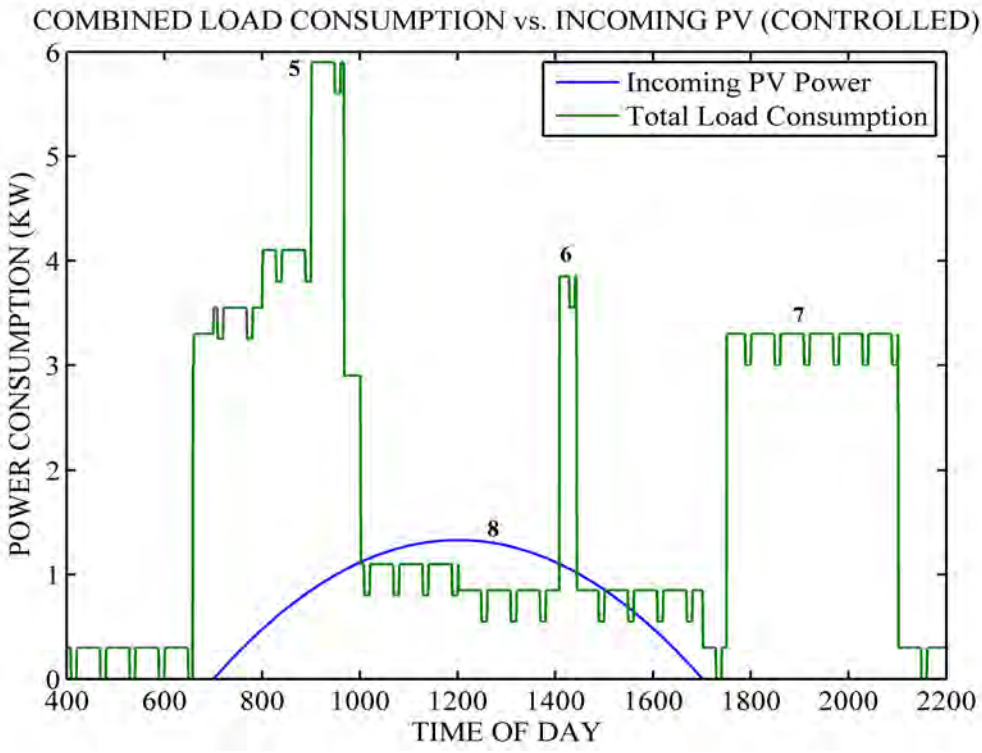

Figure 4-6: Combined load vs. incoming solar PV plot (Uncontrolled)

abovementioned parameters were the indicators of the control system performance and hence these parameters were compared for each simulation.

Table 4-3: Summary of uncontrolled simulation results

Simulation Parameter	Simulation Result
Total PV Energy Input	8.87 kWh
PV Energy Lost	1.51 kWh
Total Daily Load	35.63 kWh
Energy Cons. off Utility	28.27 kWh
Energy Cons. off PV	7.36 kWh
Percentage Utility Supplied	79.34%
Percentage PV Supplied	20.66%
Maximum Demand	5.90 kW
Overall System Efficiency	83.01%

4.5 Controlled System Simulation: Scenario 1

As described in the introduction section of this chapter, there were two scenarios which the control system needed to effectively manage. The first was a normal household day without laundry and the second was a day where laundry needed to be incorporated into the control strategy. This section discusses the simulation of the control system based on a non-laundry day.

4.5.1 MATLAB® and Simulink® Model Parameters

As can be seen from figure 4-7, there were again 8 fundamental building blocks as with the uncontrolled simulation model. Each of these fundamental blocks contributed towards the integrated model and is therefore discussed accordingly.

- **Block 1:** In an attempt to standardise the simulation results, the simulation model parameters were kept similar and therefore the parameters to generate the approximated solar PV input profile was similar as mentioned above.

Model Parameter	Value	Interpretation
Solar Panel Rating (Gain)	0.667	2 kW
Daily Energy Yield (Constant)	1.05	7.93 kWh

- **Block 2:** Control over the geyser switching times was exercised and set such that the geyser was switched on during the peak times of the solar PV power input curve. Geyser standby losses were eliminated. Therefore, the simulation block parameters were updated to those shown below.

Model Parameter	Value	Interpretation
Switching Times	1120-1200, 1300-1600	11h12-12h00 and 13h00-16h00
Geyser Power Cons.	3000	3 kW

- **Block 3:** The swimming pool pump was also controlled which permitted the swimming pool to be switched on only when sufficient incoming solar PV power was available. Also, the swimming pool was not switched on outside of daylight hours and when the geyser was switched on. The simulation block parameters was therefore updated to those shown below.

Model Parameter	Value	Interpretation
Switching Times	800-1700	08h00 to 17h00
Pool Pump Power Cons.	550	0.55 kW
Geyser Power Cons.	0	0 kW
Incoming PV Power	550	0.55 kW

- **Block 4:** The refrigerator could not be actively controlled since the compressor operated on its own closed-loop control system to regulate the temperature inside the refrigerator. However, a certain amount of control was exercised. Control over the refrigerator was exercised by switching off the refrigerator during the times when the geyser was switched on. The updated simulation block parameters are shown below.

Model Parameter	Value	Interpretation
Switching Times	0.85	85% on-time
Geyser Power Cons.	0	0 kW
Refrigerator Power Cons.	300	0.3 kW

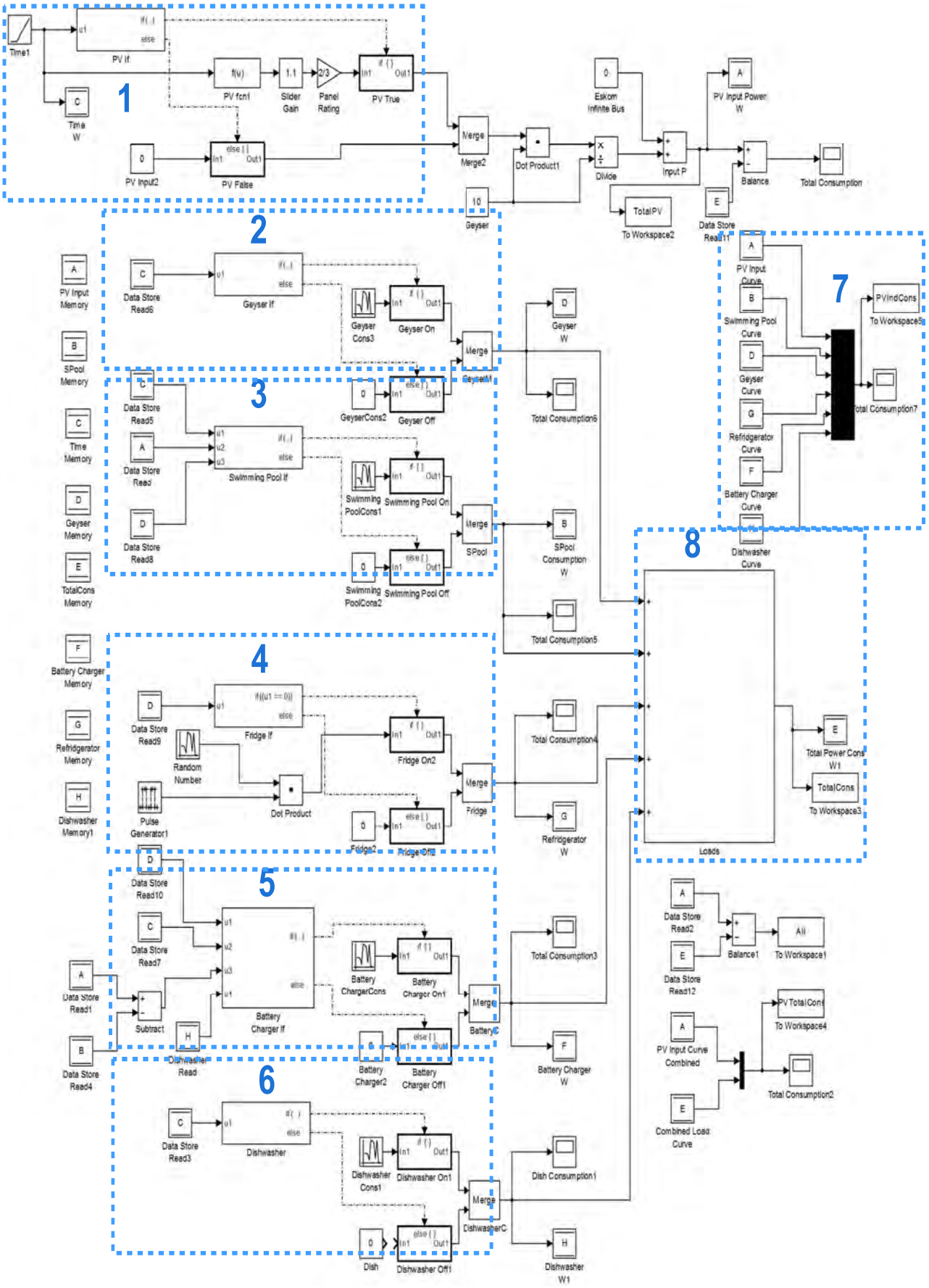

Figure 4-7: Controlled Simulink® model (Non-laundry day)

- **Block 5:** The battery charger parameters were changed such that the charger only operated once four conditions were met. The conditions were that the geyser had to be switched off, it had to be during daytime, the incoming solar PV power had to be greater than 0.25 kW and the dishwasher had to be switched off. These parameters were incorporated into the simulation block and are shown below.

Model Parameter	Value	Interpretation
Charging Start Time	250	Sufficient PV
Battery Charger Power Cons.	250	0.25 kW
Geyser Power Cons.	0	0 kW
Dishwasher Power Cons.	0	0 kW
Estimated Charge Time	400	4 hours

- **Block 6:** The dishwasher parameters were altered such that the dishwasher was switched on during the peak times of the solar PV power input curve. The dishwasher was therefore scheduled to switch on during the peak time of day and when the geyser was switched off. The updated simulation block parameters are shown below.

Model Parameter	Value	Interpretation
Washing Start Time	900	09h00
Estimated Runtime	100	1 hour
Dishwasher Power Cons.	1800	1.8 kW

- **Block 7 and 8:** These two blocks remained unchanged and still performed the tasks mentioned above.

4.5.2 Simulation Results

The exact same conditions in which the uncontrolled simulation were performed was imposed onto the controlled simulation as well. A similar solar PV input profile was injected into this simulation such that results could be compared. The individual and combined load curves are again illustrated to graphically represent the simulation data. These graphs are depicted in figures 4-8 and 4-9. The annotations made on the graphs are discussed accordingly.

- **Note 1:** This annotation illustrates that the geyser was shifted to a time where the incoming solar PV power was near its peak. It should also be noted that the standby losses of the geyser were completely eliminated. Furthermore, there were no other loads switched on along with the geyser. This significantly reduced the demand on the system.
- **Note 2:** The dishwasher was scheduled to switch on directly after the geyser was switched off. This ensured that the demand on the system was kept to a minimum and all of the solar PV energy was consumed locally.
- **Note 3:** The swimming pool pump start time was moved to a time when incoming solar PV power was equal to the power consumption of the swimming pool pump i.e. 0.55 kW. The overall runtime was also significantly reduced to minimise energy consumption.
- **Note 4:** The battery charger starting and running time was also changed to times when excessive incoming solar PV power was available. The battery charger was a

low power load compared to the rest of the loads and was the first load that switched on early in the day.

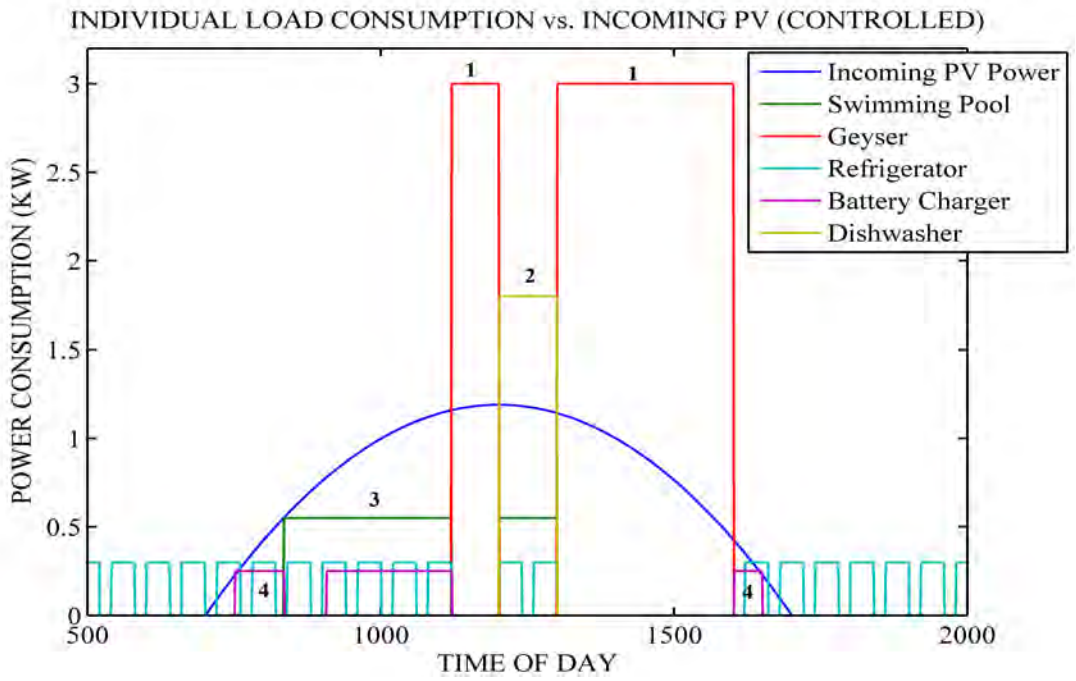

Figure 4-8: Individual load vs. incoming solar PV plot (Non-laundry day)

- **Note 5:** The combined curve illustrates that the total demand on the system was significantly reduced compared to the uncontrolled simulation. This annotation also shows that the highest amount of energy was consumed in the timespan when the incoming solar PV power was at its peak.

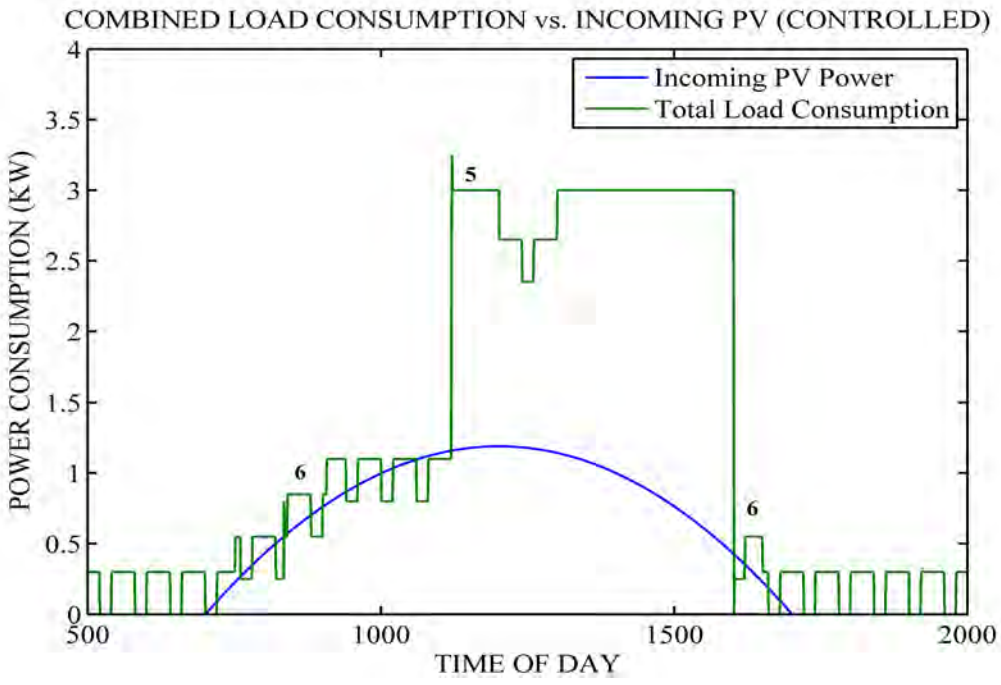

Figure 4-9: Combined load vs. incoming solar PV plot (Non-laundry day)

- **Note 6:** This annotation illustrates that as the incoming solar PV power increased and decreased early/late in the day, the loads were switched on/off such that the energy consumption increased/decreased at the same rate. During those times, the instantaneous power consumption was never greater than 1.2 times the incoming solar PV power.

A summary of the simulation results is shown in table 4-4. From the table it can be seen that the total daily energy consumption by all the loads were reduced to 26.48 kWh with the solar PV supplying 37.63% of this total (7.64 kWh). The percentage of solar PV power that was absorbed by the loads (overall system efficiency) was 96.31%. Compared to the uncontrolled system this was a significant improvement. This is further discussed in the conclusion section of this chapter.

Table 4-4: Summary of controlled simulation results (Non-laundry day)

Simulation Parameter	Simulation Result
Total PV Energy Input	7.93 kWh
PV Energy Lost	0.29 kWh
Total Daily Load	20.30 kWh
Energy Cons. off Utility	12.66 kWh
Energy Cons. off PV	7.64 kWh
Percentage Utility Supplied	62.37%
Percentage PV Supplied	37.63%
Maximum Demand	3.25 kW
Overall System Efficiency	96.31%

4.6 Controlled System Simulation: Scenario 2

The second scenario that is discussed was where laundry needed to be done. This section discusses the simulation of the control system based on a laundry day. The control strategy was very similar to the non-laundry day; however the minor differences are still worthwhile to discuss the simulation in depth.

4.6.1 MATLAB® and Simulink® Model Parameters

As can be seen from figure 4-10 there were 8 fundamental building blocks in the simulation model. Each of these fundamental blocks contributed towards the integrated model and is therefore discussed accordingly.

- **Block 1:** The simulation model parameters for this block was unchanged and therefore the parameters to generate the approximated solar PV input curve was the same as previously mentioned above.

Model Parameter	Value	Interpretation
Solar Panel Rating (Gain)	0.667	2 kW
Daily Energy Yield (Constant)	1.15	9.33 kWh

- **Block 2 and 3:** The laundry day selection added a washing and tumble drying function to the simulation which was executed during the peak times of the solar PV input curve. This replaced the dishwashing function as there were too few hours throughout the day to perform both functions. The simulation block parameters for the washing machine and tumble dryer are shown below.

Model Parameter	Value	Interpretation
Washing Start Time	1000	10h00
Drying Start Time	1100	11h00
Estimated Runtime	200	2 hours
Tumble Dryer Power Cons.	2200	2.2 kW
Washing Machine Power Cons.	550	0.55 kW

- **Block 4:** This block remained unchanged and still performed the tasks mentioned above.
- **Block 5:** This block remained unchanged and still performed the tasks mentioned above.
- **Block 6:** This block remained unchanged and still performed the tasks mentioned above.
- **Block 7:** This block remained unchanged and still performed the tasks mentioned above.
- **Block 8 and 9:** These two blocks remained unchanged and still performed the tasks mentioned above.

4.6.2 Simulation Results

As mentioned in the previous section, the similar conditions in which the uncontrolled simulation was performed were imposed onto the controlled simulation. The individual and combined load curves are again illustrated to graphically represent the simulation data. These graphs are depicted in figures 4-11 and 4-12. The annotations made on the graphs are discussed below.

- **Note 1:** This annotation illustrates that the geyser was shifted to a time where the incoming solar PV power was closer to its peak. A longer timespan was allocated for the washing machine and tumble dryer to complete their cycles.
- **Note 2:** During this stage, the washing machine and tumble dryer were switched on such that the washing and drying could be done during the peak time of the incoming solar PV profile. This ensured that the minimum amount of energy was consumed off the utility grid.
- **Note 3:** The swimming pool pump start time was moved to a time when incoming solar PV power was equal to the power consumption of the swimming pool pump i.e. 0.55 kW. The overall runtime was also significantly reduced to minimise energy consumption. The swimming pool ran for the least number of hours on a laundry day compared to non-laundry days.
- **Note 4:** Similar to the non-laundry simulation, the battery charger starting and running times were changed to times when there were excessive incoming solar PV power available. Since the battery charger was a low power load compared to the rest of the loads, it was the first load to switch on early in the day when the incoming solar PV power was low.

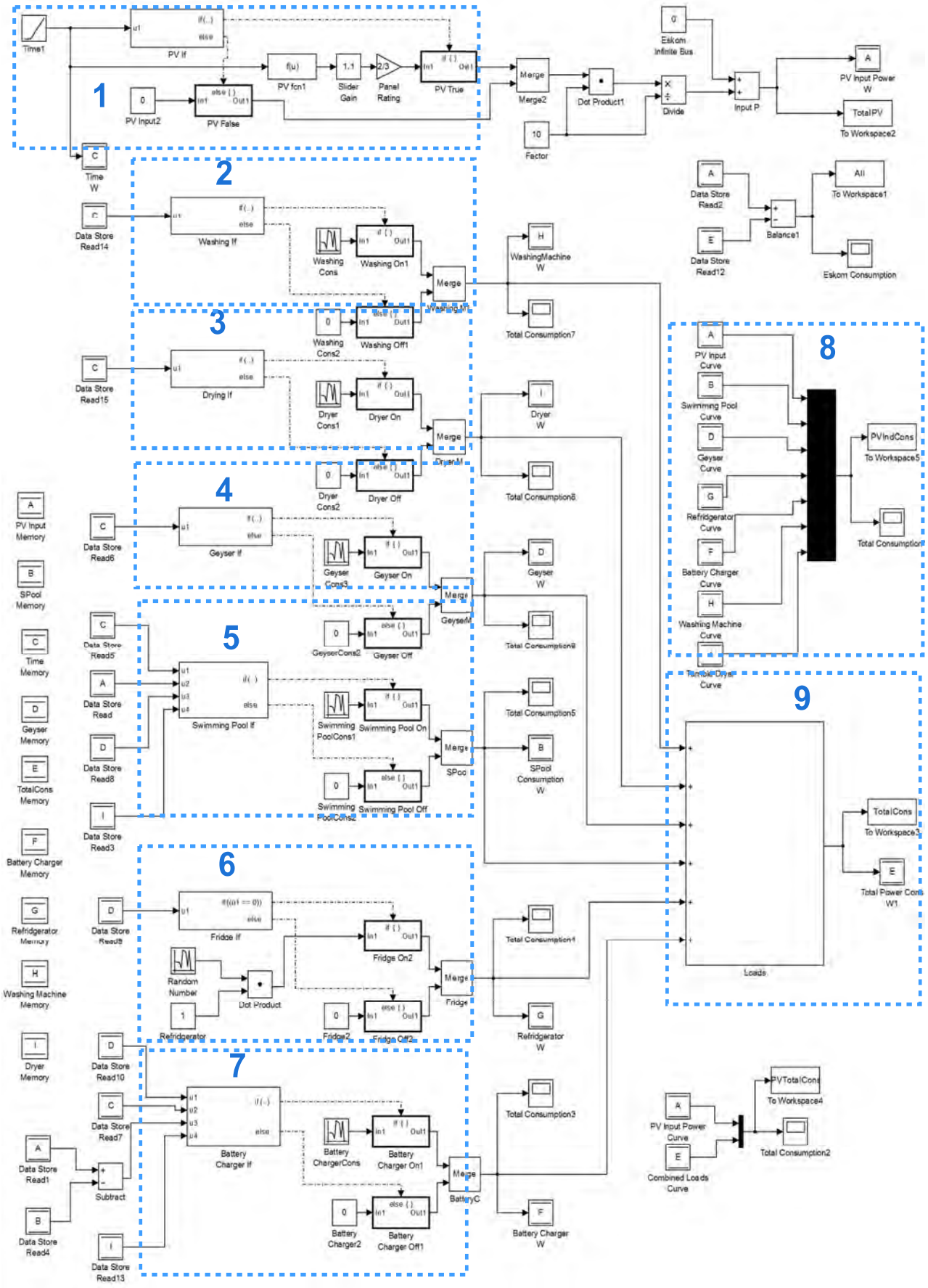

Figure 4-10: Controlled Simulink® model (Laundry day)

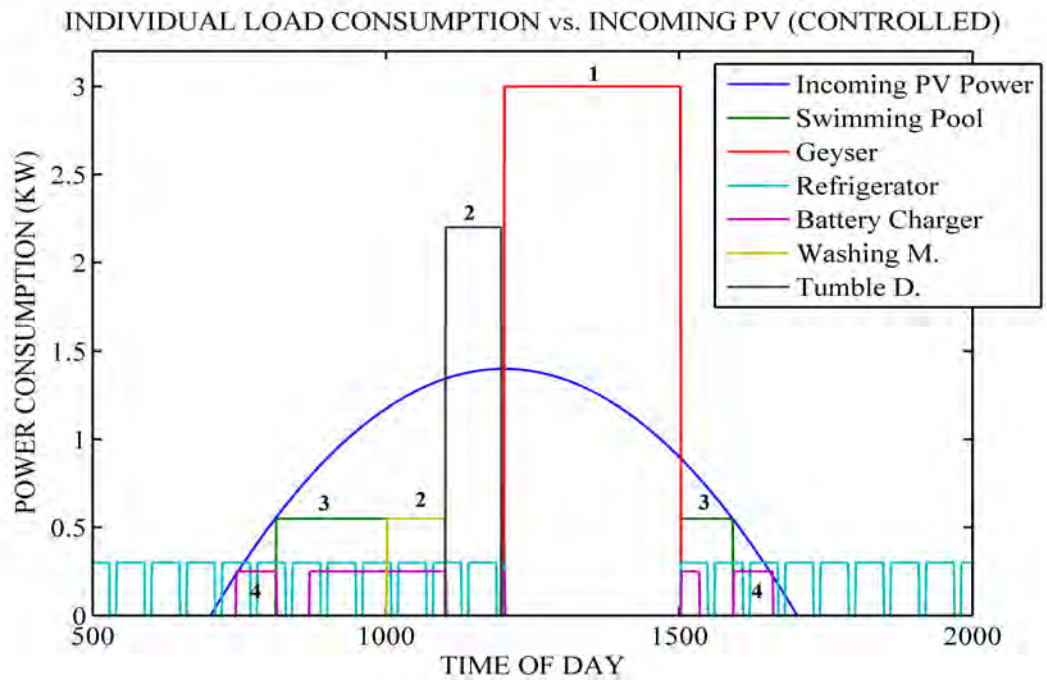

Figure 4-11: Individual load vs. incoming solar PV plot (Laundry day)

- **Note 5:** The combined curve illustrates that the total demand on the system was again significantly reduced compared to the uncontrolled simulation. This annotation also shows that the highest amount of energy was consumed in the timespan when the incoming solar PV power was at its peak.

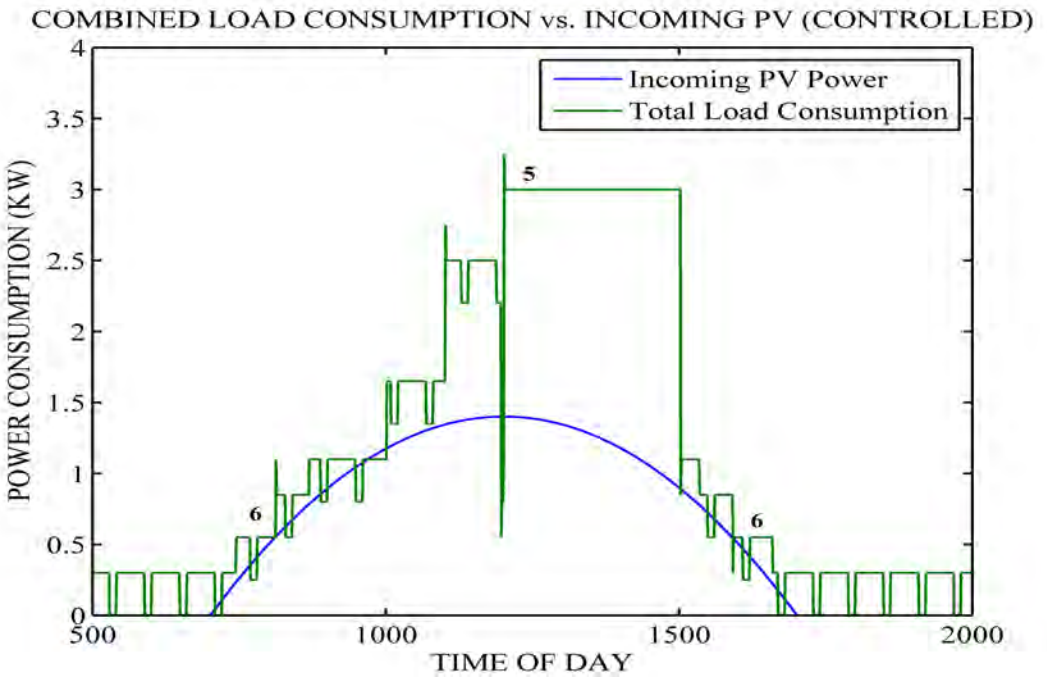

Figure 4-12: Combined load vs. incoming solar PV plot (Laundry day)

- **Note 6:** As with the non-laundry simulation, this annotation illustrates that as the incoming solar PV power increased and decreased early/late in the day, the loads

were switched on/off such that the consumption increased/decreased at the same rate. During these times, the instantaneous power consumption was never greater than 1.3 times the incoming solar PV power.

A summary of the simulation results are shown in table 4-5. From the table it is seen that the total daily energy consumption by all the loads were reduced to 19.83 kWh with the solar PV energy supplying 46.16% of this total (9.15 kWh). The percentage of solar PV power that was absorbed by the loads (overall system efficiency) were 98.07%. Compared to the uncontrolled system these were significant improvements that are discussed in the following section.

Table 4-5: Summary of controlled simulation results (Laundry day)

Simulation Parameter	**Simulation Result**
Total PV Energy Input	9.33 kWh
PV Energy Lost	0.18 kWh
Total Daily Load	19.83 kWh
Energy Cons. off Utility	10.67 kWh
Energy Cons. off PV	9.15 kWh
Percentage Utility Supplied	53.84%
Percentage PV Supplied	46.16%
Maximum Demand	3.25 kW
Overall System Efficiency	98.07%

4.7 Verification and Validation

The verification of the computer simulation models were done to confirm whether the conceptual model matched the specifications and assumptions as made in the design and simulation chapters. To ensure that the simulation model was correctly implemented, logic flow diagrams were drawn up to test the simulation model's response to a wide range of logical inputs. The model was thoroughly tested by adjusting the logical input and calculation settings of the model over a wide range. By doing so, this ensured that all possible responses of the system were gathered and ultimately verified whether the system complied to the design assumptions and specifications.

The verification process was not only used to ensure that the model complied to the assumptions and specifications. The verification process aided in the redesign and validation process which ensured that an accurate simulation model was built.

The validation of the computer simulation model was done to ensure that the results obtained from the model matched that of the real-world system. By ensuring that the simulation model represented the real-world system, the model could be used for future applications without physically building the system. The validation of the simulation model was done by comparing the results obtained from the simulation model to the results obtained from the real-world system. The validation of the simulation model is discussed in Chapter 5.

4.8 Conclusion

In this chapter, the five sections relating to the simulations were illustrated and discussed. It was found that through extensive simulation in MATLAB® and Simulink®, that the optimal power rating of the solar PV system was 2 kW. According to the simulations, a 2 kW solar PV system yielded the highest efficiencies when combined with the control system. The PVsyst simulation provided an integrated system simulation model which was used to validate and verify the compatibility between the energy system components. From the simulation, it was evident that all of the components fully integrated with one another. The report generated by PVsyst also gave insight into the expected losses and economic feasibility of the microgrid system.

When a comparison of the uncontrolled to the controlled system was made, it became evident that the control system improved the energy system efficiency and reduced the energy consumption off the grid. For a typical uncontrolled scenario as presented in section 4.4, the overall system efficiency was in the order of 83%. The controlled system with similar input parameters managed to achieve an efficiency of 98%, this was an improvement of 14%. The total energy required to supply all the loads in the uncontrolled system was 35.6 kWh. The controlled system managed to reduce the energy consumption to approximately 20 kWh. Due to the reduced energy consumption and increased system efficiency, the energy consumption off the grid was reduced from 28 kWh to 13 kWh. According to the simulations this would result in a daily electricity bill reduction of R 27.75 (R 1.85/kWh) and a monthly saving of R 832.50.

The simulation model was verified to ensure that the model matched the system specifications and assumptions. The simulation model was also validated to ensure that the model was an accurate representation of the real-world system. The validation of the simulation model along with the actual results obtained from the microgrid test station is discussed in the following chapter which is the experimental results chapter.

Chapter 5: Construction, Assembly and Testing

5.1 Introduction

In this chapter, the microgrid test station construction assembly and testing is discussed. The microgrid test station consisted of four parts namely the loads, energy system, control system and software system. The implementation of each of these four parts is discussed in detail in the sections that follow. The sections are structured as shown in figure 5-1 and discussed accordingly.

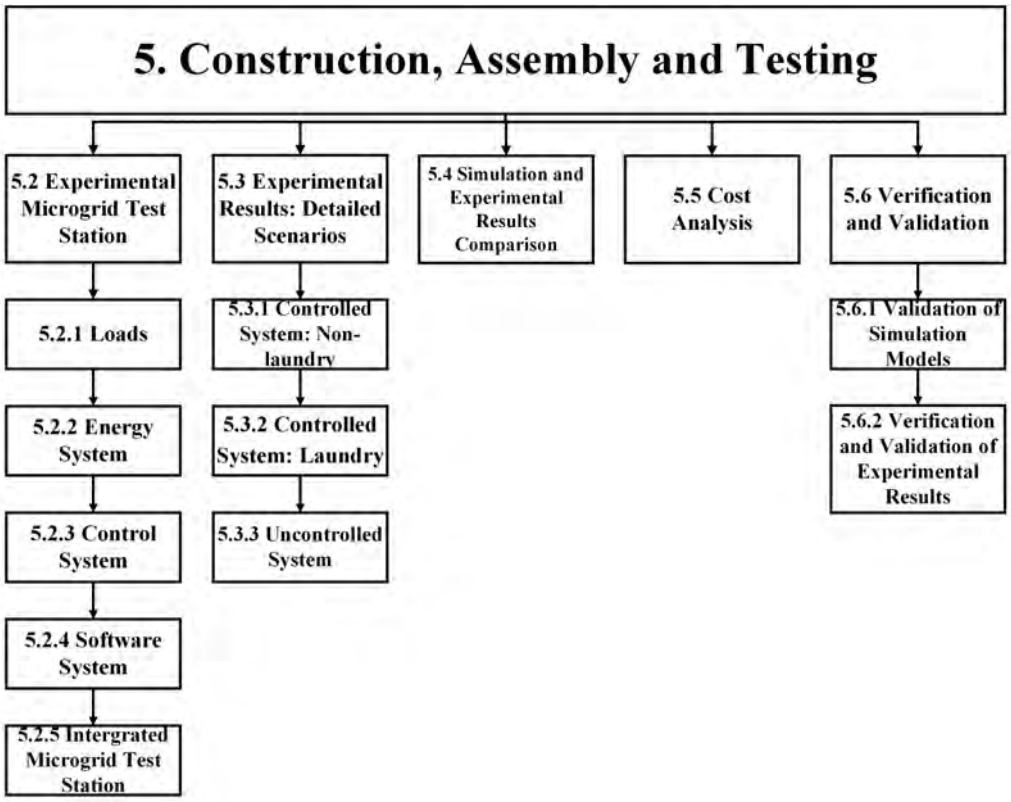

Figure 5-1: Chapter 5 structure

The discussion of the uncontrolled and controlled experimental test results is done in section 5.3 as seen in figure 5-1. After the discussion of the detailed experimental results, a comparison between the simulation and experimental results is done to determine the accuracy of the simulation model. This is also done to aid the validation of the simulation model. The validation and verification of the experimental results are also done at the end of the chapter along with a cost analysis which discusses the feasibility of the microgrid system.

5.2 Experimental Microgrid Test Station

The experimental microgrid test station consisted of the energy system, control system and loads as described in Chapter 3. This section discusses these individual components and the integration of these which led to the integrated experimental microgrid test station.

5.2.1 Loads

As mentioned in Chapter 3, the load appliances that were used for testing purposes were typical everyday household appliances. Reference to these loads is made throughout the chapter and hence the appliances are reiterated below.

1. Geyser
2. Swimming Pool Pump
3. Washing Machine and Tumble Dryer
4. Battery Charger
5. Dishwasher and Refrigerator

5.2.1.1 Geyser

The geyser that was used for testing is shown in figure 5-2. The illustrated geyser consisted of a 150 litre water tank and 3 kW heating element which was the same as the specified characteristics in the design chapter. It is evident from figure 5-2 that the geyser tank had no external insulation against environmental conditions and as a result had increased heat loss, this caused the geyser element to regularly switch on/off. However, this did not have a significant effect on the experimental results as the control system controlled the number of running hours of the geyser element.

Figure 5-2: 150 litre, 3 kW installed geyser

5.2.1.2 Swimming Pool Pump

The swimming pool pump that was used for testing is shown in figure 5-3. The swimming pool pump motor was sized accurately in terms of water circulation tempo and circulated the entire body of water through the filtration system within 5-7 hours. This was an important factor since the energy saving from the swimming pool pump was done by

reducing the number of running hours of the motor. The swimming pool pump motor was a single phase, 0.55 kW induction type with a starting and running capacitor.

(a) Swimming pool pump enclosure

(b) Installed 0.55 kW swimming pool pump

Figure 5-3: Swimming pool pump setup

5.2.1.3 Washing Machine and Tumble Dryer

The washing machine and tumble dryer that were used for testing are shown in figure 5-4a and 5-4b. These appliances were rated to carry up to 9 kg of laundry with power ratings of 0.6 kW (washing machine) and 2.2 kW (tumble dryer). These devices were only used on laundry days and hence did not operate for extended hours.

(a) Installed washing machine

(b) Installed tumble dryer

Figure 5-4: Washing machine and tumble dryer setup

5.2.1.4 Battery Charge Controller

The 20 A 12/24 V ACDC dynamics battery charge controller that was used is shown in figure 5-5a. The purpose of the charger was to recharge the battery such that the DC security light system could operate throughout the night. The battery charge controller was connected to a high efficiency AC-to-DC converter which converted 230 VAC from the GTI into 15 VDC. The lowered DC voltage was in turn PWM-ed by the charge controller to charge the battery as efficiently as possible. This was in the order of 1.1 times the measured battery voltage. The block diagram depicting the battery charge controller interconnection is shown in figure 5-5b.

(a) ACDC Dynamics 20 A battery charger

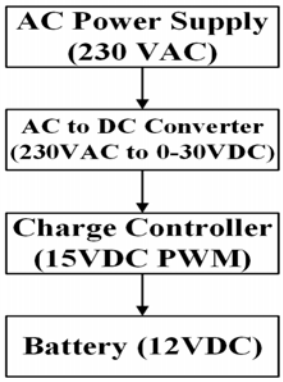

(b) Battery charger connection

Figure 5-5: Battery charger setup

5.2.1.5 Dishwasher and Refrigerator

The dishwasher and refrigerator that were used for experimental testing purposes are shown in figure 5-6a and 5-6b. The dishwasher's rated power was 1.8 kW and operated for at least an hour everyday. The refrigerator had a low power rating (0.25 kW) but operated on a continuous basis throughout the day. This made the refrigerator a high energy consumer due to its continuous operation.

(a) Installed dishwasher

(b) Installed refrigerator

Figure 5-6: Dishwasher and refrigerator setup

5.2.2 Energy System

5.2.2.1 Solar PV Panels

As mentioned in the design chapter, the solar irradiation levels at the test site location, Potchefstroom, were exceptional and hence solar PV panels were used as the DER. The Solar Frontier SF 165 W panels were installed at the residence in Potchefstroom. As seen from figures 5-7b and 5-8, there were only six solar PV panels. This yielded a total installed capacity of 990 W_p. This was half of the designed capacity of 2 kW. The reason for this was that another six solar PV panels would have significantly increased the cost of the study. However, the study's main objective was to test the response of the control system to the incoming solar PV profile and hence, the incoming solar PV instantaneous

power was multiplied by two within the software to yield the desired solar PV power rating. This way the PLC responded as if a 2 kW solar PV system was connected to the GTI. This assumption held true as another six solar PV panels would have been connected in parallel to the existing six panels and according to Kirchhoff's current law, the algebraic sum of all currents entering and leaving a node must equal zero. A visual illustration of Kirchhoff's current law and the solar PV system interconnection is shown in figures 5-7a and 5-7b.

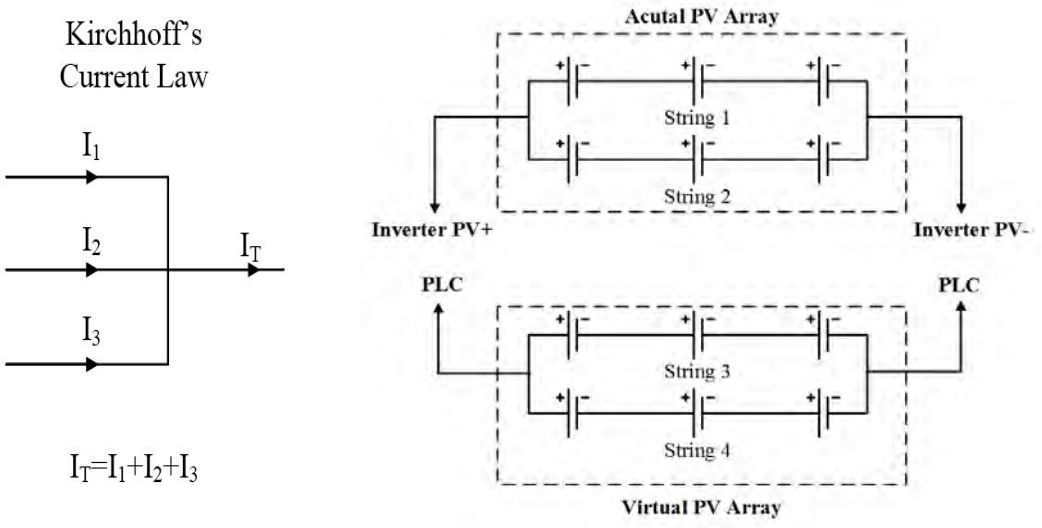

(a) Kirchhoff's current law (b) Solar PV system interconnection

Figure 5-7: Kirchhoff's current law and solar PV system interconnection

As seen from figure 5-8, the azimuth and tilt of the solar PV panels were similar to that of the simulation in the PVsyst report (report on DVD in Appendix C). The azimuth of the installation refers to the deviation in degrees from a true north orientation. Whilst every attempt was made to achieve a true north installation, a certain amount of error was factored in. Therefore, the installation azimuth was considered to be between -5 and +5 degrees. The same applied to the tilt of the solar PV panels, according to the PVsyst simulation the ideal tilt was 30°and the construction of the frame was done accordingly. Due to uneven grounding a small deviation from the 30°design specification was possible. The performance tests, operating conditions and mechanical characteristics of the Solar Frontier SF 165 W solar PV panels can be seen in the product datasheet added on the DVD (Appendix C). Therefore, these characteristics were not discussed in this section.

Figure 5-8: Installed array of solar PV panels

5.2.2.2 GTI

As previously stated in the design chapter, the Kaco Powador 2002 GTI was selected as the link between the solar PV panels and the utility grid. The rated power of the GTI was slightly less than that of the designed solar PV system which made the GTI slightly undersized. However, since the power rating of the actual solar PV system was halved, the GTI had an adequate power rating. From figures 5-9a and 5-9b, the installed GTI can be seen along with a sample of the operating parameters. The GTI used an MPPT controller to maximise the incoming solar PV power and convert the DC power into AC power. According to the datasheet, this was done at an efficiency of 95.1%. The performance tests, operating conditions and mechanical characteristics of the Kaco Powador 2002 GTI can be seen in the product datasheet added on the DVD (Appendix C).

(a) Installed Powador 2002 GTI (b) Operating parameters

Figure 5-9: Powador 2002 GTI

5.2.2.3 DC Security Light System

As stated in the design chapter, the DC light system consisted of the DC security lights, battery and charge controller. The DC security lights are shown in figure 5-10a and as per design, there were one 20 W and three 10 W LED security lights. The combined load of these LED lights equalled the design load power of 50 W. Figure 5-10b illustrates the interconnection between all the components of the DC security light system.

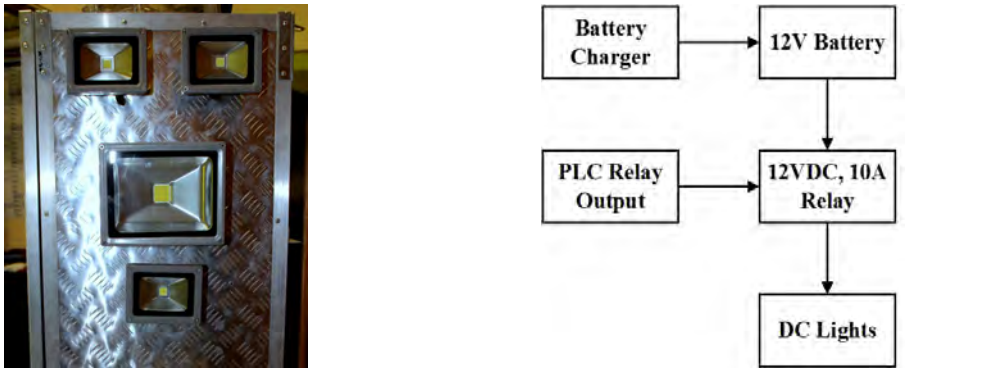

(a) LED security lights (b) DC security light system interconnection

Figure 5-10: DC security light system

The interconnection between the battery and charger controller is shown in figure 5-11.

The Maximus 12 V 105 Ah battery that was selected in the design chapter is shown on the left hand side of figure 5-11 with the battery charger in the top right hand side. As stated in the charge controller section above, an AC-to-DC converter was added to the design such that the battery could be charged from the utility grid; the AC-to-DC converter is shown on the bottom right hand side of figure 5-11.

Figure 5-11: Actual battery and battery charger interconnection

5.2.3 Control System

The control system hardware components consisted of the PLC, relays and CTs. These components are discussed in the following section along with images and diagrams of the implementation thereof. The most formidable hardware component of the control system was the PLC and hence the greatest emphasis was placed on this section.

5.2.3.1 PLC

The PLC that was used to implement the control system is shown in figure 5-12a. As shown, the PLC consisted of two modules, the CPU and AI signal module. The CPU and AI signal module are shown in figure 5-12a. The CPU was powered by a 230 VAC supply which in turn supplied the AI module with 24 VDC. The Siemens CPU made use of the Profinet Industrial Ethernet communication standard which permitted reliable communication at high speed. A simple diagram illustrating this is shown in figure 5-12b.

(a) Installed Siemens S7-1200 PLC

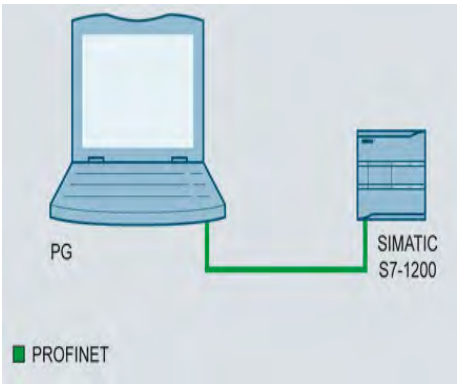

(b) CPU Profinet communication bus

Figure 5-12: Siemens PLC system and Profinet communication bus

The models of the CPU and AI signal modules are shown in figures 5-13a and 5-13b. These models are shown in conjunction with table 5-1 to illustrate the electrical connections between the CPU and AI module. As can be seen from figure 5-13a, 5-13b and table 5-1, the CPU had digital and analog inputs along with relay outputs. The CPU relay contacts were rated to carry only 3 A and therefore the internal CPU relays were used to operate 10 A (20 A when both contacts were used) double pole double throw (DPDT) relays to carry the load currents. The CPU used digital input switches (DI0, DI1) for logic purposes to enable the control and communication system.

The AI signal module performed no processing and was an extension of the CPU's functionality to read analog values. The AI signal module was used to read the values obtained from the CTs that measured the load current. The AI module converted the measured load current into scaled values ranging between -32768 and +32768. The complete list of connections and interfaces is shown in table 5-1.

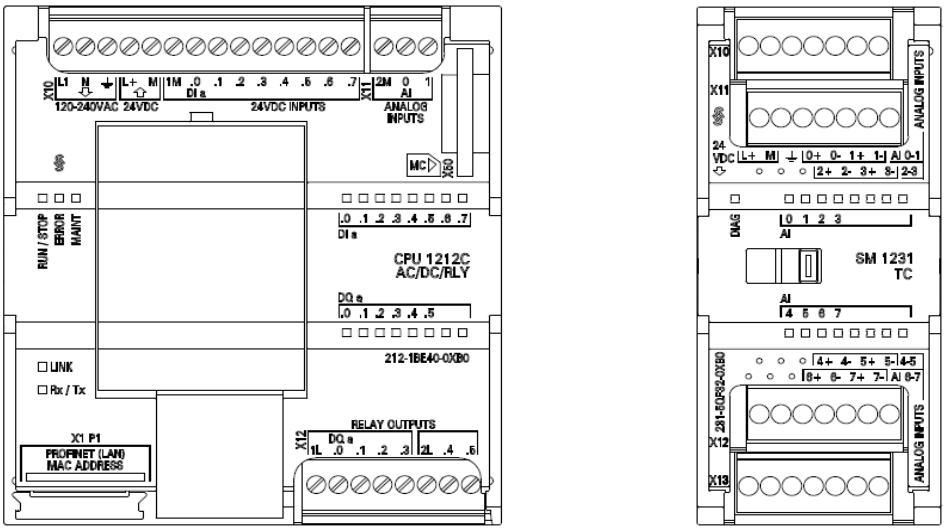

(a) Siemens S7-1200 CPU wiring diagram (b) Siemens SM1231 AI wiring diagram

Figure 5-13: System controller wiring diagram

Table 5-1: Wiring diagram reference

Siemens S7-1200 CPU		**Analog Input Module SM1231**	
ID	**Designation**	**ID**	**Designation**
L	230 VAC	AI0	CT0: Geyser
N	230 VAC	AI1	CT1: Washing M./ Tumble Dryer
GND	Grounded	AI2	CT2: Swimming Pool
AI0	Spare	AI3	CT3: Refrigerator
AI1	Spare	AI4	CT4: Battery Charger
DI0	Master Control	AI5	CT5: Dishwasher
DI1	Master Communication	AI6	Spare
DI2-DI7	Spare	AI7	Spare

DO0	CR0: NO: Geyser NC: Refrigerator	V+	24 VDC
DO1	CR1: NO: Wash. M./Tumble D. NC: Spare	V-	0 VDC
DO2	CR2: NO: Swimming Pool NC: Spare		
DO3	CR3: NO: Dishwasher NC: Spare		
DO4	CR4: NO: Battery Charger NC: Spare		
DO5	CR5: NO: DC Security Light NC: Spare		

5.2.3.2 Relays, CTs and Circuit Breakers

The circuit breakers that were used for protection purposes are shown in figure 5-14b and corresponded to the rating discussed in the design chapter. The circuit breakers were added to the microgrid test station to prevent damage to equipment in case of faults. A standard 30 mA earth leakage unit was also added to the protection scheme in case an earth fault crept in. This was primarily done to safeguard the user during testing. The secondary side of the circuit breakers was connected to primary side of the relays. These relays were controlled by the PLC's relay outputs and wired according to figure 5-13 and table 5-1. The CTs were connected between the circuit breakers and relays. The CTs fed the current drawn by the loads to the PLC which were used to operate the relays and exercise control over the loads. A schematic illustrating the wiring of the circuit breakers, CTs and relays are presented in figure 5-14a along with the installation of these components in figure 5-14b.

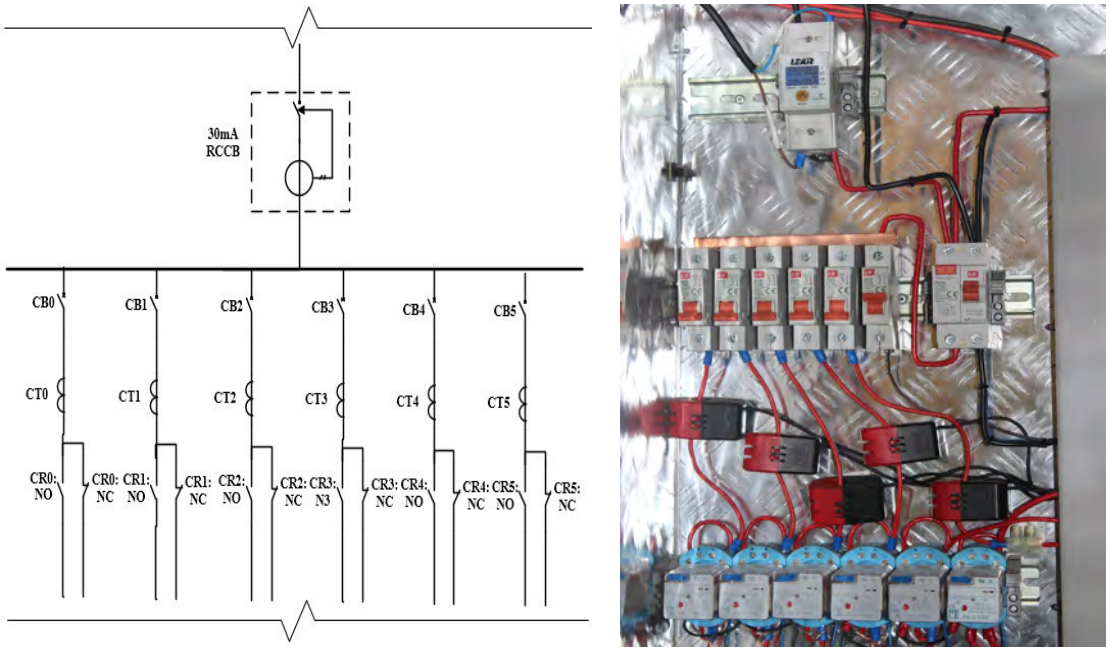

(a) CTs, circuit breakers and relays wiring diagram (b) Installed CTs, circuit breakers and relays

Figure 5-14: CTs, circuit breakers and relays

5.2.4 Software System

This section describes and illustrates the software that was used to enable communication to and from the control system. The PLC was not only responsible to exercise control over the microgrid system but also for ensuring real-time feedback on the status of the microgrid system. The feedback was received by the EMS software installed on the server which captured and recorded all the data sent by the PLC. The server also provided an interface for the user to input certain control measures such as load starting times and tariff structures. Screenshots of the PLC software structure and EMS software interface are shown in the figures below.

5.2.4.1 PLC Diagrams

Figure 5-15a illustrates the interconnection between the CPU and AI module. As seen in figure 5-15a, the PLC and AI module corresponded to the selected components in the design and simulation chapters. The program blocks that were loaded onto the CPU are shown in figure 5-15b.

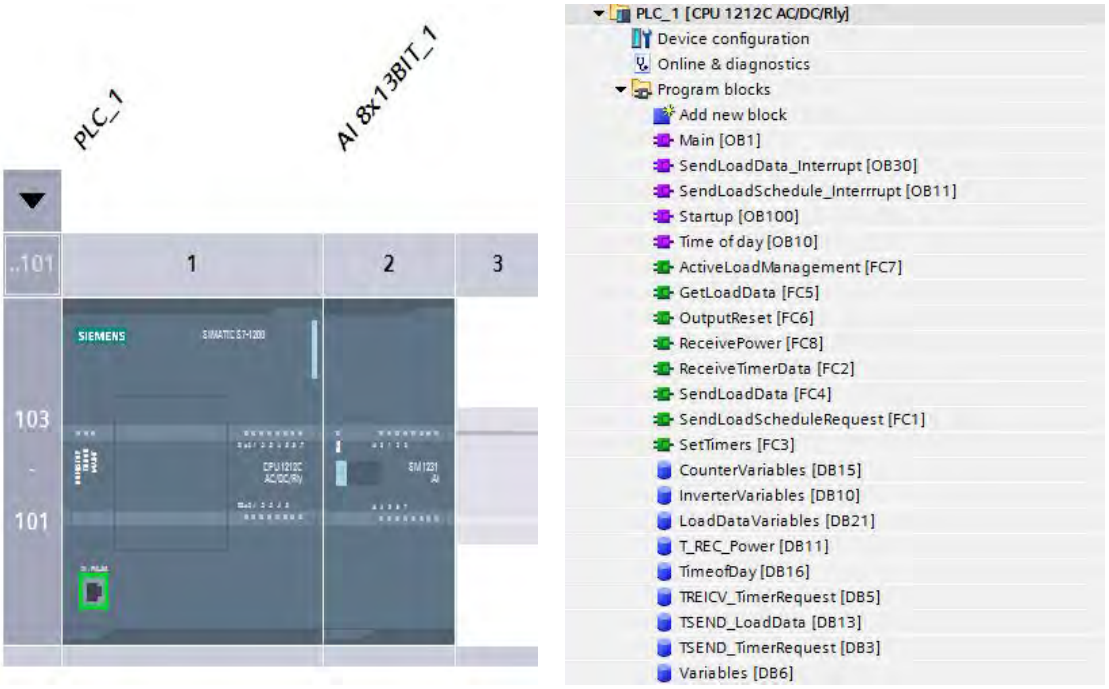

(a) PLC CPU and AI module interconnection

(b) PLC CPU program blocks

Figure 5-15: PLC interconnection and program blocks

Figure 5-15b illustrates that there was several program blocks that were loaded onto the CPU. The program blocks on the PLC were structured such that 5 interrupts, 8 functional blocks and 9 variable blocks were required. The interrupts were executed at either a specific time of the day, on a continuous cyclic time or during the start-up cycle of the CPU. The actions associated with the interrupts consisted of setting up the PLC and sending/receiving data to/from the server.

The functional blocks were responsible for the measurement of the load currents, implementing timer data settings, actively controlling EMS load conditions and extracting/combining received/sent data strings. The variable blocks were used as place holders

and memory storage blocks to simplify the memory management. Variables of all types (integer, string, double, word, boolean etc.) were used to simplify the memory management.

5.2.4.2 EMS Software Interface

The EMS software interface was divided into four main pages. The first page was the user interface where the user could input the commands to establish the network connection, select the type of day (normal or laundry day) and select the tariff structure. From this page it was also established whether all devices were communicating within the network. A screenshot of the user interface page is shown in figure 5-16.

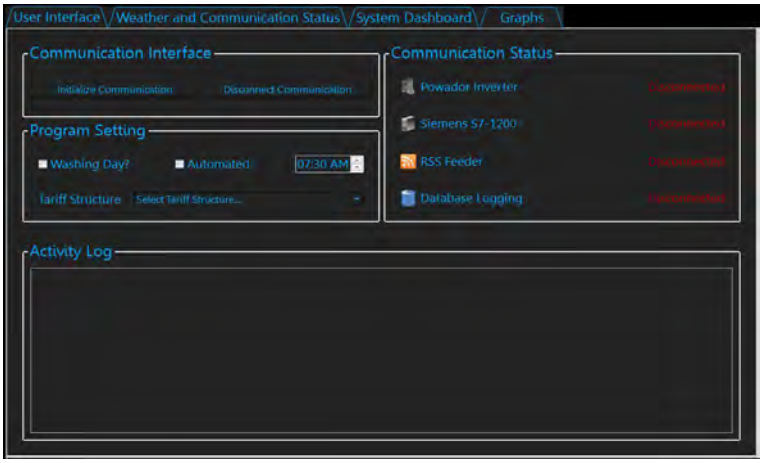

Figure 5-16: EMS software interface: User interface

On the weather and communication page, the current and predicted weather status was displayed. Apart from the described weather status, graphs visually illustrating the relative humidity, temperature and wind speed were updated in real-time. The weather and communication page is shown in figure 5-17.

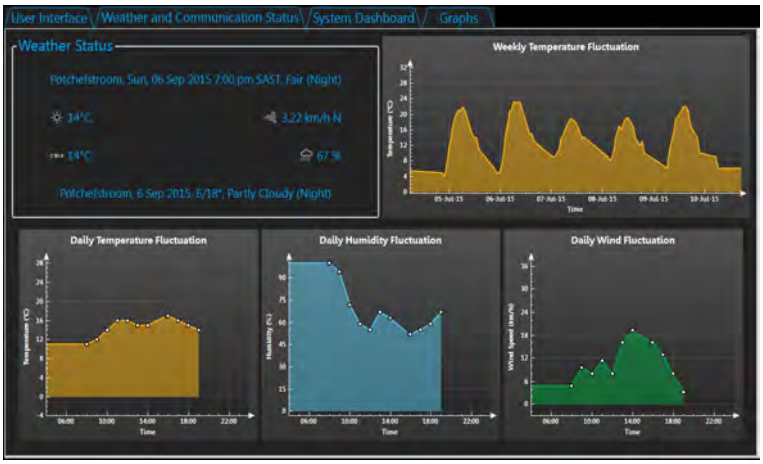

Figure 5-17: EMS software interface: Weather and communication status

The system dashboard page was designed to provide feedback to the user on the status of the system. Information such as the delivered and consumed energy, maximum power demand and consumption and daily tariff metering was presented on this page. This page

was completely autonomous and did not require any inputs from the user. The system dashboard page is shown in figure 5-18.

Figure 5-18: EMS software interface: System dashboard

The final page of the EMS software interface was the graphs page which contained real-time graphs of the incoming solar PV power and load status of the microgrid testing station. Real-time measurements from the GTI and CTs were used to compile these graphs. Also shown on this page was the forecasted solar PV input curve. The graphs page is shown in figure 5-19.

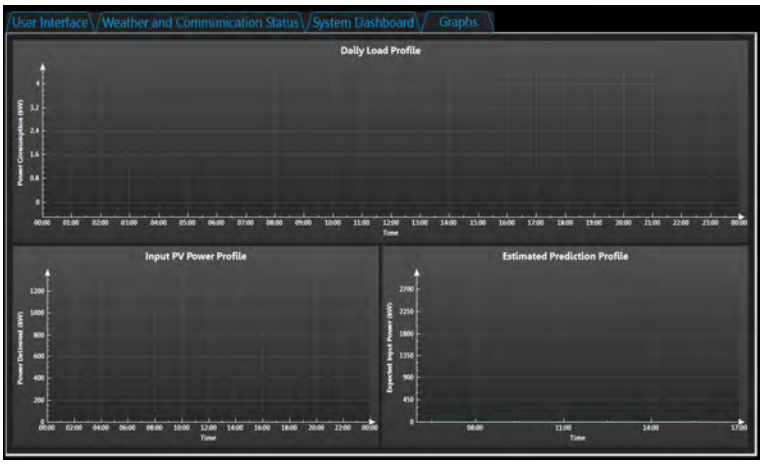

Figure 5-19: EMS software interface: Graphs

5.2.5 Integrated Microgrid Test Station

The integrated microgrid test station combined all the individual components to create a system where testing could be conducted in a safe and controlled environment. The front panel of the microgrid test station is shown in figure 5-20a which could be locked to prevent unauthorised access. The main switch shown on the front panel controlled the PLC which in turn controlled the entire system.

The large green indicator lamp next to the main switch indicated that the GTI and PLC were switched on and synchronised. The LED indicators above the main switch indicated

which relays were energised and hence acted as a warning to indicate that dangerous voltage levels was present. Within figure 5-20b, the inside of the microgrid test station is shown where all the individual components were combined.

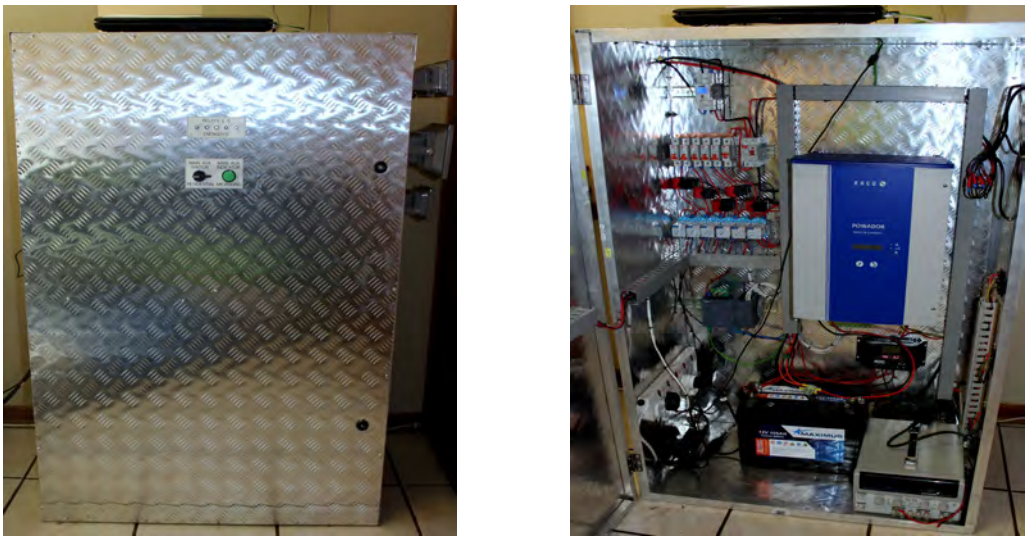

(a) Test station front panel

(b) Test station contents

Figure 5-20: Integrated test station

5.3 Experimental Results: Detailed Scenarios

The experimental results were obtained by allowing the test station to operate for a duration of 34 days. Testing could not be done for 34 consecutive days as loadshedding was taking place on a regular basis. This led to several testing days being disregarded from the experimental results. Some of the selected results that were collected were carefully analysed to ensure that no external factors such as loadshedding influenced the experimental results. To thoroughly illustrate the operation of the control system, different scenarios are illustrated below. These scenarios have differences relating to the amount of daily input energy and peak power output from the solar PV system and weather conditions such as relative humidity, wind speed and daily temperatures. Each of the scenarios below are discussed according to the input solar PV profile, weather conditions and connected loads.

5.3.1 Controlled System: Non-Laundry Day

5.3.1.1 Scenario 1

Figure 5-21 shows the temperature, wind speed and relative humidity throughout the day. It is important to take note that the relative humidity is scaled on the secondary axis of the graph. From figure 5-21 it is seen that sunrise and sunset was at 06h48 and 17h24 respectively. The day started out at a relatively low temperature (3°C), high relative humidity (77%) and no wind. As the day progressed, the temperature rose to a maximum of 20°C at 13h35. By this time the wind speed increased to 10 km/h which was defined as a light breeze. As the late afternoon set in, the temperature and wind speed gradually declined whilst the relative humidity rose. One of the factors that greatly influenced the amount of

incoming solar PV power was the cloud cover index. The captured weather data reported that there was no cloud cover during the day which was indicated as a "Clear" on the weather report.

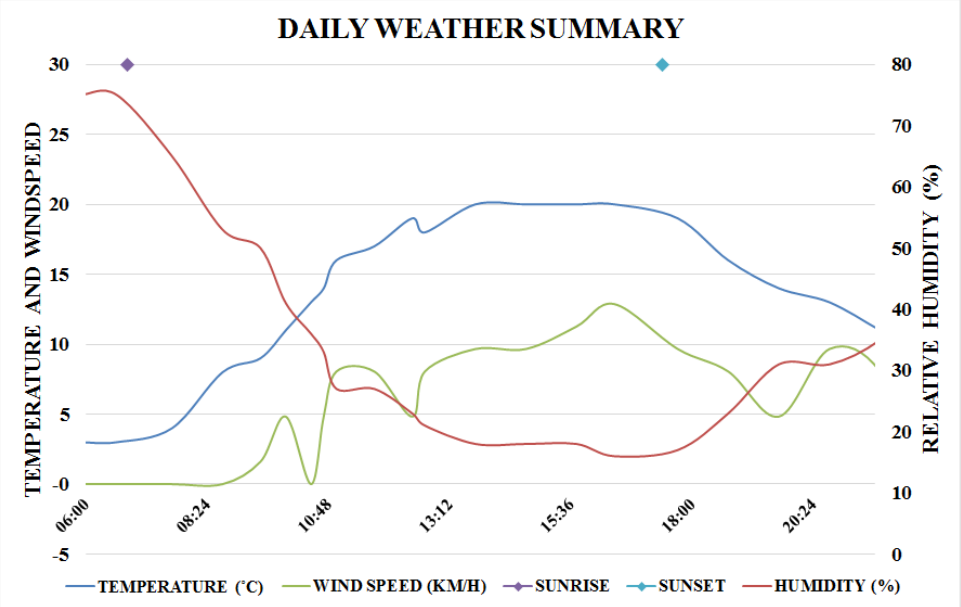

Figure 5-21: Summary of weather on 9 June 2015

The input solar PV profile and individual load curves corresponding to the weather conditions above are shown in figure 5-22. A discussion on the figure follows below where each individual load is addressed accordingly.

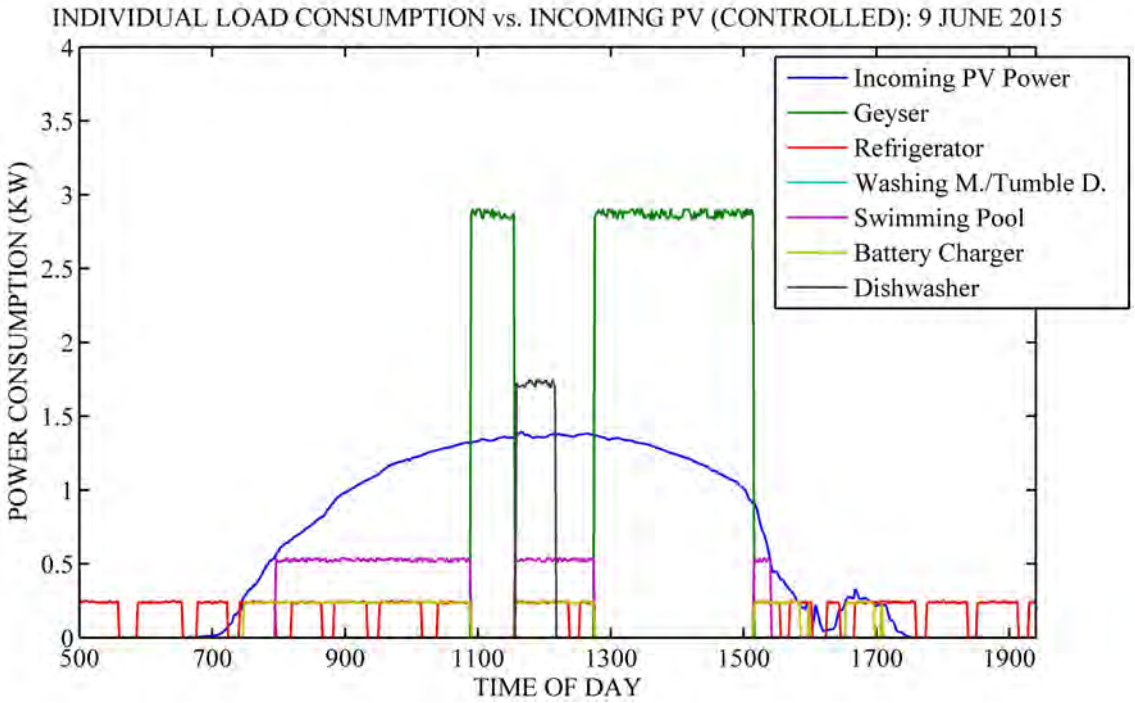

Figure 5-22: Individual load vs. incoming solar PV plot (9 June 2015)

- **Incoming PV Power:** It is seen that the incoming solar PV power steadily in-

creased to nearly 1.4 kW at noon. The output from the GTI remained steady until 15h15 where a steep drop in the incoming solar PV power was observed. This was due to the fact that a large shadow was cast over a portion of the solar PV panels during the late afternoon. Despite the disrupted solar PV profile due to the shadow, additional performance characteristics of the control system were obtained which are discussed below.

Characteristic	Experimental Result
Total Input Energy	7.81 kWh
Peak Power Output	1.39 kW
Start and Stop Time	07h01 to 17h14
Total Generating Time	10:13 Hours

- **Geyser:** The geyser was switched on at two separate occasions during the day. The first was during the late morning (10h56) hours prior to the dishwasher starting time. This preheated the water for the dishwasher which reduced the runtime of the dishwasher. The second occasion where the geyser was switched on was to heat water for bathing and showering in the evening. The steep drop in the incoming solar PV power during the late afternoon caused the geyser to switch off earlier than expected which led to the water not being heated to the desired temperature. However, the control systems' main objective was to reduce consumption off the utility grid and hence the geyser was switched off when the incoming solar PV power dropped.

Characteristic	Experimental Result
Maximum Power Demand	2.91 kW
Total Run-time	2:58 Hours
Start and Stop Time 1	10h56 to 11h32
Start and Stop Time 2	12h45 to 15h07

- **Refrigerator:** As stated previously the refrigerator could not actively be controlled since the compressor operated on its own closed-loop control system. However, control over the refrigerator was exercised by switching off the refrigerator during times when the geyser was switched on. As seen from the curve of the refrigerator, the refrigerator switched on/off spontaneously to regulate the temperature.
- **Washing Machine/Tumble Dryer:** Neither the washing machine or the tumble dryer were switched on in this scenario.
- **Swimming Pool:** The swimming pool pump was switched on during the mid-morning period as soon as the incoming solar PV power exceeded that of 0.55 kW. Whenever sufficient capacity was available, the control system switched on the swimming pool pump. The swimming pool pump was not allowed to be switched on at the same time as the geyser and was therefore switched on at three separate occasions. The steep drop in incoming solar PV power caused the swimming pool pump to switch off to reduce consumption off the utility grid. If the incoming solar PV power did not have such a sharp decrease, the swimming pool pump would have been switched on for another hour. The samples of the load current were taken every 15 seconds and hence the starting and magnetizing currents were not detected. The maximum power demand of the swimming pool pump was 0.54 kW as shown in the table below.

Characteristic	Experimental Result
Maximum Power Demand	0.54 kW
Total Run-time	4:43 Hours
Start and Stop Time 1	07h48 to 10h55
Start and Stop Time 2	11h36 to 12h44
Start and Stop Time 3	15h09 to 15h27

- **Battery Charger:** The battery charger was switched on similarly to the swimming pool i.e. whenever incoming solar PV power exceeded that of 0.25 kW. Whenever this condition was met, the control system switched on the battery charger which charged the battery. In this specific scenario, the battery was almost completely discharged and hence required a longer period of charging. Since the battery was an essential part of the DC security light system that needed to operate during night-time, the battery charger received priority over other loads. This ensured that the battery had adequate charge for the DC security light to operate through the night. Similarly to the geyser and swimming pool pump, its operation was cut short due to the shadow on the solar PV panels. However, upon closer inspection, it was seen that the battery charger was switched on for a fourth time at 16h38 due to increased solar PV power in the late afternoon. The battery charger operating time and SOC (11.62 V) suggested that the battery's charge was in the order of 15-25% of the nominal rating.

Characteristic	Experimental Result
Maximum Power Demand	0.25 kW
Total Run-time	5:54 Hours
Start and Stop Time 1	07h10 to 10h55
Start and Stop Time 2	11h36 to 12h44
Start and Stop Time 3	15h09 to 15h57
Start and Stop Time 4	16h38 to 16h51

- **Dishwasher:** The dishwasher was carefully controlled by the control system to switch on during the forecasted peak incoming solar PV power (during noon). It was no different for this scenario and the dishwasher was switched on 24 minutes before noon for 49 minutes. It was expected that the dishwasher would continue for a longer period and hence the geyser starting time was 18 minutes late. More of this is discussed in the following section.

Characteristic	Experimental Result
Maximum Power Demand	1.74 kW
Total Run-time	0:49 Hours
Start and Stop Time 1	11h36 to 12h27

Figure 5-23 shows the combined load curve versus the incoming solar PV profile. This figure provides insight into how the control system reshaped the load profile according to the available solar PV power. Figure 5-23 is discussed below according to the annotations made on the figure.

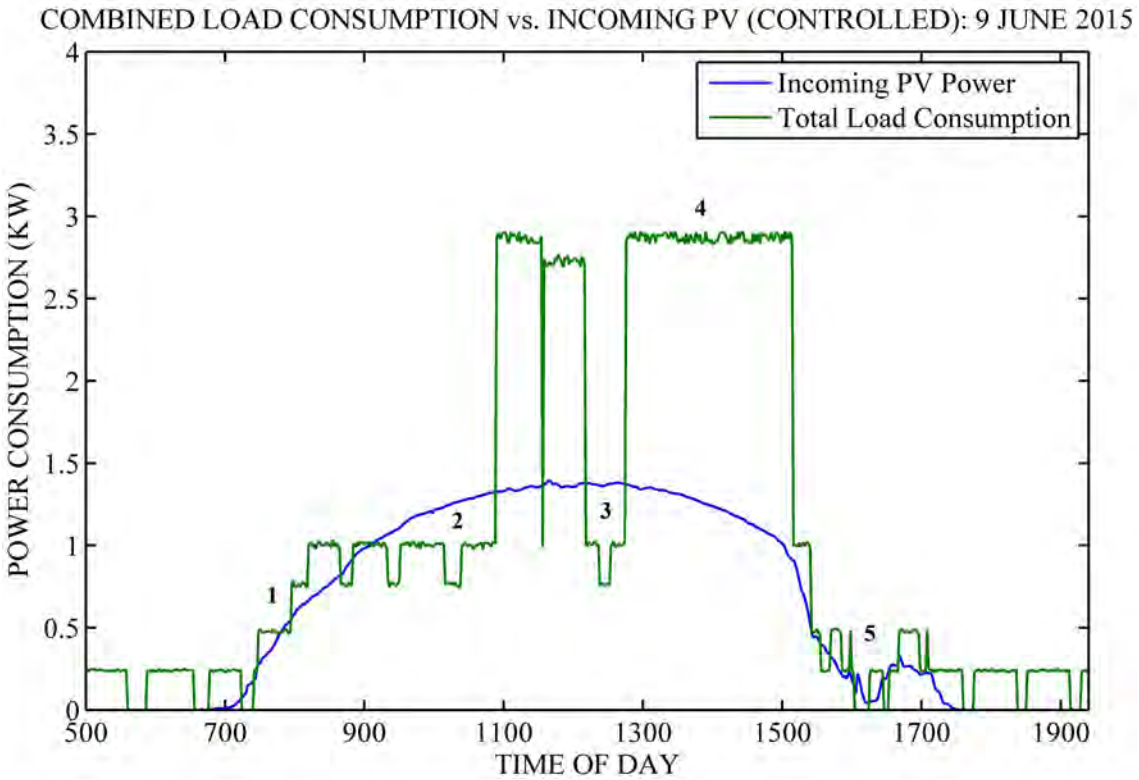

Figure 5-23: Combined load vs. incoming solar PV plot (9 June 2015)

- **Note 1:** This annotation illustrates that as the incoming solar PV power rose early in the day, the loads were switched on such that the load power consumption grew at the same rate. The instantaneous power consumption was never greater than 1.4 times the incoming solar PV power. This was greater compared to the simulation value of 1.2 times which is owed to the arbitrary switching of the refrigerator.
- **Note 2 and 3:** These annotations illustrated the area where energy was wasted due to the geyser not switching on at exactly the correct time. If the geyser was switched on at roughly 9h30 and 12h15 respectively, the wasted energy would have been minimised.
- **Note 4:** The elimination of loads being simultaneously powered reduced the peak demand to 2.91 kW.
- **Note 5:** The sudden drop in the incoming solar PV power caused the control system to suddenly drop loads. This annotation illustrates that the total load consumption was quickly reduced during this period. As the incoming solar PV power had a late afternoon increase, the control system switched on the battery charger which further charged the battery.

A summary of the experimental results is shown in table 5-2. From the table below it is noted that the total daily energy consumption by the loads were 15.25 kWh. The incoming solar PV power contributed to 46.7% of this total (7.12 kWh). The percentage of incoming solar PV power that was absorbed by the loads (overall system efficiency) was 91.3%.

Table 5-2: Summary of controlled experimental results for 9 June 2015

Parameter	Result
Total PV Energy Input	7.81 kWh
PV Energy Lost	0.68 kWh
Total Daily Load	15.25 kWh
Energy Cons. off Utility	8.13 kWh
Energy Cons. off PV	7.12 kWh
Percentage Utility Supplied	53.30%
Percentage PV Supplied	46.70%
Maximum Demand	2.91 kW
Overall System Efficiency	91.30%

5.3.1.2 Scenario 2

Figure 5-24 shows the temperature, wind speed and relative humidity on the 7th of July 2015. It is important to take note that the relative humidity are scaled on the secondary axis of the graph. From figure 5-24 it is seen that sunrise and sunset was at 06h56 and 17h28 respectively. The day started out at a moderate to low temperature (8°C), high relative humidity (81%) and light winds (10 km/h). As the day progressed, the temperature rose to a maximum of 19°C at 15h36. By this time the wind speed increased to 20 km/h which was defined as a moderate breeze. As the late afternoon set in, the temperature gradually declined whilst the relative humidity rose. The wind speed further increased during the dusk period. The captured weather data reported that there was dispersed cloud cover during the day which was indicated as a "Fair" on the weather report.

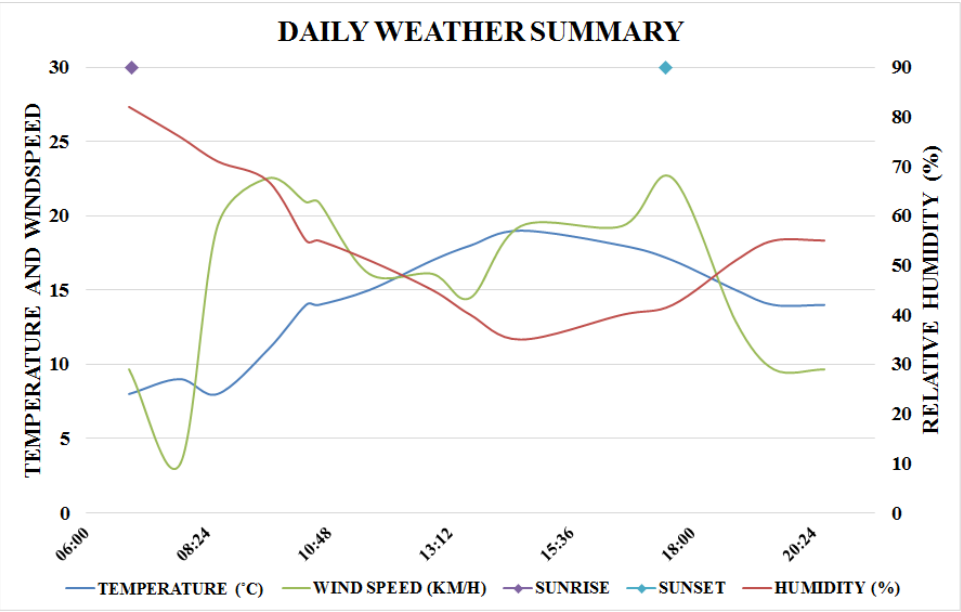

Figure 5-24: Summary of weather on 7 July 2015

The input solar PV profile and individual load curves corresponding to the weather conditions above are shown in figure 5-25. A discussion on the figure follows below where each individual load is addressed accordingly.

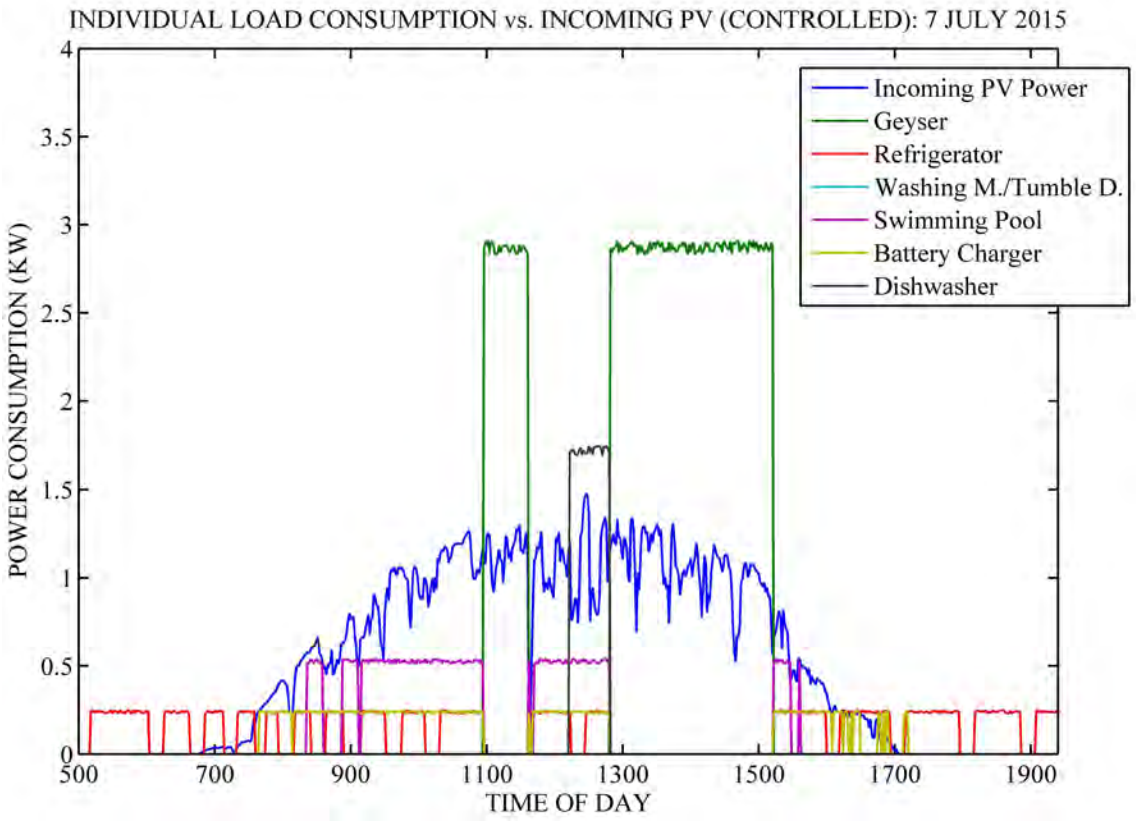

Figure 5-25: Individual load vs. incoming solar PV plot (7 July 2015)

- **Incoming PV Power:** The effect of the dispersed cloud cover was clearly visible on the incoming solar PV power profile. The incoming power gradually increased as the day progressed to noon; however there were fluctuations of the incoming solar PV power. As the afternoon set in, the incoming power gradually declined with larger fluctuations and steep drops. The excessive fluctuations caused more infrequent switching of loads which could have detrimental effects on the reliability of the appliances in the longer run. The effect of the infrequent switching of the loads require further investigation which fall beyond the scope of this study.

Characteristic	Experimental Result
Total Input Energy	6.40 kWh
Peak Power Output	1.48 kW
Start and Stop Time	06h56 to 17h24
Total Generating Time	10:28 Hours

- **Geyser:** Since the control system operated the geyser starting time based on the time of day and not on the incoming solar PV power, the fluctuations did not influence the operation of the geyser. Similar to the previous scenario, the geyser was switched on at two separate occasions during the day. The first was in the late morning (10h56) hours for a period of 36 minutes. The second followed directly after the dishwasher finished its operating cycle. Similar to the previous scenario, the control system switched the geyser off to reduce consumption off the utility grid.

Characteristic	Experimental Result
Maximum Power Demand	2.91 kW
Total Run-time	2:58 Hours
Start and Stop Time 1	10h56 to 11h32
Start and Stop Time 2	12h50 to 15h12

- **Refrigerator:** As stated above, due to the internal closed-loop control system of the refrigerator, very little control could be exercised over the refrigerator. Control over the refrigerator was exercised by switching off the refrigerator during the times when the geyser was switched on.
- **Washing Machine/Tumble Dryer:** Neither the washing machine or the tumble dryer were switched on in this scenario.
- **Swimming Pool:** The fluctuation of the incoming solar PV power caused the swimming pool pump to be switched on seven times throughout the day. This was due to the excessive solar PV power fluctuations in the morning (up to 9h15) and late afternoon (from 15h30). On a typical non-laundry day the swimming pool pump was supposed to be switched no more than three times, however the fluctuations caused an additional four switching operations. These stints of operation lasted less than 20 minutes, with the shortest being less than one minute. The additional switching on the swimming pool pump is not desirable as the motor is subjected to high starting and magnetizing current. Apart from the switching issues, the swimming pool pump operated for only 3 hours and 50 minutes which was insufficient to thoroughly circulate enough water through the swimming pool's filtration system. The start and stop times shown in the table below contains only the running times longer than 10 minutes.

Characteristic	Experimental Result
Maximum Power Demand	0.53 kW
Total Run-time	3:56 Hours
Start and Stop Time 1	08h14 to 08h29
Start and Stop Time 2	08h49 to 09h08
Start and Stop Time 3	09h12 to 10h55
Start and Stop Time 4	11h35 to 12h48
Start and Stop Time 5	15h04 to 15h30

- **Battery Charger:** The excessive fluctuations of the incoming solar PV power had a less severe effect on the battery charger during the morning compared to the swimming pool pump. This was due to the incoming solar PV power fluctuation not dropping below the 0.25 kW mark which would have caused the control system to switch off the battery charger. The late afternoon fluctuations had a more severe impact on the battery charger operation. As seen in figure 5-25, the battery charger was switched on 10 times during the entire day whereas seven of those were between 16h00 and 17h20. This excessive switching was due to two factors, the first was caused by the "trickle charging" of the battery charger and the second was due to the fluctuation around the 0.25 kW threshold. Apart from the switching problems that arose, the battery charger operated for more than five hours and managed to fully recharge the battery (12.65 V).

Characteristic	Experimental Result
Maximum Power Demand	0.25 kW
Total Run-time	5:14 Hours
Start and Stop Time 1	07h40 to 10h55
Start and Stop Time 2	11h36 to 12h48
Start and Stop Time 3	15h09 to 15h56

- **Dishwasher:** As with the geyser, the dishwasher was controlled by the control system based on time of day rather than incoming solar PV power. The control system scheduled the dishwasher to switch on during the forecasted peak incoming solar PV power (during noon). It was no different for this scenario and the dishwasher was switched on after noon for 46 minutes. As soon as the dishwasher completed its cycle, the geyser was switched on.

Characteristic	Experimental Result
Maximum Power Demand	1.76 kW
Total Run-time	0:46 Hours
Start and Stop Time 1	12h03 to 12h49

Figure 5-26 shows the combined load curve versus the incoming solar PV profile. This figure provides insight into how the control system reshaped the load profile according to the available solar PV power. Figure 5-26 is discussed below according to the annotations made on the figure.

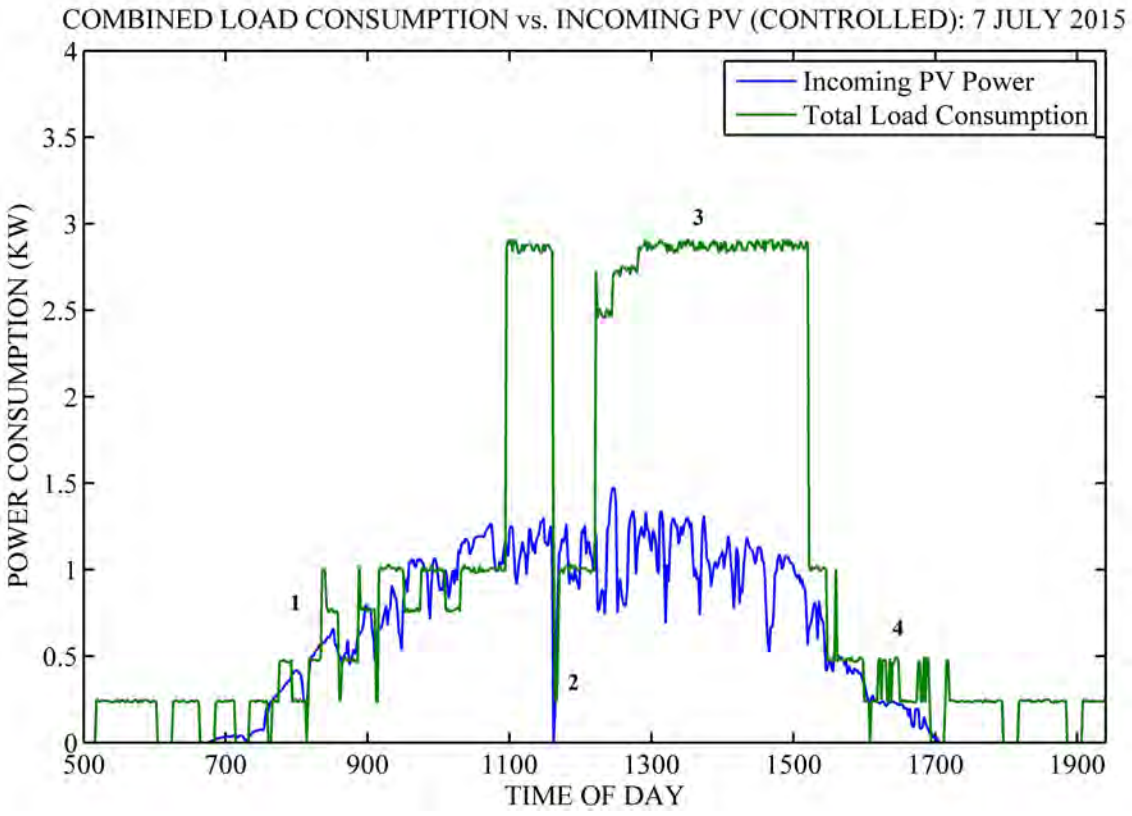

Figure 5-26: Combined load vs. incoming solar PV plot (7 July 2015)

- **Note 1:** This annotation illustrates that as the incoming solar PV power fluctuated early in the day, the loads were switched on and off to follow the incoming solar

PV profile. The incoming solar PV profile was followed as close as possible; however the large fluctuations of the incoming solar PV power significantly increased the number of switched loads. This could have a detrimental effect on the life expectancy of the appliances.

- **Note 2:** A sudden drop to nearly zero incoming solar PV power caused the control system to reduce consumption by as much as possible. This caused the control system to switch off all the loads except the refrigerator. The sudden drop in solar PV power was short lived and hence the loads were switched on as soon as the incoming solar PV power was back to the expected level.
- **Note 3:** The peak demand of the day was determined by the geyser at 2.91 kW.
- **Note 4:** Similar to the first annotation, the fluctuation of the incoming solar PV power caused excessive switching operations which is clearly visible. The excessive switching visible at this annotation was caused by the battery charger.

A summary of the experimental results are shown in table 5-3. From the table it is seen that the total daily energy consumption of all the loads were 14.83 kWh. The solar PV supplied 41.0% of this total (6.08 kWh). The percentage of solar PV power that was absorbed by the loads (overall system efficiency) was 95.1%.

Table 5-3: Summary of controlled experimental results for 7 July 2015

Parameter	Result
Total PV Energy Input	6.40 kWh
PV Energy Lost	0.32 kWh
Total Daily Load	14.83 kWh
Energy Cons. off Utility	8.75 kWh
Energy Cons. off PV	6.08 kWh
Percentage Utility Supplied	59.00%
Percentage PV Supplied	41.00%
Maximum Demand	2.91 kW
Overall System Efficiency	95.10%

5.3.1.3 Scenario 3

Figure 5-27 shows the temperature, wind speed and relative humidity on the 3rd of June 2015. Again, it is important to take note that the relative humidity is scaled on the secondary axis of the graph. From figure 5-27 it is seen that sunrise and sunset was at 06h46 and 17h24 respectively. The day started out at a moderate temperature (16°C), moderate relative humidity (77%) and gentle winds (16 km/h). The relative humidity peaked near 100% during the late morning hours as morning showers swept in. As the day progressed, the temperature rose to a maximum of 16°C at 15h11. By this time the showers had passed and the relative humidity decreased to 78%. As the late afternoon set in, the temperature gradually declined whilst the relative humidity rose. The wind speed also increased during the late afternoon reaching wind speeds of 17 km/h. The captured weather data reported that an overcast set in during the morning along with intermittent clouds for the rest of the day. Weather reports indicated that the morning were labelled as "Rain/Showers" whilst the afternoon was labelled as "Overcast".

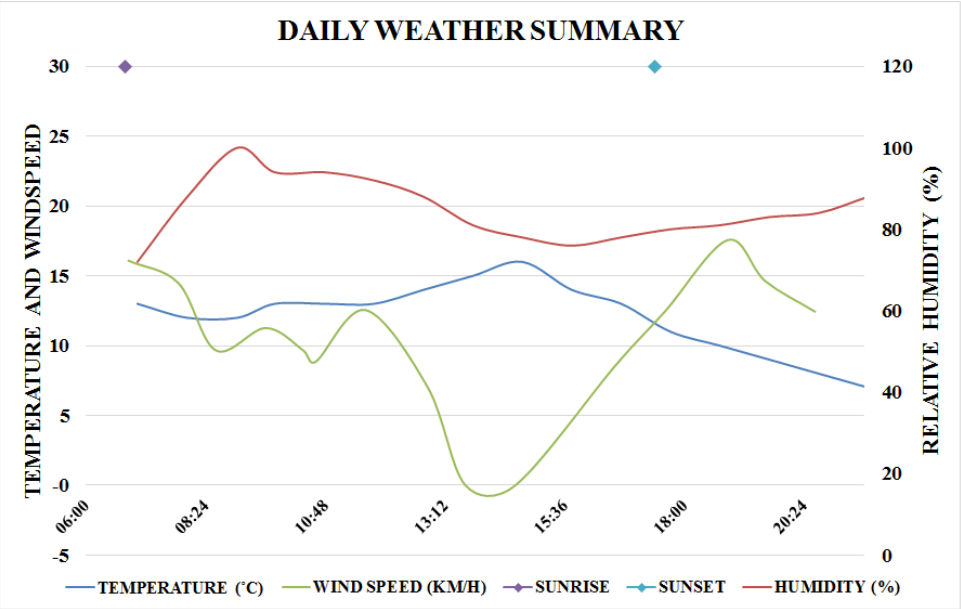

Figure 5-27: Summary of weather on 3 June 2015

The input solar PV profile and individual load curves corresponding to the weather conditions above are shown in figure 5-28. A discussion on the figure follows below where each individual load is addressed accordingly.

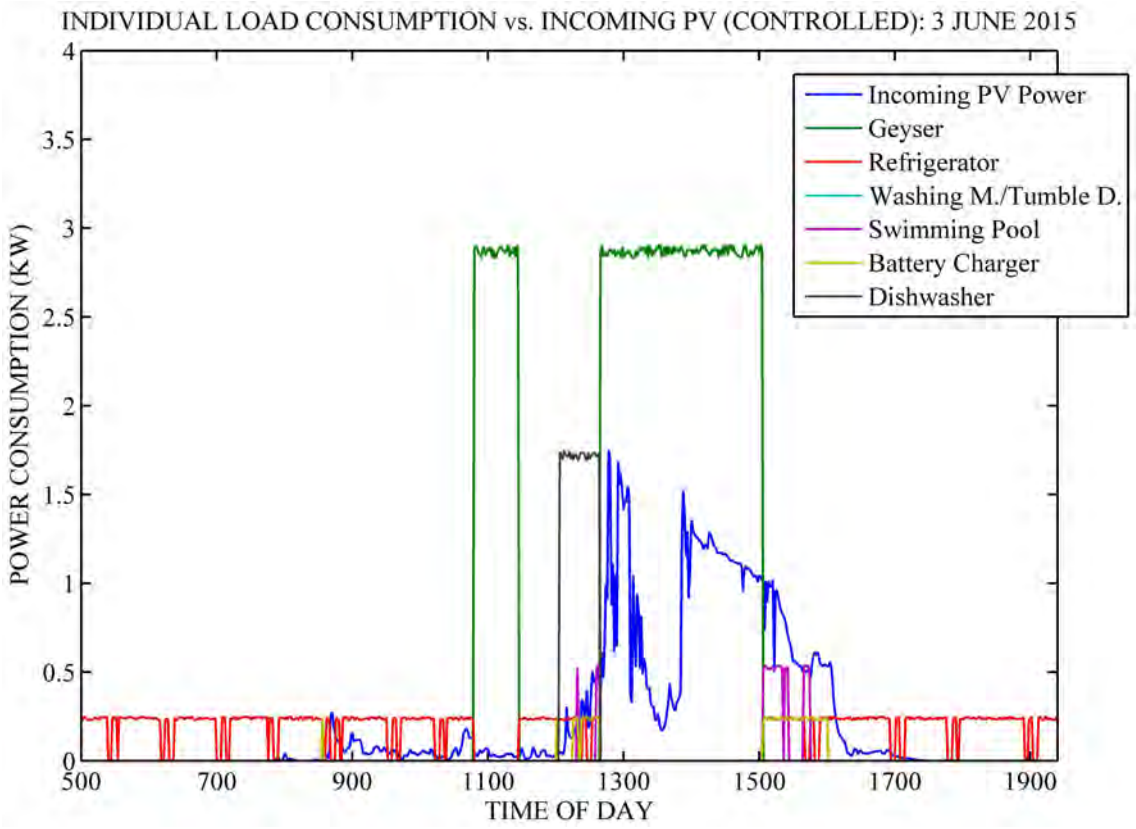

Figure 5-28: Individual load vs. incoming solar PV plot (3 June 2015)

- **Incoming PV Power:** The effect of the morning showers and afternoon overcast could clearly be seen on the incoming solar PV power profile. The incoming solar

PV power during the morning to noon was minimal and had no use. The incoming power during the morning never exceeded 0.1 kW and hence had a minimal effect on the switching of the swimming pool pump and battery charger. During the early afternoon the heavy overcast cleared somewhat which allowed solar PV power generation. This was in the timeslot when the geyser was scheduled to operate which helped decrease consumption off the utility grid. As with the previous scenario, there was large power fluctuations which caused unwanted switching in the late afternoon.

Characteristic	Experimental Result
Total Input Energy	2.76 kWh
Peak Power Output	1.74 kW
Start and Stop Time	08h06 to 17h07
Total Generating Time	09:01 Hours

- **Geyser:** The control system operated the geyser based on the time of day and not on the incoming solar PV power capacity and therefore the fluctuations did not influence the operation of the geyser. Similar to the previous scenario, the geyser was switched on at two separate occasions during the day. The first was in the late morning (10h48) hours for a period of 38 minutes. The second followed directly after the dishwasher finished its operating cycle. Similar to the previous scenario, the control system switched the geyser off to reduce consumption off the utility grid.

Characteristic	Experimental Result
Maximum Power Demand	2.91 kW
Total Run-time	3:04 Hours
Start and Stop Time 1	10h48 to 11h26
Start and Stop Time 2	12h40 to 15h03

- **Refrigerator:** As stated above, due to the internal closed-loop control system of the refrigerator, very little control could be exercised on the refrigerator. However, control over the refrigerator was exercised by switching off the refrigerator during the times when the geyser was switched on.
- **Washing Machine/Tumble Dryer:** Neither the washing machine or the tumble dryer were switched on in this scenario.
- **Swimming Pool:** Very little solar PV power during the morning caused the swimming pool pump to not be switched on until late afternoon. At 15h05 the swimming pool pump was switched on for the first time in the day. However, it was switched off after 21 minutes of operation. The fluctuations in the late afternoon caused another switching at 15h46 which lasted for less than 8 minutes. The total swimming pool pump operating time totalled less than 30 minutes.

Characteristic	Experimental Result
Maximum Power Demand	0.54 kW
Total Run-time	0:29 Hours
Start and Stop Time 1	15h05 to 15h26
Start and Stop Time 2	15h55 to 16h03

- **Battery Charger:** Similar to the swimming pool pump, the battery charger was not switched on during the morning. The battery charger was switched on for the first time at 15h05 after the geyser completed its operating cycle. The battery charger operated for a total of 52 minutes before switching off. This proved to be insufficient to fully recharge the battery. The battery was only recharged to roughly 65% SOC which translated to battery voltage of (12.3 V). This caused the DC security light to drain the battery to 13% SOC during night-time operation which reduces the life expectancy of the battery.

Characteristic	Experimental Result
Maximum Power Demand	0.25 kW
Total Run-time	0:52 Hours
Start and Stop Time 1	15h05 to 15h57

- **Dishwasher:** As with the geyser, the dishwasher was controlled by the control system based on time of day rather than incoming solar PV power. The control system scheduled the dishwasher to switch on during the forecasted peak incoming solar PV power (during noon). As with the previous scenario, the dishwasher was switched on immediately after noon for 43 minutes. As soon as the dishwasher completed its cycle the geyser was switched on.

Characteristic	Experimental Result
Maximum Power Demand	1.82 kW
Total Run-time	0:43 Hours
Start and Stop Time 1	11h58 to 12h39

Figure 5-29 shows the combined load curve versus the incoming solar PV profile. This figure provides insight into how the control system reshaped the load profile according to the available solar PV power. Figure 5-29 is discussed below according to the annotations made on the figure.

- **Note 1:** During the mid-morning period, the incoming solar PV power surpassed the 0.25 kW mark which caused the control system to switch on the battery charger. However, soon after the battery charger was switched on, the incoming solar PV power dropped below the 0.25 kW threshold which switched off the battery charger. As with the previous scenarios, the power fluctuation caused excessive switching of the loads.
- **Note 2:** The peak demand of the day was set by the geyser at 2.91 kW.
- **Note 3:** This annotation illustrates the effect that a sudden rise in incoming solar PV power had on the control system. The sudden increase in incoming solar PV power caused the control system to switch on multiple loads (battery charger and swimming pool pump) simultaneously which caused a surge in the load power consumption.
- **Note 4:** As the incoming solar PV power gradually decreased, the load curve followed soon after. In this scenario, there was a steep drop in incoming solar PV power and hence the control system switched off the battery charger and swimming pool pump instantaneously.

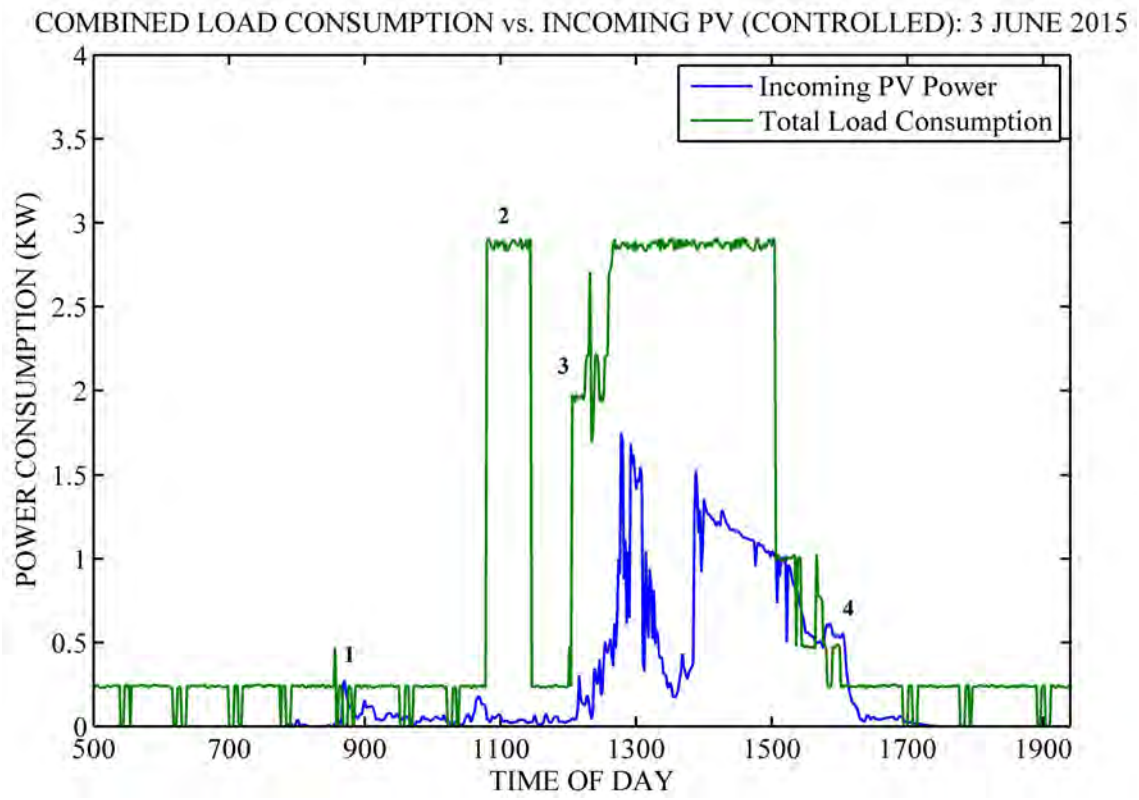

Figure 5-29: Combined load vs. incoming solar PV plot (3 June 2015)

A summary of the experimental results are shown in table 5-4. From table 5-4 it is seen that the total daily energy consumption by all the loads were 13.04 kWh. The incoming solar PV power covered only 20.35% of the total daily load (2.65 kWh). Although the percentage of incoming solar PV power that was absorbed by the loads (overall system efficiency) was 96.1%, it had very little impact on meeting the daily load requirements. However, the weather had a significant impact on the performance of the solar PV panels which did not permit the high energy yields.

Table 5-4: Summary of controlled experimental results for 3 June 2015

Parameter	Result
Total PV Energy Input	2.76 kWh
PV Energy Lost	0.11 kWh
Total Daily Load	13.04 kWh
Energy Cons. off Utility	10.39 kWh
Energy Cons. off PV	2.65 kWh
Percentage Utility Supplied	79.65%
Percentage PV Supplied	20.35%
Maximum Demand	2.91 kW
Overall System Efficiency	96.10%

5.3.2 Controlled System: Laundry Day

Figure 5-30 shows the temperature, wind speed and relative humidity throughout the day. From figure 5-30 it is noted that sunrise and sunset was at 06h50 and 17h24 respectively.

The day started out at a low to moderate temperature (7°C), moderate relative humidity (58%) and very little wind. As the day progressed, the temperature gradually rose to a maximum of 17°C around 15h36. By this time the wind speed increased to 21 km/h which was defined as a moderate breeze. As the late afternoon set in, the temperature and wind speed declined whilst the relative humidity rose. The captured weather data reported that there was no cloud cover during the day which was indicated as a "Clear" on the weather report.

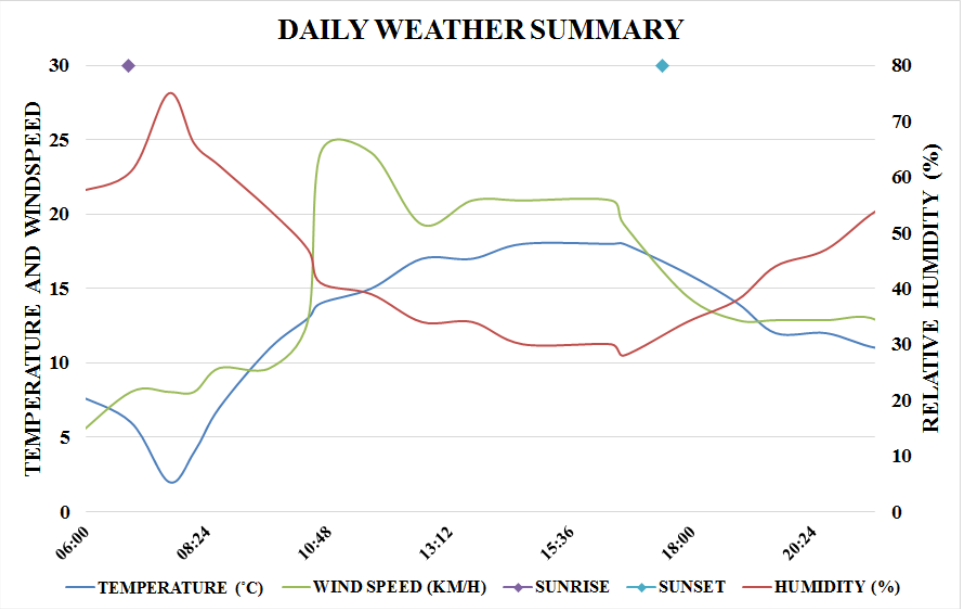

Figure 5-30: Summary of weather on 10 June 2015

The input solar PV profile and individual load curves corresponding to the weather conditions above are shown in figure 5-31. A discussion on the figure follows below where each individual load is addressed accordingly.

- **Incoming PV Power:** As seen in figure 5-31, there were no disruptions that influenced the incoming solar PV profile. No power fluctuations, shadows or intermittent cloud cover were present in this scenario. The incoming solar PV profile corresponds very well to the weather report yielding satisfactory results. The incoming solar PV power provided a longer than usual day of power generation, stretching from 06h50 to 17h25.

Characteristic	Experimental Result
Total Input Energy	8.81 kWh
Peak Power Output	1.41 kW
Start and Stop Time	06h50 to 17h25
Total Generating Time	10:35 Hours

- **Geyser:** Due to the day being allocated for laundry purposes, the geyser was switched on at only one occasion during the day. This was done prior to noon. The geyser was then switched off at 15h07 to allow the battery charger and swimming pool pump to be switched on. Since the washing machine and tumble dryer was required during the day, there were no time in the morning to switch the geyser on for additional water heating.

Characteristic	Experimental Result
Maximum Power Demand	2.90 kW
Total Run-time	3:22 Hours
Start and Stop Time 1	11h45 to 15h07

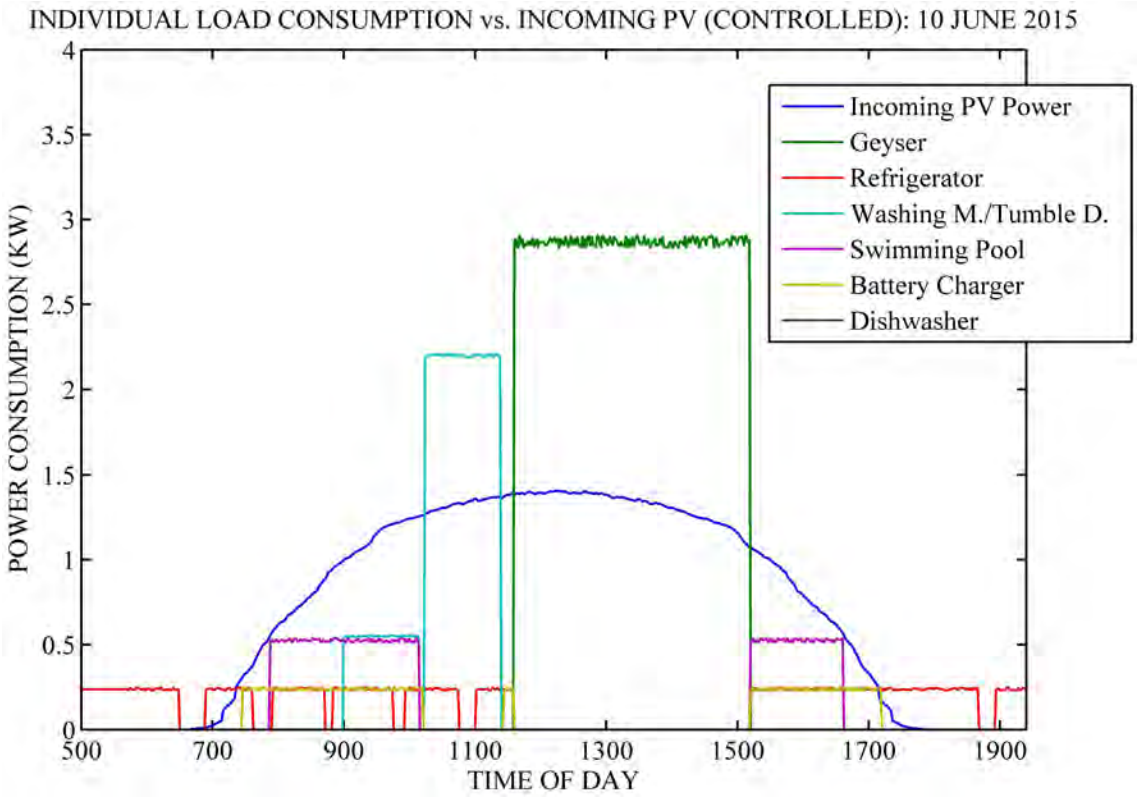

Figure 5-31: Individual load vs. incoming solar PV plot (10 June 2015)

- **Refrigerator:** Control over the refrigerator was exercised by switching off the refrigerator during the times when the geyser was switched on.
- **Washing Machine/Tumble Dryer:** The washing machine and tumble dryer were time of day controlled and set to switch on during the late morning hours when incoming solar PV power was sufficient. The washing machine had a lower power requirement than the tumble dryer and was switched on at 09h00 and finished at 09h55. Thereafter, the tumble dryer was switched on which continued until 11h15. During the operation of the tumble dryer all loads except the refrigerator was switched off to minimise consumption off the utility grid.

Characteristic	Experimental Result
Maximum Power Demand	0.56 kW and 2.18 kW
Total Run-time	2:15 Hours
Start and Stop Time 1	09h00 to 09h55
Start and Stop Time 2	09h57 to 11h15

- **Swimming Pool:** The swimming pool pump was switched on as soon as the incoming solar PV power exceeded that of 0.55 kW. This caused that whenever sufficient capacity was available, the control system switched on the swimming pool. The swimming pool was not allowed to be switched on at the same time as the geyser

and tumble dryer. The swimming pool was switched on at two separate occasions, 07h48 and 11h36 which resulted in a total operating time of 4:43 hours.

Characteristic	Experimental Result
Maximum Power Demand	0.56 kW
Total Run-time	4:43 Hours
Start and Stop Time 1	07h48 to 10h55
Start and Stop Time 2	11h36 to 12h44

- **Battery Charger:** The battery charger switched on as soon as the incoming solar PV power exceeded that of 0.25 kW. Whenever this condition was met, the control system switched on the battery charger which allowed charging of the battery to occur. In this specific scenario, the battery charger was switched on at four separate occasions. The first was at 07h10, the second at 11h36, the third at 15h08 and the last at 16h38. The total run-time for the battery charger was 5:54 hours. The 5:54 hours of battery charging ensured that the battery was charged to 95% SOC (12.61 V).

Characteristic	Experimental Result
Maximum Power Demand	0.24 kW
Total Run-time	5:54 Hours
Start and Stop Time 1	07h10 to 10h55
Start and Stop Time 2	11h36 to 12h44
Start and Stop Time 3	15h08 to 15h57
Start and Stop Time 4	16h38 to 16h51

- **Dishwasher:** The dishwasher was not switched on in this scenario due to limited time available to perform the washing and tumble drying tasks.

Figure 5-32 shows the combined load curve versus the incoming solar PV profile. This figure provides insight into how the control system reshaped the load profile according to the available solar PV power. Figure 5-32 is discussed below according to the annotations made on the figure.

- **Note 1 and 4:** The incoming solar PV profile was near perfect for the entire day and hence these results were the closest comparable to the simulation results. During the mid-morning period, the incoming solar PV power rose gradually which caused the control system to switch on the battery charger and swimming pool pump as soon as sufficient capacity was available. In a similar manner, the control system switched off the swimming pool and battery charger as the incoming power became less than the respective threshold values.
- **Note 2:** The sudden drop in power consumption was owed to the tumble dryer finishing its operating cycle 9 minutes early. During the tumble dryer's cycle all other loads except the refrigerator were already switched off. This caused the significant drop in consumption when the tumble dryer finished its cycle earlier than expected.
- **Note 3:** The peak demand of the day was set by the geyser at 2.91 kW.

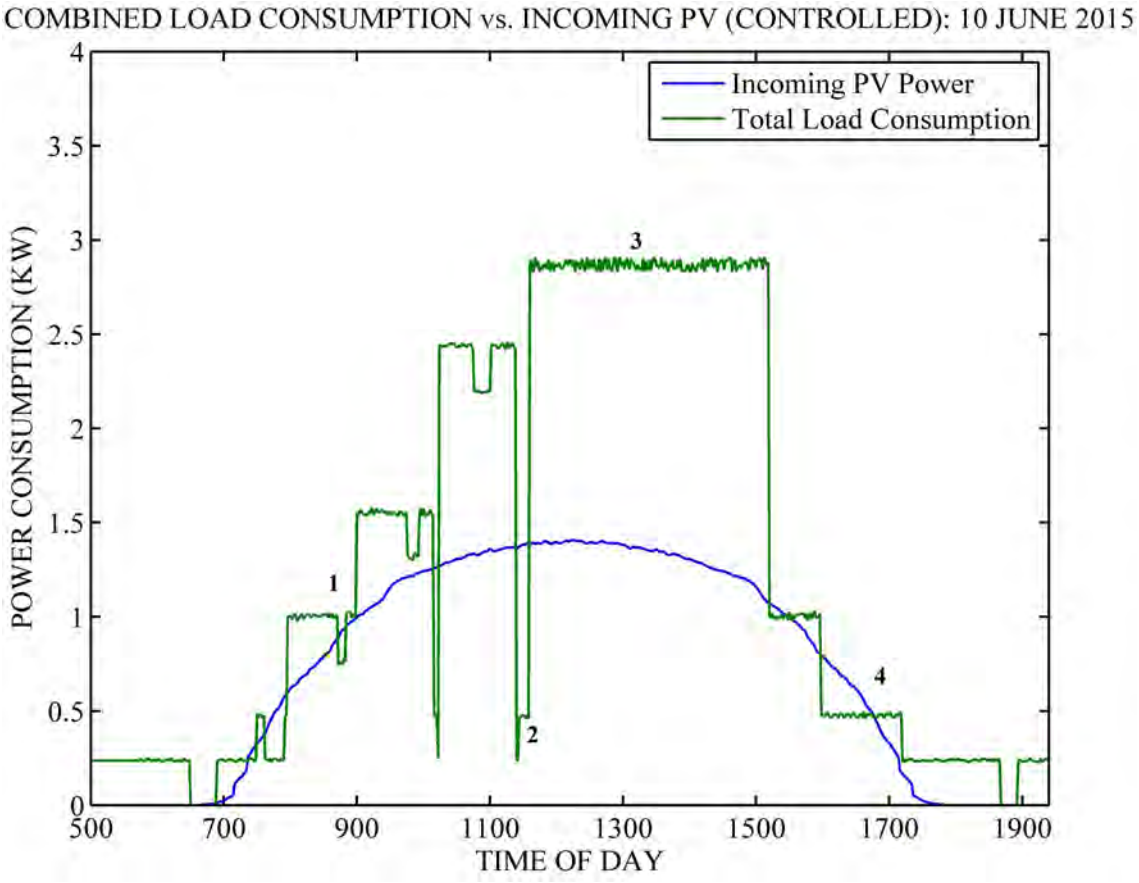

Figure 5-32: Combined load vs. incoming solar PV plot (10 June 2015)

A summary of this scenario's experimental results are shown in table 5-5. From the table it is seen that the total daily energy consumption by all the loads were 18.20 kWh with the solar PV supplying 47.75% of this total (8.50 kWh). The percentage of incoming solar PV power that was absorbed by the loads (overall system efficiency) was 96.6%. A satisfactory percentage of the load was covered by the incoming solar PV power and hence only 9.7 kWh was required from the utility.

Table 5-5: Summary of controlled experimental results for 10 June 2015

Parameter	**Result**
Total PV Energy Input	8.81 kWh
PV Energy Lost	0.29 kWh
Total Daily Load	18.20 kWh
Energy Cons. off Utility	9.70 kWh
Energy Cons. off PV	8.50 kWh
Percentage Utility Supplied	53.25%
Percentage PV Supplied	46.75%
Maximum Demand	2.91 kW
Overall System Efficiency	96.60%

5.3.3 Uncontrolled System

To directly compare the uncontrolled to the controlled system experimental results, it was necessary to have a consistent uncontrolled system load profile. The load profile was taken from a normal non-laundry day with accurate timestamps. The timestamps of the discussed solar PV input profiles were matched to the load profile's timestamps and hence accurate calculations could be performed. The individual load curve along with the various solar PV profiles are shown in figure 5-33.

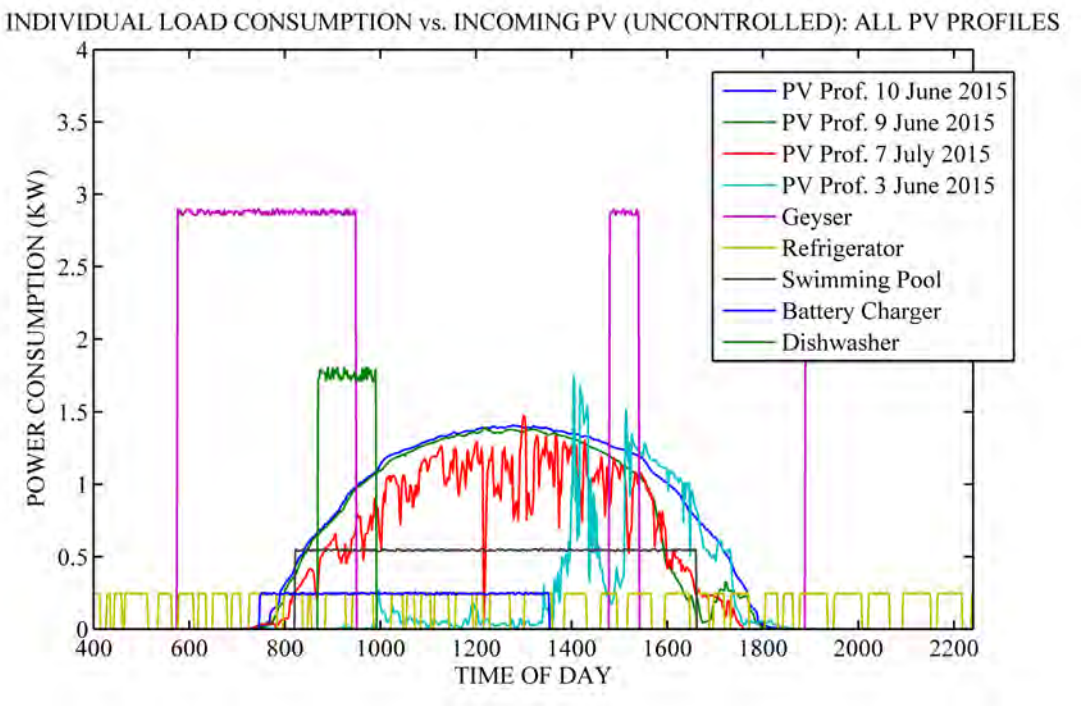

Figure 5-33: Uncontrolled individual load curve vs. various solar PV profiles

- **Incoming PV Power:** The incoming solar PV profiles were discussed in the previous sections and is not discussed in this section.
- **Geyser:** The geyser was switched on at three separate occasions during the day. The first was during the early morning hours (05h50) when the user bathed which caused hot water to flow out of the water tank and had to be replaced by cold water. The second occasion was in the early afternoon and caused the geyser to be switched on for a short period to maintain the hot water temperature. In the late afternoon, the residents used hot water for cooking and bathing purposes which triggered the geyser element to switch on for a third occasion.

Characteristic	Experimental Result
Maximum Power Demand	2.91 kW
Total Run-time	6:07 Hours
Start and Stop Time 1	05h50 to 07h58
Start and Stop Time 2	14h48 to 15h32
Start and Stop Time 3	19h25 to 22h40

- **Refrigerator:** As can be seen from the curve of the refrigerator, it was switched on/off spontaneously to regulate the temperature inside the refrigerator box.

- **Washing Machine/Tumble Dryer:** Neither the washing machine nor the tumble dryer were switched on in this scenario.
- **Swimming Pool:** The swimming pool pump was switched on at 08h15 and switched off at 16h45.

Characteristic	Experimental Result
Maximum Power Demand	0.54 kW
Total Run-time	8:30 Hours
Start and Stop Time 1	08h15 to 16h45

- **Battery Charger:** The battery charger switched on as soon as the incoming solar PV power exceeded 0 kW and switched off as soon as the battery was fully charged.

Characteristic	Experimental Result
Maximum Power Demand	0.25 kW
Total Run-time	5:55 Hours
Start and Stop Time 1	07h40 to 13h35

- **Dishwasher:** The dishwasher was manually switched on at 08h50 and finished its cycle within 1 hour and 5 minutes.

Characteristic	Experimental Result
Maximum Power Demand	1.74 kW
Total Run-time	1:05 Hours
Start and Stop Time 1	08h50 to 09h55

Figure 5-34 shows the uncontrolled combined load curve versus the incoming solar PV profiles. This figure provides insight into how the load profile was shaped without the intervention from the control system. Figure 5-34 is discussed below according to the annotations made on the figure.

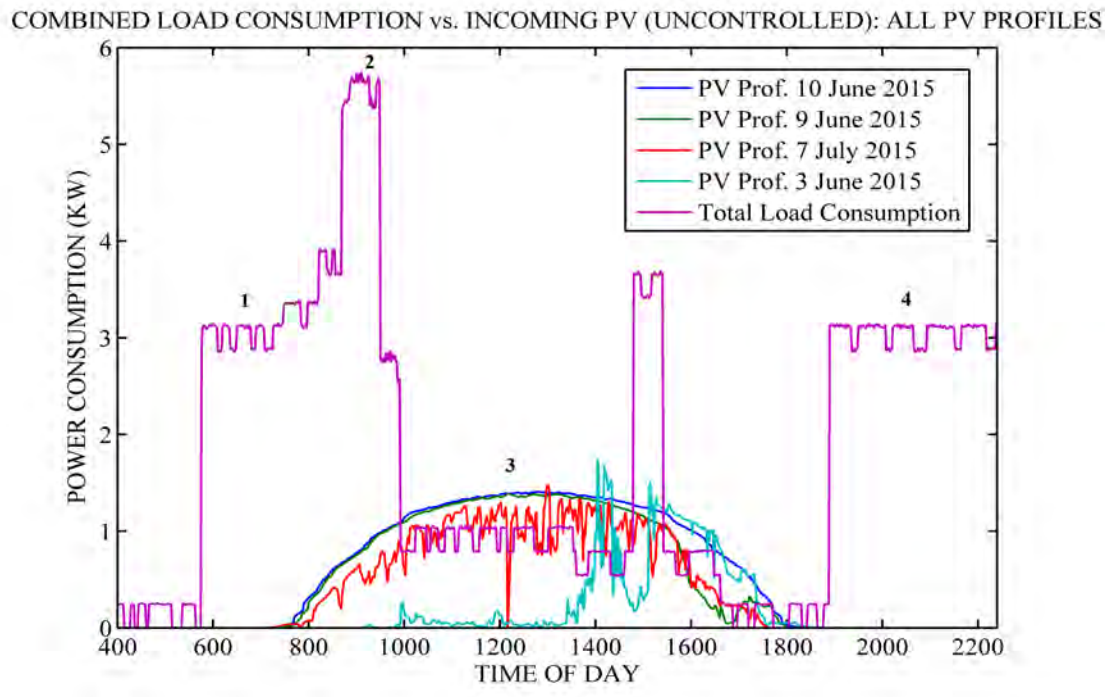

Figure 5-34: Uncontrolled combined curve

- **Note 1, 2 and 4:** These annotations illustrate that the maximum power demand of 5.75 kW was during the mid-morning period (09h00). This was undesirable as there were very little incoming solar PV power during this period. Also during the evening hours excessive energy consumption occurred.
- **Note 3:** This annotation highlights the fact that during the peak solar PV generation period, the load consumption was less than the solar PV generation. This caused the excess energy to feed into the utility grid and essentially lost.

From table 5-6 a summary of the uncontrolled results compared to the various incoming solar PV profiles are shown. It should be noted that the overall system efficiency was not only dependent on the incoming solar PV power and the load consumption. As seen, the scenario on the 7th of July 2015 yielded the highest overall system efficiency with a 6.40 kWh daily energy yield which was less than two of the other scenarios. The overall system efficiency was predominantly influenced by the incoming solar PV profile. Considering the solar PV profile of 3 June 2015, there were very little power generated in the morning by the solar PV panels. This caused the loads to consume all the solar PV power locally whereas at 14h10 a sudden surge of incoming solar PV power caused the incoming power to be greater than the load consumption. This caused the excess energy to feed into the grid which reduced the overall efficiency.

Table 5-6: Summary of uncontrolled experimental results for all solar PV profiles

Parameter	**10 Jun.'15**	**9 Jun.'15**	**7 Jul.'15**	**3 Jun.'15**
Total PV Energy Input	8.81 kWh	7.81 kWh	6.40 kWh	2.76 kWh
PV Energy Lost	2.46 kWh	1.86 kWh	1.00 kWh	0.83 kWh
Total Daily Load	34.19 kWh	34.19 kWh	34.19 kWh	34.19 kWh
Energy Cons. off Utility	27.83 kWh	28.23 kWh	28.79 kWh	32.25 kWh
Energy Cons. off PV	6.35 kWh	5.95 kWh	5.40 kWh	1.93 kWh
Percentage Utility Supplied	81.4%	82.6%	84.2%	94.4%
Percentage PV Supplied	18.6%	17.4%	15.8%	5.6%
Maximum Demand	5.75 kW	5.75 kW	5.75 kW	5.75 kW
Overall System Efficiency	72.1%	76.2%	84.4%	69.9%

5.4 Simulation and Experimental Results Comparison

A comparison between the simulation and experimental results was made to verify the accuracy of the simulation model. The scenarios that were chosen for the experimental results had a similar incoming solar PV profile than that of the simulation. There were small differences between the profiles as the simulation model represented that of a flawless incoming solar PV profile. The experimental results that fluctuated due to inclement weather could not be compared to a simulation model. This was due to issues associated with implementing the unpredictable weather patterns within the simulation environment.

The first case compared the uncontrolled scenarios with a summary of the experimental results shown in table 5-7. Each parameter of the simulation and experimental results is discussed below.

- **Total PV Energy Input:** It is seen that total daily solar PV energy of the experimental results were very similar to that of the simulation results. A difference of

0.07 kWh was noted.

- **PV Energy Lost:** The energy lost to the grid of the experimental results increased significantly which was due to the power consumption of the actual loads being less than that of the simulation model's rated power consumption. This caused the energy fed into the grid to increase and increase the lost energy.
- **Total Daily Load:** The total daily load requirement of the simulation model resembled that of the experimental results accurately. The slight deviation was owed to the same reason mentioned above.
- **Energy Cons. off Utility and PV:** These two parameters were combined to balance the total daily energy requirement parameter.
- **Percentage Utility Supplied:** The percentage of utility supplied energy of experimental results increased slightly as the lost solar PV energy parameter increased. The utility grid consumption increased to ensure that the required daily energy was supplied.
- **Percentage PV Supplied:** As the solar PV energy lost parameter slightly increased, a decrease in the percentage of the solar PV supplied energy was witnessed.
- **Maximum Demand** The maximum demand of the experimental results slightly decreased due to the power consumption of the actual loads being less than that of the simulation model's rated power consumption.
- **Overall System Efficiency:** This parameter illustrated the ratio of locally absorbed solar PV energy to the total solar PV generated energy. In simple terms, this parameter represented the percentage of the solar PV energy consumed by the loads. From table 5-7, a decrease of 11% was seen. This was owed to the increase in solar PV energy lost.

Table 5-7: Comparison of simulation and experimental results (Uncontrolled)

Parameter	Simulation Result	Experimental Result
Total PV Energy Input	8.87 kWh	8.81 kWh
PV Energy Lost	1.51 kWh	2.46 kWh
Total Daily Load	35.63 kWh	34.19 kWh
Energy Cons. off Utility	28.27 kWh	27.83 kWh
Energy Cons. off PV	7.36 kWh	6.35 kWh
Percentage Utility Supplied	79.34%	81.40%
Percentage PV Supplied	20.66%	18.60%
Maximum Demand	5.90 kW	5.75 kW
Overall System Efficiency	83.01%	72.10%

The second comparison made was that of the non-laundry day controlled scenarios with a summary of the results shown in table 5-8.

- **Total PV Energy Input:** The incoming solar PV energy of the experimental results was very similar to the simulation results with a difference of 0.12 kWh.
- **PV Energy Lost:** The solar PV energy lost to the grid of the experimental results increased slightly and was due to two reasons. The first was owed to the power consumption of the actual loads being less than that of the simulation model's rated power consumption. The second reason was caused by the small variations in the incoming solar PV power. This caused the control system to not switch off/on loads at the exact times as with the simulation model.

- **Total Daily Load:** The total daily load requirements of the simulation model were 33.3% more than that of the experimental results. The deviation was owed to the large shadow cast on the solar PV panels in the late afternoon. In turn, this caused the control system to reduce the load consumption for the same reason mentioned above.
- **Percentage Utility Supplied:** The percentage of the utility supplied energy of the experimental results decreased by 9% compared to the simulation results. This was caused by the control system which reduced the total daily load requirements whilst still ensuring that as much as possible of the solar PV energy was consumed.
- **Percentage PV Supplied:** As stated above, the control system ensured that as much as possible of the solar PV generated energy was consumed and hence this parameter increased by 9% compared to the simulation results.
- **Maximum Demand:** The maximum demand of the experimental results slightly decreased due to the power consumption of the actual loads being less than that of the simulation model's rated power consumption.
- **Overall System Efficiency:** The near unity overall system efficiency seen in the simulation model was slightly reduced in the experimental results which was caused by the fluctuations of the incoming solar PV power. The simulation results did not have the same fluctuations and was able to achieve a higher efficiency.

Table 5-8: Comparison of simulation and experimental results (Non-Laundry day)

Parameter	Simulation Result	Experimental Result
Total PV Energy Input	7.93 kWh	7.81 kWh
PV Energy Lost	0.29 kWh	0.68 kWh
Total Daily Load	20.30 kWh	15.25 kWh
Energy Cons. off Utility	12.66 kWh	8.13 kWh
Energy Cons. off PV	7.64 kWh	7.12 kWh
Percentage Utility Supplied	62.37%	53.30%
Percentage PV Supplied	37.63%	46.70%
Maximum Demand	3.25 kW	2.91 kW
Overall System Efficiency	96.31%	91.30%

The final comparison made was that of the laundry day controlled scenarios with the summary of the results shown in table 5-9.

- **Total PV Energy Input:** The incoming solar PV energy of the experimental results was slightly less than the simulation results with a difference of 0.5 kWh. This was within the accepted range which yielded useful results.
- **PV Energy Lost:** The solar PV energy lost to the grid of the experimental results increased slightly which was due to the same reasons as mentioned above.
- **Total Daily Load:** The total daily load requirement of the simulation model accurately resembled that of the experimental results. The slight deviation was owed to the power consumption of the actual loads being less than that of the simulation model's rated power consumption.
- **Percentage Utility Supplied:** The percentage of the utility supplied energy of the experimental results was very closely matched to that of the simulation results.
- **Percentage PV Supplied:** The percentage of the utility supplied energy of the experimental results was closely matched to that of the simulation results.

- **Maximum Demand:** The maximum demand of the experimental results slightly decreased due to the power consumption of the actual loads being less than that of the simulation model's rated power consumption.
- **Overall System Efficiency:** The near unity overall system efficiency seen in the simulation model was slightly reduced in the experimental results which was caused by the small fluctuations of the incoming solar PV power. The fluctuations was less than that of the non-laundry day comparison and hence the deviation from the simulation results were less.

Table 5-9: Comparison of simulation and experimental results (Laundry day)

Parameter	Simulation Result	Experimental Result
Total PV Energy Input	9.33 kWh	8.81 kWh
PV Energy Lost	0.18 kWh	0.29 kWh
Total Daily Load	19.83 kWh	18.20 kWh
Energy Cons. off Utility	10.67 kWh	9.70 kWh
Energy Cons. off PV	9.15 kWh	8.50 kWh
Percentage Utility Supplied	53.84%	53.25%
Percentage PV Supplied	46.16%	46.75%
Maximum Demand	3.25 kW	2.91 kW
Overall System Efficiency	98.07%	96.60%

5.5 Cost Analysis

Information on the tariff structures used in South Africa was needed to perform accurate calculations regarding the feasibility of the microgrid system. The South African domestic electricity consumers are supplied by either Eskom or the local municipality depending on the geographic location. In cases where the municipality supplies the residential customers, a municipal flat-rate is usually employed. These flat-rates vary according to region and in certain cases depends on the monthly energy consumption; Cape Town municipal customers that consume less than 600 kWh per month pays R 1.536 per kWh and customers that consume more than 600 kWh pays R 1.868 per kWh. Similar tariff structures are employed at other municipalities. Customers that are supplied directly by Eskom also falls within a certain tariff structure. Eskom employs the Homepower Bulk, Homepower Standard and Homelight tariff structures to their residential customers. A summary of these tariffs is added on the DVD (Appendix C). The cost analysis was done according to the Eskom Homepower Standard (>600 kWh) structure which saw a tariff of R 1.85 per kWh.

To ensure an objective feasibility study of the system was performed, it was necessary to make further assumptions apart from those made in the PVsyst report added on the DVD. The cost analysis in the PVsyst simulation report used the expected annual produced energy (4 178 kWh) to calculate the cost of produced energy (R 1.84 per kWh). However, this calculation was based on the fact that every kWh was absorbed or sold back to the utility (net-metering). Within the South African utility market, net-metering is not yet implemented and hence the calculations were adjusted according to the experimental results.

The experimental results of the uncontrolled system indicated that the percentage of

generated energy that were absorbed by local loads were in the order of 70-84%. The assumption was made that, on average 77% of the solar PV generated energy was consumed locally. Based on this, the available annual solar PV generated energy reduced to 3 217 kWh. Assuming that the daily load requirement was similar to that of the uncontrolled experimental results (35 kWh per day), the annual energy consumption equated to 12 775 kWh. The total billable energy was calculated with and without the implementation of a solar PV system. The total annual energy consumption of 12 775 kWh with no solar PV system equated to an annual cost of R 23 633.75. In the case where a solar PV system was installed with no control system, the total billable energy of 10 319 kWh equated to R 17 682.30 per year. It must be kept in mind that the solar PV system was subject to annual maintenance costs and initial investment costs. Assuming the investments costs were funded by a loan (20 years at 5%) as described in the PVsyst report, the annual maintenance and loan costs equates to R7 688.00. This increased the annual cost of electricity of the solar PV implemented system to R 25 370.30.

Based on the experimental results of the controlled system, it is seen that the percentage of the solar PV generated energy that was absorbed by local loads varied between 90-96%. The majority of the experimental results fell within the 40-50% percentile of this range and hence an assumption of 92% was made for the cost analysis. This implied that 92% of the generated energy was used to perform the cost analysis. Whilst this was a 15% increase in local absorption, it must be kept in mind that the control system reduced the daily energy consumption considerably. On average the control system reduced the daily energy consumption to approximately 18 kWh per day. The combination of the increased local absorption percentage and reduced energy consumption caused the total billable energy to reduce to 3 102 kWh per annum. This equated to R 5 739.63 annually. Including the annual maintenance and loan costs increased the annual cost to R 13 427.63. A summary of the cost analysis for the first year is shown in table 5-10. From table 5-10 it is evident that the solar PV system with the control system yielded the highest amount of savings during the first year (R 11 814). However, evaluating the feasibility of other financing options or implementing only the solar PV or control system yielded very interesting results.

Table 5-10: Summary of cost analysis

Characteristic	**No PV System Uncontrolled**	**PV System Uncontrolled**	**PV System Controlled**
Annual Residential Load (kWh)	12 775 kWh	12 775 kWh	6 570 kWh
Annual Generated PV Energy (kWh)	0 kWh	4 178 kWh	4 178 kWh
PV System Efficiency (%)	0%	77%	92%
Billable Annual Energy (kWh)	12 775 kWh	10 319 kWh	3 102 kWh
Additional Costs (kWh)	R 0.00	R 7 688.00	R 7 688.00
Annual Electricity Costs (R)	R 23 633.75	R 25 370.30	R 12 458.50

Figure 5-35 graphically illustrates the annual electricity costs for the next 20 years based on which installation was made. For reference purposes, a curve where no solar PV or control system was implemented is also shown in the figure below. The figure was drawn up based on the following assumptions:

- Annual load requirements remain constant
- Electricity prices escalate at 6% per annum
- Maintenance costs escalate at 6% per annum
- Solar PV system performance degrades by 15% every five years.

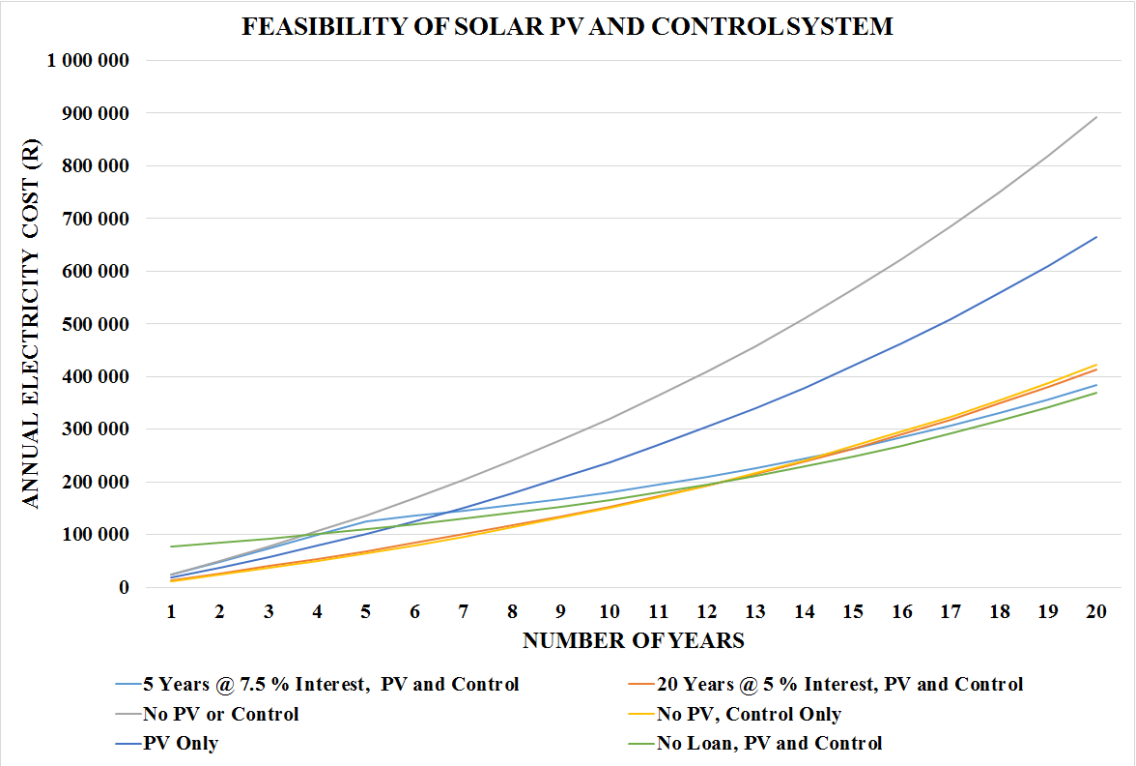

Figure 5-35: Feasibility of various implementation options

By evaluating figure 5-35 it is deduced that if no solar PV or control system would be implemented, the annual electricity cost would escalate at an exponential rate. The same is true for only implementing a solar PV system with no control system. As shown in table 5-11, the total cost of electricity after 20 years would be R 892 878 and R 664 283 respectively. However, when comparing the other options, these are stacked closely together with growth at a linear rate. The two options that are very narrowly matched are the "No PV Control Only" and "20 Years at 5%" options. By implementing either of these options, costs over 20 years could be reduced by at least R 469 936 after 20 years. A trend should be noted for the remaining options. The shorter term loan, 5 years at 7.5%, significantly decreases the total electricity costs after 20 years when compared to no solar PV and no control system (R 508 707). However, the best option that would result in the greatest amount of savings is the no loan option which saves a total of R 522 841 over 20 years. The implementation of the solar PV and the control system without a loan would recover the investment costs within four years.

By analysing figure 5-35 and table 5-11 it is clearly seen that the implementation of a

solar PV and control system is economically feasible. However, to fully utilise financial benefits, a solar PV and control system is to be implemented in conjunction with each other.

Table 5-11: Total electricity costs after 20 years

No PV No Control	PV Only No Control	No PV Control Only	20 Years at 5%	5 Years at 7.5%	No Loan, PV and Control
R 892 878	R 664 283	R 422 942	R 413 171	R 384 171	R 370 037

5.6 Verification and Validation

5.6.1 Validation of Simulation Models

As mentioned in the conclusion of Chapter 4, the simulation models needed to be validated against the experimental results. The validation was done by comparing the accuracy of the simulation results to that of the experimental results. This was done in the previous section and the accuracy of the simulation model compared to the experimental results is summarised in table 5-12 below.

Table 5-12: Validation of simulation models

Parameter	Uncontrolled	Controlled (Non-Laundry)	Controlled (Laundry)
Total PV Energy Input	0.68%	1.51%	5.57%
Percentage Utility Supplied	2.06%	9.07%	0.59%
Percentage PV Supplied	2.06%	9.07%	0.59%
Maximum Demand	2.54%	10.46%	10.46%
Overall System Efficiency	11.09%	5.01%	1.47%

Bearing in mind the predictability of the weather and its effect on solar PV profiles, the simulation models matched the experimental results with reasonable accuracy. The uncontrolled simulation model managed an overall system similarity of 11.09%, where the controlled simulation models (non-laundry and laundry) managed an overall similarity of 5.01% and 1.47% respectively. These results were adequate for the validation of the simulation models.

5.6.2 Verification and Validation of Experimental Results

Verification and validation is usually considered only applicable to simulation models and the design thereof. However, it is important to also verify and validate the experimental results. The validation process was done by ensuring that the hardware such as the solar PV panels, GTI, PLC controller and loads have all been used in real-world applications. From the sections above, it is evident that the equipment used in this study has been widely implemented in industry. The Powador GTI has been implemented in a number of rooftop solar PV system installations across the globe. The solar PV panels connected to the GTI have also been widely used in solar PV systems owing to its high open-circuit

voltage. The Siemens PLC is one of the global leaders in the automation industry and has numerous installations across the world. The industry wide implementation of these pieces of equipment attributed towards the validation of the experimental results.

The verification process was done by ensuring that the equipment used in the study adheres to applicable standards commonly used in industry. The applicable standards of each piece of equipment are listed below. These applicable standards all contributed towards the verification of the experimental results.

- Powador GTI 2002
  - Safety of Unit: EN62103:2007, EN50178:1997
  - Interference of Immunity: EN61000-6:2007
  - Effects on the Grid: EN61000-3:2006
- Siemens S7-1200 PLC
  - Electromagnetic Compatibility: IEC61000-4
  - Degree of Protection: EN60529
- Solar Frontier CIS Solar PV Panels
  - Solar PV Module Design Specification: IEC61646
  - Fire Rating: IEC61730
  - Safety Class: IEC61140
- Current Transformers
  - Although the CT core was not designed to a specific standard, an accuracy error of less than 2% was guaranteed. This was confirmed by performing laboratory measurements using a TiePie HandyScope.
- TiePie HandyScope
  - Accuracy of Measurements: EN55011:2009, EN55022:2006, EN61000-6-1:2007 and EN6100-6-3.

5.7 Conclusion

This chapter discussed the implementation and applicability of the individual loads, energy, control and software system. The integration of these components was also discussed along with the integrated microgrid station where tests was conducted in a safe and controlled environment. The microgrid test station was tested with real-world components to obtain real-world experimental results. The experimental results were compared to the simulation models in order to validate the accuracy of the simulation model. Based on the experimental results, significant reductions in energy consumption off the utility grid was achieved. An uncontrolled system with no solar PV or control system was compared to a controlled system which employed a 2 kW solar PV system with active load management. The daily energy data obtained from the system is shown in the table below. This table compared the uncontrolled and the controlled systems based on the fact that the controlled system was financed on a 5-year loan at 7.5% interest. Based on this, it was deduced that within 5 years the loan could be paid off and the electricity bill per month would reduce to R 1 332.02. If the controlled system was not implemented and the energy consumption remained the same, the equivalent monthly electricity bill would increase to R 2 706.83. Therefore, the implementing the system is technically and economically feasible. A thorough results discussion of the study follows in Chapter 6 along with future work that can be done to improve the study.

Table 5-13: Comparison of uncontrolled and controlled system

Parameter	Uncontrolled System	Controlled System
Total Daily Load	34.19 kWh	15.25 kWh
Energy Cons. off Utility	34.19 kWh	8.13 kWh
Percentage Utility Supplied	100.0%	53.3%
Percentage PV Supplied	0%	43.7%
Maximum Demand	5.75 kW	2.91 kW
Monthly Electricity Bill	R 1897.55	R 2020.83

Chapter 6: Conclusion and Recommendations

6.1 Introduction

The following chapter aims to provide closure of the dissertation. The main topics covered in previous chapters are highlighted conclusively. Emphasis is placed on the simulation and experimental results along with the financial feasibility of the microgrid system. After the discussion of the abovementioned, recommendations and future work ideas are discussed. The chapter concludes by summarising how validation and verification was ensured throughout the duration of the study.

6.2 Discussion

The introductory chapter presented background information of microgrids and how these systems fit into the modern power system. It was highlighted that microgrids are usually grid-connected or standalone systems. For the purpose of this study, only grid-connected microgrids was considered. Within South Africa, not all distribution entities permit net-metering and feeding electricity into the grid. Without proper net-metering policies, consumers whom are injecting back into the grid are essentially losing that energy without receiving remuneration. The study was based on this problem and addressed this by designing an EMS which focussed on ensuring that locally generated power from a DER was absorbed within the residence. The introductory chapter also included the abstracts and citations of articles that were submitted for peer reviews. A total of three articles was written throughout the duration of the study. The first article focussed on summarising the design and simulations of the EMS and was accepted and presented at the International Conference on the Domestic Use of Energy (DUE). The second article summarised the experimental results obtained from the system and was submitted to the Journal of Energy in South Africa (JESA). The third and final article was a review article that presented a method for selecting an appropriate system controller for energy management systems. This article was submitted to the International Journal of Energy Conversion and Management. Each of these articles are added in Appendix A.

The literature study chapter discussed all the relevant literature associated with the research study. Topics included the applicable sources of energy, renewable and non-renewable, that could be implemented in a residential microgrid. The renewable energy sources that were under consideration included wind and solar energy. Non-renewable energy sources that were considered included diesel and petrol; however, upon further investigation these were found not financially feasible solutions and were disregarded from the study. It was evident that renewable energy sources were the only financially feasible solution. Careful consideration was taken before deciding between wind and solar energy. Solar irradiation and mean wind speed data were analysed for the location where the experimental test station would be installed and it was found that solar energy would

be the best source of energy given the geographical location.

A market scan of the applicable system controllers was also included in the literature study chapter. The applicable system controllers were classified as PLCs, MCUs or SBCs. All three controller technologies were adequate to host the EMS; however it was decided that the PLC deemed most applicable as a result of its robustness, ease of implementation and after sales support. The PLC also required the least amount of expansion boards which also favoured its adoption. Furthermore, discussions on possible energy storage systems and communication protocols were included in the literature study.

The design chapter integrated the knowledge obtained in the literature study to compile a detailed system design. The design chapter firstly listed the requirements and specifications that had to be met for the integrated system. This consisted of characteristics of a typical residence where a residential microgrid could be installed. These characteristics were based on a typical LSM group 8 residence. Based on the requirements and specifications, a conceptual and detailed design were compiled which were divided into the energy, control and communication systems. The energy system detail design discussed the load selection, GTI, solar PV and DC security light application design. The control and communication system detail design discussed how the PLC would be used to control the energy system. Furthermore, a discussion on the three EMS software phases (initialisation, once-off and continuous) followed which described the exact procedure of the operating cycle of the control system. The final section in the design chapter briefly described the mechanical design of the enclosure that would be used to house the microgrid system.

One of the main purposes of the simulation chapter was to establish the optimal solar PV power rating for the residence by making use of Simulink® and statistical analysis. It was found that the optimal power rating was 2 kW. All of the energy system components selected in the design chapter were combined to set up a PVsyst simulation model. The PVsyst simulation model was simulated with meteorological data near the test site location to obtain the expected daily energy yields. These results were used to improve the accuracy of the MATLAB® and Simulink® uncontrolled and controlled (non-laundry and laundry day) simulation models. The results of the uncontrolled simulation model were used as a base case to which the results of the other models could be compared to.

The uncontrolled simulation model yielded a total daily load requirement of 35.63 kWh of which 28.27 kWh was supplied by the utility grid. The other portion was supplied by the solar PV system; however, only 83.0% of the solar PV generated energy was absorbed locally. The non-laundry controlled system simulation yielded a significantly reduced total daily load of 20.30 kWh. Of this total, 12.66 kWh was utility supplied and 96.3% of the solar PV generated energy was consumed locally. Similar results were obtained from the laundry day simulation with the total load requirement equating to 19.83 kWh. The utility grid supplied 10.67 kWh of the total and 98.07% of the solar PV generated energy was absorbed locally. The simulation results were compared to the experimental results in the results chapter.

The two main objectives of the results chapter were to discuss all aspects that related to the experimental test station and the experimental results. The first part of the chapter was

dedicated to illustrating the experimental microgrid test station. The selected loads, energy, control and software systems were thoroughly covered in this section which included photos, wiring and logic diagrams. The second part of the results chapter focussed on the experimental testing of the microgrid system. The experimental testing was conducted in a similar manner as with the simulation results. The experimental system was tested in various scenarios which included weather conditions such as clear skies, intermittent cloud cover and overcast/showers. These factors were the major drivers that influenced the performance of the EMS and were discussed accordingly in the results chapter. The testing of the experimental system was conducted over a period of 34 days. The experimental results that were obtained proved to be sufficient as a repetition of similar results occurred. The experimental results of these scenarios proved that the percentage of the solar PV generated energy absorbed locally ranged between 69.9% to 84.4%. It further showed that the utility grid supplied at least 81.4% of the daily energy requirement on days when the solar PV energy yield was exceptional.

The first scenario of the controlled system's experimental test (non-laundry day) was conducted when the weather status was classified as "Clear Skies". This implied a significant amount of daily solar PV energy yield. The percentage of the solar PV generated energy absorbed locally increased to 91.3% with the percentage of energy supplied by the utility reducing to 53.3%. In the second scenario, the weather status was classified as "Fair" which translated to intermittent cloud cover. The results were similar to the clear skies scenario with the exception of the increased percentage of the utility supplied energy. The percentage of the solar PV generated energy absorbed locally further increased to 95.1% with the percentage of energy supplied by utility increasing to 59.0%. The third and final scenario translated to a weather status of "Overcast/Showers". The energy yield from the solar PV system decreased significantly and could clearly be seen in the percentage of energy supplied by the utility. The percentage of the solar PV generated energy absorbed locally further increased to 96.1% with the percentage of energy supplied by utility increased to 79.65%.

The laundry day controlled system's experimental test was conducted when the weather status was classified as "Clear Skies". Other scenarios were not discussed as these correlated to the non-laundry day results. The percentage of the solar PV generated energy absorbed locally increased to 96.6% with the percentage of energy supplied by utility grid reducing to 53.25%. A comparison between the simulation and experimental results were made in the results chapter and showed a strong correlation. The differences between the simulation and experimental results were owed to small fluctuations in the solar PV input profiles that could not be factored into the simulation models.

To conclude the research study, a financial feasibility study based on the experimental results of the microgrid system was performed. It was found that by implementing the microgrid system and EMS, electricity costs spanning over 20 years would be significantly reduced (R 522 841) provided that the investment is made without a loan. The savings on the electricity monthly and yearly electricity bill makes the implementation of a residential microgrid a feasible solution.

6.3 Key Research Questions

This section is included in the final chapter to address the research questions that was set up at the start of the study. The questions are restated below from the introductory chapter and are addressed after each question.

1. Is it financially feasible to implement a residential microgrid with an EMS?

   As stated in the detailed cost analysis (Chapter 5), the implementation of an EMS controlled microgrid system is a financially feasible solution. Significant savings would be made if such a system is implemented.

2. If net-metering is to be implemented in the South African utility network, how does this influence the feasibility of a residential microgrid with an EMS? How does the benefits of net-metering weigh up against localised consumption (self consumption)?

   For the EMS controlled microgrid system to be a feasible solution, net-metering feed-in tariffs per kWh should be less than half the cost of buying a kWh from the utility. As stated in the introductory chapter, feed-in tariffs implemented by the City of Cape Town and Nelson Mandela Bay municipalities are well-below the cost per kWh. Therefore, if these tariffs remain low, self consumption trumps the benefits of net-metering.

3. Technically, how much energy reduction is possible without excessively disrupting the daily routine of residential energy consumers?

   During the experimental testing, the daily routine of the residents was disrupted to a noticeable extent. The residents had to ensure that bathing and showering were done at a very particular time (early evening) otherwise the geyser water temperature would not be warm enough. The washing/drying cycle also disrupted the regular routine to a significant extent as it did not occur on a fixed daily time but only on certain days at very specific times. Other disruptions to the normal routine was not noticed; however, the bathing and showering at fixed times introduced a certain amount of discomfort. The daily energy requirement was nearly halved but brought discomfort to the residents. The residents reported that they did not want to plan ahead showering/bathing times. Based on this, by eliminating the geyser energy management strategy from the EMS, an additional 60 to 100 kWh per month should be added to the electricity bill.

6.4 Future Work and Recommendations

This section describes the possible areas for further study. The purpose of this chapter is to present relevant areas of study that would lead to further improvements. These study areas were identified throughout the duration of the research study.

- In terms of design, one topic that would significantly influence the performance of the EMS is the implementation of tariff structures into the control strategy. In cases where time of use (TOU) tariff structures are implemented, the EMS could take this into account and further minimise energy consumption during peak periods.

- The accuracy of the simulation model can be significantly improved if the simulation model can include weather conditions such as cloud cover and rain into the input solar PV profile. This would cause the EMS to respond to a solar PV input profile that represents a real-world system. By doing so, an accurate dynamic response of the EMS can be obtained through simulation.
- The performance of the system can greatly be increased if the system is to be tested during other seasons of the year i.e. summer, autumn etc. The timespan of this study only permitted testing during the winter season when solar PV input energy was at its lowest. It is anticipated that greater savings can be achieved during summer, autumn and spring. The control strategy can be altered according to season if testing is conducted and results are obtained.

6.5 Validation and Verification

This section summarises the validation and verification processes that was followed to ensure that the design, simulation and results of the study were validated and verified. The detail design was the first section in the dissertation that was validated and verified. The validation of the detail design was ensured by designing the energy, control and software system according to the specifications and requirements compiled at the start of the study (Section 3.7). The design was performed in accordance with industry standards to further ensure validity. The verification of the design was performed in the simulation chapter where the design was extensively simulated to ensure that the response to inputs were as expected (Section 4.7).

The simulation models were verified in a similar manner as the design which consisted of testing the response of the simulation model to various inputs (Section 4.7). The purpose of this was to ensure that the response of the simulation model matched that of the design response. By doing so, this ensured that all possible responses of the system were gathered and ultimately verified whether the system complied to the design assumptions and specifications. The validation of the simulation model was done to ensure that the results obtained from the model matched that of the real-world system (Section 5.6.1). This was done by comparing the results obtained from the simulation model to the experimental results obtained from the real-world system.

Finally, the experimental results were validated by ensuring that the equipment used in the construction and assembly of the microgrid system was widely implemented throughout the industry (Section 5.6.2). It was evident from the experimental results chapter that only industry preferred equipment was used where possible. The verification of the experimental results was done by ensuring that the equipment used in the study adhered to standards typically used in industry (Section 5.6.2). The standards that applied to the equipment were listed in the results chapter and ultimately contributed to the verification of the experimental results. A summary of the validation and verification processes are visually illustrated below in figure 6-1.

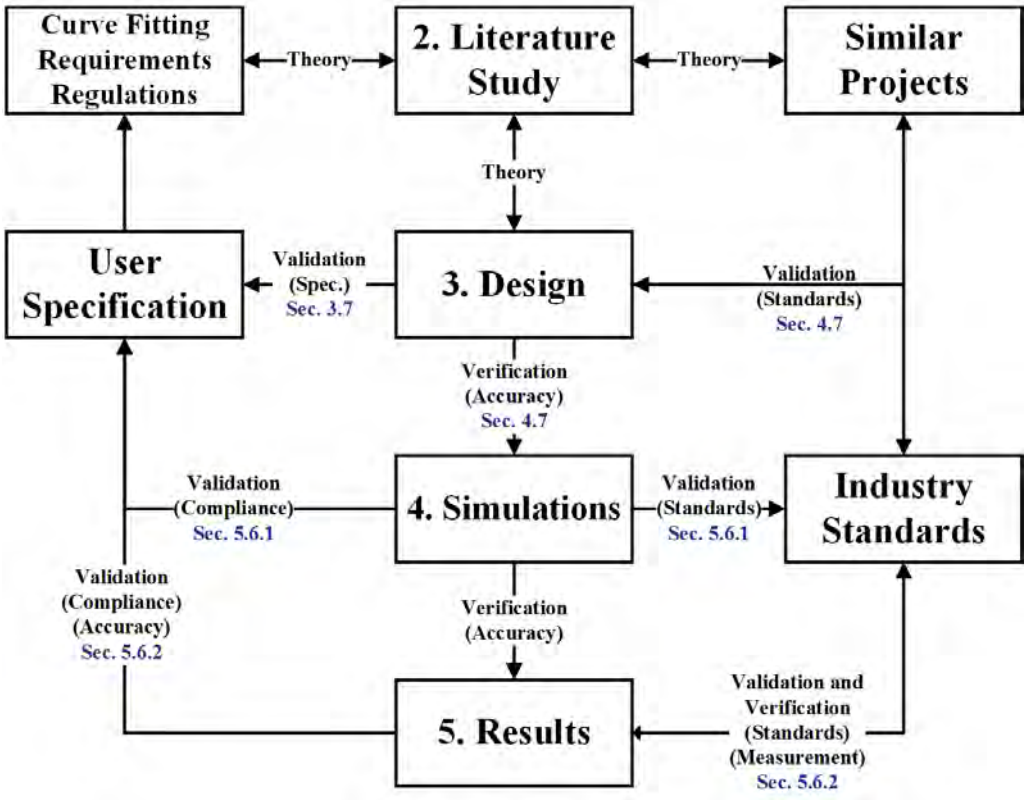

Figure 6-1: Validation and verification of dissertation

6.6 Closure

The research project that was undertaken in January 2014 addressed a real-world problem relating to the absence of net-metering policies in South Africa. A solution to address the shortcoming of net-metering policies was presented in this dissertation. Throughout the duration of the study, a great deal of knowledge regarding distributed generation, energy management systems and net-metering policies were obtained. These fields of engineering are growing at an alarming rate as the need for self-generation and renewable energy are becoming more popular. The work presented in this dissertation is my humble contribution toward these fields of engineering. The dissertation is concluded with a quote that holds true for all aspects of engineering.

If you can find a path without any obstacles, it probably doesn't lead somewhere. - Christopher Brian Bridges

List of References

[1] H. Kim and M. Thottan, "A two-stage market model for microgrid power transactions via aggregators," *Bell Labs Technical Journal*, vol. 16, no. 3, pp. 101 –107, 2011, ISSN: 10897089. [Online]. Available: http://onlinelibrary.wiley.com/doi/10.1002/bltj.20524/abstract.

[2] Q. Jiang, M. Xue, and G. Geng, "Energy management of microgrid in grid connected and stand-alone modes," *IEEE Transactions on Power Systems*, vol. 28, no. 3, pp. 3380 –3389, 2013, ISSN: 08858950. [Online]. Available: http://ieeexplore.ieee.org/xpl/articleDetails.jsp?arnumber=6472268.

[3] Power Engineering International. (2010). Achieving a smart energy ecosystem, [Online]. Available: http://www.powerengineeringint.com/articles/print/volume-18/issue-5/features/achieving-a-smart-energy-ecosystem.html.

[4] D. Robinson, "Microgrids for energy reliability," *ASHRAE Journal*, vol. 55, no. 11, B14 –B17, 2013, ISSN: 00012491. [Online]. Available: www.bacnet.org/Bibliography/BACnet-Today-13/Robinson-2013.pdf.

[5] A. A. Aminou, M Adonis, and A. K. Raji, "Energy management system in autonomous microgrid," in *Proceedings of the 23rd Southern African Universities Power Engineering Conference*, (University of Johannesburg, Jan. 28, 2015), SAUPEC, Ed., Southern African Universities Power Engineering Conference, Jan. 2015, p. 97, ISBN: 978-0-86970-786-9.

[6] Y. Guo, M. Pan, and Y Fang, "Optimal power management of residential customers in the smart grid," *Parallel and Distributed Systems, IEEE ...*, vol. 23, no. 9, 2012. [Online]. Available: http://ieeexplore.ieee.org/xpls/abs_all.jsp?arnumber=6127869.

[7] S Aman, "Energy management systems: state of the art and emerging trends," *Communications Magazine ...*, no. January, pp. 114–119, 2013. [Online]. Available: http://ieeexplore.ieee.org/xpls/abs_all.jsp?arnumber=6400447.

[8] M. Nandy and S. Bhattacharya, "Energy Issues in India and South Africa," *ICFAI Journal of Infrastructure*, vol. 7, no. 2, pp. 69 –90, 2009. [Online]. Available: www.iupindia.in/609/IJI_Energy_Issues_in_India_69.html.

[9] R. de Groot, V. van der Veen, and A. Sebitosi, "Comparing solar PV (photovoltaic) with coal-fired electricity production in the centralized network of South Africa," *Energy*, vol. 55, no. 0, pp. 823 –837, 2013, ISSN: 0360-5442. [Online]. Available: http://www.sciencedirect.com/science/article/pii/S0360544213002910.

[10] Eskom Media Desk, *Following significant achievements over winter, Eskom urges all South Africans to "Live Lightly" this summer*, Media Statement, Aug. 2013. [Online]. Available: http://www.eskom.co.za/OurCompany/MediaRoom/Documents/MediaStatementQuarterlyStateSystem.pdf.

[11] Eskom Generation Communication, *COP17 fact sheet: Eskom's generation plant mix*, Fact Sheet, Aug. 2011. [Online]. Available: http://www.eskom.co.za/AboutElectricity/FactsFigures/Documents/Generation_Mix.pdf.

[12] Modern Power Systems, "Old coal helps Eskom keep the lights on," *Modern Power Systems*, vol. 33, no. 11, pp. 26 –27, 2013, ISSN: 02607840. [Online]. Available: http://connection.ebscohost.com/c/articles/92768357/old-coal-helps-eskom-keep-lights-on.

[13] N. Odendaal, "IFM shuts furnace in new Eskom buy-back deal," *Mining weekly*, vol. 19, no. 3, p. 7, 2013, ISSN: 15629619. [Online]. Available: http://www.miningweekly.com/article/ifm-shuts-furnace-in-new-eskom-buy-back-deal-2013-01-24.

[14] T. Creamer, "Eskom signs up 11 buy-back deals to provide maintenance cushion," *Engineering News*, vol. 33, no. 2, p. 10, 2013. [Online]. Available: http://www.miningweekly.com/article/eskom-signs-up-11-buy-back-deals-to-provide-maintenance-cushion-2013-01-14.

[15] Eskom Integrated Demand Management, *How to guide for Aggregated Standard Product Programme*, Guideline, May 2013. [Online]. Available: http://www.eskom.co.za/sites/idm/Documents/20130515_How_to_Guide_Aggregated_SPP_V1.0.pdf.

[16] Eskom Integrated Demand Management. (2014). Switch and save residential mass roll out, [Online]. Available: http://www.eskom.co.za/sites/idm/Pages/Switch%20And%20Save%20Residential%20Mass%20Roll%20Out.aspx.

[17] M. Mikati, M. Santos, and C. Armenta, "Electric grid dependence on the configuration of a small-scale wind and solar power hybrid system," *Renewable Energy*, vol. 57, pp. 587–593, Sep. 2013, ISSN: 09601481. [Online]. Available: http://www.sciencedirect.com/science/article/pii/S0960148113001274.

[18] L. R. Brown, "Exciting news about renewable energy," *Mother Earth News*, no. 254, p. 44, 2012, ISSN: 00271535. [Online]. Available: http://www.motherearthnews.com/renewable-energy/energy-policy/clean-energy-zm0z12onzmar.aspx.

[19] M. A. Delucchi and M. Z. Jacobson, "Meeting the world's energy needs entirely with wind, water, and solar power.," *Bulletin of the Atomic Scientists*, vol. 69, no. 4, pp. 30 –40, 2013, ISSN: 00963402. [Online]. Available: http://www.its.ucdavis.edu/research/publications/publication-detail/?pub_id=1925.

[20] S. Ramakrishnan and S. Ramakrishnan, "WoT (Web of Things) for energy management in a smart grid-connected home," *Issues in Informing Science and Information Technology*, vol. 10, pp. 461 –472, 2013, ISSN: 15475840. [Online]. Available: http://iisit.org/Vol10/IISITv10p461-472Ramakrishnan0048.pdf.

[21] D. Lipschitz. (2010). Grid tying and net-metering for systems under 1 MW, [Online]. Available: http://www.engineeringnews.co.za/article/grid-tying-and-net-metering-for-systems-under-1-mw-2010-10-22 (visited on 04/30/2014).

[22] NERSA, *Renewable energy feed-in tariff phase 2*, Jul. 2009. [Online]. Available: http://www.nersa.org.za/Admin/Document/Editor/file/Electricity/REFIT%20Phase%20II%20150709.pdf (visited on 04/30/2014).

[23] Eskom, *Small and micro generation (SMG) bulletin 1*, Newsletter, Sep. 2015. [Online]. Available: www.eskom.co.za/Whatweredoing/Documents/SMG_Bulletin1.pdf.

[24] Nelson Mandela Bay Municipality. (2014). Renewable energies pilot project, [Online]. Available: http://www.nelsonmandelabay.gov.za/Content.aspx?objID=369.

[25] City of Cape Town Municipality. (2014). Electricity tariffs, [Online]. Available: https://www.capetown.gov.za/en/electricity/Elec%20tariffs%20201415/Residential%20Electricity%20Tariffs%20Explanation.pdf.

[26] C. A. Visagie, "De Zalze residential estate electricity plan implementation," in *Proceedings of the Twenty Third Conference on the Domestic Use of Energy*, Cape Town, South Africa: Cape Peninsula University of Technology, Apr. 2015, pp. 109–113.

[27] M. Schulze and P. C. Del Granado, "Implementation of feed-in tariffs into multi-energy systems," *International Journal of Electrical Power and Energy Systems Engineering*, no. 2, p. 85, 2010, ISSN: 2070-3767. [Online]. Available: http://www.eeh.ee.ethz.ch/uploads/tx_ethpublications/Schulze_Implementation_of_Feed_in_Tariffs_into_Multi_Energy_Systems.pdf.

[28] Department of Labour, "Occupational Health and Safety Act 85 of 1993," Government, Act, 1993. [Online]. Available: http://www.labour.gov.za/DOL/downloads/legislation/acts/occupational-health-and-safety/amen-dments/Amended%20Act%20-%20Occupational%20Health%20and%20Safety.pdf.

[29] Microsoft, *Visio clip art drawings*, 2015. [Online]. Available: https://products.office.com/en/visio/flowchart-software.

[30] M. A. Delucchi and M. Z. Jacobson, "Meeting the world's energy needs entirely with wind, water, and solar power," *Bulletin of the Atomic Scientists*, vol. 69, no. 4, pp. 30 –40, 2013, ISSN: 00963402. [Online]. Available: http://www.fing.edu.uy/iq/cursos/qica/industria/Adicional,%20part%20III.pdf.

[31] V. Smil, "The long slow rise of solar and wind," *Scientific American*, vol. 310, no. 1, pp. 52 –57, 2014, ISSN: 00368733. [Online]. Available: http://www.vaclavsmil.com/wp-content/uploads/scientificamerican0114-521.pdf.

[32] T. Trainer, "Can the world run on renewable energy? a revised negative case," *Humanomics*, vol. 29, no. 2, pp. 88–104, 2013. [Online]. Available: http://www.scopus.com/inward/record.url?eid=2-s2.0-84878261846&partnerID=40&md5=35d499b6e814a90765d5cd8da3f6a8c3.

[33] O. Anaya-Lara, N. Jenkins, J. Ekanayake, P. Cartwright, and M. Hughes, *Wind Energy Generation: Modelling and Control*. Chichester, West Sussex, UK: John Wiley and Sons Ltd., 2009, ch. 1-6, pp. 1–36,5796–, ISBN: 978-0-470-71433-4.

[34] D. Devitt, "A wind energy plan that fits America's resources," *Power*, vol. 157, no. 12, pp. 52 –55, 2013, ISSN: 00325929. [Online]. Available: http://www.powermag.com/a-wind-energy-plan-that-fits-americas-resources.

[35] Wikipedia, *Darrieus windmill*, 2007. [Online]. Available: http://commons.wikimedia.org/wiki/File:Darrieus-windmill.jpg#filelinks.

[36] K. Aggeliki, *Vertical windmills - a survey of types and designs*, 2011. [Online]. Available: http://www.brighthub.com/environment/renewable-energy/articles/92978.aspx.

[37] NERSA, *Grid Connection Code for Renewable Power Plants (RPPs) Connected to the Electricity Transmission System (TS) or the Distribution System (DS) in South Africa*, version 2.6, Jul. 2014. (visited on 04/13/2014).

[38] NERSA, *Grid code requirements for wind turbines connected to distribution or transmission systems in South Africa*, version 4.4, 2010. [Online]. Available: http://www.nersa.org.za/Admin/Document/Editor/file/Electricity/TechnicalStandards/RSA%20Grid%20Code%20Connection%20Requirements%20for%20Wind%20Energy%20Facilitie.pdf (visited on 03/26/2014).

[39] Earth Policy Institute, *World cumulative installed wind power capacity and net annual addition*, 2013. [Online]. Available: http://www.earth-policy.org/?/data_center/C23/.

[40] 3Tier. (2012). Global mean wind speed at 80m, [Online]. Available: http://dupont-consulting.files.wordpress.com/2012/01/3tier_5km_global_wind_speed.jpg.

[41] T. Markvart, "Solar cells," in *Solar Electricity*, 2nd ed. Chichester, West Sussex, UK: John Wiley and Sons Ltd., 2004.

[42] USA Department of Energy. (2005). Solar cell, [Online]. Available: http://en.wikipedia.org/wiki/File:Solar_cell.png.

[43] Solar Energy Technology Co. (2008). Polycrystalline solar cell, [Online]. Available: http://img.hisupplier.com/var/userImages/2008-10/21/nbsolar$164726530-(s).jpg.

[44] Earth Policy Institute, *World solar PV production*, 2013. [Online]. Available: http://www.earth-policy.org/?/data_center/C23/.

[45] SolarGIS. (2013). World map of global horizontal irradiation, [Online]. Available: http://solargis.info/doc/_pics/freemaps/1000px/ghi/SolarGIS-Solar-map-World-map-en.png.

[46] SolarGIS. (2012). Global horizontal irradiation: Southern Africa, [Online]. Available: http://solargis.info/doc/_pics/freemaps/1000px/ghi/SolarGIS-Solar-map-Southern-Africa-en.png.

[47] T. Maphelele, R. Stanford, and B. Kooverji, *South africa solar energy technology road map*, version 2, 2013. (visited on 03/10/2013).

[48] UCS. (2011). Biomass energy, [Online]. Available: http://www.ucsusa.org/clean_energy/our-energy-choices/renewable-energy/how-biomass-energy-works.html#.VS_HGPmUd8E.

[49] R. Curley, "Biomass," in *Alternative Energy Sources*. Springer, 2012, ch. 10, pp. 287–311, ISBN: 978-3-642-20950-5.

[50] B. Block. (2013). Study: Biofuels more efficient as electricity source, [Online]. Available: http://www.worldwatch.org/node/6109.

[51] F. Energy, *Ultra-clean, efficient, reliable power*, 2013. [Online]. Available: http://www.fuelcellenergy.com/assets/Fuel-Cell-Technology-White-Paper.pdf.

[52] R. Curley, "Petroleum fuel products," in *Fossil Fuels. Energy: Past, Present and Future*. Brittanica Educational Publishing, 2012, ch. 1, pp. 19–21, ISBN: 978-1-61530-540-7.

[53] W. Glasburch. (Jun. 2012). Residual fuel oil, [Online]. Available: http://commons.wikimedia.org/wiki/File:Residual_fuel_oil.JPG (visited on 04/22/2015).

[54] T. Olivo, "Analysis of ultra capacitors as ups energy storage devices," in *IEEE SoutheastCon 2010 (SoutheastCon), Proceedings of the*, Mar. 2010, pp. 398–401. DOI: 10.1109/SECON.2010.5453845.

[55] J. Song, A. Toliyat, D. Turtle, and A. Kwasinski, "A rapid charging station with an ultracapacitor energy storage system for plug-in electrical vehicles," in *Electrical Machines and Systems (ICEMS), 2010 International Conference on*, Oct. 2010, pp. 2003–2007.

[56] A. Xu, S. Xie, and X. Liu, "Dynamic voltage equalization for series-connected ultracapacitors in EV/HEV applications," *Vehicular Technology, IEEE Transactions on*, vol. 58, no. 8, pp. 3981–3987, Oct. 2009, ISSN: 0018-9545.

[57] Maxwell Technologies, *Datasheet: K2 Series Ultracapacitors*, 2014. [Online]. Available: https://www.maxwell.com/images/documents/K2Series_DS_1015370_5_20141104.pdf.

[58] D. Tuite, "Get the low down on ultracapacitors," *Electronic Design*, vol. 55, no. 26, p. 45, Oct. 2007, ISSN: 27759973.

[59] C. K. Dyer, P. T. Moseley, Z. Ogumi, D. A. Rand, and B. Scrosati, "Electric vehicles: Batteries," in *Encyclopedia of Electrochemical Power Sources*, J. Garche, Ed. 2009, pp. 219–235, ISBN: 978-0-444-52093-7.

[60] S. McCluer and J. Christin, *Comparing data center batteries, flywheels and ultracapacitors*, Rev. 2, White Paper, 2011. [Online]. Available: http://www.apcmedia.com/salestools/DBOY-77FNCT/DBOY-77FNCT_R2_EN.pdf (visited on 04/14/2014).

[61] F. DeLattre, "Flywheels: A power protection alternative," *Control Engineering*, vol. 57, no. 4, p. 51, 2010. [Online]. Available: http://connection.ebscohost.com/c/articles/49762570/flywheels-power-protection-alternative.

[62] R. E. Hebner, J. D. Herbst, and A. L. Gattozzi, "Pulsed power loads support and efficiency improvement on navy ships," *Naval Engineers Journal*, vol. 122, no. 4, pp. 23–32, 2010, ISSN: 1559-3584.

[63] G. Dunning, "Welcome to the World of Programmable Logic Controllers," in *Introduction to Programmable Logic Controllers*, 3rd. Clifton Park, NY: Delmar Cengage Learning, 2006, ch. 1, pp. 4–24, ISBN: 978-1-4018-8426-0.

[64] Siemens, *Siemens S7-1200 CPUs*, 2015. [Online]. Available: http://w3.siemens.com/mcms/programmable-logic-controller/en/basic-controller/s7-1200/cpu/Pages/Default.aspx?tabcardname=standard%20cpus.

[65] E. Schnieder, L. Schnieder, and J. R. Müller, "Conceptual foundation of dependable systems modelling," in *Dependable Control of Discrete Systems*, (École Normale Supérieure de Cachan, Italy), M. Fanti and M. Dotoli, Eds., vol. 2.1, 2009, pp. 198–202.

[66] I. Felea, S. Dzitac, F. Popentiu-Vladicescu, and I. Dzitac, "Models of Availability Maximization Applied to "K from N" Structures for Electro-energetic Systems," in *Proceedings of the ESREL Anual Conference*, R. Bris, Z. Vintr, C. Guedes-Soares, and S. Martorell, Eds., 2009.

[67] E. Gergely, L. Coroju, and F. Popentiu-Vladicescu, "Analysis of PLC Architectures for Dependable Industrial Applications," *Journal of Computer Science and Control Systems*, vol. 3, no. 2, pp. 26–30, 2010, ISSN: 18446043. [Online]. Available: http://connection.ebscohost.com/c/articles/56563313/analysis-plc-architectures-dependable-industrial-applications.

[68] National Electrical Manufacturers Association, *NEMA IA 2.1 standard*, 2005. [Online]. Available: http://www.nema.org/Standards/pages/default.aspx.

[69] C. Yilmaz, "Implementation of Programmable Logic Controller-Based Home Automation," *Journal of Applied Sciences*, vol. 10, no. 14, pp. 1449–1454, 2010, ISSN: 18125654. [Online]. Available: http://www.researchgate.net/publication/49591498_Implementation_of_Programmable_Logic_Controller-Based_Home_Automation.

[70] L. Balasevicius, G. Dervinis, and K. Sarkauskas, "Renewable Energy Sources-Receiver Switching," *Electronics and Electrical Engineering*, no. 114, pp. 89–92, 2011, ISSN: 13921215. [Online]. Available: http://connection.ebscohost.com/c/articles/67415786/renewable-energy-sources-receiver-switching.

[71] D Kolokotsa, K Kalaitzakis, E Antonidakis, and G. Stavrakakis, "Interconnecting smart card system with PLC controller in a local operating network to form a distributed energy management and control system for buildings," *Energy Conversion and Management*, vol. 43, no. 1, pp. 119–134, 2002, ISSN: 0196-8904. [Online]. Available: http://www.sciencedirect.com/science/article/pii/S0196890401000139.

[72] M. Predko, "Microcontrollers," in *Programming and Customizing the PIC Microcontroller*. New York, NY: McGraw-Hill, 1998, ch. 1, 9, pp. 1–5, 237284–, ISBN: 0-07-913645-1.

[73] D. Otten and J. Mach, "MCUs help meet design demands in low-power, high-performance industrial applications," *ECN: Electronic Component News*, vol. 55, no. 6, p. 14, 2011, ISSN: 15233081. [Online]. Available: components-asiapac.arrow.com/file.../id.../Microchip_mar2013_en.pdf.

[74] N. Barsoum, "Temperature and light control of three phase induction motor speed drive by PIC," *AIP Conference Proceedings*, vol. 1239, no. 1, pp. 185 –191, 2010, ISSN: 0094243X. [Online]. Available: http://scitation.aip.org/content/aip/proceeding/aipcp/10.1063/1.3459747.

[75] R. Shipley, Ed., *Microcontrollers - No Experience Necessary*, vol. 97, 5 May 2013, *Applied Science and Technology Source*, *Applied Science and Technology Source*, pp. 39-43.

[76] Arduino. (2015). Arduino Mega 2560, [Online]. Available: http://www.arduino.cc/en/Main/ArduinoBoardMega2560.

[77] B. Belvedere, M. Bianchi, A. Borghetti, C. Nucci, M. Paolone, and A. Peretto, "A microcontroller-based power management system for standalone microgrids with hybrid power supply," *Sustainable Energy, IEEE Transactions on*, vol. 3, no. 3, pp. 422–431, Jul. 2012, ISSN: 1949-3029.

[78] M. K. Ghodki, "Microcontroller and solar power based electrical energy management system for renewable energy applications," *International Journal of Electrical Power and Energy Systems*, vol. 44, no. 1, pp. 852 –860, 2013, ISSN: 0142-0615. [Online]. Available: http://www.sciencedirect.com/science/article/pii/S0142061512004899.

[79] I. Pisica, G. Taylor, C. Chousidis, D. Trichakis, L. Tomescu, and L. Laurentiu, "Design and implementation of a prototype home energy management system," cited By (since 1996)0, 2013. [Online]. Available: http://www.scopus.com/inward/record.url?eid=2-s2.0-84894138047&partnerID=40&md5=0d060b8540091d4a0db8e497d8137b60.

[80] R. Heeks and A. Robinson, "Ultra low-cost computing and developing countries," *Communications of the ACM*, vol. 56, no. 8, pp. 22 –24, 2013, ISSN: 00010782. [Online]. Available: http://dl.acm.org/citation.cfm?id=2492016.

[81] H. Uhan and A. Akbas, "Designing a system allowing high-definition video transfer with minimum latency and multi-use access to projection device by wireless," in *Proceedings of 2012 International Conference on Complex Systems, ICCS 2012*, Institute of Pure and Applied Sciences, Yalova University, 2012. [Online]. Available: http://www.researchgate.net/publication/261273444_Designing_a_system_allowing_high-definition_video_transfer_with_minimum_latency_and_multi-use_access_to_projection_device_by_wireless.

[82] K. Dewald and D. Jacoby, "Signal processing in embedded systems," *Latin America Transactions, IEEE (Revista IEEE America Latina)*, vol. 11, no. 1, pp. 664–667, Feb. 2013, ISSN: 1548-0992.

[83] PandaBoard. (2015). Panda Board ES Setup, [Online]. Available: http://pandaboard.org/content/resources/references.

[84] M. M. Ramses, E. D. L. Victoria, and A. S. Raúl, "Mobile remote control for home automation," *International Journal of Interactive Mobile Technologies*, vol. 7, no. 4, pp. 21 –26, 2013, ISSN: 18657923. [Online]. Available: http://www.researchgate.net/publication/270069303_Mobile_Remote_Control_for_Home_Automation.

[85] dSPACE, *Datasheet: DS1103 PPC controller board*, 2013. [Online]. Available: http://www.dspace.com/shared/data/pdf/2013/DS1103.pdf.

[86] Zeltom. (2015). RAPCON Board, [Online]. Available: http://zeltom.com/products/rapcon.

[87] A. Mermoud, *PVSyst*, Sottware Package, 2015. [Online]. Available: http://www.pvsyst.com/en/about-us/contact-our-team.

[88] C. Ricelli. (2014). Solar panel installation cost, [Online]. Available: http://www.riccellicreative.com/solar-panel-installation-cost/.

[89] B. Richard, C. Gudel, and S. Rollier, "What you need to know about solar design," *POWERGRID International*, vol. 17, no. 1, pp. 89 –93, 2012, ISSN: 15476723. [Online]. Available: http://www.elp.com/articles/powergrid_international/print/volume-17/issue-1/features/what-you-need-to-know-about-solar-design.html.

[90] E. Boldt. (2013). Pulse width modulation with analogwrite, [Online]. Available: http://robotic-controls.com/learn/arduino/pulse-width-modulation-analogwrite.

[91] F. Gotte, S. Mott, and C. Quintana. (2013). The project, [Online]. Available: https://intelligentsolar.wordpress.com/about.

[92] Javvin Technologies, "TCP/IP based protocols," in *Network Protocols Handbook*. 2005.

[93] Y. Bai, "Serial protocols," in *The Windows Serial Port Programming Handbook*. CRC Press LLC, 2005, ISBN: 0-8493-2213-8.

[94] A. Knoll and R. Prasad, "Wireless robotics: a highly promising case for standardization," English, *Wireless Personal Communications*, vol. 64, no. 3, pp. 611–617, 2012, ISSN: 0929-6212. DOI: 10.1007/s11277-012-0604-8. [Online]. Available: http://dx.doi.org/10.1007/s11277-012-0604-8.

[95] E. Perez, H. Beltran, N. Aparicio, and P. Rodriguez, "Predictive power control for pv plants with energy storage," *IEEE Transactions on Sustainable Energy*, vol. 4, no. 2, pp. 482–490, Apr. 2013. DOI: 10.1109/TSTE.2012.221255.

[96] I. Lampropoulos, P. Garoufalis, P. Van den Bosch, and W. King, "Hierarchical predictive control scheme for distributed energy storage integrated with residential demand and photovoltaic generation," *IET Generation, Transmission and Distribution*, vol. 9, no. 15, pp. 2319–2327, Jul. 2015. DOI: 10.1049/iet-gtd.2014.0908.

[97] M. Ahmed, H. Shareef, A. Mohamed, J. Ali, and A. Mutlag, "Rule base home energy management systemconsidering residential demand response application," *Applied Mechanics and Materials*, vol. 785, no. 1, pp. 526–531, Apr. 2015. DOI: 10.4028/www.scientific.net/AMM.785.526.

[98] P. Romero, G. Lozano, R. Cadaval, and L. Tello, "Local energy management unit for residential applications," *Elektronika IR Elektrotechnika*, vol. 19, no. 7, pp. 61–64, May 2013. DOI: 10.5755/j01.eee.19.7.5164.

[99] J. Pascaul, J. Barricarte, P. Sanchis, and L. Marroyo, "Energy management strategy for a renewable-based residential microgrid with generation and demand forecasting," *Applied Energy*, vol. 158, no. 1, pp. 12–25, Nov. 2015, ISSN: 0306-2619.

[100] Department of Energy. (2012). A survey of energy-related behaviour and perceptions in South Africa, The residential sector, [Online]. Available: http://www.energy.gov.za/files/media/Pub/Survey%20of%20Energy%20related%20behaviour%20and%20perception%20in%20SA%20%20Residential%20Sector%20-%202012.pdf.

[101] South African Audience Research Foundation. (2012). SAARF Segmentation-Tools, [Online]. Available: http://www.saarf.co.za/lsm-presentations/2012/LSM%20Presentation%20-%20February%202012.pdf.

[102] G. M. Bokanga, A. K. Raji, and M. T. E. Kahn, "Design of a low voltage DC microgrid system for rural electrification in South Africa," *Journal of Energy in Southern Africa*, vol. 25, no. 2, p. 9, May 2014, ISSN: 96902815. [Online]. Available: http://connection.ebscohost.com/c/articles/96902815/design-low-voltage-dc-microgrid-system-rural-electrification-south-africa.

[103] Victor Energy, *Datasheet: Gel and AGM Batteries*. [Online]. Available: http://www.victronenergy.com/upload/documents/Datasheet-GEL-and-AGM-BatteriesEN.pdf.

[104] G. Delport, "The geyser gadgets that work/don't work," in *Proceedings of the 13th Domestic Use of Energy Conference*, N. Beute, Ed., Cape Town, 2005, pp. 139–144.

[105] Q. Catherine, J. Wheeler, R. Wilkinson, and G. De Jager, "Hot water usage profiling to improve geyser efficiency," *Journal of Energy in Southern Africa*, vol. 23, no. 1, 2012.

[106] A. Harris, M. Kilfoil, and E. Uken, "Options for residential water heating," in *Proceedings of the 16th Domestic Use of Energy Conference*, N. Beute, Ed., Cape Town, 2008, pp. 141–148.

[107] Solar Frontier, *Datasheet: SF Series*, 2014. [Online]. Available: http://www.solar-frontier.com/eng/cs/groups/co_en_corporate/documents/co_en_attachment/mdaw/mdi1/~edisp/c025365.pdf (visited on 11/15/2014).

[108] Kaco, *Datasheet: Powador 2002-6002*, 2012. [Online]. Available: http://kaco-newenergy.com/fileadmin/data/downloads/products/Galvanically%20Isolated%20String%20Inverters%20Powador%202002-6002/Data%20Sheets/DTS_PW_2002-6002_en_140711.pdf (visited on 11/15/2014).

[109] SMA, *Datasheet: Sunnboy 3000TL*, 2014. [Online]. Available: http://files.sma.de/dl/15330/SB5000TL-21-DEN134924W.pdf (visited on 11/15/2014).

[110] Steca, *Datasheet: Coolcept*, 2014. [Online]. Available: http://www.steca.com/index.php?coolcept-StecaGrid-1500-4200-en#productdownload (visited on 11/15/2014).

[111] K. Sangani, "Light work for domestic LEDs," *Engineering and Technology*, vol. 9, no. 4, pp. 40–43, 2014, ISSN: 17509637. [Online]. Available: http://ieeexplore.ieee.org/xpl/articleDetails.jsp?arnumber=6809531.

[112] Victron Energy, *Datasheet: Gel and AGM batteries*, 2012. [Online]. Available: http://www.victronenergy.com/upload/documents/Datasheet-GEL-and-AGM-Batteries-EN.pdf (visited on 01/15/2015).

[113] SANWS, *Weather data for the period from January 2010 to September 2014*, 2014. [Online]. Available: http://www.weathersa.co.za/compliments-complaints/company-details.

[114] Z. A. Samani, "Estimating solar radiation and evapotranspiration using minimum climatological data," *Journal of Irrigation and Drainage Engineering*, vol. 126, no. 4, pp. 265–267, 2000, ISSN: 1943-4774.

[115] A. Ugwu and J. Ugwuanyi, "Performance assessment of Hargreaves model in estimating solar radiation in Abuja using minimum climatological data," *International Journal of the Physical Sciences*, vol. 6, no. 31, pp. 7285–7290, 2011, ISSN: 1992-1950.

Appendix A: Publications and Peer Reviews

Throughout the duration of the study, a conscious effort was made to gather as much external input on the research topic as possible. This included attending conferences, obtaining feedback from subject matter experts, writing scientific articles and presenting papers at international conferences. The list below summarises the conferences that was attended, the citations of the publications and the pending peer reviews. All written articles are added after the listings below.

Conferences

- Schneider Electric Xperience Efficiency Conference, 18-20 Aug. 2014, Visitor.
- Suid-Afrikaanse Akademie vir Wetenskap en Kuns Conference. 07-08 Nov. 2014 (South African Journal for Science and Arts), Paper Delivered.
- Domestic Use of Energy (DUE) Conference, 31 Mar-01 Apr. 2015, Paper Delivered.
- Africa Utility Week, 12-14 May 2015, Visitor.
- Powergen and Distributech Conference, 15-17 Jul. 2015, Delegate.

Publications

- W.A. Bisschoff and R. Gouws, “Energy management system for a residential grid-tied micro-grid,” in Proceedings of the Twenty Third Conference on the Domestic Use of Energy, Cape Town, South Africa: Cape Peninsula University of Technology, Apr. 2015, pp. 85–91, ISBN: 978-0-9922041-8-1.
- W.A. Bisschoff and R. Gouws, "Ontwerp van ‘n energiebestuurstelsel vir optimale energie verbruik en effektiwiteit van ‘n distribusievlakmikrokragnetwerk," Studentesimposium in die Natuurwetenskappe, Pretoria, South Africa, Nov. 2014, pp. 21.

Pending Peer Reviews

- W.A. Bisschoff and R. Gouws, "Experimental Energy Management System for Residential PV Systems in Non-feed-in Tariff Countries", Submitted to the Journal of South Africa (JESA) on 6 November 2015. ISSN: 1021-447X.
- W.A. Bisschoff and R. Gouws, “Practical considerations for controller selection in residential energy management systems: A review”, Submitted to the Journal of Energy Conversion and Mangement on 13 November 2015. ISSN: 0196-8904.

PROCEEDINGS

of the

Twenty Third Conference on the

DOMESTIC USE OF ENERGY

31 March-1 April 2015

Organised by

The Cape Peninsula University of Technology

In association with
IEEE: Chapters of IAS, IES, PELS and Power & Energy Society
The South African Association of Energy Service Companies
The South African Institute of Electrical Engineers
Association of Municipal Electrical Undertakings
The Southern Association for Energy Efficiency
Sustainable Energy Society Southern Africa
National Energy Efficiency Agency
University of Stellenbosch
University of Cape Town
North-West University
City of Cape Town
Eskom

Published by

Cape Peninsula University of Technology, Cape Town, South Africa

ISBN 978-0-9922041-8-1

Energy Management System for a Residential Grid-Tied Micro-Grid

Wilhelm A. Bisschoff and Rupert Gouws

Abstract—With the national power grid under tremendous pressure, there are enormous pressure exerted on residential electricity consumers to cut-back on electricity consumption to ensure a reliable supply. This has led to residential electricity users wanting to generate their own electricity through solar and wind systems, more formally known as distribution energy resources (DERs). The possibility of DERs currently exists within the centralized power grid, but is currently not well supported by Eskom and local municipalities. There are currently very little widely implemented policies regarding net-metering and feed-in tariff structures amongst Eskom and municipalities. Thus, excess generated energy fed into the grid is used elsewhere without any benefit going to the owner of the DER. By implementing an active energy management system (EMS) alongside the grid integrated system, electricity generated by the DER can be consumed locally by the residential loads. The EMS achieves an electricity consumption reduction of 23.4 % compared to a system with no EMS. Further results show that the EMS compensated system shows a cost saving of R19.17 per day which translates to a reduction of 51.4 % compared to a system with no EMS.

***Index Terms*—Energy Management, Micro-grids, Renewable Energy**

1 Introduction

Recent press releases and media announcements made by the South African state-owned utility company, Eskom, indicates that the South African national power grid is under severe pressure. The uncertainty of the utilities' future has sparked ideas for residential energy consumers to become independent of Eskom and start generating their own electricity. Most of these energy consumers have resorted to considering micro-grid topologies into their homes.

A micro-grid is defined as a small independent power system consisting of locally generated alternative energy sources that can function independently or in accordance with the centralized power grid [1],[2]. Micro-grids can be integrated with the centralized grid on transmission or distribution level depending on the purpose of the system. For a residential micro-grid, the system is integrated on the low voltage (LV) distribution level network where the power generation mediums are referred to as distributed energy resources (DERs) [2]. Typical examples of DERs include small scale wind turbines, photovoltaic (PV) systems, microturbines, diesel-generators, fuel cells etc.

Conventional micro-grids are connected in a topology that enables the system to be grid-tied or to be disconnected from the grid (island-mode) [3]. The grid-tie topology is the most-common and simplest to implement, since the energy balance between the generated and consumed energy is maintained. However, in the case where the DERs connected to the micro-grid generates excess energy, it is fed into the centralized grid to maintain the energy balance [2],[4]. In island mode it is not that simple since there is no additional loads to which excessive energy can be fed to maintain the energy balance. This complication is overcome by using a large battery bank as a buffer between the DER and the loads. The PV modules are used only to charge the batteries and thereafter the batteries supply the load. Fig. 1 illustrates the concept of DERs within the centralized grid.

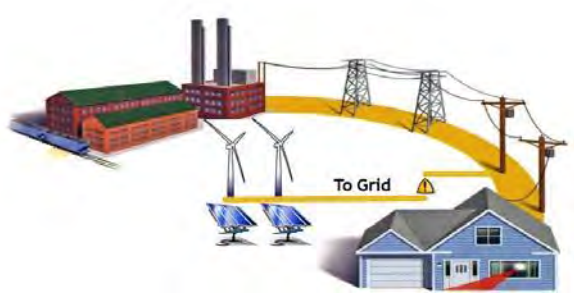

Figure. 1. Visual illustration of micro-grid topology.

With the rising electricity prices, more and more residential electricity consumers are considering grid-tied micro-grid systems consisting of small scale renewable energy sources such as wind turbines and photovoltaic systems. According to [5] and [6], the implementation of residential grid-tied micro-grids can drastically improve reliability and decrease the monthly electricity bill whilst reducing pressure off the grid. However, achieving the above mentioned, it requires the utility companies to support the residential electricity users by allowing the installation of bi-directional meters into their homes [5],[6]. Unfortunately, according to [7] and [8], connecting small scale (<1 MW) energy sources that feed electricity back into the grid is still fairly unsupported in South Africa and therefore cannot be remunerated as in other countries such as the United State of America (USA), Belgium, Switzerland etc. [9]. First world countries offer these electricity feed-in tariffs to promote the adoption of renewable DERs. However, South Africa has not yet

W. A. Bisschoff, School of Electrical, Electronic and Computer Engineering, North-West University, Potchefstroom, South Africa (e-mail: wabisschoff@gmail.com).

R. Gouws, School of Electrical, Electronic and Computer Engineering, North-West University, Potchefstroom, South Africa (e-mail: rupert.gouws@nwu.ac.za).

reached this point which is mainly due to the lack of appropriate billing processes that can accommodate net metering.

This makes the installation of a residential grid-tied micro-grid inefficient as excess energy fed into the centralized grid goes to waste. There are very little micro-grid systems combining an energy management system (EMS) to ensure that locally generated energy is consumed within the interconnected loads rather than feeding the excess energy into the grid. A well-designed EMS that exhibits a control system that can process information such as generation data, load data, consumption patterns, weather predictions and economic factors can be utilized to use the generated energy in the most efficient manner.

2 ENERGY MANAGEMENT SYSTEM DESIGN

The primary objective of the EMS is to reduce the monthly electricity bill by implementing various energy saving strategies to minimize the energy consumption off the centralized grid. The secondary objective of the EMS is to ensure that as much as possible of the energy generated by the DER are consumed locally rather than fed into the grid. By achieving the secondary objective, the primary objective will be met.

2.1 Design Requirements

According to the design requirements, the EMS is to be installed into a middle-class home which consists of the physical attributes listed below. Take note that the characteristics below are set-up according to typical South African homes.

i. Three Bedrooms, with one bedroom having an en-suite bathroom

ii. Two Bathrooms, one independent and one en-suite

iii. An outside living area next to the swimming pool

iv. A kitchen with a built-in gas stove and oven with a separate washing room fit for a washing machine and tumble dryer

Taking the physical attributes into account, electrical attributes and appliances for a residence described above would be but not limited to:

v. Two 3 kW geysers, with one geyser wired to supply only the en-suite bathroom and the other geyser wired to supply the washing room along with the standalone bathroom

vi. One 9 kg washing machine along with a 9 kg tumble dryer

vii. An automated dishwashing machine with an instantaneous power consumption of less than 2 kW

viii. A typical 550 W AC swimming pool pump is used to circulate the water

ix. A standard refrigerator with an instantaneous power consumption of not more than 300 W

x. The residence must host a DC security light system that activates during night time and remains switched on for the duration of the night without any interruptions. The DC light system must be used to provide light to the pool area and the rest of the yard. The maximum allowed instantaneous power consumption of the DC light system may not exceed 75 W.

xi. The system may include a battery bank, but it may not exceed a storage capacity of 2 kWh.

xii. The DER, PV, WTG etc., may not be used as a standalone system but rather as a supplement along with the grid.

A floor plan of a residence adhering to the above mentioned requirements is shown in fig. 2. Fig. 2 will be used as a basis from which the detail design decisions are made.

Figure. 2. Floor plan showing illustrating the design requirements.

The *"S"* areas shown in fig. 2 indicates a zone where security lighting is required throughout the night.

2.2 Distributed Energy Resource (DER)

Taking into consideration the availability and feasibility of renewable energy sources in South Africa, there are two that comes to mind, Wind and Solar. These two forms of energy are both available at the coastal and inland regions of South Africa. Fig. 3 and 4 illustrate the annual wind speed and solar irradiation levels across the southern parts of Africa [10],[11]. When analysing fig. 3 and 4, it becomes evident that the coastal regions are more suited for wind energy harvesting and inland areas for solar energy harvesting. The testing station made available for the data collection hosts a 3 kW grid-tied PV system and is based in the north western part of the South Africa and hence the EMS design is done in accordance with a PV system as DER for the micro-grid.

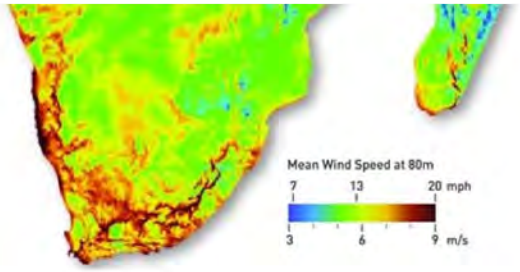

Figure. 3. Southern Africa mean wind speed measured at 80 m above ground level [10].

Figure. 4. Annual average sum of solar irradiation for Southern Africa [11].

2.3 DC Security Light System

According to the specifications set out in the design requirements, the security light system may not exceed an instantaneous power consumption of more than 75 W and hence the design weighs towards a low-power light emitting diode (LED) based security light system. Since there are 4 zones that require security lighting through the night, 4 LED floodlights (3x10 W and 1x20 W at 12 V) have been selected to provide the necessary lighting. This brings the power consumption of the DC light system to a total of 50 W, which falls within the requirements.

The design specifications requires that the battery bank must be able to supply the 50 W DC security light system for a minimum of 10 hours and a maximum of 12 hours, depending on the season. The selected system voltage as mentioned above is 12 V. Taking into account the above mentioned design considerations, the depth of discharge of a battery can greatly influence the number of service years as shown in fig 5. Taking into consideration that the ideal design would be to choose a depth of discharge (DOD) close to the knee of the curve shown in fig 5. This would represent a 30 % DOD (only 30 % of the battery's capacity is used) and would increase initial investment costs. Therefore, the cycle depth design specification has been set at a maximum DOD of 50 % and translates to roughly 1000 cycles.

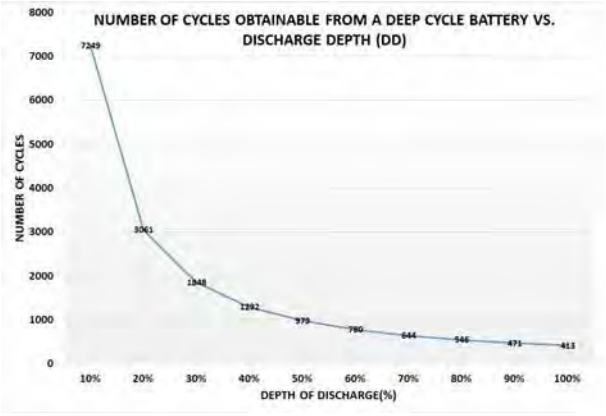

Figure. 5. Number of cycles from a deep-cycle battery vs. depth of discharge (DOD).

The final design consideration that must be taken into account is the percentage of available storage capacity which is primarily influenced by the ambient air temperature at which the battery operates. The graph illustrated in fig. 6 shows the influence of ambient temperature on the available storage capacity of a battery [12].

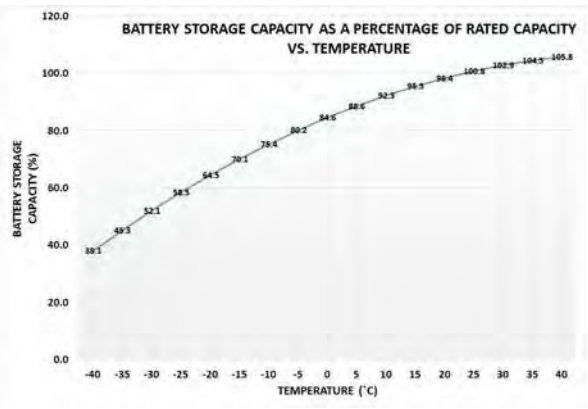

Figure. 6. Battery storage capacity vs. Temperature [12].

Hence from this graph, the storage capacity of a battery declines as the ambient temperature decreases. The storage capacity of the battery will therefore be at its lowest during the winter season and these conditions are considered when choosing the storage capacity reduction factor for the design. Average winter temperatures vary greatly throughout the regions of South Africa, however the average winter temperatures for the town of Potchefstroom, where testing will be conducted, are shown in fig. 7 (provided by the South African National Weather Service (SANWS)) [13].

By examination of the weather data, an assumption regarding the minimum average temperature during winter months can be made. The majority of the temperatures during the night seldom drops below 0°C, however a worst-case design approach is followed and therefore the design specification is set at 0°C. By analysing the curve shown in fig. 6, it can be seen that at 0°C, a battery storage capacity reduction of 15.4 % is applicable. A summary of the battery design specifications are summarized in Table I.

Table I. Summary of battery sizing specifications.

Description	Design Specifications
Load power consumption (W)	50 W
System voltage (V)	12 V
Hours of operation	12 hrs
Days without charging	0
DOD (%)	50 %
Battery storage reduction factor (%)	15 %

The majority of battery's capacity ratings are given in ampere-hours (Ah) and therefore the design requirements will be calculated to match this unit. To calculate the required Ampere-hour rating to meet the specifications set out in Table I, the formula shown in (1) must be applied.

$$Ah_{rating} = \frac{(P_{load})(T_{operation})}{(\gamma)(1-\delta)(V_{systen})(n+1)} \quad (1)$$

Where γ represents DOD, δ represents the reduction factor and n implies days without charging. When applying (1) for the requirements in Table I, it can be seen that a battery capacity rating of 117 Ah would be sufficient.

2.4 Residential Energy Saving

In a study presented by [14], it was found that the electricity consumption within a typical residential home can be broken down as shown in fig. 8.

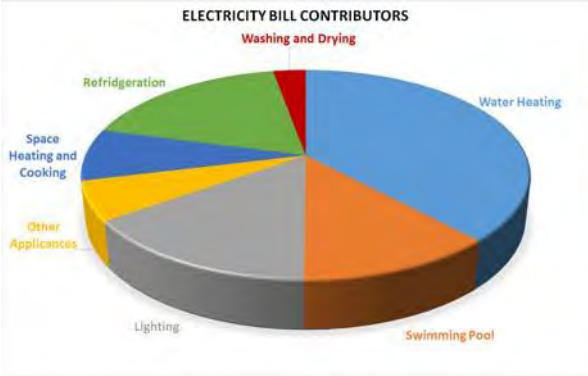

Figure. 8. Major electricity bill contributors in a home.

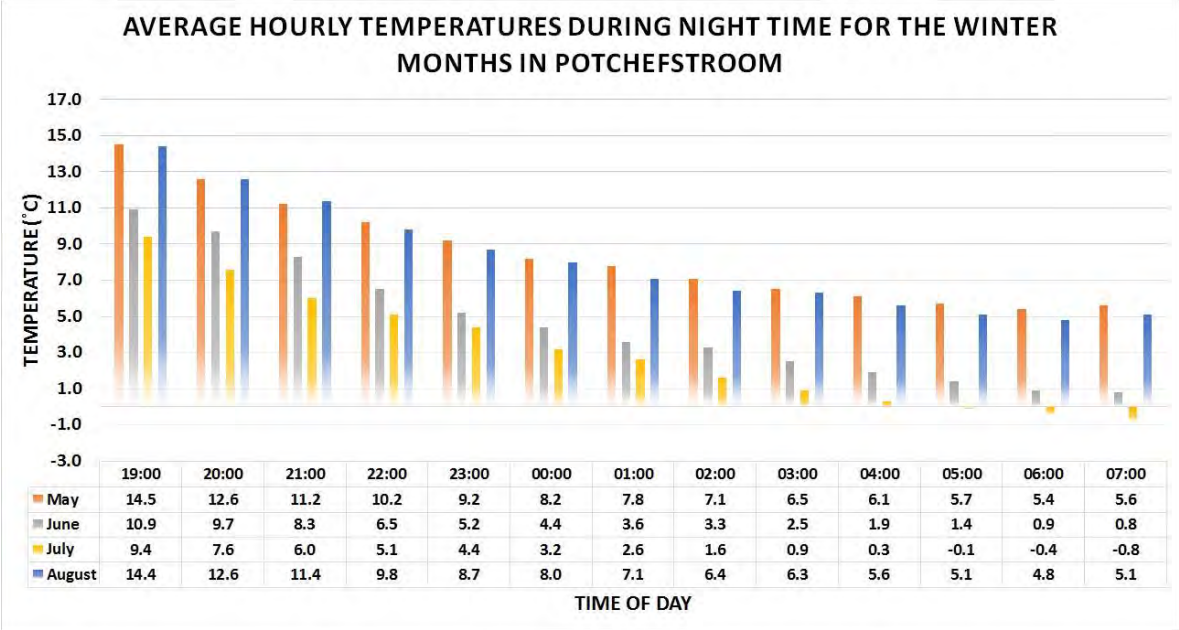

	19:00	20:00	21:00	22:00	23:00	00:00	01:00	02:00	03:00	04:00	05:00	06:00	07:00
May	14.5	12.6	11.2	10.2	9.2	8.2	7.8	7.1	6.5	6.1	5.7	5.4	5.6
June	10.9	9.7	8.3	6.5	5.2	4.4	3.6	3.3	2.5	1.9	1.4	0.9	0.8
July	9.4	7.6	6.0	5.1	4.4	3.2	2.6	1.6	0.9	0.3	-0.1	-0.4	-0.8
August	14.4	12.6	11.4	9.8	8.7	8.0	7.1	6.4	6.3	5.6	5.1	4.8	5.1

Figure. 7. Hourly average temperatures during the winter months in Potchefstroom.

As expected the majority of electricity consumption within a residence are due to loads running on a continuous basis such as the geyser heater, refrigerators etc. Based on this known fact, the EMS is designed to effectively manage continuous running loads with the exception of loads such as a washing machine and tumble dryer. By actively controlling the geyser, refrigerator, swimming pool pump, washing machine, tumble dryer and battery charge controller, significant energy savings can be achieved whilst ensuring that a high percentage of the load is supplied by the PV system.

2.4.1 Geyser Energy Saving

Geysers are cylindrical insulated water tanks which are used to heat the incoming cold water to a temperature that is suitable for use within a household. A geyser basically consists of a heating element and thermostat with a controllable switch. The thermostat is set to a desired temperature. When the water temperature is below the set point, the controllable switch is closed and the geyser element is switched on. These elements are usually in the range of 3 kW for a 150 litre tank and 4 kW for a 200 litre unit [14]. Once the water is heated to the desired temperature, the controllable switch opens and the geyser is switched off. Electricity within a geyser is used in two ways [15]:

xiii. The first begin when hot water is used, it is drawn from the geyser into the pipes which then needs to be replaced by cold water. The mixture of hot and cold water causes the geyser's temperature to stabilize well below the desired temperature and the element is switched on.

xiv. The second begin when the geyser temperature drops as a result of the temperature difference between the ambient and the geyser's temperature. This is known as standing losses. The greater the difference, the greater the heat loss. This causes the geyser to switch on and off

periodically to maintain the geyser temperature. Fig. 9 illustrates the concept of standing losses. This figure is based on the assumption that no hot water is drawn from the geyser.

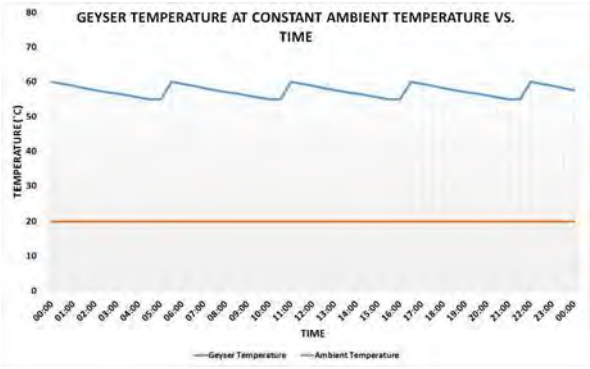

Figure. 9. Geyser Temperature at constant ambient temperature [14],[16].

According to experimental data collected in [16], standing losses can vary from 1.012 to 2.531 kWh/day which equates to a cost of at least R 51.22 per month (R1.48 per kWh). Hence the EMS is to minimize standing geyser losses as this can result in significant monthly savings.

Table II. Summary of geyser standby losses.

Description	kWh/month	Cost (R)
Standby losses	1.01-2.53 kWh	R 51.22-R 128.06

2.4.2 Swimming Pool Energy Saving

There are lots of energy efficient swimming pool pumps that are available on the market designed to reduce energy consumption [17]. However, these high efficiency pumps often require a significant initial investment. An alternative energy saving incentive that can be implemented, is to reduce the running time of the swimming pool pump. On average, swimming pool pumps run the filtration system for a period of roughly 10 hours per day (8 AM to 6 PM). Studies made Eskom, have shown that if the swimming pool pump is correctly sized to the volume of the swimming pool, a runtime of 4 to 5 hours would circulate the every litre of water which would be sufficient for filtration and cleaning [17].

Assuming a 550 W single speed swimming pool pump running for 10 hours per day would result in a monthly energy consumption of 165 kWh. Running the same motor for a total of 6 hours per day would result in a consumption of 99 kWh, which is a 40 % reduction in consumed energy. This translates to a saving of R 97.68 (R 1.48 per kWh) per month.

Table III. Summary of swimming pool consumption.

Runtime	kWh/month	Cost (R)
10 hours	165 kWh	R 244.20
6 hours	99 kWh	R 146.52

3 EMS SIMULATION DATA

3.1 Simulation Setup

In order to make the simulation data as realistic as possible, each residential appliance adopted in the simulation has been researched or measured in a real-time system to produce accurate load emulations. The designed EMS is divided into two profiles, days that require washing clothes and days that does not require washing. Each profile of the EMS acts differently on these days. The EMS also reacts differently depending on the amount of PV energy that comes in. As mentioned previously, the EMS' objectives are to maximize energy consumption from the locally generated electricity and reduce the monthly electricity bill. To illustrate the proof of concept, the simulation results compares the non-washing day of an uncompensated system that has no energy management with the compensated system that has full on energy management.

3.2 PV Input Profiles

The PV input profiles was collected from a 3 kW grid-tied PV installation at the North-West University in Potchefstroom. The PV profiles consisted of 15 minute samples throughout the day. A series of equations (not shown) fitting the data presented in fig. 10 was then derived to be used for simulation purposes. The PV profiles were measured during all four seasons, however only data from the month of August 2014 is shown to illustrate proof of concept. The profiles that were filtered from the data all corresponded to days with clear skies and high average temperatures. The filtered profiles are shown in fig. 10.

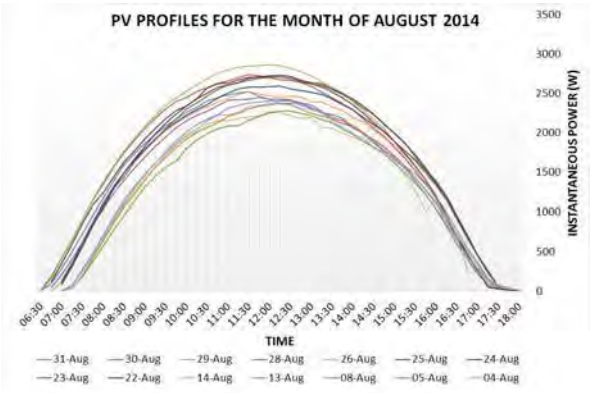

Figure. 10. PV profiles for the month of August 2014.

3.3 Uncompensated System

For a non-washing day, the uncompensated individual load profile is shown in fig. 11 with the combined load profile shown in fig. 12. The results of the uncompensated simulation is shown in Table IV.

Table IV. Summary of uncompensated simulation.

Characteristic	Result
PV Energy Input (kWh)	15.37 kWh
PV Energy Lost (kWh)	4.94 kWh
PV Energy Consumed (%)	67.7 %
Total Load Requirement (kWh)	35.63 kWh
Utility Supplied (%)	70.7 %
PV System Supplied (%)	29.3 %

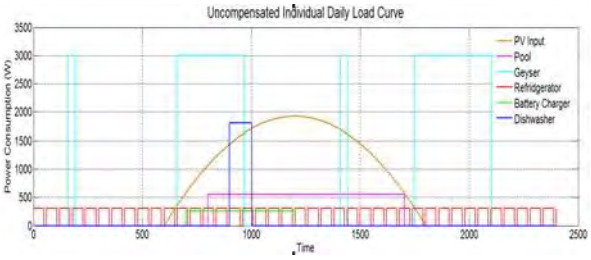

Figure. 11. Uncompensated individual load curve.

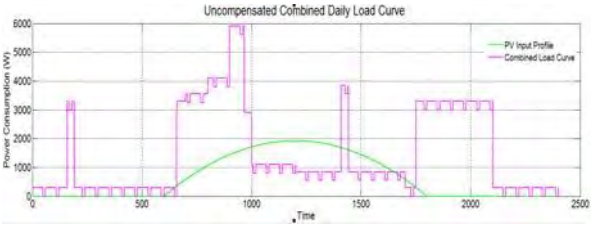

Figure. 12. Uncompensated combined load curve.

3.4 Compensated System

For a non-washing day, the compensated individual load profile is shown in fig. 13 with the combined load profile shown in fig. 14. The results of the compensated simulation is shown in Table V.

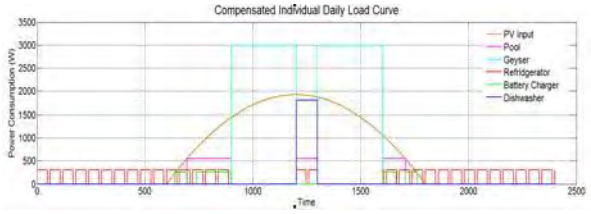

Figure. 13. Compensated individual load curve.

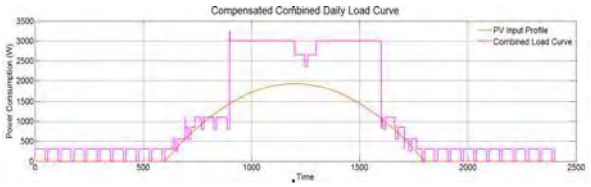

Figure. 14. Compensated combined load curve.

Table V. Summary of compensated simulation.

Characteristic	Result
PV Energy Input (kWh)	15.37 kWh
PV Energy Lost (kWh)	0.35 kWh
PV Energy Consumed (%)	97.7 %
Total Load Requirement (kWh)	27.26 kWh
Utility Supplied (%)	44.9 %
PV System Supplied (%)	55.1 %

3.5 Additional Simulations

This section adds another result obtained from a lower PV input profile. The results are summarized in Table VI and Table VII.

Table VI. Summary of uncompensated simulation.

Characteristic	Result
PV Energy Input (kWh)	12.58 kWh
PV Energy Lost (kWh)	3.07 kWh
PV Energy Consumed (%)	75.6 %
Total Load Requirement (kWh)	35.63 kWh
Utility Supplied (%)	73.3 %
PV System Supplied (%)	27.7 %

Table VII. Summary of compensated simulation.

Characteristic	Result
PV Energy Input (kWh)	12.58 kWh
PV Energy Lost (kWh)	0.14 kWh
PV Energy Consumed (%)	98.9 %
Total Load Requirement (kWh)	26.89 kWh
Utility Supplied (%)	53.7 %
PV System Supplied (%)	46.3 %

4 DISCUSSION

4.1 Uncompensated Load Curves

The uncompensated individual load curve was derived from measurements taken in residences along with researched load patterns of South African residences [12],[14]. These measurements were mainly time-based to determine the consumption behaviour of the residence inhabitants. As can be seen in fig. 11, all of the loads are switched on uncontrolled through the entire day and night. The uncompensated combined load curve in fig. 12 presents the combined consumption of all the loads. As can be seen in the early to mid-morning, consumption and demand is exceptionally high during this period. The demand reaches a peak of almost 6 kW. This is mainly due to several loads being switched on at the same time. During this period, the incoming PV is not at a maximum and consumption outweighs input by roughly 2 to 3 times. This causes excessive electricity consumption off the centralized grid and increases the monthly bill.

Further analysis of fig. 12 sees that during the peak hours of incoming PV energy, very little loads are switched on and the incoming energy exceeds that of the connected load. This causes the excess energy to be fed into the centralized grid and get lost without any benefit to the home owner. Analysing the data presented in Table IV, the total load requirement for the uncompensated system was 35.63 kWh. Of this quantity 70.7 % of the load was supplied by the centralized grid and only 29.3 % by the DER. Running the financial implication for this, it would result in a total of R37.28 per day (R 1.48 per kWh) for the electricity consumed off the centralized grid. This result is based on a day with fine weather with clear skies and moderate sunshine. Of the total delivered energy from the DER, only 67.7 % was consumed locally which translates to 4.94 kWh that was lost to the centralized grid. This equates to R 7.31 per day.

4.2 Compensated Load Curves

Analysing fig. 13, it can be seen that the EMS has altered the load curve such that all the loads are more in the shape of the PV profile. With the reshaping of the load curve as shown in fig. 14, the EMS has achieved following:

xv. The total electricity consumption has been reduced from 35.63 to 27.26 kWh which is a reduction of 23.4 %.

xvi. More importantly, of the 27.26 kWh, 55.1 % thereof is supplied by the DER and only 44.9 % is supplied by the centralized grid.

xvii. This translates to a daily cost of R 18.11 (R 1.48 per kWh) per day for the electricity consumed from the centralized grid. Comparing the system with no EMS installed, a cost reduction of R19.17 or 51.4 % is possible.

xviii. Of the total DER generated electricity, only 0.35 kWh or 2.3 % was lost to the centralized grid. This equates to a total of R 0.52 per day.

To conclude the discussion, Table VIII provides a summary of the costs.

Table VIII. Summary of costs.

Characteristic	Uncompensated	Compensated
Daily Cost	R 37.28	R 18.11
Monthly Cost	R 1118.40	R 543.30

REFERENCES

[1] H. Kim and M. Thottan, "A two-stage market model for micro-grid power transactions via aggregators.," Bell Labs Technical Journal, vol. 16, no. 3, pp. 101 –107, 2011, ISSN: 10897089. [Online]. Available: http://nwulib.nwu.ac.za/login?url=http://search.ebscohost.com/login.aspx?direct=true&db=buh&AN=67365656&site=eds-live.

[2] Q. Jiang, M. Xue, and G. Geng, "Energy management of micro-grid in grid-connected and stand-alone modes.," IEEE Transactions on Power Systems, vol. 28, no. 3, pp. 3380 –3389, 2013, ISSN: 08858950. [Online]. Available: http://nwulib.nwu.ac.za/login?url=http://search.ebscohost.com/login.aspx?direct=true&db=buh&AN=89267630&site=eds-live.

[3] Power Engineering International. (2010). Achieving a smart energy ecosystem, [Online]. Available: http://www.powerengineeringint.com/articles/print/volume-18/issue-5/features/achieving-a-smart-energy-ecosystem.html.

[4] D. Robinson, "Micro-grids for energy reliability." ASHRAE Journal, vol. 55, no. 11, B14 –B17, 2013, ISSN: 00012491. [Online]. Available: http://nwulib.nwu.ac.za/login?url=http://search.ebscohost.com/login.aspx?direct=true&db=aph&AN= 91960786&site=eds-live.

[5] M. Mikati, M. Santos, and C. Armenta, "Electric grid dependence on the configuration of a small-scale wind and solar power hybrid system," Renewable Energy, vol. 57, pp. 587–593, Sep. 2013, ISSN: 09601481. [Online]. Available: http://www.sciencedirect.com/science/article/pii/S0960148113001274.

[6] S. Ramakrishnan and S. Ramakrishnan, "Wot (web of things) for energy management in a smart grid-connected home.," Issues in Informing Science and Information Technology, vol. 10, pp. 461 – 472, 2013, ISSN: 15475840. [Online]. Available: http://nwulib.nwu.ac.za/login?url=http://search.ebscohost.com/login.aspx?direct= true&db=aci&AN=91510547&site=eds-live.

[7] D. Lipschitz. (2010). Grid tying and net metering for systems under 1 MW, [Online]. Available: http://www.engineeringnews.co.za/article/grid- tying- and-netmetering-for-systems-under-1-mw-2010-10-22

[8] NERSA, Renewable energy feed-in tariff phase 2, 2009. [Online]. Available: http://www.nersa.org.za/Admin/Document/Editor/file/Electricity/REFIT%20Phase%20II%20150709.pdf.

[9] M. Schulze and P. C. Del Granado, "Implementation of feed-in tariffs into multienergy systems." International Journal of Electrical Power and Energy Systems Engineering, no. 2, p. 85, 2010, ISSN: 2070-3767. [Online]. Available: http://nwulib.nwu.ac.za/login?url=http://search.ebscohost.com/login.aspx?direct=true&db=edsgea&AN=edsgcl.221760386&site=eds-live.

[10] 3Tier. (2012). Global mean wind speed at 80m, [Online]. Available: http://dupontconsulting.files.wordpress.com/2012/01/3tier_5km_global_wind_speed.jpg.

[11] SolarGIS. (2012). Global horizontal irradiation: southern africa, [Online]. Available: http://solargis.info/doc/_pics/freemaps/1000px/ghi/SolarGIS- Solar-mapSouthern-Africa-en.png.

[12] Victron Energy, Datasheet: Gel and AGM batteries, 2012. [Online]. Available: http://www.victronenergy.com/upload/documents/Datasheet-GEL-and-AGM-BatteriesEN.pdf.

[13] South African National Weather Service (SANWS). Weather data provided for the period of Jan. 2010 to Sept. 2014.

[14] A. Harris, M. Kilfoil and E.A. Uken. (2008). Options for residential water heating. Proceedings of the 16th Domestic Use of Energy Conference, Cape Town, 2008, Cape Peninsula University of Technology: pp. 141-148.

[15] G.J. Delport, (2005). The Geyser Gadgets that work/ do not work. Proceedings of the 13th Domestic Use of Energy Conference, Cape Town, March 2005, Cape Peninsula University of Technology: pp. 139 – 144.

[16] Q. Catherine, J. Wheeler, R. Wilkinson and G. de Jager. (2012). Hot water usage profiling to improve geyser efficiency. Journal of Energy in Southern Africa, Vol. 23(1), pp. 39-45.

[17] Eskom IDM. (2011). Trimming 10% is easier than you think. [Online]. Available: http://www.eskom.co.za/OurCompany/MediaRoom/Documents/10pcsavingsBrochure.pdf.

AUTHORS BIOS AND PHOTOGRAPHS

Wilhelm A. Bisschoff received the B.Eng degree in Electrical Engineering from the North-West University Potchefstroom Campus in 2013. From 2014 he was a Research Assistant for the NWU Potchefstroom Campus Unit for Energy Systems. He is currently pursuing his M.Eng in Electrical Engineering and is registered as a Candidate Engineer-in-Training with ECSA and the SAIEE.

Rupert Gouws holds a Ph.D. degree in Electrical and Electronic Engineering from the North-West University (Potchefstroom campus). He consulted to a variety of industry and public sectors in South Africa and other countries in the fields of energy engineering and engineering management. Currently he is appointed as an associate professor specialising in energy engineering, electrical machines and control at the North-West University. The Engineering Council of South Africa (ECSA) registered him as a Professional Engineer and the Association of Energy Engineers (AEE) certified him as a Certified Measurement and Verification Professional (CMVP).

Presenting author: Wilhelm A. Bisschoff

Experimental Energy Management System for Residential PV Systems in Non-feed-in Tariff Countries

Wilhelm A. Bisschoff and Rupert Gouws

Abstract— Currently within South Africa and other developing countries, net-metering policies are not yet widely implemented which hinders the adoption of residential PV systems. Without proper net-metering policies in place, the benefits of residential PV systems are limited to self-consumption as all energy fed into the utility grid is lost without remuneration. This leads to an inefficient and non-profitable PV system. To improve the efficiency and feasibility of the PV system in countries with no feed-in policy, it is of utmost importance that an energy management system (EMS) that optimises self-consumption, of the generated energy, be employed. The EMS presented in this paper focusses on self-consumption and reducing the energy consumption off the utility grid. Experimental results obtained from a real-world system showed that the local energy consumption percentage increased by 15-20% when compared to a PV system with no EMS.

Index Terms—Energy Management, Distributed Generation

1 Introduction

Rising electricity prices and unreliable supply are driving more residential electricity consumers to installing grid-tied distributed energy resources (DERs) that consist of small scale renewable energy sources such as wind turbines and solar photovoltaic (PV) systems (Jiang, et al., 2013), (Robinson, 2013) . According to (Mikati & Santos, 2013) and (Ramakrishnan & Ramakrishnan, 2013), implementing grid-tied DERs have the ability to drastically improve the reliability of supply whilst decreasing the annual electricity bill. According to (Schulze & Del Granado, 2010) achieving the abovementioned requires widespread net-metering policies that permit residential electricity consumers to "sell" excess generated electricity back to distribution utilities.

A statement made by (Schulze & Del Granado, 2010) that across the globe, first world and developed countries have these net-metering policies in place; countries such as the Americas, Belgium and Switzerland offers competitive feed-in tariffs which have substantial financial benefits. However, in third world and developing countries these policies are absent (Eskom , 2015), (Eskom Newsdesk, 2015). This is owed to safety concerns, a lack of proper electrical infrastructure and poor distribution system management. According to (Mikati & Santos, 2013) and (Ramakrishnan & Ramakrishnan, 2013) without proper net-metering policies in place, the benefits of grid-tied DERs are limited to self-consumption as all energy fed into the utility grid is lost without remuneration. This leads to an inefficient and non-profitable DER system. To improve the efficiency and feasibility of the DER system in areas with no feed-in policy, it is of utmost importance that an energy management system (EMS) that optimises self-consumption be implemented.

For the purpose of this study, an EMS was designed for a PV DER. The EMS was implemented as a real-world application by installing a PV system, a grid-tie inverter (GTI), auxiliary relay contacts and the EMS. The EMS system controller was a Siemens S7-1200 programmable logic controller (PLC) and was responsible for exercising control over the residential loads. An overview of the integrated system is shown in Figure 1 and explains the interconnection between the main components.

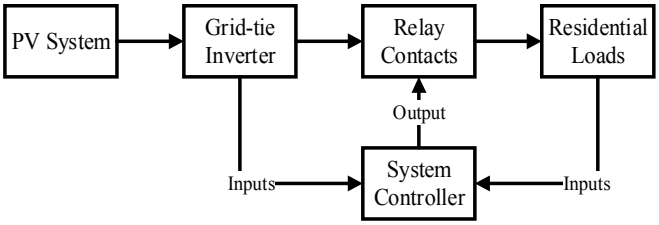

Figure 1. Overview of integrated system

2 Load Requirements

The system was specifically designed for the South Africa market and made extensive use of the NRS034-1:2007 standard which describes electricity consumption patterns of different income groups in South Africa, namely living standards measure (LSM). Within the NRS034-1:2007, the electricity demand and consumption profiles of the various income groups were described. Research on the various LSM groups identified which group would most likely adapt a residential PV system and based on these findings, associated residential loads and load profiles were determined. The identified loads that would be controlled were as follows:

- A 150 litre geyser (3 kW)
- A 9 kg washing machine (0.55 kW) and 9 kg tumble dryer (2.2 kW)
- An efficient swimming pool pump (0.6 kW)
- A standard two door refrigerator (0.3 kW)
- A standard dishwashing machine (1.8 kW)

In the study, (Bokanga, et al., 2014) illustrated that a significant energy consumption reduction was possible by implementing low power LED DC lights. The implementation of DC security lights was therefore included in the design.

W. A. Bisschoff, School of Electrical, Electronic and Computer Engineering, North-West University, Potchefstroom, South Africa (e-mail: wabisschoff@gmail.com).

This study was supported by the National Research Foundation of South Africa.

R. Gouws, School of Electrical, Electronic and Computer Engineering, North-West University, Potchefstroom, South Africa (e-mail: rupert.gouws@nwu.ac.za).

3 DESIGN OVERVIEW

The integrated system was divided into the three sub-systems as illustrated in Figure 2. The first sub-system, namely the energy system, solely consisted of hardware and was responsible for the physical connection between the PV system, GTI, charge controller and loads. The communication and control sub-systems operated alongside each other to manage the hardware as efficiently as possible. The control and communication sub-systems consisted of both hardware and software.

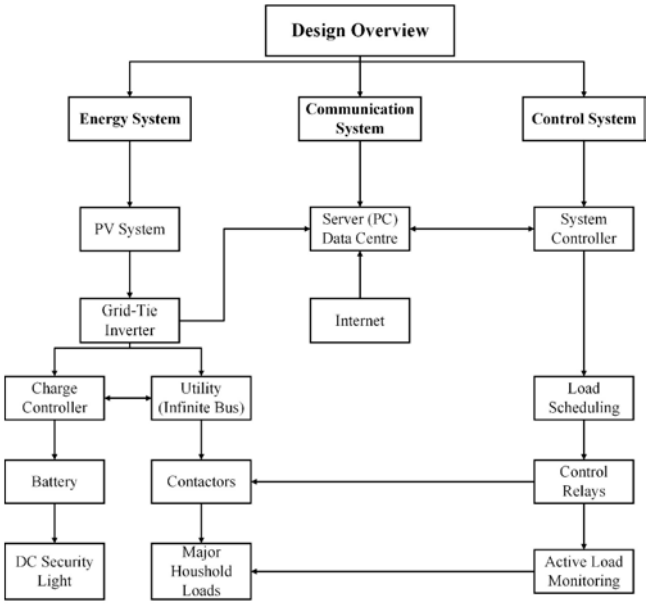

Figure 2. Design overview

3.1 Energy System Design

The energy system was a combination of a DC security light system, PV system, GTI and controllable household loads. As can be seen in Figure 2, the objective of the energy system was to integrate the PV system, battery, GTI and other hardware into a topology that could be integrated with each other and the utility. The PV system was connected via the GTI to the utility grid such that energy generated by the PV system could supply the loads connected in the residence. To actively control the loads in the residence, it was essential that electronically controllable switches, such as contactors relays, were installed in series with the loads that needed to be controlled. By doing so, full control could be exercised over which loads are connected/disconnected to/from the utility and PV system. Figure 3 illustrates the integrated energy system concept along with how the DC security light system fits into the energy system.

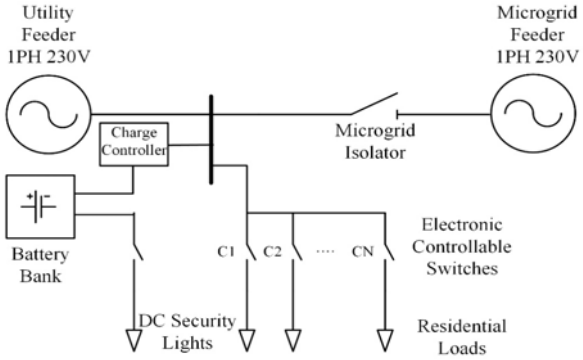

Figure 3. Grid integration and load control

3.2 Control System Design

The control system made use of multiple control strategies which was based on short and long-term inputs. Primarily, for the short-term inputs, the control system ensured that as much as possible of the energy generated by the PV system was consumed locally and power consumption off the grid was minimised. In the case where power generation exceeded power consumption, more loads were switched on to reduce the excess energy. The state-of-charge (SOC) of the battery was also fed to the system controller that aided in the decision-making processes regarding the DC security light system. Long-term inputs included daily expected energy, weather patterns, user priority settings and daily electricity tariff structures. The main purpose of the long-term inputs was to further ensure the optimising of the energy usage within the system. The control system made use of these inputs to schedule the loads according to the expected energy input profile. A summary of the short and long-term inputs that were used are shown in Figure 4.

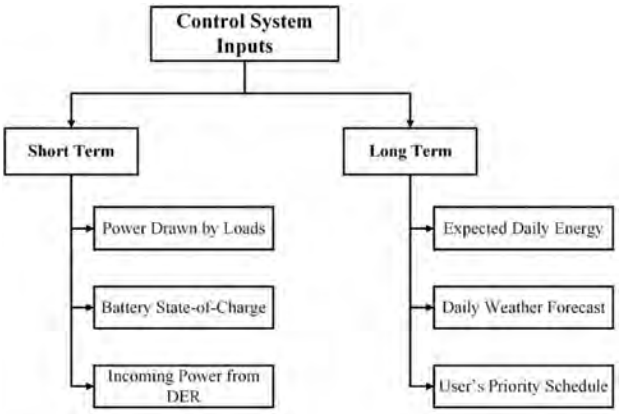

Figure 4. Summary of short and long term inputs to the control system

3.3 Communication System Design

The communication system was used to ensure that short and long-term data are communicated and synchronised across the integrated system network. The short-term control strategy communicated the current drawn by the loads, the battery SOC and incoming power from the PV through the network to a centralised server. This allowed the server to analyse the received measurements, create an energy consumption profile and alter the short-term control strategy to balance incoming power with the power drawn by the loads. Further objectives of the communication system was to obtain weather predictions from an internet RSS feed, accepting user inputs and storing all relevant information in a MySQL database for further analysis. The data was presented in the EMS software interface; the communication system's topology is illustrated in Figure 5.

Figure 5. Communication system topology

4 EXPERIMENTAL TEST STATION

As mentioned in the energy system design section, the system was designed for the South African market and therefore the integrated test station was installed in the town of Potchefstroom in the north-western part of South Africa. The Solar Frontier panels were installed at a residence in Potchefstroom as seen in Figure 6. As seen from Figure 6 the azimuth and tilt of the solar PV panels were directed in a true north orientation at approximately 30˚ inclination. This was in accordance with design recommendations from the PVsyst simulation software.

Figure 6. Installed PV modules

The integrated test station combined all the individual components to create a system where testing could be conducted in a safe and controlled environment. The integrated test station hosted the GTI, contactor relays, system controller and DC security light system. The integrated test station along with the individual components is shown on the left hand side of in Figure 7. On the right hand side of Figure 7, the DC security lights along with the plugs for the loads are shown.

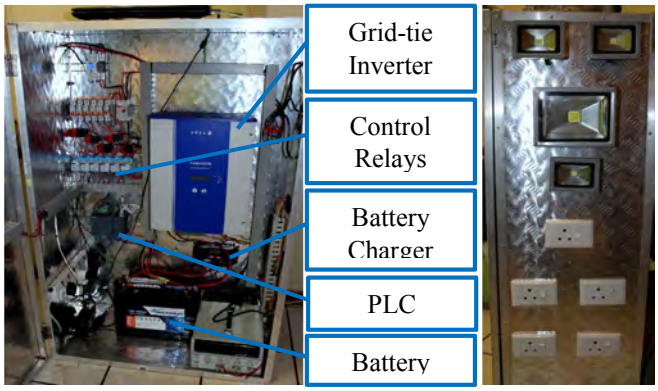

Figure 7. Integrated test station

5 EMS SOFTWARE INTERFACE

The EMS software interface was divided into four main pages. The first page was the user interface where the user could input the commands to establish the network connection, select the type of day (normal or laundry day) and select the tariff structure. From this page it was also established whether all devices were communicating within the network. On the weather and communication page, the current and predicted weather status was displayed. Apart from the described weather status, graphs visually illustrating the relative humidity, temperature and wind speed were updated in real-time. This data was used to predict the expected daily energy input and optimise the performance of the system. The weather and communication page is shown in Figure 8.

The system dashboard page was designed to provide feedback to the user on the status of the system. Information such as the delivered and consumed energy, maximum power demand and consumption and daily tariff metering were presented on this page. This page was completely autonomous and did not require any inputs from the user. The final page of the EMS software interface was the graphs page which contained real-time graphs of the incoming solar PV power and load status of the testing station. Real-time measurements from the GTI and measurement devices were used to compile these graphs. Also shown on this page was the forecasted solar PV input curve.

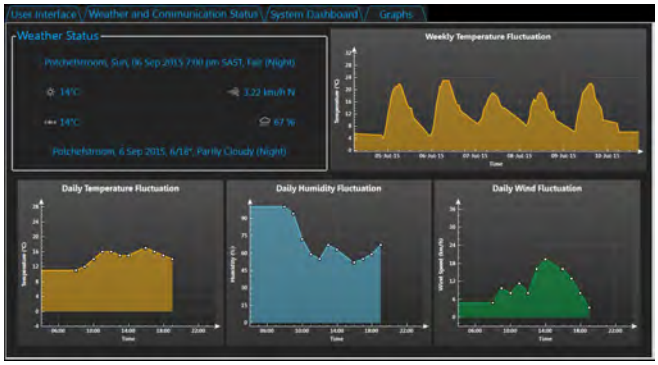

Figure 8. EMS software interface

6 EXPERIMENTAL RESULTS

The experimental results were obtained by allowing the test station to operate for a duration of 34 days. Some of the selected results that were collected were carefully analysed to ensure that no external factors influenced the experimental results. To thoroughly illustrate the operation of the control system, different scenarios are illustrated below. These scenarios have differences relating to the amount of daily input energy and peak power output from the solar PV system and weather conditions such as relative humidity, wind speed and daily temperatures. Each of the scenarios below is discussed according to the input solar PV profile, weather conditions and connected loads.

The EMS was designed according to two scenarios. In the first scenario, the loads that were connected throughout the day included the geyser, swimming pool, battery charger, refrigerator and dishwasher. This scenario was classified as a non-laundry day. The second scenario included the laundry cycle and added the washing machine and tumble dryer to the list of daily loads. The results below are presented according to these two scenarios and are compared to a case where no EMS intervention occurred.

6.1 EMS Controlled System: Non-Laundry Day

Figure 9 shows the temperature, wind speed and relative humidity throughout the day of testing. It is important to take note that the relative humidity is scaled on the secondary axis of the graph. From Figure 9 it is seen that sunrise and sunset was at 06h48 and 17h24 respectively. The day started out at a relatively low temperature (3˚C), high relative humidity (77%) and no wind. As the day progressed, the temperature rose to a maximum of 20˚C at 13h35. By this time the wind speed increased to 10 km/h which was defined as a light breeze. As the late afternoon set in, the temperature and wind speed gradually declined whilst the relative humidity rose. One of the factors that greatly influenced the amount of

incoming solar PV power was the cloud cover index. The captured weather data reported that there was no cloud cover during the day which was indicated as a "Clear" on the weather report.

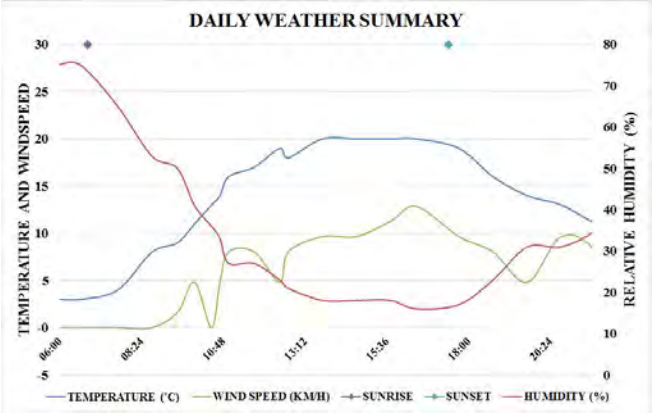

Figure 9. Summary of weather on 9 June 2015

The input solar PV profile and individual load curves corresponding to the weather conditions above are shown in Figure 10. A discussion on the figure follows below where each individual load is addressed accordingly.

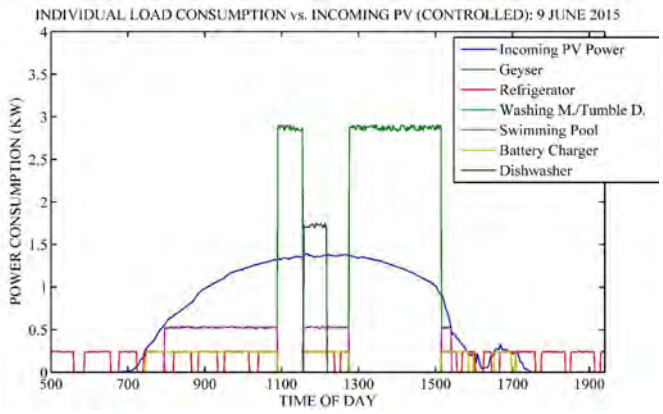

Figure 10. Individual load vs. incoming solar PV plot (9 June 2015)

Incoming PV Power: It is seen that the incoming solar PV power steadily increased to nearly 1.4 kW at noon. The output from the GTI remained steady until 15h15 where a steep drop in the incoming solar PV power was observed. This was due to the fact that a large shadow was cast over a portion of the solar PV panels during the late afternoon. Despite the disrupted solar PV profile due to the shadow, additional performance characteristics of the control system were obtained which are discussed below.

Characteristic	Experimental Result
Total Input Energy	7.81 kWh
Peak Power Output	1.39 kW
Start and Stop Time	07h01 to 17h14
Total Generating Time	10:13 Hours

Geyser: The geyser was switched on at two separate occasions during the day. The first was during the late morning (10h56) hours prior to the dishwasher starting time. This preheated the water for the dishwasher which reduced the runtime of the dishwasher. The second occasion where the geyser was switched on was to heat water for bathing and showering in the evening. The steep drop in the incoming solar PV power during the late afternoon caused the geyser to switch off earlier than expected which led to the water not being heated to the desired temperature. However, the control systems' main objective was to reduce consumption off the utility grid and hence the geyser was switched off when the incoming solar PV power dropped.

Characteristic	Experimental Result
Maximum Power Demand	2.91 kW
Total Run-time	2:58 Hours
Start and Stop Time 1	10h56 to 11h32
Start and Stop Time 2	12h45 to 15h07

Refrigerator: As stated previously the refrigerator could not actively be controlled since the compressor operated on its own closed-loop control system. However, control over the refrigerator was exercised by switching off the refrigerator during times when the geyser was switched on. As seen from the curve of the refrigerator, the refrigerator switched on/off spontaneously to regulate the temperature.

Washing Machine/Tumble Dryer: Neither the washing machine or the tumble dryer were switched on in this scenario.

Swimming Pool: The swimming pool pump was switched on during the mid-morning period as soon as the incoming solar PV power exceeded that of 0.55 kW. Whenever sufficient capacity was available, the control system switched on the swimming pool pump. The swimming pool pump was not allowed to be switched on at the same time as the geyser and was therefore switched on at three separate occasions. The steep drop in incoming solar PV power caused the swimming pool pump to switch off to reduce consumption off the utility grid. If the incoming solar PV power did not have such a sharp decrease, the swimming pool pump would have been switched on for another hour. The samples of the load current were taken every 15 seconds and hence the starting and magnetizing currents were not detected. The maximum power demand of the swimming pool pump was 0.54 kW as shown in the table below.

Characteristic	Experimental Result
Maximum Power Demand	0.54 kW
Total Run-time	4:43 Hours
Start and Stop Time 1	07h48 to 10h55
Start and Stop Time 2	11h36 to 12h44
Start and Stop Time 3	15h09 to 15h27

Battery Charger: The battery charger was switched on similarly to the swimming pool i.e. whenever incoming solar PV power exceeded that of 0.25 kW. Whenever this condition was met, the control system switched on the battery charger. In this specific scenario, the battery was almost completely discharged and hence required a longer period of charging. Since the battery was an essential part of the DC security light system that needed to operate during night-time, the battery charger received priority over other loads. This ensured that the battery had adequate charge for the DC security light to operate through the night. Similarly to the geyser and swimming pool pump, its operation was cut short due to the shadow on the solar PV panels. However, upon closer

inspection, it was seen that the battery charger was switched on for a fourth time at 16h38 due to increased solar PV power in the late afternoon. The battery charger operating time and SOC (11.62 V) suggested that the battery's initial charge was in the order of 15-25% of the nominal rating.

Characteristic	Experimental Result
Maximum Power Demand	0.25 kW
Total Run-time	5:54 Hours
Start and Stop Time 1	07h10 to 10h55
Start and Stop Time 2	11h36 to 12h44
Start and Stop Time 3	15h09 to 15h57
Start and Stop Time 4	16h38 to 16h51

Dishwasher: The dishwasher was carefully controlled by the control system to switch on during the forecasted peak incoming solar PV power (during noon). It was no different for this scenario and the dishwasher was switched on 24 minutes before noon for 49 minutes. It was expected that the dishwasher would continue for a longer period and hence the geyser starting time was 18 minutes late.

Characteristic	Experimental Result
Maximum Power Demand	1.74 kW
Total Run-time	0:49 Hours
Start and Stop Time 1	11h36 to 12h27

Figure 11 shows the combined load curve versus the incoming solar PV profile. This figure provides insight into how the control system reshaped the load profile according to the available solar PV power. Figure 11 is discussed below according to the annotations made on the figure.

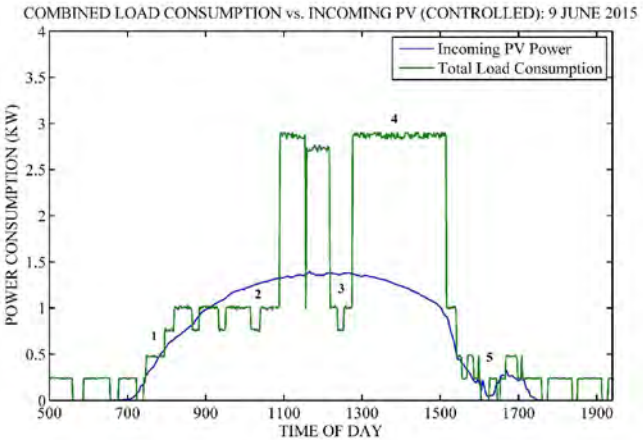

Figure 11. Combined load vs. incoming solar PV plot (9 June 2015)

Note 1: This annotation illustrates that as the incoming solar PV power rose early in the day, the loads were switched on such that the load power consumption grew at the same rate. The instantaneous power consumption was never greater than 1.4 times the incoming solar PV power during this period. This was greater compared to the simulation value of 1.2 times which is owed to the arbitrary switching of the refrigerator.

Note 2 and 3: These annotations illustrated the area where energy was wasted due to the geyser not switching on at exactly the correct time. If the geyser was switched on at roughly 9h30 and 12h15 respectively, the wasted energy would have been minimised.

Note 4: The elimination of loads being simultaneously powered reduced the peak demand to 2.91 kW.

Note 5: The sudden drop in the incoming solar PV power caused the control system to suddenly drop loads. This annotation illustrates that the total load consumption was quickly reduced during this period. As the incoming solar PV power had a late afternoon increase, the control system switched on the battery charger which further charged the battery.

A summary of the experimental results are shown in Table 1**Error! Reference source not found.**. From the table below it is noted that the total daily energy consumption by all the loads were 15.25 kWh. The incoming solar PV power contributed to 46.7% of this total (7.12 kWh). The percentage of incoming solar PV power that was absorbed by the loads (overall system efficiency) was 91.3%.

Table 1. Summary of results (9 June 2015)

Parameter	Result
Total PV Energy Input	7.81 kWh
PV Energy Lost	0.68 kWh
Total Daily Load	15.25 kWh
Energy Cons. off Utility	8.13 kWh
Energy Cons. off PV	7.12 kWh
Percentage Utility Supplied	53.30%
Percentage PV Supplied	46.70%
Maximum Demand	2.91 kW
Overall System Efficiency	91.30%

6.2 EMS Controlled System: Laundry Day

Figure 12 shows the temperature, wind speed and relative humidity throughout the day of testing. From Figure 12 it is noted that sunrise and sunset was at 06h50 and 17h24 respectively. The day started out at a low to moderate temperature (7˚C), moderate relative humidity (58%) and very little wind. As the day progressed, the temperature gradually rose to a maximum of 17˚C around 15h36. By this time the wind speed increased to 21 km/h which was defined as a moderate breeze. As the late afternoon set in, the temperature and wind speed declined whilst the relative humidity rose. The captured weather data reported that there was no cloud cover during the day which was indicated as a "Clear" on the weather report.

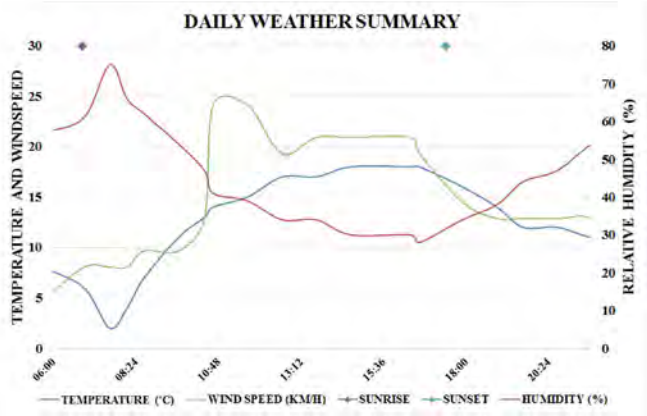

Figure 12. Summary of weather on 10 June 2015

The input solar PV profile and individual load curves corresponding to the weather conditions above are shown in Figure 13. A discussion on the figure follows below where each individual load is addressed accordingly.

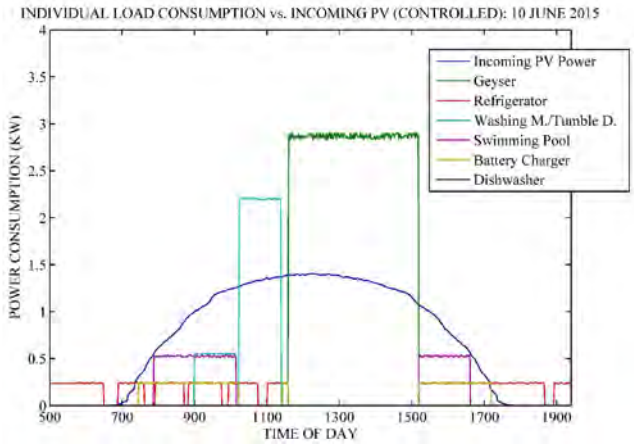

Figure 13. Individual load vs. incoming solar PV plot (10 June 2015)

Incoming PV Power: As seen in Figure 13, there were no disruptions that influenced the incoming solar PV profile. No power fluctuations, shadows or intermittent cloud cover were present in this scenario. The incoming solar PV profile corresponds very well to the weather report yielding satisfactory results. The incoming solar PV power provided a longer than usual day of power generation, stretching from 06h50 to 17h25.

Characteristic	Experimental Result
Total Input Energy	8.81 kWh
Peak Power Output	1.41 kW
Total Generating Time	10:35 Hours
Start and Stop Time	06h50 to 17h25

Geyser: Due to the day being allocated for laundry purposes, the geyser was switched on at only one occasion during the day. This was done prior to noon. The geyser was then switched off at 15h07 to allow the battery charger and swimming pool pump to be switched on. Since the washing machine and tumble dryer was required during the day, there was no time in the morning to switch the geyser on for additional water heating.

Characteristic	Experimental Result
Maximum Power Demand	2.90 kW
Total Run-time	3:22 Hours
Start and Stop Time	11h45 to 15h07

Refrigerator: Control over the refrigerator was exercised by switching off the refrigerator during the times when the geyser was switched on.

Washing Machine/Tumble Dryer: The washing machine and tumble dryer were time of day controlled and set to switch on during the late morning hours when incoming solar PV power was sufficient. The washing machine had a lower power requirement than the tumble dryer and was switched on at 09h00 and finished at 09h55. Thereafter the tumble dryer was switched on which continued to 11h15. During the operation of the tumble dryer all loads except the refrigerator was switched off to minimise consumption off the utility grid.

Characteristic	Experimental Result
Maximum Power Demand	0.56 kW and 2.18 kW
Total Run-time	2:15 Hours
Start and Stop Time 1	09h00 to 09h55
Start and Stop Time 2	09h57 to 11h15

Swimming Pool: The swimming pool pump was switched on as soon as the incoming solar PV power exceeded that of 0.55 kW. This caused that whenever sufficient capacity was available, the control system switched on the swimming pool. The swimming pool was not allowed to be switched on at the same time as the geyser and tumble dryer. The swimming pool was switched on at two separate occasions, 07h48 and 11h36. This resulted in a total operating time of 4:43 hours.

Characteristic	Experimental Result
Maximum Power Demand	0.56 kW
Total Run-time	4:43 Hours
Start and Stop Time 1	07h48 to 10h55
Start and Stop Time 2	11h36 to 12h44

Battery Charger: The battery charger switched on as soon as the incoming solar PV power exceeded that of 0.25 kW. Whenever this condition was met, the control system would switch on the battery charger which allowed charging of the battery to occur. In this specific scenario, the battery charger was switched on at four separate occasions. The first was at 07h10, the second at 11h36, the third at 15h08 and the last at 16h38. The total run-time for the battery charger was 5:54 hours. The 5:54 hours of battery charging ensured that the battery was charged to 95% SOC (12.61 V).

Characteristic	Experimental Result
Maximum Power Demand	0.24 kW
Total Run-time	5:54 Hours
Start and Stop Time 1	07h10 to 10h55
Start and Stop Time 2	11h36 to 12h44
Start and Stop Time 3	15h08 to 15h57
Start and Stop Time 4	16h38 to 16h51

Dishwasher: The dishwasher was not switched on in this scenario due to limited time available to perform the washing and tumble drying tasks.

Figure 14 shows the combined load curve versus the incoming solar PV profile. This figure provides insight into how the control system reshaped the load profile according to the available solar PV power. Figure 14 is discussed below according to the annotations made on the figure.

Note 1 and 4: The incoming solar PV profile was near perfect for the entire day and hence these results were the closest comparable to the simulation results. During the mid-morning period, the incoming solar PV power rose gradually which caused the control system to switch on the battery charger and swimming pool pump as soon as sufficient capacity was available. In a similar manner, the control system switched off the swimming pool and battery charger

as the incoming power became less than the respective threshold values.

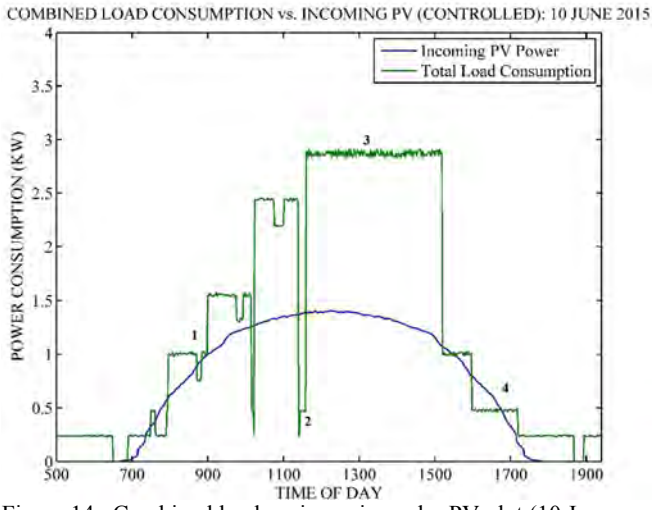

Figure 14. Combined load vs. incoming solar PV plot (10 June 2015)

Note 2: The sudden drop in power consumption was owed to the tumble dryer finishing its operating cycle 9 minutes early. During the tumble dryer's cycle all other loads except the refrigerator were already switched off. This caused the significant drop in consumption when the tumble dryer finished its cycle earlier than expected.

Note 3: The peak demand of the day was set by the geyser at 2.91 kW.

A summary of this scenario's experimental results are shown in Table 2. From the table it is seen that the total daily energy consumption by all the loads were 18.20 kWh with the solar PV supplying 47.75% of this total (8.50 kWh). The percentage of incoming solar PV power that was absorbed by the loads (overall system efficiency) was 96.6%. A satisfactory percentage of the load was covered by the incoming solar PV power and hence only 9.7 kWh was required from the utility.

Table 2: Summary of results (10 June 2015)

Parameter	Result
Total PV Energy Input	8.81 kWh
PV Energy Lost	0.29 kWh
Total Daily Load	18.20 kWh
Energy Cons. off Utility	9.70 kWh
Energy Cons. off PV	8.50 kWh
Percentage Utility Supplied	53.25%
Percentage PV Supplied	46.75%
Maximum Demand	2.91 kW
Overall System Efficiency	96.60%

6.3 Uncontrolled System

To directly compare the uncontrolled to the controlled system experimental results, it was necessary to have a consistent uncontrolled system load profile. The load profile was taken from a normal non-laundry day with accurate timestamps. The timestamps of the discussed solar PV input profiles were matched to the load profile's timestamps and hence accurate calculations could be performed. The individual load curve along with the various solar PV profiles is shown in Figure 15.

Incoming PV Power: The incoming solar PV profiles were discussed in the previous sections and are not discussed in this section.

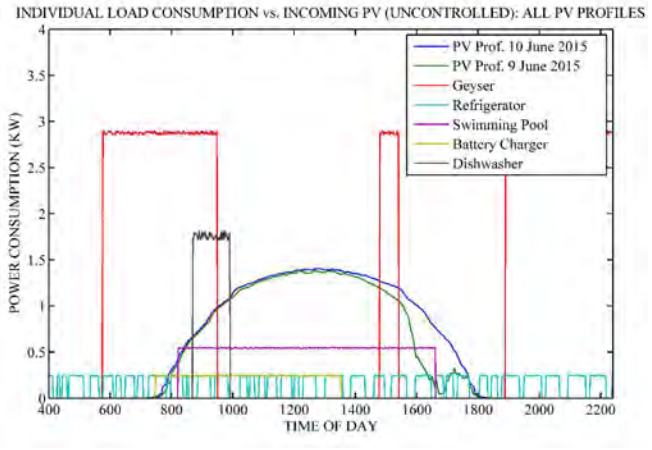

Figure 15. Uncontrolled individual curve

Geyser: The geyser element was switched on at three separate occasions during the day. The first was during the early morning hours (05h50) when the user bathed which caused hot water to flow out of the water tank and had to be replaced by cold water. The second occasion was in the early afternoon and caused the geyser element to be switched on for a short period to maintain the hot water temperature. In the late afternoon, the residents used hot water for cooking and bathing purposes which triggered the geyser element to switch on for a third occasion.

Characteristic	Experimental Result
Maximum Power Demand	2.91 kW
Total Run-time	6:07 Hours
Start and Stop Time 1	05h50 to 07h58
Start and Stop Time 2	14h48 to 15h32
Start and Stop Time 3	19h25 to 22h40

Refrigerator: As can be seen from the curve of the refrigerator, it was switched on/off spontaneously to regulate the temperature inside the refrigerator box.

Washing Machine/Tumble Dryer: Neither the washing machine nor the tumble dryer was switched on in this scenario.

Swimming Pool: The swimming pool pump was switched on at 08h15 and switched off at 16h45.

Characteristic	Experimental Result
Maximum Power Demand	0.54 kW
Total Run-time	8:30 Hours
Start and Stop Time	08h15 to 16h45

Battery Charger: The battery charger switched on as soon as the incoming solar PV power exceeded 0~kW and switched off as soon as the battery was fully charged.

Characteristic	Experimental Result
Maximum Power Demand	0.25 kW
Total Run-time	5:55 Hours
Start and Stop Time	07h40 to 13h35

Dishwasher: The dishwasher was manually switched on at 08h50 and finished its cycle within 1 hour and 5 minutes.

Characteristic	Experimental Result
Maximum Power Demand	1.74 kW
Total Run-time	1:05 Hours
Start and Stop Time	08h50 to 09h55

Figure 16 shows the uncontrolled combined load curve versus the incoming solar PV profile. This figure provides insight into how the load profile was according to the available solar PV power without the control system. Figure 16 is discussed below according to the annotations made on the figure.

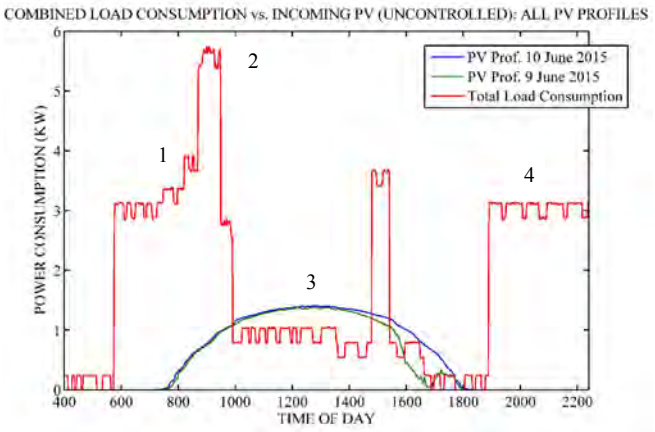

Figure 16. Uncontrolled combined curve

Note 1, 2 and 4: These annotations illustrate that the maximum power demand of 5.75 W was during the mid-morning period (09h00). This was undesirable as there were very little incoming solar PV power during this period. Also during the early evening hours excessive energy consumption occurred.

Note 3: This annotation highlights the fact that during the peak solar PV generation period, the load consumption was less than the solar PV generation. This caused the excess energy to feed into the utility grid and was lost.

From Table 3, a summary of the uncontrolled results compared to the various incoming solar PV profiles are shown. It should be noted that the overall system efficiency was not only dependent on the incoming solar PV power and the load consumption. The overall system efficiency was predominantly influenced by the incoming solar PV profile.

Table 3: Summary of results (Uncontrolled)

Parameter	10 June 2015	9 June 2015
Total PV Energy Input	8.81 kWh	7.81 kWh
PV Energy Lost	2.46 kWh	1.86 kWh
Total Daily Load	34.19 kWh	34.19 kWh
Energy Cons. off Utility	27.83 kWh	28.23 kWh
Energy Cons. off PV	6.35 kWh	5.95 kWh
Percent. Utility Supplied	81.4%	82.6%
Percent. PV Supplied	18.6%	17.4%
Maximum Demand	5.75 kW	5.75 kW
Overall System Eff.	72.1%	76.2%

7 CONCLUSION

The experimental results of these scenarios proved that the percentage of the solar PV generated energy absorbed locally ranged from 72.1% to 76.2% when no EMS was implemented. It further showed that the utility grid supplied at least 81.4% of the daily energy requirement on days when the solar PV energy yield was quite high.

The first scenario of the controlled system experimental test (non-laundry day) was conducted when the weather status was classified as "clear skies". A significant improvement was seen compared to the uncontrolled system. The percentage of the solar PV generated energy absorbed locally increased to 91.3% with the percentage of energy supplied by the utility reducing to 53.3%. This translated to an energy saving of approximately 20 kWh per day. When converted to South African currency, this is equal to R 36.80 per day based on a tariff of R 1.84 per kWh.

In the second scenario (laundry day), the weather status was also classified as "clear skies". The results were similar to the non-laundry day scenario with the exception of the increased percentage of the utility supplied energy (8.81 kWh). The percentage of the solar PV generated energy absorbed locally further increased to 96.6% with the percentage of energy supplied by utility totalling to 53.25%. This translated to an energy saving of approximately 18 kWh per day or R 33.12.

To conclude, the EMS operating alongside a residential PV system increases the local energy consumption percentage by 15-20% when compared to a PV system with no EMS. This translates to a daily energy saving in the range of R 32.50 to R 37.00 which makes this EMS a feasible solution to implement along with a residential PV system.

REFERENCES

Bokanga, G. M., Raji, A. K. & Kahn, M. T. E., 2014. Design of a low voltage DC microgrid system for rural electrification in South Africa. Journal of Energy in Southern Africa, 25(2), p. 9.

Eskom, 2015. Tariffs and Charges 2015/2016. [Online] Available at: http://www.eskom.co.za/CustomerCare/TariffsAndCharges/WhatsNew/Documents/Tariff%20brochure%20v9%20lowres.pdf [Accessed 1 November 2015].

Eskom Newsdesk, 2015. Small and Micro Generation (SMG) Bulletin 1. [Online] Available at: www.eskom.co.za/Whatweredoing/Documen-ts/SMG_Bulletin1.pdf [Accessed 1 November 2015].

Jiang, Q., Xue, M. & Geng, G., 2013. Energy Management of Microgrid in Grid-Connected and Stand-Alone Modes. IEEE Transactions on Power Systems, 28(3), pp. 3380-3389.

Mikati, M. & Santos, M., 2013. Electric grid dependence on the configuration of a small-scale wind and solar power hybrid system. Renewable Energy, Volume 57, pp. 587-593.

Ramakrishnan, S. & Ramakrishnan, S., 2013. WoT (Web of Things) for Energy Management in a Smart Grid-Connected Home. Issues in Informing Science and Information Technology, Volume 10, pp. 461 - 472.

Robinson, D., 2013. Microgrids for Energy Reliability. ASHRAE Journal, 55(11), pp. B14 - B17.

Schulze, M. & Del Granado, P., 2010. Implementation of feed-in tariffs into multi-energy systems. International Journal of Electrical Power and Energy Systems Engineering, Volume 2, p. 85.

Practical considerations for controller selection in residential energy management systems: A review ☆

W.A. Bisschoff[a,*], R. Gouws[a]

[a] *Faculty of Engineering, School of Electrical, Electronic and Computer Engineering, North-West University, Potchefstroom, 2520, South Africa*

Abstract

A review of the wide variety of system controllers available on the market along with the practical applicability of each is discussed in this paper. The system controllers that are discussed include programmable logic controllers, microcontrollers and single board computers. These controllers are generally not competing for the same market share however, some of the capabilities of these controllers overlap with one another which makes the selection of an appropriate system controller a complex decision. The practical considerations of controller selection are discussed in this article along with a practical example thereof. The practical example that was used to illustrate controller selection was a residential energy management system which would be installed alongside a grid-tied 2 kWp photovoltaic system. The aim of the energy management system is to ensure that all the photovoltaic generated energy is consumed locally within the residence and not fed into the distribution network. Such a system is applicable in areas where no net-metering policies are in place.

Keywords:
Programmable Logic Controller, Microcontroller, Single Board Computer

1. Introduction

The popularity of control systems and the drive towards automation is causing more system controllers to be introduced into the market. Over the past decade, numerous controllers apart from programmable logic controllers (PLCs) and microcontrollers (MCUs) have come to light in the form of single board computers (SBCs) [1]. Some of the most popular modern SBCs are the Raspberry Pi, Panda and Rapcon Boards which are all driven by open-source software [2] [3], [4], [5]. These controllers form part of the SBC family which possesses processing power similar to earlier generation computers [2], [4], [6].

Although MCUs, PLCs and SBCs are generally not competing for the same market share, some of the capabilities of these controllers overlap with one another. PLCs have been the preferred controller choice for all industrial automation processes since the introduction of digital control [7]. However, both SBC and MCU manufacturers have already started exploring the opportunities in the industrial market [8]. Generally MCUs and SBCs are more popular in smaller scale and development control systems [4], [6]. Typical applications of MCUs include switch mode power supplies, inverters and other power electronic equipment [9]. SBCs have become more popular with digital signal processing (DSP) and cloud driven applications due to their superior processing power and software accessibility [10]. However, with the addition of expansion boards, any control system application can be realised by making use of one of the controllers listed in figure 1. The controllers mentioned in this figure are discussed below.

2. Modern Controllers

Modern controllers comes in a wide variety of capabilities ranging from basic input/output (I/O) to complex DSP. This section provides a review of the controllers that are typically used in modern industrial and small scale control systems. The performance and success of a control system can be compromised by selecting an

☆ Supported by the National Research Foundation of South Africa.
* Corresponding Author.
Email addresses: wabisschoff@gmail.com (W.A. Bisschoff), rupert.gouws@nwu.ac.za (R. Gouws)

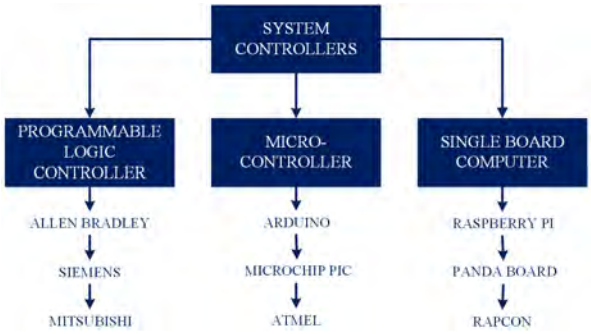

Figure 1: Summary of system controllers

unsuitable controller. The controllers discussed in this section include 1) PLCs 2) MCUs and 3) SBCs.

2.1. Programmable Logic Controllers

A PLC is a solid-state digital computer used to control and automate electromechanical processes such as production lines in factories, building energy management systems and heating, ventilation and air conditioning (HVAC) systems [11]. PLCs are renowned for their robustness and capability to withstand harsh environments such as excessive temperatures, dusty/smoke conditions and vibration. Apart from the robustness and reliability under extreme conditions, the simple programming techniques that is used to set the PLC's parameter makes this a favourable controller in all applications. [12], [13].

The programming techniques associated with a PLC are based on logical structure such as AND, OR, NOT, XOR etc. [11]. This structure of programming permits the use of logical gates and basic truth tables to control the PLC in a desirable manner. These logical structures are also presented in graphical forms to ensure an user friendly programming environment; the most widely used graphical environments include ladder and functional block diagrams. Another notable advantage of PLCs are the simplified redesign of established circuits. Alterations to the circuit are easily done without rewiring the entire circuit, only logical program code alterations need to be made. This ensures a time-efficient solution to rectify a fault or alteration to an established circuit [11]. These devices have a built-in non-volatile memory bank hosting an independent operating system which makes standalone and real-time automation possible. Automation through these devices is made possible by the fact that inputs can be obtained from sensors, calculations can be performed in real-time and the appropriate outputs can be activated [11]. The architecture of a PLC controlled system is shown in figure 2 [11], [14].

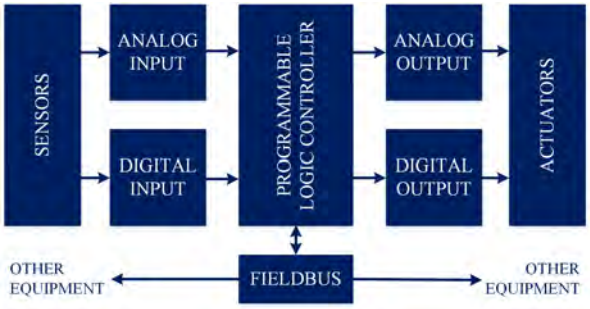

Figure 2: PLC application architecture [11], [14]

A summary of the practical advantages and disadvantages associated with PLCs are summarised in table 1. The table highlights benefits and shortcoming that are commonly found in industry and experimental control systems.

Table 1: Advantages and disadvantages of PLCs

Advantages	**Disadvantages**
Rugged and tested in harsh conditions	Lots of wiring makes fault investigations timely
Simple integration of modules i.e. I/O, Comms.	Expensive to set-up control system
Simple programming language	Integration issues between manufacturers' PLCs
Small controllers can control multiple machines	Semiconductors are temperature dependent
Real-time simulation prior to commissioning	
Reliable industrial controller	

2.1.1. Industry and Development Applications

In a study by Yilmaz (2010), a home automation system implementing a PLC was designed and constructed [15]. The main purpose of this system was to automatically control the lighting, wall outlets, gas and water system of a home to optimise energy consumption. The control of the wall outlets came from connecting several of the outlets onto the relays controlled by the PLC. In a similar manner, the distribution panel lighting switches were also connected to the PLC's relays; however, the control of these lighting switches was performed using a single keypad as input device.

The keypad was strategically placed within the home which allowed centralised lighting control. With a low pressure gas system present in the home, Yilmaz (2010) decided to implement a gas safety system into the home which shuts down the gas inflow in case of a leakage [15].

In a study presented by Balasevicius, Dervinis and Sarkauskas (2011), a small building energy management system consisting of renewable energy sources and a diesel generator were developed [16]. Solar PV and wind power plants of up to 5 kW was considered alongside a 10 kW diesel generator. The aim of the project was to minimise energy consumption from the national grid and expend all the locally generated energy. According to Balasevicius et al. (2011), the small building was divided into ten sections of electric loads, each connected to a triac-bank which is connected to the sources of energy [16]. The control system consisted of a power meter connected at each load section. The control strategy that was followed was to first connect the building to the utility company's grid and determine the power required by each section. Once this was established, the available energy from the wind, solar and diesel generator was determined. Based on these measurements, the PLC determined and controlled which load sections could be connected to the sources of energy.

A study presents a building energy management system that offers distributed control of the indoor comfort level whilst reducing the energy consumption. According to Kolokotsa et al. (2002), the system used a smart card unit, controlled by a user, to adjust the indoor illuminance and HVAC settings according to the user's smart card [17]. In cases where a smart card was not presented, the system assumed no-one was present and switched off all the lights and HVAC. A PLC performed fuzzy logic algorithms to determine the sensor inputs, actuator outputs and to send data across a communication network. There were several illuminance and temperature sensors connected to the control system which determined the comfort level according to the user's inputs. In addition, the PLC collected data from various users' smart cards and stored the data to adapt the control strategy.

2.2. Microcontrollers

Microcontrollers are comparable to a small computers since similarities in architectural design exist. Similar to a computer, an MCU has a reduced instruction set computer (RISC) processor, variable random access memory (RAM) and input/output (I/O) peripherals [18]. A MCU also contains an instructions set which hosts the program code embedded by the programmer. These devices contain numerous features which make these embedded devices very attractive when considering simplified control systems.

Some of the main features of MCUs are reduced size, weight and cost compared to other controllers consisting of a separate processor, memory module and I/O devices. The reduction to a single integrated circuit (IC) permits the implementation of cost effective embedded systems. The downside to MCUs is that in cases where high processing power is required, the MCU may fall short of the expected demand. Another shortcoming associated with MCUs is the low-level programming language knowledge that is required to set the parameters of these devices. However, advances made in the field of MCUs have seen the development of MCUs, such as Arduino, that are programmable with high-level programming languages. These languages are not as efficient and requires more memory as their low-level language counterparts.

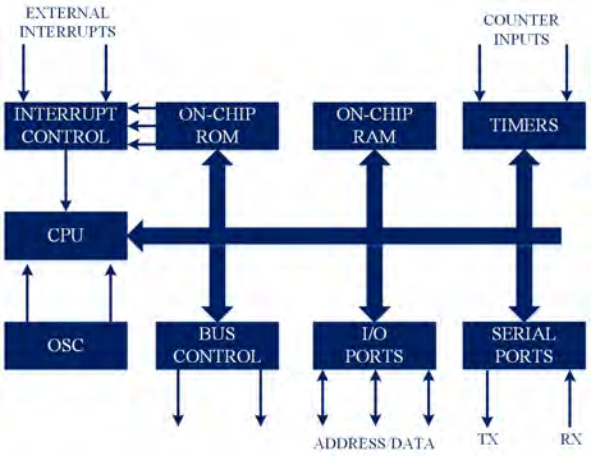

Figure 3: MCU generic architecture [19]

2.2.1. Industry and Development Applications

MCUs are conventionally not used in heavy current applications as the control unit; however, there are exceptions which are discussed below.

In a case study, Belvedere et al. (2012) presented an energy management system that consisted of a battery storage system, fuel cells and solar PV emulator [20]. The system was interconnected in such a way that a small distributed network of 4.5 kW was formed which was not connected to the utility grid but rather

Table 2: Advantages and disadvantages of microcontrollers

Advantages	Disadvantages
Real-time simulation prior to commissioning	Requires custom built printed circuit board (PCB)
Permits numerous peripherals	Complex programming language
No unnecessary components on the PCB	Not fit for harsh conditions such as high temperatures
Small controllers can control multiple devices	Time intensive to debug
Cost effective	Limited to control signals (no on-board relays)

formed its own 230 V AC bus. The two networks were isolated from one another and is never connected simultaneously. A 5 kW load emulator was connected to the bus to emulate various loads connected to the network. The main objective of the control strategy for the MCU system was to connect and disconnect the fuel cells and solar PV emulator to optimise the charging of the battery bank. Based on the battery bank state-of-charge, the MCU decided which source of energy, battery or utility grid, should supply the loads [20].

In a case study, Ghodki (2013) presented a study which contained a distribution system consisting of solar PV power and the utility grid [21]. A monitoring system employing smart metering was used to measure the amount of electrical energy consumed by the load and based on these measurements, the MCU controlled the power flow. The control of the power flow was established by using relays to connect the solar PV system and the utility grid in a parallel connection to the load [21]. The MCU measured the power consumed by the load and based on the capacity of the solar PV system, a decision was made regarding which source of energy, solar PV or utility, was used to power the load [21].

In a case study presented by Pisica et al. (2013) a prototype home energy management system was designed and implemented [22]. The main objective of this study was to make use of dynamic tariff monitoring and scheduling home appliances operation according to those tariffs. This way loads was shifted to a time frame where more generation capacity and a lower tariff was available. In this manner, electricity savings was increased by a scheduling pattern. The system also consisted of a web page that hosted all the scheduling, time frames and connected appliances. According to Pisica et al. (2013), the additional distributed generation was advised to further increase electricity savings [22].

2.3. Single Board Computers

Single Board Computers are fast becoming popular as embedded computer controllers due to their compact size and high processing [23]. Similarly to conventional computers, SBCs also consist of an embedded processor, memory module and I/O ports. Although these are low-end 8/16 bit processors, basic dynamic RAM and a limited number of I/O peripherals, these devices still offer competitive computation power at a fraction of the cost and size of conventional computers. The majority of SBCs are driven by Linux based operating systems; some these operating systems include Ubuntu, Android and Angstrom.

SBCs are similar to microcontrollers in the sense that the need for expansion boards are much higher than with PLCs. SBCs and microcontrollers are both only capable to produce low power control signals. Additional actuator expansion boards are required to control any real-world system. However, SBCs have a distinct advantage over all other compact controllers when comparing the number of connectible peripherals, communication protocols and processing power.

Table 3: Advantages and disadvantages of SBCs

Advantages	Disadvantages
Real-time simulation prior to commissioning	Limited to control signals (no on-board relays)
Permits numerous peripherals	Complex programming language
Capable of handling complex control systems	Not fit for harsh conditions such as high temperatures
Small controllers can control multiple devices	Time intensive to debug
Cost effective	Fairly new technology with little reliability tests
Multiple communication protocols	

2.3.1. Industry and Development Applications

There is a shortfall of energy management studies using SBCs which is due to the fact that SBCs are fairly new on the market and studies have not yet

been conducted in this manner. However, there is a home automation system powered by SBCs which is discussed below.

In the study presented by Ramses et al. (2013), a home automation system was implemented to control various loads by using a mobile device [24]. A Raspberry Pi SBC was used as a server to connect the home onto the internet. The user was then able to access the server through the mobile device's internet connection and control several of the loads from a centralised point. The main actuator was controlled through wireless network communication received from the SBC and relays were used to connect and disconnect the loads [24].

In the study presented by Raja et al. (2014), a secured smart home energy monitoring system using a Raspberry PI was designed [25]. The system included a home automation system that was controlled by a mobile device through a web-application. The loads that were controlled included a television and microwave. Furthermore, the system controlled the residence's video security system which was activated when motion control sensors were triggered.

3. Practical Considerations

Development and industrial controllers usually come in the form of a base model with very basic features and capabilities. However, expansion modules are always available from manufactures to enhance and improve the features of the base model. It is therefore considered a complex procedure when performing a trade-off analysis when selecting an appropriate controller for a specific application. The most important practical consideration regarding the controller that should be kept in mind are listed below.

a) Supply Voltage
   (i) Alternating (AC) or direct current (DC)
   (ii) Voltage level and range (i.e. 85-264 VAC)
b) Input Ports
   (i) Digital inputs
      - Number of inputs
      - Maximum permissible voltage
      - High and low threshold values
      - Isolated or non-isolated
   (ii) Analog inputs
      - Number of inputs
      - Acceptable input type and range (i.e. 0-10 V or 4-20 mA)
      - Resolution (i.e. 13 bits)
      - Sampling rate
      - Differential inputs
c) Output Ports
   (i) Digital outputs
      - Number of outputs
      - Type of outputs (i.e. transistor or relay)
      - Output protection (i.e. short circuit)
      - Output current capability
      - Switching frequency
      - Operating cycles
   (ii) Analog outputs
      - Number of outputs
      - Output ranges (i.e. 0-10 V or 4-20 mA)
      - Resolution (i.e. 10 bits)
      - Differential outputs
d) Communication
   (i) Protocol (i.e. serial, ethernet, bluetooth etc.)
   (ii) Data transfer rate
   (iii) Architecture (i.e. client-server)
e) Environmental
   (i) Degree of Protection (i.e. ingress protection (IP) 54)
   (ii) Operating temperature
   (iii) Vibration
f) Processor Capability
   (i) Work memory
   (ii) Load memory (i.e. internal and expandable)
   (iii) Processing times (i.e. cycle, operation, calculation etc.)
   (iv) Number of timers, counters, flags etc.

4. Experimental System Controller Selection

A system controller for a residential energy management system (EMS) needs to be selected. The EMS will be installed along with a residential grid-tied photovoltaic (PV) system and will aim to ensure that all the locally generated energy is absorbed in the residence. This is applicable in areas where no net-metering policies are present and all energy that is fed into the utility network is essentially lost. The loads will be controlled by energising relay contacts which will ultimately supply the loads. The loads that need to be controlled is the electric geyser, refrigerator, dishwasher, washing machine, tumble dryer and swimming pool pump. Details regarding the loads are illustrated in table 4.

The solar PV system will have an installed capacity of 2 kWp. The PV modules will be connected to a

Table 4: Load power levels

Load	Power Rating	Voltage Rating	Current Draw
Geyser	3 kW	220 V	13.6 A
Swimming Pool Pump	0.55 kW	220 V	2.5 A
Washing Machine and Tumble Dryer	0.55 kW 2.2 kW	220 V	2.5 A 10 A
Dishwasher	1.8 kW	220 V	8.1 A
Refrigerator	0.25 kW	220 V	1.2 A

Kaco Powador 2002 grid-tie inverter (GTI) which uses the RS-232 protocol to communicate the incoming and outgoing power, current and voltage. This information will be used to optimise local energy consumption by switching on/off the loads according to the incoming solar PV profile. The loads' power consumption will be measured by making use of current transformers (CTs) and feeding the load currents back to the controller. This way it can be ensured that the total load current exceeds the incoming generation current.

The home-owner should be able to switch off/on the EMS with a push-button and also isolate the loads from the PV system in case of emergency. Based on the discussion in the previous section, the practical considerations and specifications will be set out accordingly.

a) Supply Voltage
   (i) An AC voltage is readily available without the need for any converters; however a DC voltage can be easily obtained by installing a AC-DC converter.
   (ii) The nominal voltage readily available in the residence is at 220 VAC; however with an AC-DC converter any DC voltage can be obtained. It is decided that the controller will be supplied by 24 VDC as this will also be used to power the control circuitry.

b) Input Ports
   (i) Digital inputs
   - The system requires a total of two digital inputs. One for the switch off/on button and also one for the emergency stop button.
   - The control circuitry voltage is supplied from the AC-DC converter that supplies the controller and hence will be 24 VDC.
   - The threshold values of each controller varies; however there seem to be a trend that the low threshold seems to be at 45% of the rated control voltage. For a 24 VDC system this translates to approximately 10.8 VDC.
   - Isolated inputs are required when higher than the rated input voltage are present near the controller and the possibility exists that the controller may be exposed to that voltage level. In this case, the controller may be exposed to 220 VAC which will cause permanent damage to the controller if there are no isolated inputs.

   (ii) Analog inputs
   - The number of inputs is directly linked to the number of CTs that will be used to measure the load currents; therefore a total of five analog inputs are required.
   - The CTs will be terminated by a burden resistor and hence the analog input type needs to be voltage. The CTs output a low current (in the order of mA) that will be run through the burden resistor to generate a voltage of less than 10 V. Therefore, an analog input module permitting a voltage swing of between -10 and 10 V would be adequate.
   - Since the accuracy of the measurements will be determined by the CTs (less than 2%), the resolution of the analog input module will not be the limiting factor. Adequate resolution for the measurements will be 8 bits.
   - Sampling rate
   - Differential inputs

c) Output Ports
   (i) Digital outputs
   - The number of outputs is determined by the number of loads that need to be controlled. The total number of loads that must be controlled is six and therefore six outputs is required.
   - Continuous current draw applications is best controlled by making use of relay outputs.
   - External short circuit protection is needed at the relay outputs.
   - Based on the data presented in table 4, the current draw of the loads determines the

Table 5: Controllers trade-off analysis

	Evaluation Criteria							
Controllers	**Cost**	**Life Expectancy**	**Ease of Implementation**	**After Sales Support**	**Software Ease of Use**	**Robustness**	**Size**	**Score**
Weight	0.15	0.2	0.2	0.1	0.2	0.1	0.05	**1**
PLC	2	5	5	5	5	5	2	**4.4**
MCU	5	3	4	5	5	2	5	**4.1**
SBC	4	3	3	4	2	2	5	**3.05**

continous current capability rating of the outputs.

- Relay outputs cannot be switched at high frequencies due to the mechanical design; however the loads do not require switching at high frequencies.
- The mechanical design of the relays is designed and built for numerous switching operations; however the switching on loads will not require a great deal of switching throughout the day.

(ii) Analog outputs

- No analog outputs are required

d) Communication

(i) The communication protocols required between the controller and other equipment is established through RS-232 communication.

(ii) The transfer rate of the GTI is set at 9600 baud (9.6 kbps).

(iii) The network topology will be client-server.

e) Environmental

(i) The controller will be installed in an enclosure indoors and hence does not require an IP rating that is rated for excessive vibration, humidity and temperature.

Each of the controllers mentioned in the preceding sections deemed adequate with the addition of expansion boards. A practical evaluation was performed to determine the correct controller for the application and is shown in table 5. From table 5 it was evident that the PLC is the best suited system controller for the given application. The decision is mainly driven by the fact that the reliability and after sales support of the PLC are superior compared to the MCU and SBC. The selection of the PLC requires an additional analog input module to be added to meet the number of required analog input ports. Furthermore, a serial communication board is also required to permit communication in the system.

5. Conclusion

This paper provided a review on the three families of modern system controllers used in industry and development control systems. The three controllers that were discussed included PLCs, MCUs and SBCs. PLCs are still considered to be the favourite in industrial control systems. The development of open-source hardware and software at reasonable prices has opened the possibilities for SBCs and MCUs to enter the industrial market. However, the lack of after sales support of open-source products is a limiting factor in the absorption in industrial control systems.

The paper further discussed the practical considerations that need to be considered when selecting a controller for a control system. Factors that primarily influence controller selection are the supply voltage, number of I/O ports, I/O type (analog/digital/relay), communication protocols and environmental conditions. Within the primary influencing factors, detailed secondary factors need to be taken into account. An example of a residential EMS was used to practically illustrate the design considerations that need to be taken into account. The system controller had to control the various residential loads and the communication between the equipment to ensure that the EMS efficiently managed the system. It was found that for the residential EMS that performed load shifting, a PLC was best suited as it had the necessary specifications to

control the EMS. Some of these specifications included a 220 VAC supply, 6 relay outputs, 8 digital inputs, 8 analog inputs an additional RS-232 communication module.

Bibliography

[1] Microcontrollers-No Experience Necessary, pp. 39-43 (5 2013).

[2] How the raspberry pi sparked a maker revolution., Popular Science 286 (6) (2015) 20.

[3] Arduino, Arduino mega 2560 (2015).
URL http://www.arduino.cc/

[4] PandaBoard, Panda board es setup (2015).
URL http://pandaboard.org/

[5] Zeltom, Rapcon board (2015).
URL http://zeltom.com/products/rapcon

[6] H. Uhan, A. Akbas, Designing a system allowing high-definition video transfer with minimum latency and multi-use access to projection device by wireless., in: Proceedings of 2012 International Conference on Complex Systems, ICCS 2012, no. Proceedings of 2012 International Conference on Complex Systems, ICCS 2012, Institute of Pure and Applied Sciences, Yalova University, 2012.

[7] K. Hans B., R. Helmut A., PLCs: Programmable Logic Controllers, McGraw-Hill Professional, 2012.

[8] Rs components distributes industrial shields plcs and panel pcs., Wireless News.

[9] N. Barsoum, Temperature and light control of three phase induction motor speed drive by pic., AIP Conference Proceedings 1239 (1) (2010) 185 – 191.

[10] K. Dewald, D. Jacoby, Signal processing in embedded systems, Latin America Transactions, IEEE (Revista IEEE America Latina) 11 (1) (2013) 664–667.

[11] G. Dunning, Welcome to the World of Programmable Logic Controllers, 3rd Edition, Delmar Cengage Learning, 2006, Ch. 1, pp. 4–24.

[12] E. Schnieder, L. Schnieder, J. R. Mller, Conceptual foundation of dependable systems modelling, in: M. Fanti, M. Dotoli (Eds.), Dependable Control of Discrete Systems, Vol. 2, 2009, pp. 198–202.

[13] I. Felea, S. Dzitac, F. Popentiu-Vladicescu, I. Dzitac, Models of availability maximization applied to "k from n" structures for electro-energetic systems, in: R. Bris, Z. Vintr, C. Guedes-Soares, S. Martorell (Eds.), Proceedings of the ESREL Anual Conference, 2009.

[14] Siemens, Siemens S7-1200 CPUs (2015).
URL http://www.siemens.com

[15] C. Yilmaz, Implementation of programmable logic controller-based home automation., Journal of Applied Sciences 10 (14) (2010) 1449–1454.

[16] L. Balasevicius, G. Dervinis, K. Sarkauskas, Renewable energy sources-receiver switching., Electronics and Electrical Engineering (114) (2011) 89–92.

[17] D. Kolokotsa, K. Kalaitzakis, E. Antonidakis, G. Stavrakakis, Interconnecting smart card system with {PLC} controller in a local operating network to form a distributed energy management and control system for buildings, Energy Conversion and Management 43 (1) (2002) 119–134.

[18] M. Predko, Microcontrollers, McGraw-Hill, 1998, Ch. 1, 9, pp. 1–5, 237–284.

[19] D. Otten, J. Mach, Mcus help meet design demands in low-power, high-performance industrial applications., ECN: Electronic Component News 55 (6) (2011) 14.

[20] B. Belvedere, M. Bianchi, A. Borghetti, C. Nucci, M. Paolone, A. Peretto, A microcontroller-based power management system for standalone microgrids with hybrid power supply, Sustainable Energy, IEEE Transactions on 3 (3) (2012) 422–431.

[21] M. K. Ghodki, Microcontroller and solar power based electrical energy management system for renewable energy applications, International Journal of Electrical Power and Energy Systems 44 (1) (2013) 852 – 860.

[22] I. Pisica, G. Taylor, C. Chousidis, D. Trichakis, L. Tomescu, L. Laurentiu, Design and implementation of a prototype home energy management system, 2013.

[23] R. Heeks, A. Robinson, Ultra-low-cost computing and developing countries., Communications of the ACM 56 (8) (2013) 22 – 24.

[24] M. M. Ramses, E. D. L. Victoria, A. S. Ral, Mobile remote control for home automation., International Journal of Interactive Mobile Technologies 7 (4) (2013) 21 – 26.

[25] S. Raja, C. Viswanathan, D. Sivakumar, M. Vivekanandan, Secured smart home energy monitoring system (SSHEMS) using raspberry PI, Journal of Theoretical and Applied Information Technology 66 (1) (2014) 305 – 314.

Appendix B: Turnit-In Report

The report added in this appendix illustrates a similarity report generated by the Turnit-In software package which compared the written report to previous written university reports, international journals, conference papers and all other published documents. This report provided proof that the work performed in this study was unique and original. From the report shown below it is seen that the similarity of the dissertation equated to 6%.

The majority of the similarities are owed to common technical report phrases such as "shown in figure", "shown in table" and so on. The other portion of the similarities are due to technical engineering terms and phrases covered in the literature study that can only be explained in a certain manner. This produced similarities to other sources that covered similar topics.

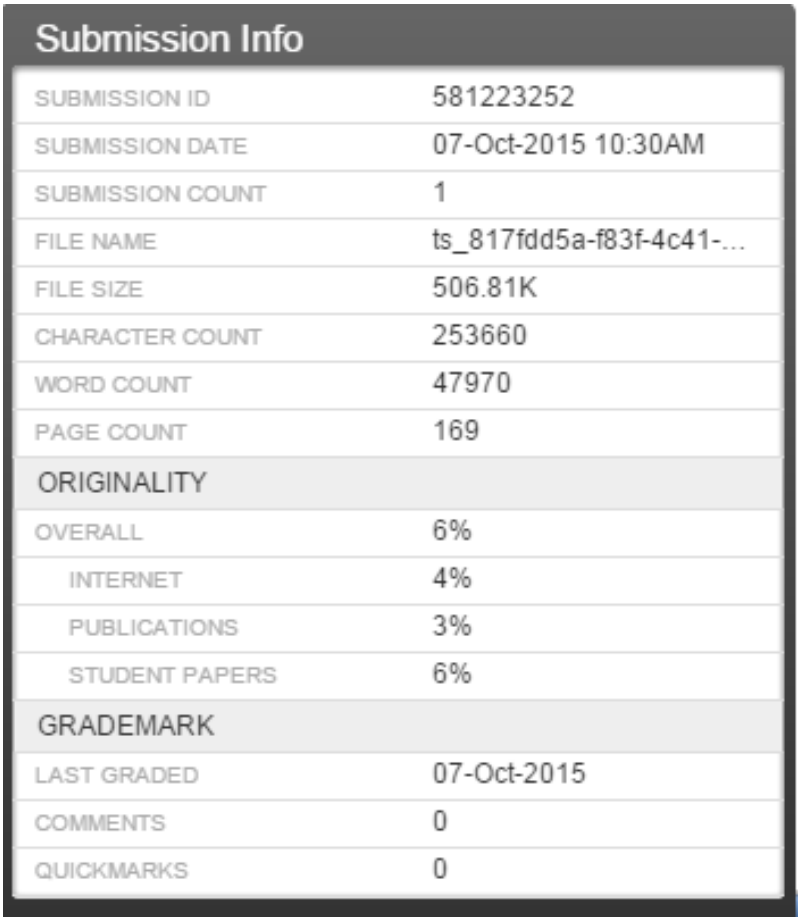

Submission Info	
SUBMISSION ID	581223252
SUBMISSION DATE	07-Oct-2015 10:30AM
SUBMISSION COUNT	1
FILE NAME	ts_817fdd5a-f83f-4c41-...
FILE SIZE	506.81K
CHARACTER COUNT	253660
WORD COUNT	47970
PAGE COUNT	169
ORIGINALITY	
OVERALL	6%
INTERNET	4%
PUBLICATIONS	3%
STUDENT PAPERS	6%
GRADEMARK	
LAST GRADED	07-Oct-2015
COMMENTS	0
QUICKMARKS	0

Figure B-1: Turnit-In report

Appendix C: DVD Content

This appendix describes the contents of the added DVD. The structure of the DVD is listed below with each topic added in a separate folder.

C.1 Datasheets

The datasheets have been added for reference purposes to support the detailed design. All the applicable datasheets used during the design and construction of the microgrid system can be found on the DVD under the "C.1 Datasheets" folder. The datasheets added in the folder are listed below.

1. Solar Frontier SF 165 W Solar Panel
2. Kaco Powador 2002 Grid-tie Inverter
3. Siemens S7-1200 1212C CPU
4. Siemens S7-1200 AI Module
5. Current Transformer
6. Maximus Battery

C.2 Eskom Tariff Structures

This folder contains the tariff structures implemented by Eskom to their residential distribution customers. These tariffs are valid for the 2015/2016 financial year. Eskom employs three tariff structures for their urban residential customers with tariffs ranging from R 0.99 to R 1.85 per kWh. The applicable tariff structures are added in folder "C.2 Eskom Tariff Structures".

C.3 MATLAB® and Simulink® Simulation Models

The models added in the "C.3 MATLAB® and Simulink® Simulation Models" folder were extensively used to simulate all aspects of the study. These simulations were performed to obtain meaningful simulation results. The folder contains the three simulation models that was used to represent the real-world system.

C.4 Solar PV Panels Power Rating

This folder shows additional information that was used to determine the optimal power rating for the solar PV system. Within this folder, the probability density functions and expected daily energy yield for the months of June and July are shown. These were the

months when most of the testing was conducted and hence was deemed relevant to only show this data. These graphs can be seen in the "C.4 Solar PV Panels Power Rating" folder.

C.5 PVsyst Simulation Report

The PVsyst simulation report was extensively used to aid in the design and simulation of the uncontrolled and controlled system. The PVsyst simulation allowed the addition of very detailed parameters which ultimately led to an accurate real-world representation. The sections in the simulation report consisted of geographical, installation, loss and economic evaluation parameters. The full report is added in the "C.5 PVsyst Simulation Report" folder where all the information was gathered from.